UiT
THE ARCTIC
UNIVERSITY
OF NORWAY

FACULTY OF SCIENCE AND TECHNOLOGY
Department of Geology

Late Triassic channel systems at the Loppa High, SW Barents Sea

Agafonova Olga
Master thesis in GEO-3900
December 2015

Abstract

The study is based on the 3D seismic dataset (LN09M01). The study area is located in the southwest Barents Sea, south-western flank of the Loppa High. In the SW Barents Sea, the Middle to Late Triassic interval incorporates relatively thick and widespread fluvial system in the Snadd Formation, which is characterized by distinctive abundance of channel bodies of varying shape and extend. During Triassic, the Barents Sea Basin was gradually filled with sediments, sourced from Caledonian mountains in the southeast, by prograding alluvial to deltaic plain.

The Middle to Late Triassic Snadd Formation is dominated by distinctive abundance of channel bodies. This master thesis has the overall objective to increase knowledge about the distribution and evolution of fluvial depositional systems of Snadd Formation, also focusing on channel dimensions, geomorphology and control over sediment deposition. By analyzing 3D seismic volume and investigating stratigraphic evolution, this thesis reveals evidence of the presence of fluvial depositional systems and variety of fluvial geomorphological features, such as point bar, concave-bank, channel fill and levees deposits.

The results of this study provide a basis sedimentology insight of the Snadd formation, evolution and migration of ancient fluvial channel, and in broader scale, it provides insight into spatio-temporal development of channel sandstone bodies.

Acknowledgements

I would like to thank my supervisors Srefan Buenz for giving me this great opportunity to work on this interesting project. This thesis was a great experience for me and I have learnt and analyzed a lot. I appreciate all of your input and help.

For advice and consultation, I would also like to thank to: Iver Martens, who was a great Petrel instructor, and also gave me advice regarding velocity modelling. I would like to thank all of my friends for supporting me and for being exactly the way they are, and fellow master students for creating a good working environment. I gratefully acknowledge the friendship and support extended to me by the faculty members of the department during my years at the University of Tromsø.

Last but not least, I would like to thank all my family members for great support. I am grateful to have you all. A very special thank you belongs to Anton Skvortsov, for always standing by my side. This thesis is dedicated to you.

Contents

Chapter 1 - Objectives

By investigating stratigraphic evolution of the area, this study reveals the presents of fluvial features, including paleo-channel belts, its evolution patterns, point-bar systems and its migration and preservation processes. The main objective of this master thesis is to utilize 3D seismic data to map, visualize and describe in terms of their morphology and architecture paleo-channel systems of the study area and improve our understanding of the channel evolution and development. This new regional understanding of the fluvial succession gives a good insight into basis sedimentology of the Snadd formation and it provides insight into spatio-temporal development of channel sandstone bodies. Unfortunately, no borehole penetrated paleo-channel in the study area, and the data are therefore not further used except for stratigraphic correlations with the seismic data.

This master thesis concentrates on paleo-channel systems in the Triassic sediments on the southwestern flank of the Loppa High, SW Barents Sea (LN09M01)

Figure 1 The south-western Barents Sea with location of main structural elements and study area on the south-western flank of the Loppa High, shown with black rectangle. Figure modified from (NPD, Factmaps, 2014).

(Figure 1). The Loppa High area has been of increasing interest within the hydrocarbon industry, because of the previous findings of Skrugard in 2011, Havis in 2012 (Npd, 2012) and Gohta in 2013 (Lundin, 2013). The study of channels is of great importance in hydrocarbon exploration, since they can act as conduits for sediments transported to deep basins, act as repositories of coarse-grained sediment, and hence could represent promising exploration targets. The morphology and architecture of the channels in the area will be identified in seismic data by using different seismic attributes. The present study will benefit from examples with comprehensive channels in the Gulf of Mexico, in continental margin of North America, Canada, Africa and Russia.

Chapter 2 - Environments of Erosion and Deposition

2.1 Introduction

The significance of rivers as being main sediment transfer agents and the fact that alluvial sediments form large parts of the temporary and long-term rock records have long been recognized. Comparatively recent studies of sediment transport processes, behavior of different river channel types and ancient sequences go back to 1950s, when first attempts have been made to recognize that the lateral migration of the channel generates fining-upwards sequence (Collinson, 1996).

Climate and geology are the primary forces shaping the Earth's landscape. The combination of these processes control water discharge, sediment supply, and channel slope, which determine a river channel's pattern (Wooster, 2002). River channels also play major role in the Earth's biogeochemical cycling of materials and influence global climate (Hudson-Edwards, 2006), besides they are major erosive and sediment transport agents. Rivers have been eroding, transporting, and depositing fluvial sediments since the Earth's hydrosphere came into existence. Fluvial environments occur on every continent on Earth and in every climatic zone (Hudson-Edwards, 2006). Fluvial deposits are those transported by, suspended in, or laid down by a stream. They are predominantly clastic, ranging in grain size from finest mud to coarsest boulder conglomerates (Miall, 1992), deposited at river channel, banks, floodplains, fluvial fans, and commonly contain economically important resources such as water, oil, gas, placer minerals, peat and coal, building stone, and sand and gravel (Bridge & Demicco, 2008). Fluvial deposits are sensitive paleo-environment indicators as they reflect tectonic slope changes, source area geology, sea-level and climate. They contain an important record of the morphology, flow and sedimentary processes of the rivers and floodplains in the past (Bridge J. S., 1999). Fluvial deposits are also important aquifers and hydrocarbon reservoirs. A particularly important aspect of ancient fluvial deposits is the geometry, proportion and spatial distribution of coarse-grained channel belt deposits (Bridge J. S., 1999). Major non-renewable recourses such as petroleum, gold, coal and uranium are therefore hosted in fluvial deposits in the USA (e.g., Alaska, Texas), Russia, China, Argentina, Venezuela, South Africa and the northwest Europe (Miall, 1992).

2.2 Geomorphic zones

Most of the time water flow in rivers and streams is concentrated within channels, which are depressions or scours in the land surface that contain the flow (Bridge & Demicco, 2008), and which are confined into series of interconnected channels. Present day river drainage network is strongly influenced by climatic and tectonic factors (Veiga-Pires, et al., 2007), but also by flow rate, flood-related sedimentary processes and the amount of sediment discharge (Hudson-Edwards, 2006). Discharge (also known as streamflow, flow, or flow rate) is expressed in dimensions of volume per unit (LeRoy, et al., 1997). All river flows ultimately are the result of precipitation (temperate or tropical regions), or of some combination of surface runoff, soil water, and ground water (LeRoy, et al., 1997, Bridge, et al., 2008). Rainwater flowing down slopes comes together to form a stream flow. The area that supplies water into a river channel is the drainage basin (Matsuda, 2004). The position and orientation of river channels in drainage basins are controlled by geological structure, the areal distribution of different types of surface material, and drainage conditions (Miall, 1992). A river system is composed of the mainstream and several tributaries (Matsuda, 2004). Many rivers develop various landforms and flow either parallel or transverse to the main structural units and have valleys in long established (over many millions of years) lowlands (Bridge, et al., 2008). In channels connected to the oceans, the sea level defines the "base level" of all the depositional system of rivers which flow into it (Dalla Valle & Gamberi, 2011). However, the lack of connection to the ocean means that everything brought in by water from erosional areas, as bed load, suspended load, is deposited within the channel, and consequently, the base level in the channel will be determined by tectonic subsidence and sediment supply (Nichols, 2007). Sediment is supplied into the river channel due to weathering processes over exposed rocks, mass wasting of loose material under gravity force, or with the assistance of the overland water. The materials brought to the channel are sediment load, which is deposited to form an alluvial plain. There three basic channels patterns are distinguished in alluvial plains: braided, meandering and straight.

Three geomorphic zones are recognized within fluvial and alluvial systems (Figure 2) erosional, transfer and depositional zone. Erosional zone is characterized by

erosional processes, which are actively downcutting and removing bedrock via downslope movement (Bridge, et al., 2008). At large scale, floods scour cohesive fine sediments to form channels (Collinson, 1996), which act essentially as a conduit for the throughput of channelized sediment gravity flows (Pickering & Clark , 1996). This zone contributes a substantial proportion of the clastic sediment for deposition in other sedimentary environments. The reasons for erosion to occur are climate change, which can affect the balance of a hydrological and sediment supply, and global or local sea-level fall (Leeder & Mack, 2007). Once channel has been initiated, it may expand and shift its position due to combination of vertical incision and lateral migration (Collinson, 1996). Incision is the vertical cutting into the previous depositional surface, when streambed deepens over time, (Michael R. Leede, et al., 2007; Nichols, 2007; Collinson, 1996), while a rising bed elevation is indicative of an "aggrading" stream channel (Castro, 2003). Seismic volume may also reveal wide and deep incised channels. Truncation of reflections usually indicates that the channel is incised into previous deposits. Seismic section AA' across the Shijiutuo Uplift, Bohai Bay Basin, China (Figure 3) has a well-defined signature on the seismic horizon slices as discontinuous seismic reflection configurations with seismic facies units filling a negative relief (Evy Glørstad-Clark, et al., 2010; Jair Weschenfelder, et al., 2010).
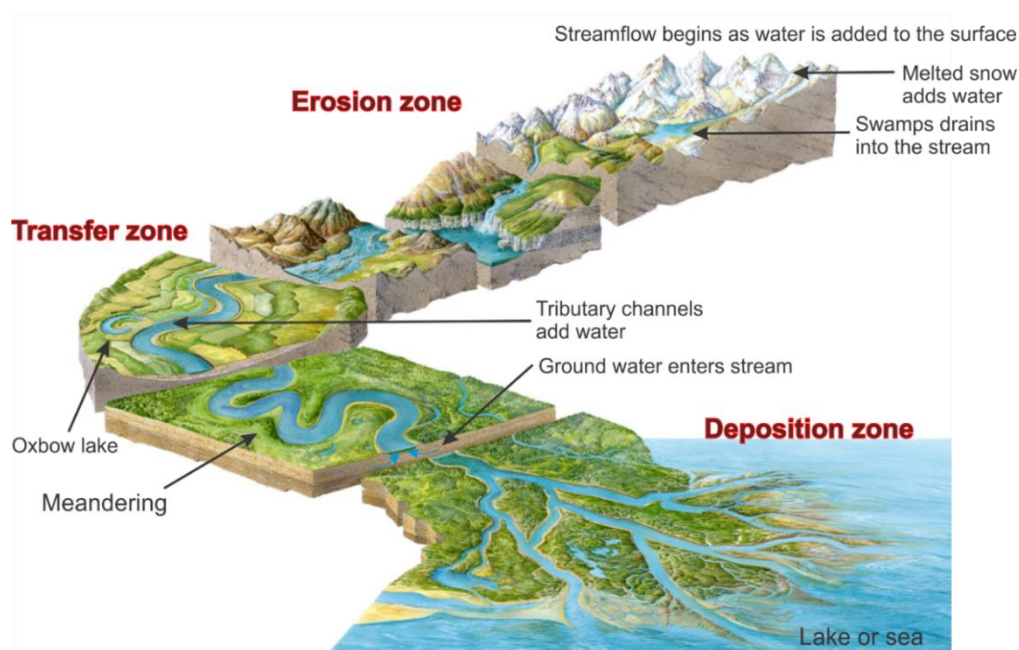

Figure 2. Schematic view of different geomorphic zones within fluvial systems: erosional zone, transfer zone and deposition zone. Figure modified from (Bridge & Demicco, 2008).

The incised valley morphology is presented in Figure 3 (inset table), with infilling style and seismic appearance. Incising or aggrading streams are considered vertically unstable, since vertical stability refers to the relative constancy over time period of streambed elevation (Castro, 2003). Local variations in bed elevation which are inherent in streams due to both scour and fill processes should not be considered as vertical instability. There are two methodologies (channel evolution and longitudinal profiles) presented to evaluate an existing vertically unstable conditions. Cannel evolution over time is the progression from a stable channel, to unstable channel via channel incision and widening, and to stabilization (Figure 4 A). Even though the rate and timing might vary dramatically, the general trend is well documented (Castro, 2003). Stage 2 indicates that the primary mechanism of channel evolution is incision of the channel bed. If bank erosion is the primary process, then the channel is at Stage 3. Stage 4 indicates some channel stability and sediment deposition near the bank. Distinguishing between Stage 1 and Stage 5 might be difficult since it requires a longitudinal profile. Longitudinal profiles (Figure 4 B, C) establish the elevation of the existing water surface, channel bottom, floodplains and terraces (Harrelson, 1994).
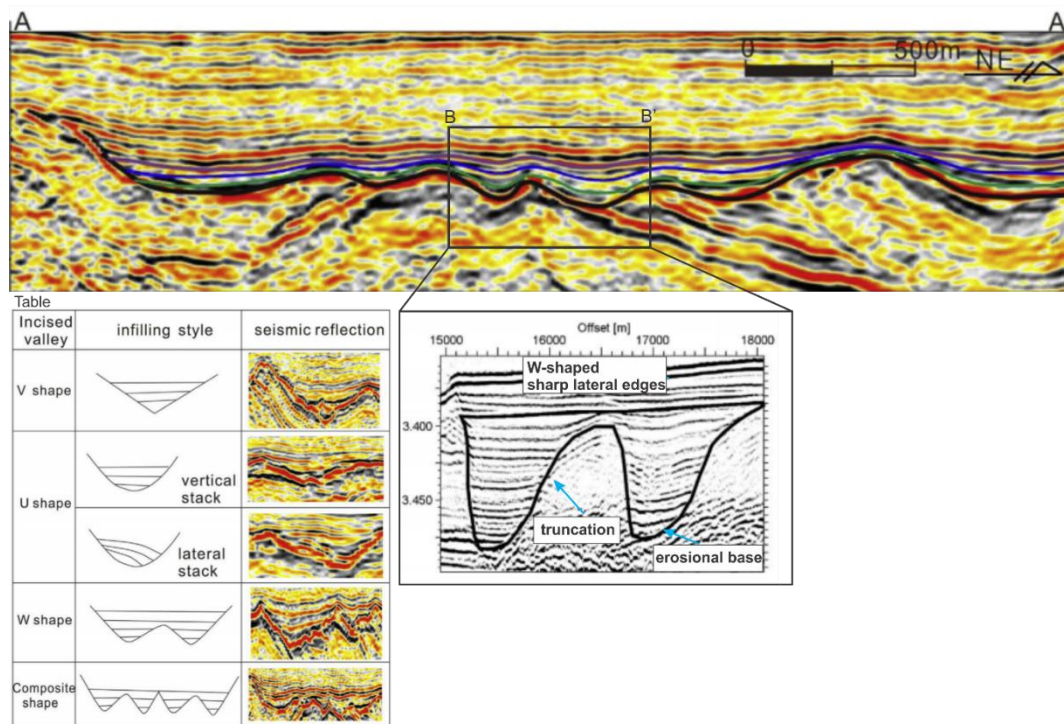

Figure 3. Seismic cross section AA' showing incised valleys and characteristics of filled internal reflection configuration and external forms. Channel fill facies are encircled by black solid line. Inset table displays the shapes of incised valleys, which generally changes from V through U and up to W shaped. Figure modified from (T. Schwenka, et al., 2005) and (Hongtao Zhu, et al., 2014).

Longitudinal changes and stream character changes with flow distance from headwater toward downstream end (Figure 4), and are therefore used to provide information about overall stream gradient, unit length and spacing, profile breaks or headcuts, and bed roughness and variation (Castro, 2003).
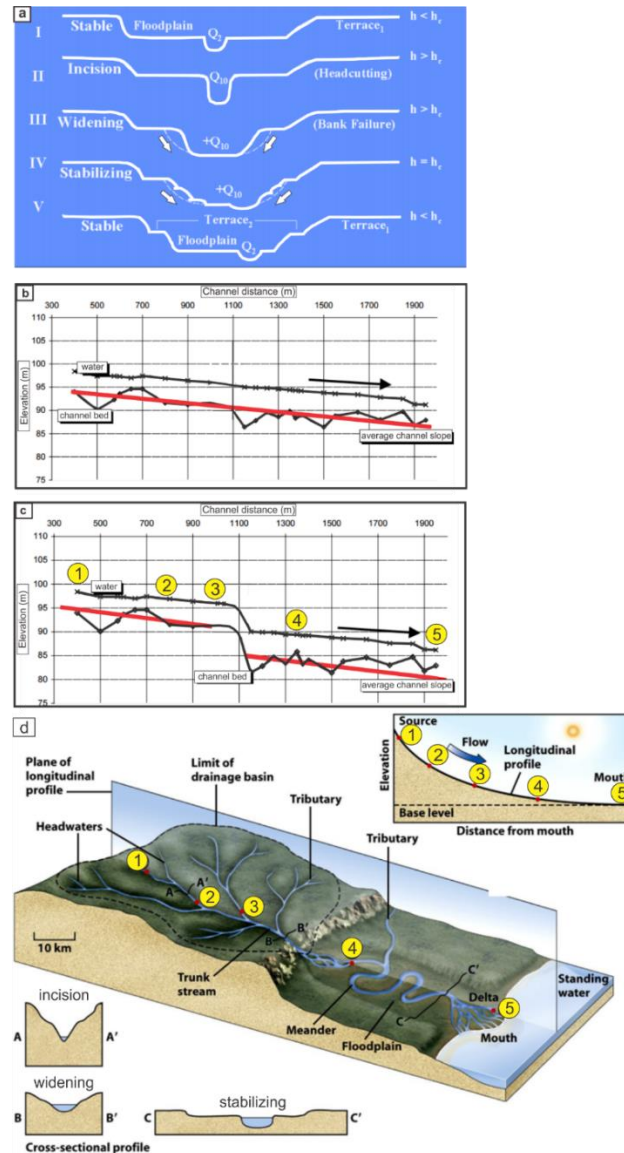

Figure 4 A) Channel Evolution model over time, showing the progression from a stable channel, to unstable channel via channel incision and widening, and to stabilization, where h is bank high and hc – critical bank high. B) Example of longitudinal profile without bed elevation off-set, C) Example of longitudinal profile with bed elevation off-set. Modified from (Castro, 2003). D) Schematic diagram of longitudinal changes, showing how stream character changes with flow distance.

Erosional processes dominate updip parts of longitudinal profiles (Figure 4 B, C), and as the slope decreases in a downstream direction, depositional processes take place (Dru Germanoski & S. A. Schumm, 1993). Erosion and sediment reworking in updip parts of the profile favor the development of bypass sediments. A fall in

longitudinal profiles (Figure 4 C) of the channel results in the flows eroding and dowcuting (incising) into underlying strata (Dru Germanoski, et al., 1993). Erosion by rivers is a primary mechanism by which landscape adjusts to climatic or tectonic forcing (M. E. Oskin, et al., 2014). Channel incision can be initiated in numerous ways, where the most common initiator is a change in peak discharge (Castro, 2003), influenced by climate change, lowered sea level and infrastructure. During response to base-level retreat, channel profile is expected to progress through a continuum sequential changes (D. Bowman, et al., 2009). Vertical deepening may be accompanied by lateral widening or migration. Lateral migration occurs over variable timeframes, ranging from gradual lateral migration to the complete shift of the channel to a new location, the process is known as avulsion (2.6.3 Lateral accretion and Avulsion) (Leeder M. R., 2011). It is associated with lateral erosion of bank material and involves removal of the loose overbank material by fluid scour (common for non-cohesive sand and gravel) or gravity-driven mass movement, when material collapses and falls into the stream (common for cohesive fine-grained bank material) (Collinson, 1996). Channel deposits, as a result, are largely concentrated within incised valleys, to the sides of which lie exposed areas, which are the subject for alternation and paleosoil formation (Nichols, 2007).

The lower part of the system is depositional zone (Figure 2). It is also the main phase of channel infill where sediments are deposited in the river channels and on the floodplains (Pickering, et. al., 1996). For sediments to get deposited flow rates should drop below the fall velocity for a particle of a given size (Hudson-Edwards, 2006). Generally, tectonics creates and controls the potential space for deposition by changing the gradient and differential tilting allowing either deposition or erosion (Michael R. Leeder, et. al., 2007).

In a transfer zone (Figure 2) gradient is lower than in erosional and depositional zones, and stream is not eroding, but nor is depositing (Bridge, et. al., 2008). Transfer zone might be associated with river confluence or bifurcation. Distinguishing between these two features is very important, because of the importance of these features to river networks and routing of flow and sediment (Jonathan M. Nelson, et al., 2011).

Figure 5. Longitudinal and stream character changes observed with flow distance away from headwater toward downstream end (along Apaporis River in Colombia and Pechora River in Russia). Modified from Google picture search.

Here, the concept of confluence or junction is where two channels meet to become a single channel. River channel confluences are a feature common to fluvial networks and are the points, which are significant contributions of water and sediment added to main channel (Best, 1987). Bifurcations or splits, where a single channel divides into one or more distributaries (Jonathan M. Nelson, et al., 2011), it is commonly observed associated with transfer zones. Modern examples of variety of geomorphic zones have been reported from various climatic zones (examples from western Colombia and Russia) (Figure 5).

2.3 Sediment transport and flow regimes

There are several factor witch influence sediment transport, deposition and hydraulics. Among them are climate, seasons, stream flow, water depth, flow dynamics, bed surface structures or sedimentary structures, grain size and texture (Hudson-Edwards, 2006). The relationship between hydrodynamic regime (water level, currents, waves, bed shear stress, channel morphology and sedimentary regime), erosion, sediment transport and accumulation is well established, allowing to predict the distribution behavior of different size particles, density, and shape, and the formation of bed forms (Einsele, 1992).

Sediment is transported in rivers by two mechanisms, traction currents and sediment gravity flows. Traction currents are those which transport cohesionless sediment as dispersed grains, each moving independently (Henry W. Posamentier & Roger G. Walker, 2006). Where large grains are generally moved by sliding or rolling along the river bed (bedload), smaller grains though, usually bounce along the bed or are swept along for some distances in suspension (Figure 6 B).
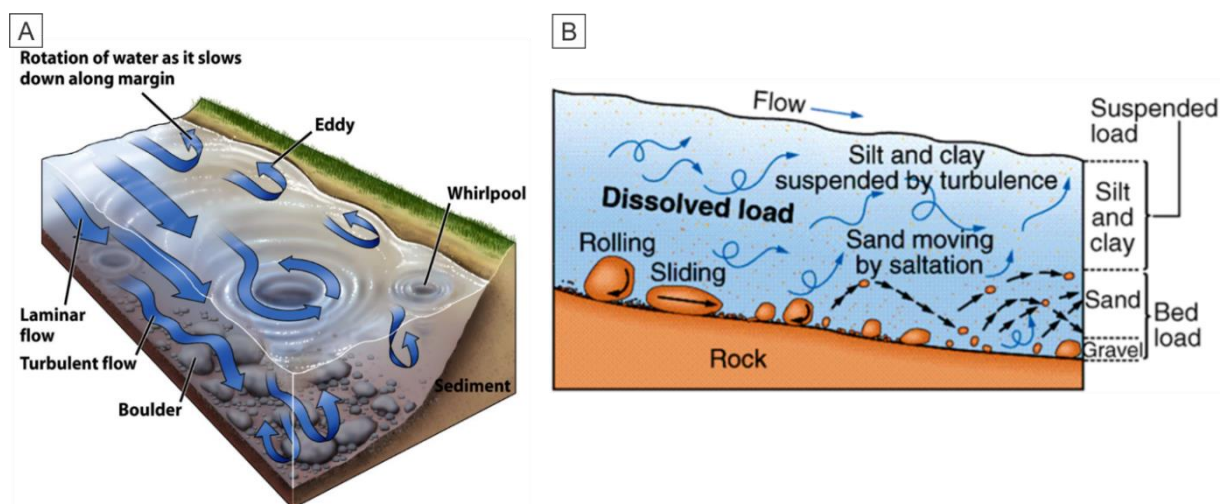

Figure 6. A) Laminar low velocity, transitional and turbulent river flows B) The processes of sediment movement within flowing water: (a) rolling; (b) saltation; (c) suspension. Modified from (Hudson-Edwards, 2006)

Suspended load is the mixture of finer sediments with a large relative surface area (commonly fine particles of silt and sand, <0.0625 mm) (Hudson-Edwards, 2006), which are transported in form of suspension (Figure 6 B) (Collinson, 1996). Suspended load is carried in flowing water where particles are suspended primarily due to turbulence (J. Dufek & G. W. Bergantz, 2007; Collinson, 1996), moves at the same

velocity as the flow and have slow settling velocity (Robert W. Dalrymple, 2010). The Hjulstrom curve (Figure 7) illustrates that higher velocity is required to entrain fine particles of clay and silt than coarse sand, however, once the fine sediment is in suspension, a much lower velocity is required to keep it in suspension (Keylock, 2004). Significant volumes of silts and sands are therefore found in channels, on levees and on fan surfaces accumulated at period of flooding (e.g. crevasse splays).

Bedload (>0.0625 mm) consist of coarser non-coheseve particles which are deposited in the topographically low and move within thin zone called bedload layer, directly above the channel bed. Within this zone grains move by several mechanisms including rolling and saltation (Figure 6 B), (Robert W. Dalrymple, 2010; Hudson-Edwards, 2006). Sediment in the bedload layer is always poorly sorted than sediment in suspension, as it is reflected in the nature of deposits (Robert W. Dalrymple, 2010).

Even though most alluvial sediment are deposited from traction currents, in certain settings sediment gravity play important role in sediment transport. These typically occur when large masses of loose sediment are mobilized by liquefaction on a sloping surface (Henry W. Posamentier, et. al., 2006). The flow may start as a land slide, and develop itself into moving body of unsorted sediment termed debris flow. Debris flows are mobile, gravity-driven, high-density, highly concentrated mixtures of sediment and water, composed of poorly sorted rock, soil and organic matter (Major, 1996). They "freeze" to deposit poorly sorted massively textured unit ranging in size from clay to cobbles and boulders meters in diameter with matrix-supported fabric once the applied shear stress (downslope gravity component) falls through lateral expansion and no longer exceeds their strength or through loss of gradient or as flows lose fluid (Major, 1996; Collinson, 1996). Debris flows are commonly occur in both subaerial and subaqueous parts of channels, and are important agents of transport and deposition of alluvial fans (Collinson, 1996). The flow ceases when the floe loses momentum on a flat basin floor, resulting in apparently chaotic deposits of poorly sorted debris, with large pebbles and cobbles mixed together and usually separated by finer sand, silt and mud.

River flow varies on time scales of hours, days, seasons and longer. Flow regimes show regional pattern that are largely determined by five components: the

magnitude of discharge, the frequency of occurrence, the duration of the period of time associated with specific flow conditions, the timing or regularity, the rate of change or flashiness (LeRoy, et. al., 1997). A flow through a channel can be classified in many ways:
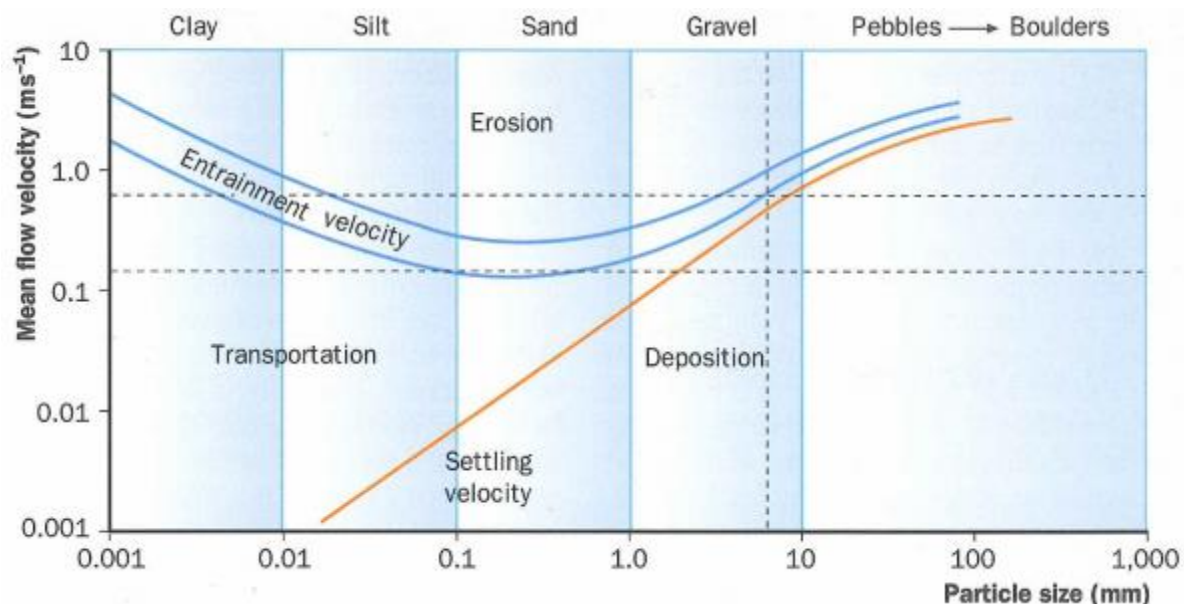

Figure 7. Hjulstrom curve demonstrates the relationship that exists between the velocity of fluid flow and grain size. Modified from (Keylock, 2004).

- Steady and unsteady flows, which are often easiest to recognize as the distinction is associated with flow properties dependence on time;

- Laminar (flow streamlines run parallel, flow velocity is low and viscosity is high (Chris Perry & Kevin Taylor, 2007), transitional and turbulent flows (streamlines move in a series of random eddies, flow velocity is high and viscosity is low (Chris Perry, et al., 2007) (Figure 6 A, Figure 8 A), which are characterized by rate of mixing and velocities;

- Uniform and non-uniform flows, which are characterized by velocity vector identity through the flow, rotational and irrotational flows, viscous and inviscous flows, incompressible and compressible flows, separated and unseparated flows (McDonough, 2007). Within fluvial systems, current flow through a channel is nearly always unidirectional and progressive reworking of fine sediment commonly leads to the finest material being transported furthest downstream (Chris Perry, et al., 2007).
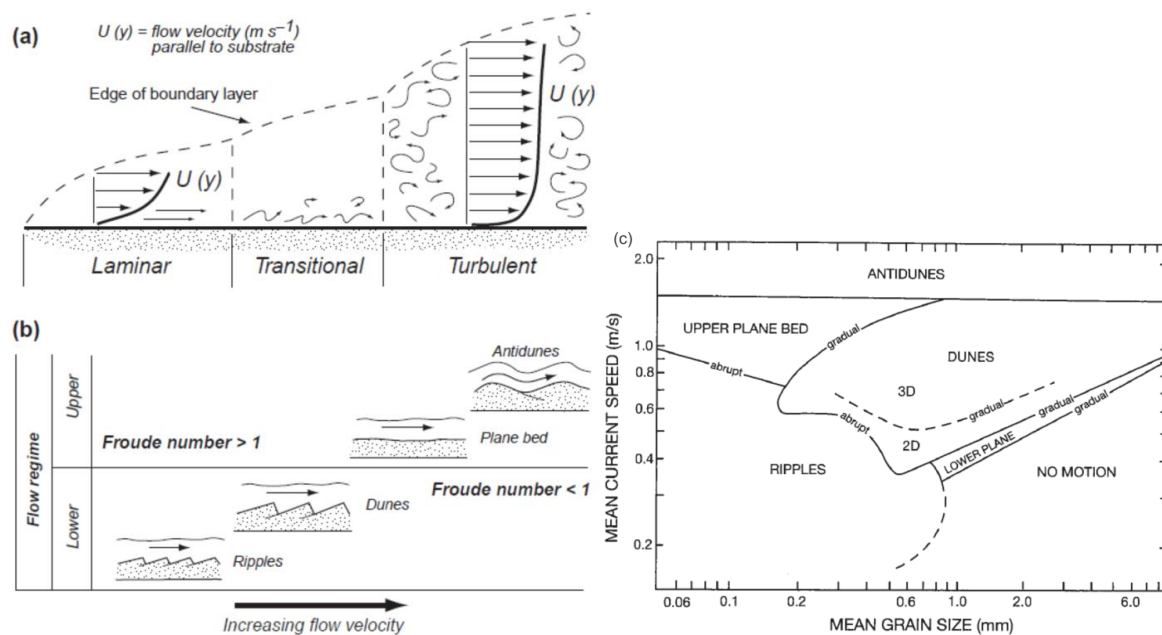
Figure 8. A) The nature of flow regimes within a fluid medium, B) The relationship between flow regime and sediment bedform development. As flow velocity increases from lower to upper flow, the amount and size of sediment that can be entrained and transported increase, leading to a change in sediment bedform structure (modified from (Hudson-Edwards, 2006). C) Current speed-grain size section through the three-dimensional phase diagram for the occurrence of current-generated bedforms (modified from (Robert W. Dalrymple, 2010).

As flow increases, the velocities required entraining sediment particles are reached, and at this stage, the sediment particles start to move by rolling and saltation (Chris Perry, et al., 2007). However, particles of sand or gravel, which are moved by the flowing water, are seldom all in the simultaneous motion, unless particles are far apart or their number is very small. Once set in the motion, the speed of the particle is affected by the proximity of the neighboring moving particles, which means that the grain speed is slower when the grain density is higher (Langbein & Leopold, 1968). The result of these grains interaction and movement is to intensify any initial grains grouping, thus any random influx of the grains into channel will set up wavelike forms - that is groups of grains separated by open spaces. That process leads to development of ripples and, at slightly higher velocities, dunes (Figure 8 B).

2.3.1 Small-scale bedforms

Fluvial sediments may represent different accumulation conditions in fluvial settings (Collinson, 1996). Fluvial (also known as alluvial) deposits are characterized by a huge variety of actively migrating bed forms and sedimentary structures, which are well-described by (Collinson, 1996; Bridge, et al., 2008). Movement of fluvial

sediments causes bed to deform into series of bedforms. Deformation occurs at a wide range of scales and forms including ripples, dunes, plane beds and standing waves (Collinson, 1996). The variation of sediment-transport rate and the bed sediment size are the most fundamental properties of siliclastic sediments, because of its control on sediment transport behavior. Also it exerts a strong influence on the nature of sedimentary structures present, as shown by current speed-grain size section through the three-dimensional phase diagram for the occurrence of current-generated bedforms (Figure 8 C) (Robert W. Dalrymple, 2010). Accumulation of grains is by no means composed always of the same particle sizes. At different flow stages when bed grains are in constant motion, there is a continuous trading of particles as some are swept away and replaced by others (Langbein, et al., 1968). In rivers that carry a wide range of grain sizes, different sizes are deposited over different ranges of discharge. Size variability has a tendency to increase as discharge decreases (Collinson, 1996).

As flow velocities increase, sediment bedforms are initially smoothed out to form planar beds and eventually antidunes, which are generated at upper flow regimes (Froude number $\geq$ 1) (Figure 8 B) (Chris Perry, et al., 2007). As flow velocity is reduced, current ripples, dunes, small-scale trough cross-bedding, wavy and horizontal lamination are generated at low flow regime stage (Froude number $\leq$ 1) (Figure 8 B). Hence, through cycles of river flooding, the mechanisms and processes of sediment movement change with flow velocity. Transition zone itself is characterized by plane beds and planar lamination (Gonzalo D. Veiga, et al., 2007). As flow velocity increases from lower to upper flow and associated with this is an increase in the amount and size of sediment that can be entrained and transported. This, in turn, will influence the structure of the sedimentary bedforms that develop (Chris Perry, et al., 2007). The preservation potential, however, for small units to become buried and preserved is successively low (Miall, 1992).

With increasing current velocity, very fine, medium and very coarse sands respond differently by depositing in different bedforms, thus the occurrence of both ripples and dunes are limited by critical values of grain size. Channel units comprise large- and small-scale channels, identified by complex of sedimentary bodies, which are comprised by minor, medium–sized and large-scale depositional structures

(Collinson, 1996). The evolution of fluvial environments and their infill, which can be from exclusively sandy to heterolithic, is recorded, and is characterized by the alternation of fine-grained sandstone/mudstone couplets (Gonzalo D. Veiga, et al., 2007).

2.3.2 Large-scale bedforms.

Fluvial strata comprise substantial hydrocarbon reservoirs across the globe, and it is well established that the sedimentologic and architectural complexity of associated fluvial deposits imparts a strong control on hydrocarbon recovery (Stephen M. Hubbard, et al., 2011). Fluvial deposits occur in a wide range of tectonic settings. They are an important component of stratigraphic record and are sensitive indicator of tectonism and sea level change (Miall, 1992) and they serve as sites of sediment storage.

Natural river channel are neither smooth nor regular in form features. Movement of sand grains via bedload transport causes the bed to deform into a series of bedforms including ripples, riffles, sand and pebble/cobble clusters, chutes, dunes (Hudson-Edwards, 2006; Collinson, 1996), which have repetitive tendency. Repetitive bedforms commonly construct higher-order components, such as bars (Collinson, 1996). Bars are referred to as sandy or gravelly macroforms in channels. Braided rivers (2.4.2 Bedload (Braided) river channels) are characterized by a dominance of braid or mid-channel bars; in meandering rivers (2.4.3 Meandering (mixed load and suspended load) river) coarse sediments deposited attached to the bank as point bars (Figure 9, Figure 10). Bars are examples of the lateral accretion architectural elements, where sediments are continuously deposited laterally rather than horizontally as channel moves sideways due to erosion on the outer bank and deposition of sediments on inner bank, leading to lateral migration (Bridge, et al., 2008). In meandering rivers laterally accreted deposits develop on the inside of the meander bends as the bend widens or migrates downstream (Henry W. Posamentier, et al., 2006). The meandering river facies sequence, as the result, consists of fining upward layers of channel, point bar, and flood plain deposits (Figure 9 B). Each bed in the sequence is deposited under decreasing energy as individual meander loops migrate, leaving the channel aside, and each bed is also formed in the different part of the channel (Collinson, 1996).

Continued enlargement of a meander loop results in increased sinuosity. Bars move until the channel moves sideways, this process is called avulsion, leaving the bar out of the main flow of the water, or until a cut bunk incise into an adjacent reach of the channel, resulting in point bar being cut-off by chute (2.5.3 Chute cutoffs). Point bar deposition begins with medium to fine trough cross-beds with rippled surface, and ends with fine sand and silt containing climbing ripples and cross-laminae (Leeder M. R., 2011). After channel has moved, flood plain muds with mud cracks and roots accumulate. The sequence (Figure 9 B) would normally be formed within a single pass of meander loop.
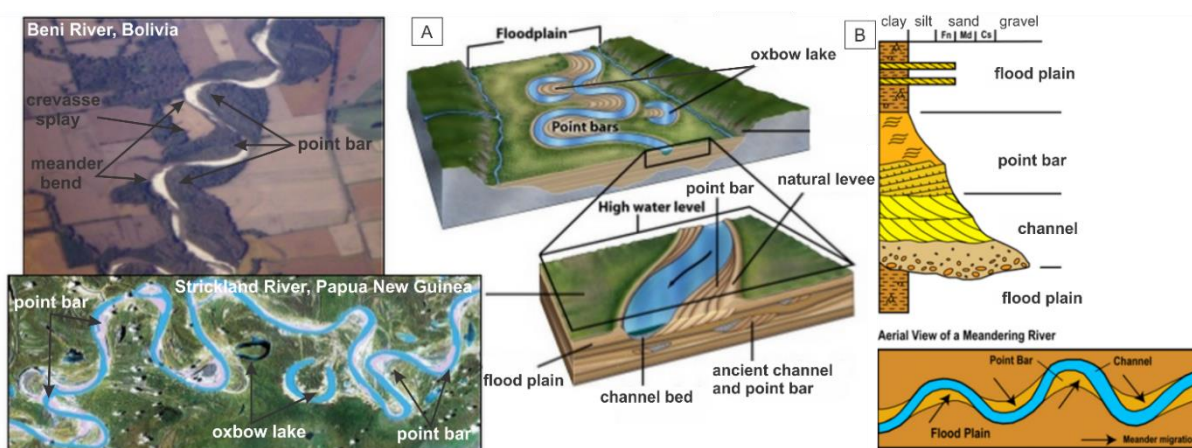

Figure 9. Examples of large, sand-bed meandering rivers, illustrating the location of meander bends, point bars, natural levees and oxbow lakes. A) The development pathway typical of bends undergoing meander development, where cut bank erodes on outer bend and point bar accretes on inner bend. B) Meandering river facies sequence and typical point bar model for meandering stream. Figure modified from (Bevis, 2013). Inset pictures on the left side show examples of large, sand-bed meandering rivers (Beni River in Bolivia and Strickland River in Papua New Guinea), illustrating the location of meander bends, point bars, crevasse splay and oxbow lakes.

Coarse sediments deposited attached to the channel base are mid-channel bars (Figure 10 A) (Collinson, 1996), are primary common for braiding stream deposits. In the simplest view, in terms of flow dynamics, a mid-channel bar is simply a double-sided point bar, yet the essential difference is that the mid-channel bar is constantly moving downstream (Leeder M. R., 2011). Braid bars separate the flow into distinct braid channels, they are elongate, oriented parallel or sub-parallel to the main flow (Dru Germanoski, et al., 1993). However, mid-channel bar dynamics are not as well understood as those of point bars. The dominant processes are double-sided later accretion by curved-crested dune migration leads to distinctive 3D architecture (Leeder M. R., 2011). Bars have sand or gravel composition due to exceeded river capacity

(abundant sediment supply) or highly variable discharge related to seasonal variations (Miall, 1992). Mid-channel bars, from which flow is spitted, often termed longitudinal bars, which are elongate bedforms, roughly parallel to current flow. Both mid-channel and longitudinal bars have a distinctive depositional process. It is represented by clasts lodgement on top of the bar showing downstream reduction in clasts size (Figure 10 B), where at downstream ends fine channel gravels contrast sharply with coarse clasts of the adjacent channel floor over which they are advancing (Collinson, 1996). The flow is generally strongest between the bars and erosion of the upstream side of the bar may occur (Collinson, 1996; Bridge, et al., 2008). Some bars originate from a change in accumulation of dunes, or, in other cases, low-relief dunes accrete and build a mid-channel "sandflat" (Collinson, 1996).
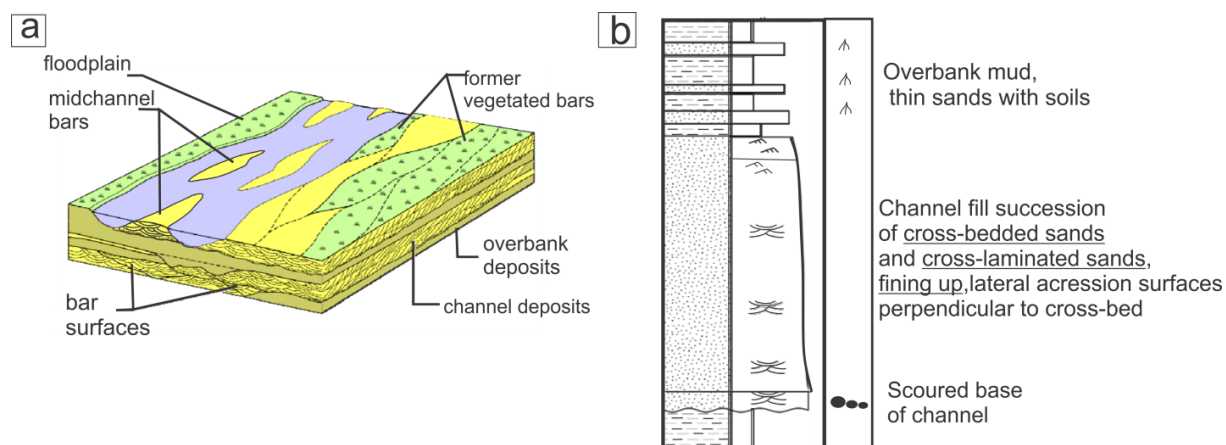

Figure 10. A) Mid-channel bar model for a braided stream, showing various types of fluvial sedimentary deposit of channel valley. B) A schematic braided river facies sequence diagram of the distribution of bedload grain size and sub-bar-scale bed forms in sandy and gravelly rivers at the bankfull flow stage. Modified from (Collinson, 1996).

Numerous researchers have described the systematic reduction of grain size resulting in fining-up succession along point bars in meandering and mid-channel bars in braided fluvial systems (Figure 9 B, Figure 10 B) (Phillip A. Labrecque, et al., 2011). On the lower parts of bars, high flow velocities sweep fine bedload up the surface, so that coarser particles lag behind. The succession ranges from coarse material at the base to fine material at the top (Collinson, 1996). In relatively low-energy streams, however, mud may be laid down on point bar upper surfaces, these mud layer due to its particles cohesion will not be eroded (Collinson, 1996). Phillip A. Labrecque (2011, p. 147) attributed this to: 1) weaker current flow at the top of the bar, around the

bend apex and subsequent selective deposition of fine material from suspension; and 2) abrasion, associated with erosion of larger clasts into smaller ones. Important processes relevant to bar migration include lateral and downstream accretion, as well as a component of vertical accretion. Accretion units that comprise the primary reservoir units are characterized by inclined heterolithic stratification (John S. Bridge & Ian A. Lunt, 2005). As channel migrates, the deposits from different parts of channel bars become vertically superimposed (e.g. bar head deposits overlying bar tail deposits, and bar tail deposits overlying confluence scour deposits). Relatively thick, fining-upward sequences form as bar-tail regions migrate downstream. Systematic spatial variations in the thickness of channel bar deposits, and the inclination (is mainly <10° but approaches the angle of repose (35°) in places) and orientation of large-scale strata, are due to bed topography and the mode of channel migration (John S. Bridge, et al., 2005). Furthermore, most of the internal structure of unit bars is cross-stratified, which is due to the bedforms (dunes, ripples, bedload sheets) migrating over them (John S. Bridge, et al., 2005). Bars are modified and reorganized due to changes between lower and higher water stages in channel system (Einsele, 1992). During high flow stages, the channels and bars are covered with dunes, although there may be restricted areas of upper-stage plane beds and ripples near bar tops (John S. Bridge, et al., 2005). Both the bedload and suspension transport rate and the grain size over sandy point bars and braid bars during the channel-forming flow stage increase with the depth-averaged flow velocity (Bridge, et al., 2008). All of these parameters are largest near the inner bank at the upstream end of a bar and near the outer bank at the downstream end (Bridge, et al., 2008). Bars are the basic depositional elements of the river, and can be subdivided into architectural elements, which are characterized by distinctive facies assemblage, internal geometry (2.6.2 Internal geometry) and external form (2.3.1 Small-scale bedforms) (Miall, 1992).

2.4 Types of fluvial systems and river classification

2.4.1 Alluvial fans and fan deltas

Alluvial fans are highly complex, steeply-sloping fluvial system found at the base of mountain range (Einsele, 1992). Fan, cone-shaped, lobate accumulations (lobe) (Figure 11) of alluvial fans have a focused source of sediment supply, usually an incised

canyon channel (Galloway, 1996), formed at the foot of highlands in response to high rate sediment supply (Leeder M. , 2011). Fans are depositional geomorphic features (Galloway, 1996), which show significant changes down fan from proximal debris flow deposits to mid-fan braided stream deposits to distal fan sheet flow deposits beyond the fan toe (Figure 11). The fan toe grades gently into a basin floor environment (Leeder M. , 2011), fan deltas are thus built into a lake or the sea (Einsele, 1992) showing characteristic progradational geometries, associated with coarsening up general stratigraphic style, and modification by current waves (Galloway, 1996).
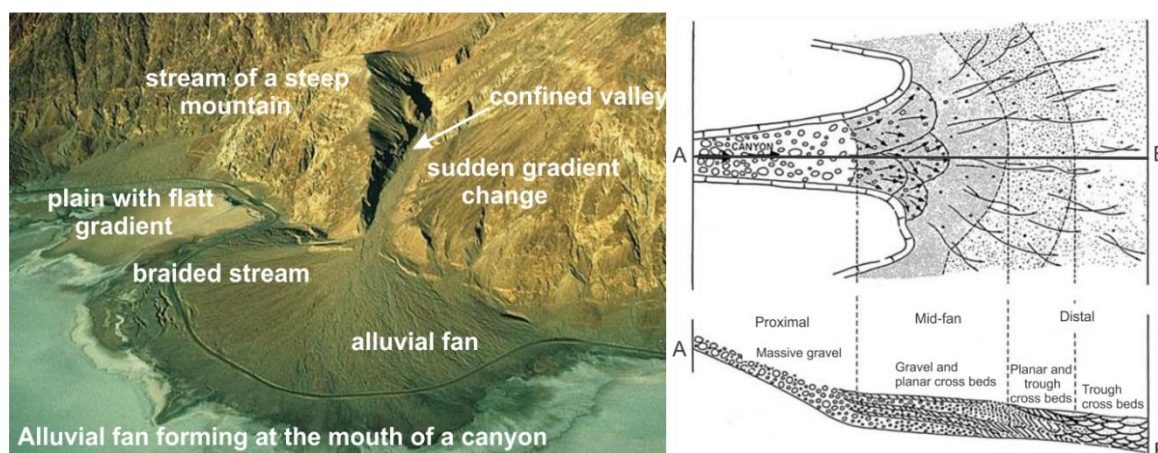

Figure 11. Inset picture on the left showing alluvial fan forming at the mouth of a canyon. Fugure modified from Google image search. Diagram on the right shows general depositional model for ancient alluvial fans developed based on Devonian examples of Norway. Figure modified from (Gloppen & Stell, 1980).

Sedimentation on alluvial fans starts where the streams lose some of the transport efficiency is comprised by stream deposits and sediment gravity flows (Einsele, 1992). As flow channels migrate laterally they generate a broad, low angle fan-shaped body of sediment (Leeder M. , 2011), which may be referred as a fluvial distributary system (Nichols, 2007). Major depositional episodes correspond to the periods when amount of deposition is controlled by local rainfalls amount and the availability of detritus (Leeder M. , 2011). According to Leeder M. (2011, p. 330) fans are subdivided into debris-flow-dominated alluvial fans, stream-flow-dominated alluvial fans. Debris-flow-dominated alluvial fans occur both in humid and semiarid climates and high mountain locations and are triggered by floods on steep surfaces of unconsolidated clay-rich sediment (Galloway, 1996), and comprise a main rockhead confined valley which may pass into a distributive network of fan channels and mid-fan lobes. Stream-flow-dominated alluvial fans receive perennial or seasonal stream

flow, where migration of channel streams dominate the sequences produced on such fans, they may show proximal-distal change from coarse alluvial deposited in rapidly shifting braided channels to finer sediment of meandering channel and overbank flood deposits.

2.4.2 Bedload (Braided) river channels

A large proportion of European, Russian and North American aquifers were formed by former braided river systems (P. Huggenberger & C. Regli, 2009). Braided rivers and their deposits are important components of the Earth's surface, since ancient braided rivers might be indicators of past Earth surface environments, and may also contain significant reserves of water and hydrocarbons (John S. Bridge, et al., 2005). Knowledge of the nature of channel and bedform migration is also essential for interpreting the origin of river deposits.

Braided river channel (Figure 12 A) was identified by (Wooster, 2002) as "one which flows in two or more anastomosing channels around alluvial islands", and "a braiding stream is characterized by having a number of alluvial channels with bars or islands between meeting and dividing again, and presenting from the air the intertwining effect of a braid." Braiding is typically referred to as repeatedly dividing and joining channels, splitting around numerous bars, which represent temporary sediment storage (Miall, 1992). Braided rivers are also distinctive because of their high stream power (product of water gravity, high values of valley slope, and discharge) and subsequent high rates of erosion and therefore high bedload transport rates, and deposition compared to other river types (Wooster, 2002). The principal morphological components of the braided rivers are braid channels, submerges migrating bedforms and mid-channels bars (Dru Germanoski, et. al., 1993). Braided stream systems with channels of low sinuosity tend to form in environments of large sediment supply and steep gradients with high width/depth ratios (Einsele, 1992). Bedload (braided) channel fills are mostly coarse-grained and contain little suspended-load material (Collinson, 1996).
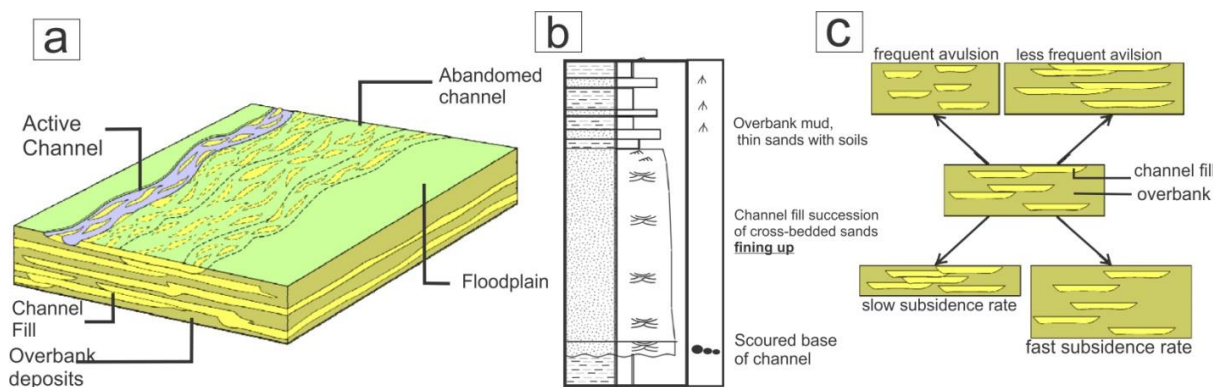
Figure 12 A) Depositional architecture of braided river, showing later migration if active channel and abandonment bars, B) Vertical sequence showing schematic graphic sedimentary log of braided river deposits, C) Architecture of fluvial deposits. Modified form (Collinson, 1996).

The complexity of depositional and erosional processes in braided river systems leads primary to highly heterogeneous distributions of hydrogeological parameters such as hydraulic conductivity and porosity, whereas hydraulic conductivity variations are of primary importance in hydrocarbon migration (P. Huggenberger, et al., 2009).

2.4.3 Meandering (mixed load and suspended load) river

The term 'meandering' applies only to actively migrating high-sinuosity channelst set within alluvial floodplains (Grenfell, 2012). Meandering river (Figure 13 A) characteristically occurs on alluvial plains, on valley floors and between terraces (Collinson, 1996) at relatively lower slopes and carrying predominantly fine grained sediments, (Miall, 1992; Collinson, 1996). Meandering rivers are generally single-thread, as it follows a sinuous path as it moves from one side to another along the length of the channel. Theoretical understanding of the meanders formation follows from unstable straight channel configuration (W. M. van Dijk, et al., 2012), including planimetrically unstable configuration or bend instability and altimetrically or bar instability. Consequently, initially straight channel alignment grows to form meandering pattern. The closest bank to the thalweg has relatively fast flowing water against it. It results in erosion of this bank and meander development accompanied by deposition on the opposite bank of the channel where the flow is sluggish and the bedload can no longer be carried (Bridge, et al., 2008). Due to continued erosion of the outer bank and deposition of bedload on the inner bank the channel develops a bend and meander loops (Figure 13 A). Maximum velocities and depth occur close to the outer bank so that the channel has an asymmetric cross-section (Collinson, 1996).
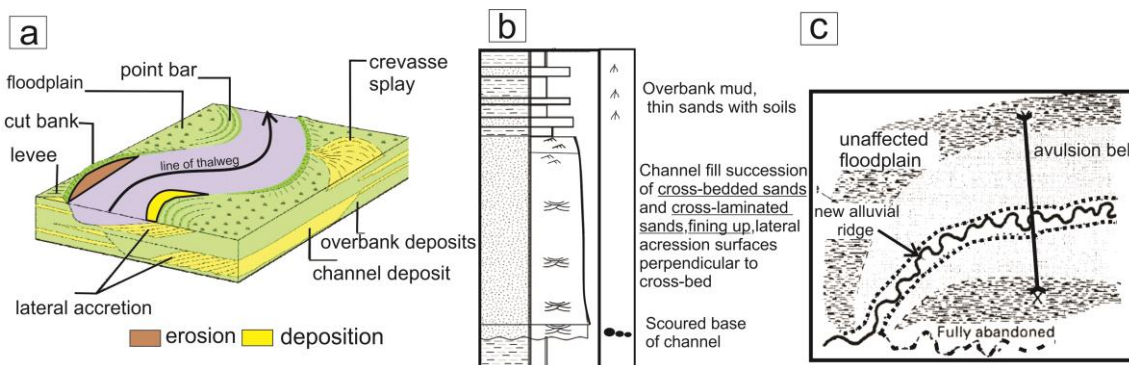
Figure 13 A) Main morphological features of meandering river, B) Vertical sequence showing schematic graphic sedimentary log of meandering river deposits, C) Channel, initiating the growth of a new alluvial ridge. Modified form (Collinson, 1996).

The wave length and the width of the meanders grow with increasing river discharge and slope of the river valley or fluvial plain (Einsele, 1992). The physical processes operating within channels particularly associated with turbidity current flow (Pickering, et al., 1996). Meandering river deposits consist of fine-grained sediment as sand (Einsele, 1992; Collinson, 1996) and minor proportions of silts, muds and (locally) backswamp carbonaceous muds and clays (Einsele, 1992).
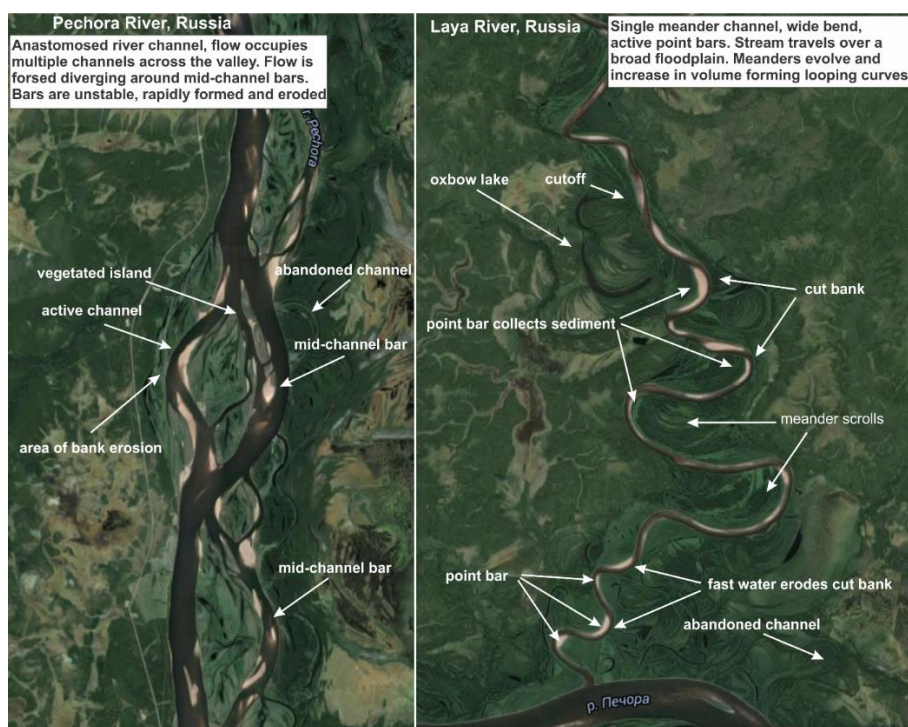

Figure 14 Comparison of Pechora River in Russia large anastomosed river (picture on the left), illustrating the location of mid-channel bars, areas of bank erosion, vegetated island, abandoned channel and Laya River in Russia (picture on the right) large, sand-bed meandering rivers, illustrating the location of meander bends, point bars, cut bank and oxbow lakes. Modified from Google maps.

2.4.4 Anastomosed rivers

Anastomosing rivers have distinctive fluvial style and are an important category of laterally stable in their position highly sinuous interconnected channels with multiple coexisting channel belts on alluvial plains that enclose floodbasins (Makaske, 2000; Miall, 1992). Makaske (2000, s. 149) showed, that anastomosing channel patterns may consist of straight, meandering or braided channel which can all be parts of anastomosed river, including bars, abandoned channel segments, crevasse splays and levees (Figure 15 A, B, C). Anastomosing rivers are usually formed by avulsions, i.e., flow diversions that cause the formation of new channels on the floodplain (Einsele, 1992). Anastomosed rivers have highly variable sinuosity ranging from 1.51 to 1.75, due to that fact it can be concluded that the rate of sinuosity is not suitable factor for distinguishing anastomosed rivers.
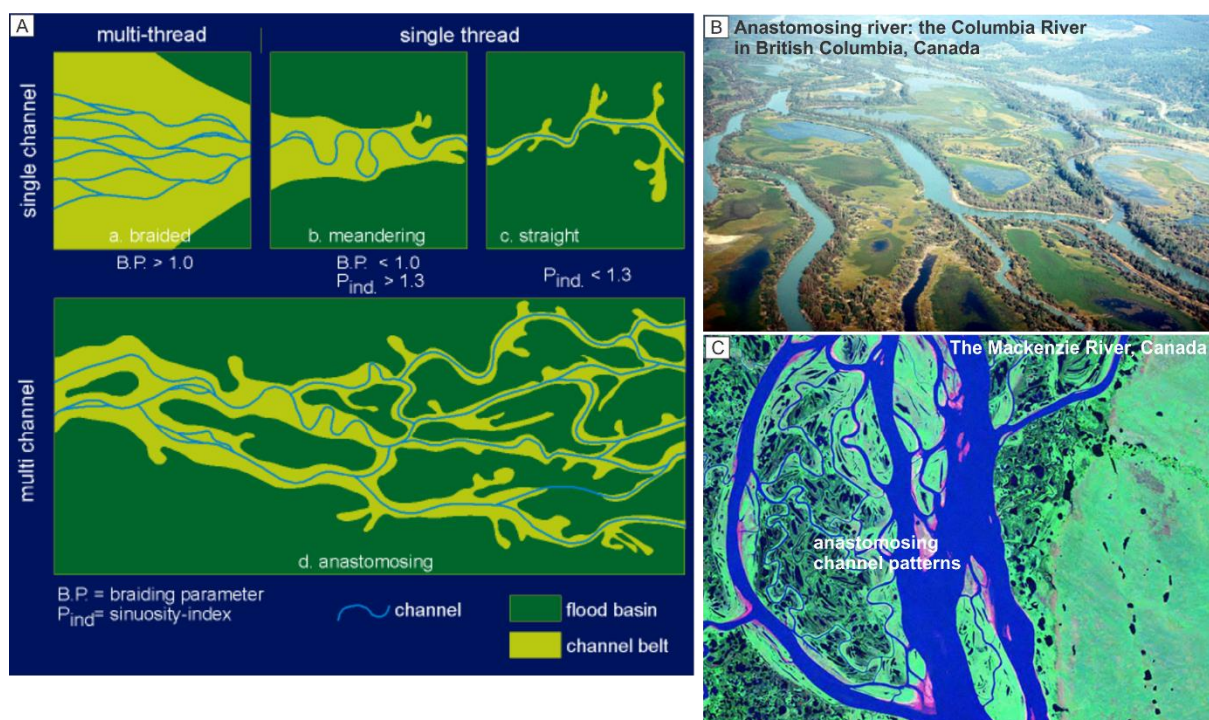

Figure 15 A) Proposed classification of alluvial river types based on channel pattern and floodplain geomorphology. Anastomosing rivers (below) are classified as a composite form of which the individual channel belts may have braided, meandering or straight channels (above). Modified from (Makaske, 2000). Inset pictures B and C on the right show Columbia River in Canada (note wet flood basins on the islands, which are enclosed by largely tree-covered, natural levees) and the Mackenzie River are on large scale characterized by anastomosing patterns. Figure modified from Google image search.

Channels (Figure 15 B, C, Figure 14, left figure) are classified as anastomosing due to its composite form of which the individual channel bels are braided, meandering and straight, and because they have relatively large islands, with various shapes and

sizes. Modern anastomosing rivers have been reported from various climatic zones (examples from western Canada, British Colombia and Russia) contrasts with braided and meandering river patterns described above (Figure 14, right figure).

2.4.5 River classification

The (Rosgen, 2007) river classification system emphasized hydraulic parameters to define river systems (Figure 16). It is based on the parameters such as width to depth (aspect) ratios, sinuosity and channel gradient (Sylvia Nordfjord, et al., 2005). Measured hydraulic variabilities of the discussed below channel systems can be directly compared with the morphological features of the proposed (Rosgen, 2007) classification.

Stream Types	Aa+	A	B	C	D	DA	E	F	G
SIN.	< 1.2		> 1.2	> 1.4	< 1.1	1.1-1.6	> 1.5	> 1.4	> 1.2
W/D	< 12		> 12	> 12	> 40	< 40	< 12	> 12	< 12
SLOPE (degrees)	.04-.099		.02-.039	< .02	< .02	< .005	< .02	< .02	.02-.039
	Straight		Low sinuosity	Meandering	Braided	Anasto-mosed	Stable Meandering	Entrenched Meandering	Gullies

Figure 16 Classification of rivers, after (Rosgen, 2007), based on the morphological characteristics of river channels. The number of active channels, width to depth (aspect) ratio, cross-section patterns, sinuosity, channel slope gradient and nature of bed material are the characteristics used to classify a river segment. The (Rosgen, 2007) system classifies only river reaches (a straight portion of the river) and not entire river systems.

There are number of different methods used in order to analyze stream paramers and label them in descriptive manner. Method of river classification after (Rosgen, 2007) is currently the most used classification system.

Table 1 Classification of rivers sinuosity, after (Rosgen, 2007), based on the morphological characteristics of river channels.

	Single-Thread Channels			
	Low	Moderate	High	Very high
Sinuosity	<1.2	>1.2	<1.5	>1.5

2.5 Overbank environments

2.5.1 Floodplains and Channel-levee system (CLS)

Adjacent to river channels are areas of periodically flooded wetlands, that stretches from the banks of its channel to the base of the enclosing valley-called floodplain (Wikipedia, 2015). Floodplains are sites of sediment accumulation within river basin (Chris Perry, et al., 2007) and whose organic richness is due to the fact that they are exposed to flooding events, when nutrients, habitats and soils are preserved (Leeder M. R., 2011). The water outside the channel will normally be very shallow and have low flow velocity and fine grained sediments, which have been transported in a suspension and then deposited as overbank sediments, which may built up into elevated bank called levee (Bjorlykke, 2010). Alteration of channel and levee sediments in stratigraphic section emphasizes that the process of alluvial architecture depended on dynamic interaction in time and space between channel and floodplain. In the period of flood, most sand is dumped on the levees- areas adjacent to the channel (Figure 17 A) where it is deposited unless the deceleration of floodwater leads to fine sediments deposition (Leeder M. R., 2011). Thus, channel-levee deposits are divided by into two "end-member" facies: sand rich, with high flow velocity and high deposition rate, showing parallel lamination, ripple cross-lamination and climbing ripple cross-lamination are channel-proximal, and mud rich, with abundant starved ripples, indicating limited volume of sand-size sediments are channel-distal (Figure 17 B) (Ian

A. Kanea, et al., 2007). Levee deposits are the largest and most extensive sand-prone architectural element of channel belt (M. Janocko & W. Nemec, 2012).

Both sandstone thickness and sandstone proportion are decaying from channel-proximal to channel-distal localities (Figure 17 B). As the levee accretes vertically the levee crest migrates in a channel-distal direction, this process requires increase in flow magnitude combined with channel floor aggradation (Jair Weschenfelder, et al., 2010). Channel-levee geometries forms as a result of relatively continuous migration of a single channel form (Zoltán Sylvester, et al., 2010). Deposition on floodplains depends on flood characteristics such as frequency, duration and suspended sediment concentrations. Major floods may cover the areas beyond the levees, and clay and silt will be deposited on these floodplains (Bjorlykke, 2010), as the deceleration of floodwater leads to a gradual deposition of finer sediment from channel margin (Leeder M. R., 2011). Sediments, deposited on channel-levee system, have a special interest since they are sites of soils, habitats and organic remains preservation. These depositions, if not remobilized through physical erosion, can also become sources as a result of post-depositional processes (Chris Perry, et al., 2007). The channel-levee sediments are highly variable, depending on climate, they characteristics change, thus in humid-tropical regions coal may be found if the overbank has developed as a raised swamp (Miall, 1992).
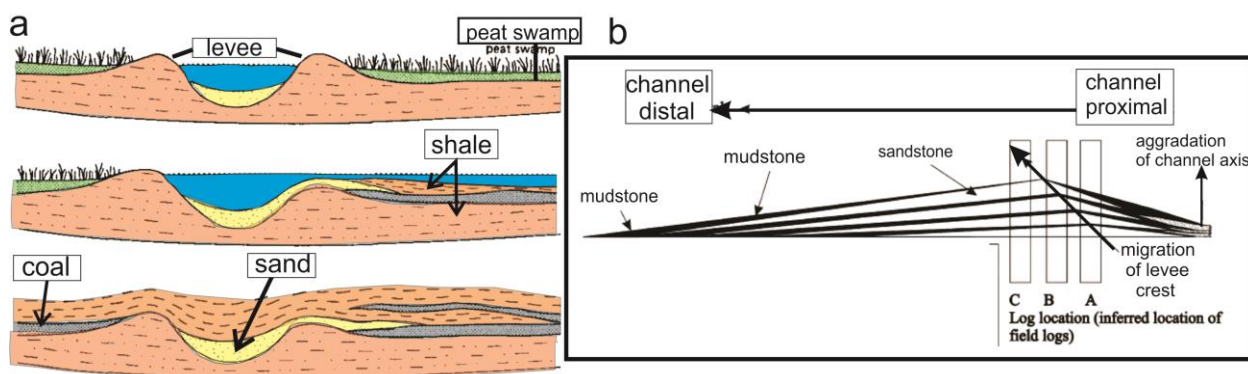

Figure 17 A) Schematic diagram showing how periodic flooding produced splits from overbank or crevasse-splay deposits (Lawrence M. Gochioco, 1990), B) schematic levee growth showing thinning sandstone from log A to B, and thickening upward trend for log C. Figure modified from (Ian A. Kanea, et al., 2007).

2.5.1 Crevasse-splay

Water flow and sediment transport on floodplains is complicated by variable floodplain width and surface topography (such as crevasse splays, depressions, and

channels). Another form of overbank deposits is the crevasse splay (Figure 18 A). Crevasse channels and splays commonly cut through discontinuous levees (levee breach) during rising-flow stage and into the overbank environments, indicating that current has spilled out of the channel (Bridge, et al., 2008). Near channel levees and crevasse splays pass into more distal floodplians (Collinson, 1996). The geometry of crevasse splay deposits is different from that of levee deposits. In fact, crevasse channels can have their own levees and mouth bars. Channel-bar and channel-fill deposits are common in crevasse splays (Bridge, et al., 2008), that is why it might be difficult to distinguish from the main channel deposits. Crevasse splay channels are expected to be smaller than those in main channels and are characterized by a short channel leading away from the main channel (Henry W. Posamentier, et al., 2006), however some crevasse channels may be similar in size to main channels (especially immediately prior to an avulsion) (Bridge, et al., 2008). Within crevasse splays, groups of flood-generated stratasets may occur in distinctive vertical sequences (Figure 18 B), which are on average up to meters thick, and hundreds of meters in lateral extent (Henry W. Posamentier, et al., 2006). A typical crevasse splay deposits tend to be coarse grained and thicker than levee deposits (Bridge, et al., 2008), and contain abundant plant roots and transported plant material. Spatial decrease in sediment transport rate is mainly responsible for the deposition. The stratigraphic architecture of crevassed splay deposits is characterized by amalgamated turbidities near the apex of the splay, becoming less amalgamated with distance away the splay apex (Henry W. Posamentier, et al., 2006). The prevailing internal structures may resemble sandy turbidities, showing some grading, horizontal lamination and ripple cross-bedding (Einsele, 1992). The most distinctive sedimentary structure associated with crevasse-splay deposits is climbing current ripples, which results in rapid sedimentation from suspension once flow cuts through the levees crevasse (Bridge, et al., 2008). Avulsion is associated with crevasse splay and may be initiated by extensive enlargement of channels on crevasse splay or by intersection of the main channel.
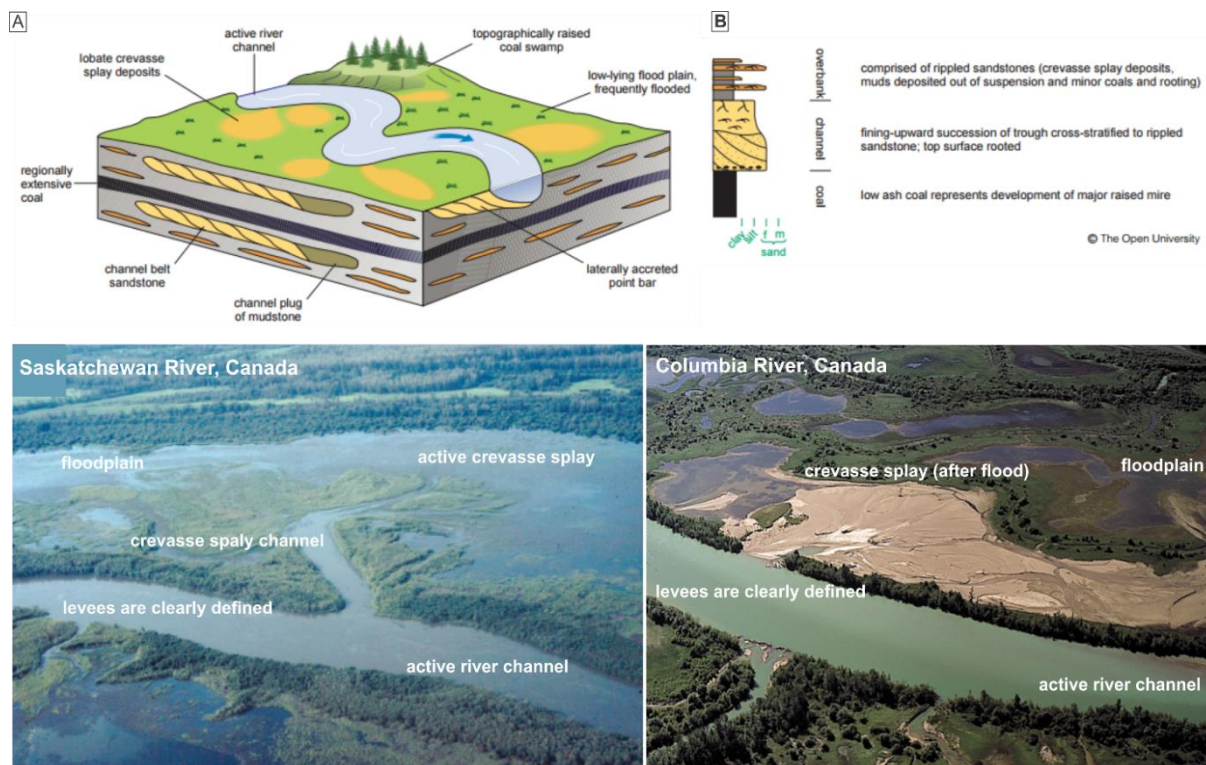
Figure 18 Geometry of floodplains. A) Schematic representation of single meandering channel, showing crevasse -splay deposits and other various types of fluvial sedimentary deposits. B) Vertical sequence showing schematic graphic sedimentary log of meandering river deposits. Crevasse splay deposits comprised by alternating thin beds of mudstone and fine-grained sandstones to siltstone with ripples on top, and plant fragments (Einsele, 1992). Inset picture (right), showing active river channel, levees and active crevasse splay from Saskatchewan River, Canada, (left) showing crevasse splay developed after flood from Columbia River in Canada (note floodbasin is bordered by older channel belt (background). Pictures modified from Google image search.

If the discharge-slope product and sediment transport rate of an overbank flow can exceed that of the channel flow, sediment transport rate increases from the channel to floodplain, end erosion and enlargement of crevasse channel is possible (Henry W. Posamentier, et al., 2006). Modern examples of crevasse splays have been reported from various climatic zones (examples from western Canada and British Colombia) (Figure 18).

2.5.3 Chute cutoffs

Meander bend development and sinuosity growth are sometimes limited by the occurrence if non-linear processes such as chute cutoffs and channel adjustment following the cutoff (W. M. van Dijk, et al., 2012). Point bars are sometimes cut off by chutes, which commonly are most active at high discharge (Collinson, 1996). Single bend cutoffs occur as a meander bend migrate laterally. Bank erosion and lateral movement of the bend produces a higher amplitude bend (W. M. van Dijk et al., 2012).

The formation of chute channel at meander bend requires some mechanism to force the flow over developing point bar. As overbank flow becomes more significant, channel geometry changes, which causes flow diversion at the outer bank (W. M. van Dijk, et al., 2012). The flow diversion into chute maybe further reduce entire flow capacity (Grenfell, 2012). Early studies of large meandering rivers identified a prevalence of meander bends cut off by chute formation had resulted in relatively stable 'chute cutoff islands' (Strickland River, Papua New Guinea, Beni River, and Paraguay River) (Figure 19, figures on the left) (Grenfell, 2012).

Various processes can lead to a chute cutoff (W. M. van Dijk, et al., 2012). The probability of chute cut-off increases as sinuosity increases (Bridge & Demicco, 2008). However, the entire process of chute formation remains poorly understood. It has been suggested, that the formation of chute cutoff would be favored at bends with particular characteristics, such as high meander bend sinuosity, lower values of curvature and bend geometry (Grenfell, 2012). Single bend cutoffs occur as the meander bend growth proceeds due to downstream migration, lateral expansion and bank erosion produces a higher amplitude bend (Figure 19 A) (W. M. van Dijk, et al., 2012). Overbank flow occurs in response to in-channel sedimentation and channel geometry change. Downstream sedimentation transport decreases as sinuosity increases and lowers stream gradient. The decrease in stream gradient causes a decrease a decrease in flow velocity, so that water level rises, starting overbank flow at the outer bank (Figure 19 B) (W. M. van Dijk, et al., 2012). Diverted flow leads to further sediment transport reduction and overbank flow become more focused as it rapidly incises a chute channel in the outer bank (Figure 19 C) (W. M. van Dijk, et al., 2012).

As flow wanes, chute is cut off from main significant flow during low discharge and becomes oxbow lake or abandoned meander (Collinson, 1996). Once the channel has been abandoned, the channel is progressively filled. The infill typical for chute channels is sandy and gravel framework, migrating sand bedforms and suspended load fines (Collinson, 1996). Dunes with curved crestlines are the most common bed forms on chutes floor, sandy unit bars, point bars, and braid bars during the high-flow stage occur locally in shallow areas of high flow velocity (Bridge & Demicco, 2008).
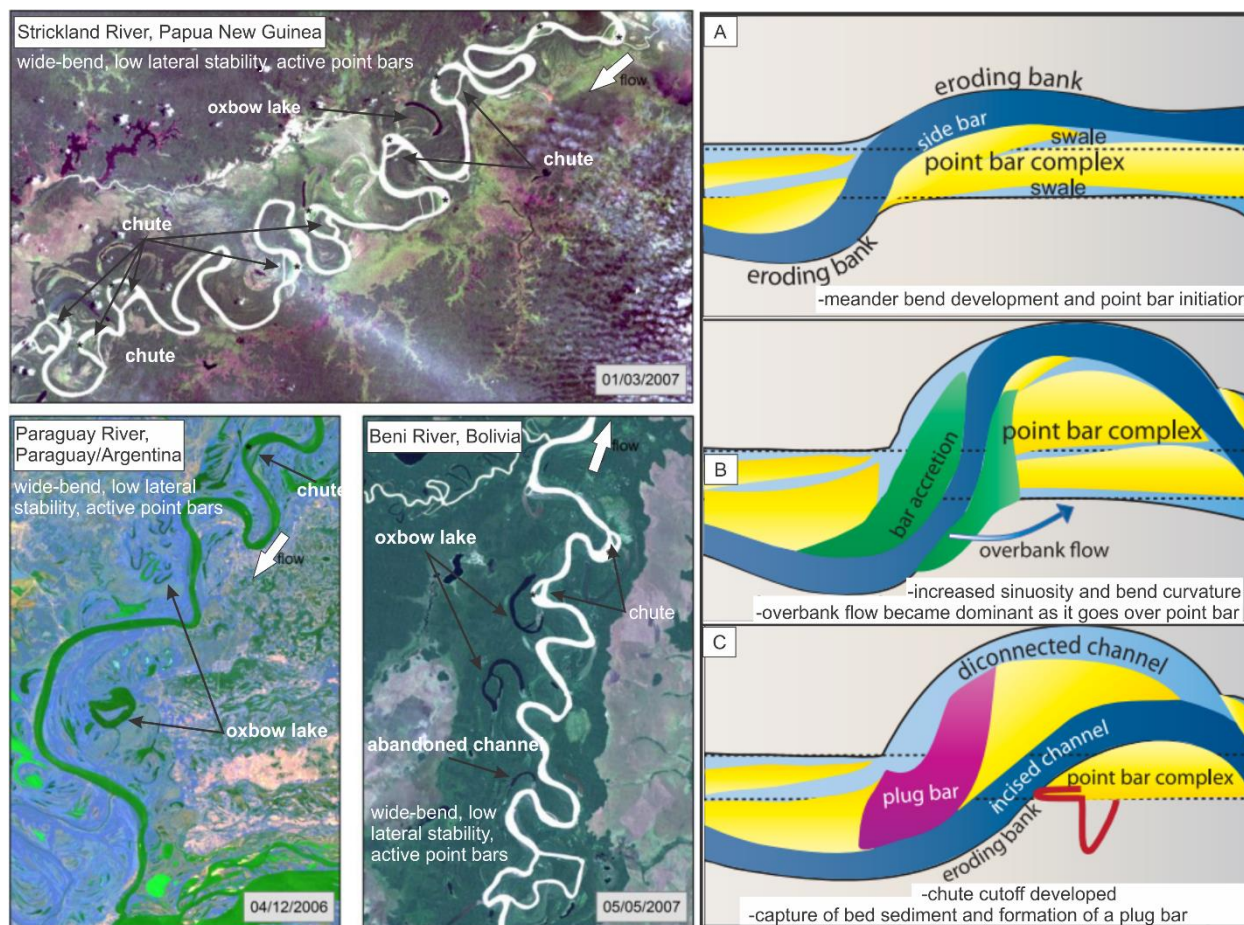
Figure 19 Cute cutoff, formed by scroll-slough development, are common in sand-bed river channels. Figures on the right illustrates examples of large, sand-bed meandering rivers (Strickland River, Paraguay Riverand Beni River) with wide-bend, active point bars and stable chute channels, illustrating the location of stable chute channels and oxbow lakes. Modified from (Grenfell, 2012). Figures on the left illustrate morphology of a bifurcate meander bend. (A-C) The development pathway typical of bends undergoing meander chute cutoff, illustrating the formation of stable chute channel, where A) conceptual model for chute development in meandering river with meander bend development, B) Model shows how overbank flow goes over point bar and eventually becomes dominant , C) Model shows incising upstream propagated chute channel. Bed sediment are captured in a form of plug channel bar, which eventually disconnects the meander from the channel. Modified from (W. M. van Dijk, et al., 2012).

Ripples are normally restricted to areas of slow-moving water near banks. In planform terms, chute channels indicate a transition from single-thread meandering to braiding channel. Antidunes and transverse ribs occur only rarely in fast, shallow water (Bridge & Demicco, 2008). Fluvial channel deposits of gravel and sand sediments which are transported as a bedload under current certain velocity form either gravelly sand or clast-supported gravel bed when most of sands has been sorted out, or lag deposits when the velocity is slower (Einsele, 1992), or river beds dominated by sand (gravel lag) (Collinson, 1996).

2.6 Fluvial architecture

2.6.1 Types of channel architecture

Another classification of channels is applicable to channels, where they are divided into three types according to their architectural styles i.e., erosional, depositional and mixed, depending upon channel sedimentation with respect to intrabasin tectonic and sea level controls (Figure 20) (D.V. Ramana, et. al, 2006; Pickering, et al., 1996). Erosional processes dominate updip parts of the profile, and as the slope straitens in a downstream direction, depositional processes take place (Figure 20) (Faruk O. Alpak, et al., 2013). Thus, erosional channels are associated with low sinuosity, steep slopes, turbidity currents having high concentrations of coarser sediments and show sights of erosional architectural elements (e.g., scours, cut-downs, and the deposition of residual facies) (Pickering, et al., 1996). The aggradational or depositional channels (Figure 20) are associated with high sinuosity in lower slopes and fine-grained sediments suspended in turbidity currents (e.g., the Amazon, Mississippi, and Indus channels) (Pickering, et al., 1996). These channels commonly have well-developed levees made up of relatively fine-grained material spilled over from the channel part. The aggradational channels grow with deposition along channel axis concurrently depositing finer sediments in the levees. In this process vertical aggradations of channel levee complex takes place (see chapter) (D.V. Ramana, et. al., 2006; Pickering, et al., 1996).
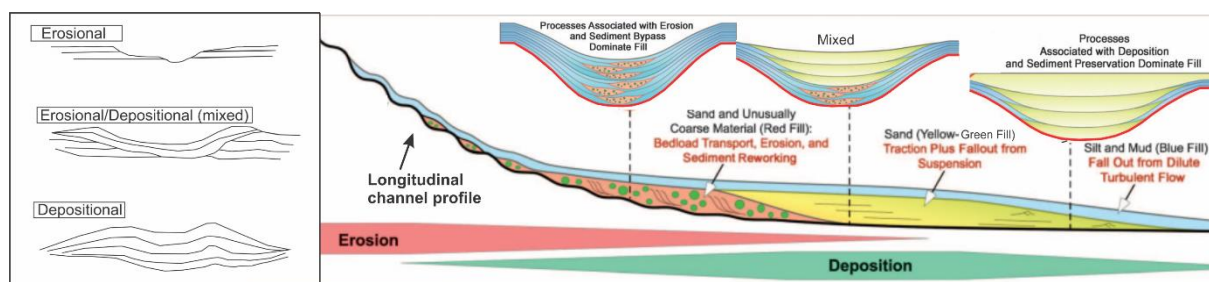

Figure 20 Schematic diagram illustrating types of channel architecture expected along a longitudinal channel profile. The inset Sketch in the right corner showing three channel types: erosional, mixed and depositional. Figure modified from (D.V. Ramana, et al., 2006).

In the mixed type (Figure 20), erosion and aggradations go on hand–in-hand. On many occasions the well-developed depositional channel-levee systems are partly eroded by younger erosional channels due to sea level changes or sudden huge

discharge by feeding rivers, leading to major channel flow lateral migration or avulsion, which is wholesale shift in channel position (D.V. Ramana, et al., 2006).

2.6.2 Internal geometry

The geometry of channel system may show the diversity of strataset of various scales, which is related to the geometry and migration of the associated bedforms (Bridge, et al., 2008). The smallest scale channel-form element is referred to as channel storeys, composed of relatively conformable stacked set of bedsets bounded by erosional surface base (Dru Germanoski, et al., 1993). Bedset of each individual channel may be represented by distinctive external geometry of sets such as small- to large-scale complex to simple ribbons (Gonzalo D. Veiga, et al., 2007). The multiscale stratigraphic architecture of channel systems is schematically illustrated in Figure 21 and Figure 22 C. Multi-storey channel belts, stacked vertically upon each other with or without significant offset, are typically refered to as channel-belt complexes (M. Janocko, et al., 2012). The length and thickness of stratasets can be related to the length and height of formative bedforms (John S. Bridge, et al., 2005). Migration of unit bars forms simple sets of large-scale inclined strata, whereas dune migration forms medium-scale sets of cross strata and small-scale cross strata from ripple migration (John S. Bridge, et al., 2005). The geometry and orientation of large-scale inclined strata reflect mainly lateral and downstream migration of the bars and dunes.

A channel story is a stratigraphic product, which at a smaller scale consist of ribbon structure, also known as lenticular storeys (Figure 21), which in its turn is associated with passage of dunes, ripples, and bed-load sheets (Bridge & Demicco, 2008). Lenticular storeys geometry of ribbons with fining upward succession, composed of trough cross-bedded sets (David Macdonald, et al., 2007). Rapid vertical aggradation and as a result climbing ripples can occur in soft sediments on top, if only sediment input into the system is high enough (Einsele, 1992). Channel unit may show the lenticular bodies fill including inclined surfaces (Figure 21) roughly perpendicular to the main channel orientation or trough cross-bedded sets and dipping toward the flow direction. Lenticular bodies also may grade upwards toward fine-grained deposits in the set to small-scale cross lamination (Gonzalo D. Veiga, et al., 2007). Channel

story fills display distinctive bed stacking pattern that range from vertically aggrading to lateraly accreting (Dru Germanoski , et al., 1993).

Migration of river channel and bars control the geometry an orientation of large-scale inclined strata (Bridge, et al., 2008). The presence of inclined surface structures, represented by ribbons within channel deposits, with almost perpendicular orientation, with respect to the main channel orientation, suggests the accretion structures of relatively highly sinuous channels (Gonzalo D. Veiga, et al., 2007). The presence of inclined surfaces represented by isolated ribbons within floodplain deposits suggests a single-channel pattern, which if combined with the lateral accretion structures, may suggest the development of meandering channels (Gonzalo D. Veiga, et al., 2007).

Coarse particles have a tendency to increase roundness downstream, and form characteristic fabrics with their long axes perpendicular to the flow direction (Einsele, 1992). Both these criteria together with cross-bedded sets inclination indicate the paleocurrent direction, which was responsible for the formation (Gonzalo D. Veiga, et al., 2007; Einsele, 1992). The upper section of individual channel is usually eroded, although lenticular mudstones can be found at the tops of these complexes (Gonzalo D. Veiga, et al., 2007). The external structure of small-scale channels can be simple, and filled with cross-bedded and cross-laminated sandstones.
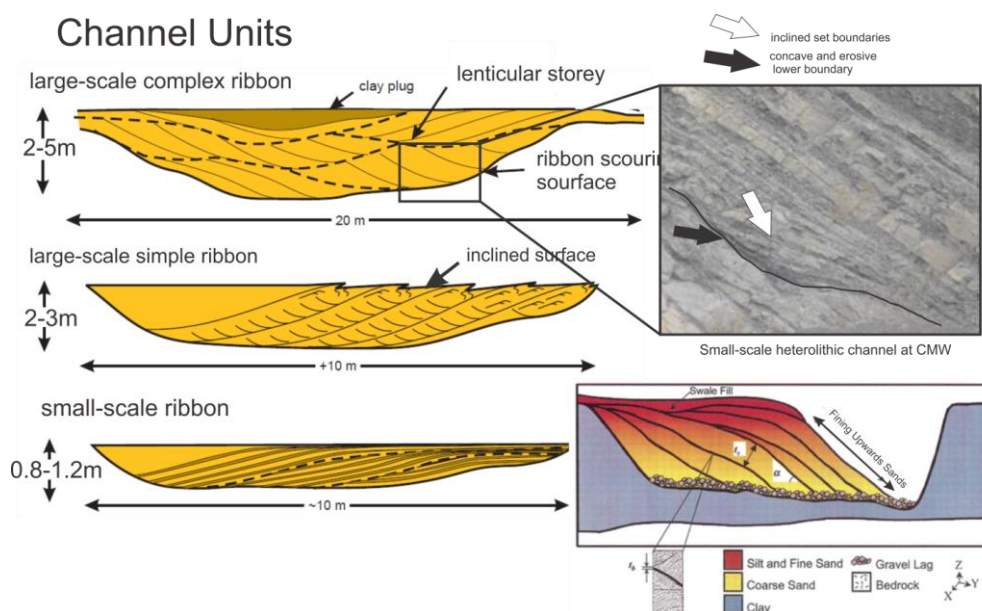

Figure 21 Inclined sedimentary units identified for the Avile Member. Figure modified from (Gonzalo D. Veiga, et al., 2007).

2.6.3 Lateral accretion and Avulsion

Downstream fining is a significant geomorphological characteristic of the channel deposits (Phillip A. Labrecque, et al., 2011). The channel fill succession is built up by lateral accretion of the active channel part or bedforms, which together create lateral facies successions (Robert W. Dalrymple, 2010). Accretion might be vertical (Figure 23 B, C) and lateral (Figure 22 A, B, C), whereas both lateral and vertical accretion of channels means that sediment are accumulating at the side of a channel or bank. The growth of lateral accretion deposits or sidebars is toward the channel axis, whereas cross bedding dips parallel to channel axis (Edie, 2005). Altogether, a river channel style is likely to be characterized by layer of very distinctive, gradual, diverse channel accretionary deposits with general progradational aspect (Leeder M. R., 2011). Vegetated accretionary deposits would certainly retard channel migration, leading instead to the stabilisation of multiple small channels that shifted by avulsion (University of Cambridge, 2008).
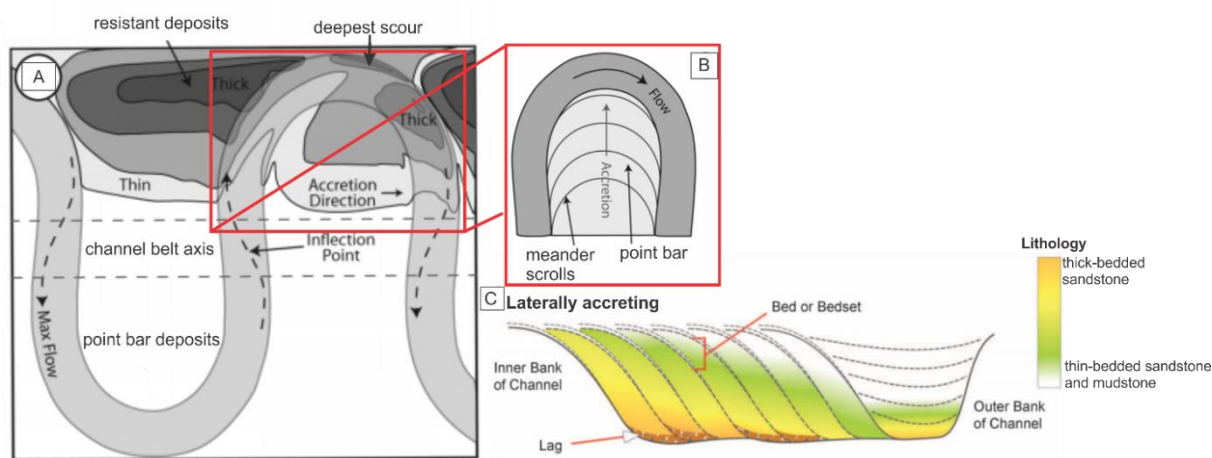

Figure 22 Lateral accretion of point-bar. A) Point bars migrate laterally and in the downstream direction. B) Meander scrolls on laterally accreting point bars, formed by lateral migration of the meander bend (Phillip A. Labrecque, et al., 2011). C) Schematic diagram illustrating stratigraphic architecture of the laterally accreting channel system, which consists of dipping channel-form elements. Modified from (Faruk O. Alpak, et al., 2013).

Prolonged occupation of an area by river leads to the production of a channel or avulsion belt (Figure 13 C) (Leeder M. R., 2011), occupied by active and abandoned channels. Overbank sedimentation is most rapid close to an active channel, leading to the growth of an alluvial ridge above the surrounding floodplain (Figure 13 C) (Collinson, 1996). The process when channel completely changes position on the floodplain and gets infilled is known as avulsion (Leeder M. R., 2011). Accumulation

and possible preservation of river channel deposits can only occur if the river avulses (Bridge & Demicco, 2008). These abandonments are accompanied by the exposure of the higher areas of the pre-existing braidplain surface to subaerial processes, including soil development and vegetational colonization (University of Cambridge, 2008). Where channel displacement is large and rapid, channel system may be more prone to avulsion, moving laterally toward the topographic low or hanging-wall syncline, associated with faulting or subsidence. The resultant sand-body geometry may be one of elongate ribbons of sand, laterally segregated by finer grained sediments. From a reservoir perspective, vertical connectivity would be relatively poor, whereas lateral connectivity would be relatively poor as well. (Ian A. Kanea, et al., 2007). Where, on the other hand, channel displacement is small, the channel may gradually laterally migrate to produce a composite sand body with a sheet-like geometry, which may be laterally limited but vertically connected, depending on the available accommodation space and bypass rates, claiming for good reservoir quality prediction (Ian A. Kanea, et al., 2007).

2.6.4 Stacking architecture

The stacking or aggradational architecture of channel sand bodies reveals channel growth patterns, forming from the interaction between lateral and vertical migration processes during the growth of the channel system. Aggradation is the process of building up a surface by sediment deposition and it is likely to be related to sinuosity, rate of sediment accumulation, sand/mud ratio of sediment supplied (net/gross ratio), and the degree of channel confinement (Pickering & Clark , 1996). Stacking architecture can be observed from both outcrops and seismic section (Figure 23 C). The lateral stacking patterns indicate a frequently lateral channel migration, while the vertical stacking patterns show a stable channel (Hongtao Zhu, et al., 2014).

In terms of reservoir prediction, sand body geometry and the effect of channel growth pattern have a strong control on the interconnectivity of individual channel-fill elements and the width (Pickering & Clark , 1996) and palaeochannels are acting as effective longitudinal drains for the fluids to migrate (A. Gay, et al., 2005).
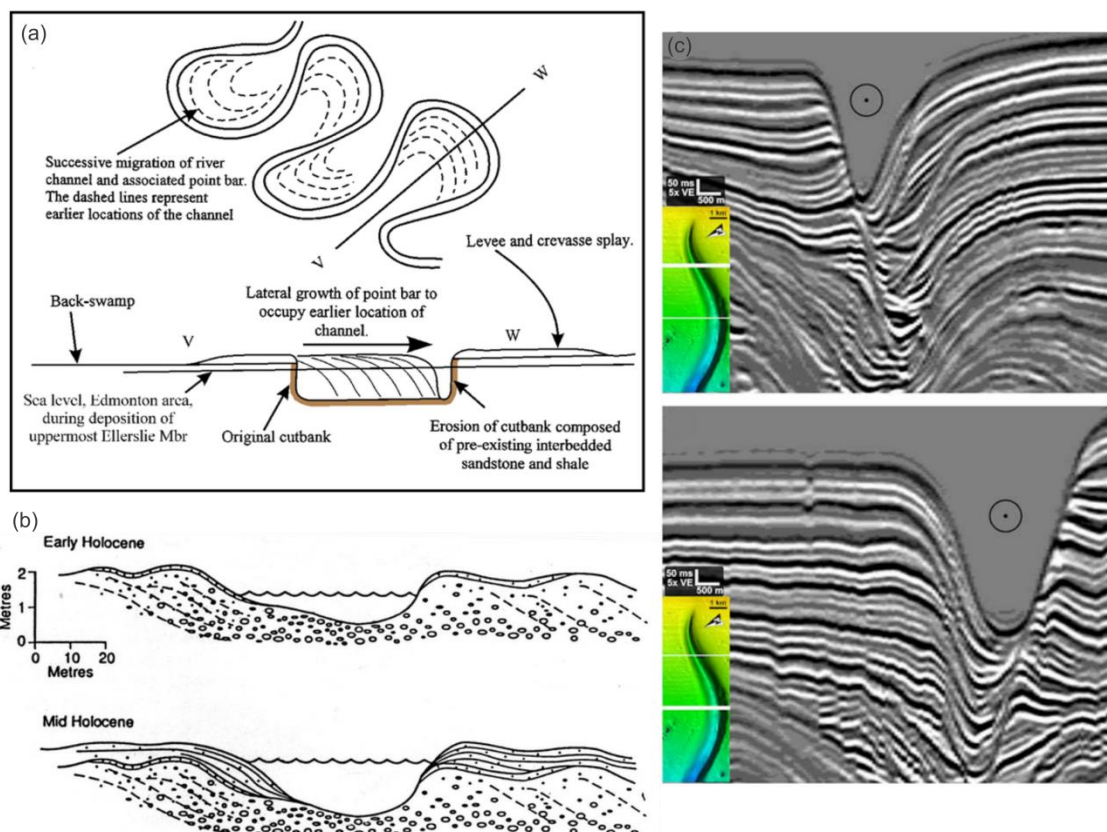
Figure 23 Stacking architecture through lateral and lateral accretion. A) Diagram showing lateral accretion models (Edie, 2005). B) Diagram showing model of floodplain and channel evolution through vertical accretion in narrow valley, (C) shows modern seafloor, where submarine channel displays lateral accretion associated with its meandering. The aggradational trajectory is slightly migration in the direction of lateral accretion-right to left in (C upper) and left to right in (C lower), modified from (Jobe, 2013)

2.7 Implication

The implication for petroleum exploration lie in the prediction of sand-rich, sinuous channels locations, which are important reservoir elements (Ian A. Kane, 2010). They may be found as distinctive features of individual lenses of sandstone bodies, which can act as good hydrocarbon reservoirs with heterogeneity, degree of lateral continuity and vertical connectivity being crucial components in reservoir geometry of a channel in terms of possible HC prospectivity (Pickering & Clark , 1996). Fluvial sandstones typically represent mid-channel or point bar sequences in braided or meandering river system respectively. The lateral accretion of bars will deposit sandstone layer extending to the width, but limited in thickness by river depth. The primary thickness at the time of deposition is reduced by 10-30% or more by later compaction (Bjorlykke, 2010). The overbank deposits of muds, on the other hand, will become tight shale, which will subsequently reduce the vertical permeability.
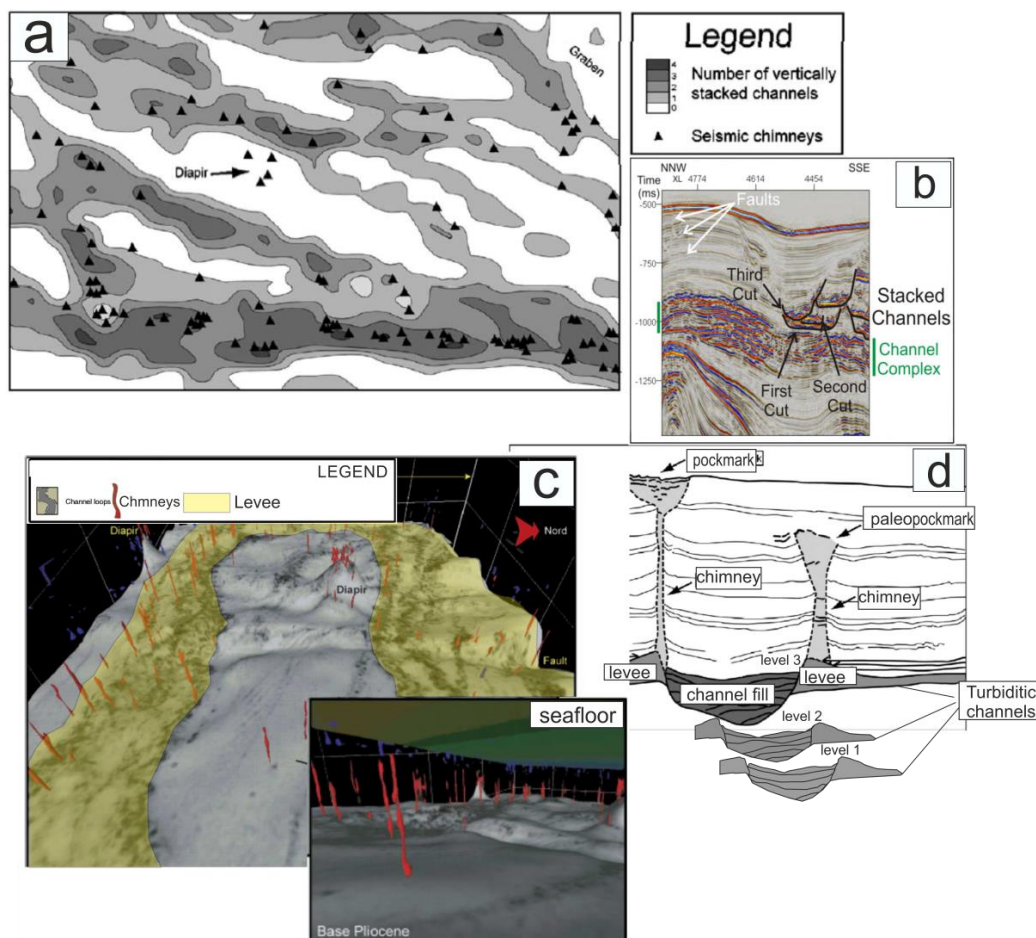
Figure 24 A) Frequency map of vertical stacked palaeochannels. This figure shows large bands, 2–8 km wide, of stacked palaeochannels. The triangles represent the position of seismic chimney. Modified from (A. Gay, et al., 2005), B) Typical vertical seismic section with interpreted stacked channels (from Atributes Thesis), C) Basinward perspective view within the 3D seismic block, showing turbiditic palaeochannels. The channel levee system is highlighted in yellow. The seismic chimneys, extracted from the 3D seismic block are represented. The base of the vertically elongated seismic chimneys seems to connect with levee system of turbiditic palaeochannels. However, isolated chimneys may connect to deeper palaeochannels. Modified from (A. Gay, et al., 2005), D) The Pockmark and paleopockmark (sealed pockmark) seems to take root at the channel–levee interface of buried palaeochannel from (A. Gay, et al., 2004)

Fining upward sequence shows that the highest permeability is near the base, where coarse-grained sediments are deposited. Deep fluids produced within source rocks are preferentially entrapped within the channel-levee system sandy bodies. Fluids can migrate from one palaeochannel level to another one along faults, which develops on at the crest of channel-levee system, or along sand sill and dykes, or through vertical stacking pattern of palaeochannels (Figure 23 B, C, Figure 24 A, B) (A. Gay, et al., 2005). According to A. Gay, et al. (2005, p. 35) the ability of fluids migration from a sand body to another depends on: 1) Lithology, as the coarse nature of deposits (grain flows, debris-flows or high-density turbidity currents) determines the

ability of fluids to migrate longitudinally through turbiditic palaeochannels. However, once channel is abandoned, very cohesive and difficult to erode mud is deposited, limiting the fluid upward migration. 2) Vertical stacking of palaeochannels as the turbiditic palaeochannels have surfaces that separate sandstone-dominated lithologies from overlying shale-dominated lithologies. 3) Connectivity as sand-rich intrusions, such as sill and dykes, may represent a preferential pathway for fluids to connect turbiditic palaeochannels, overpressure and differential compaction.

As fluid migrate from one level to another one through stacking paleochannels, migration pathways (chimneys) (Figure 24 C, D) are more concentrated when underlain by three to four stacked palaeochannels (A. Gay, et al., 2005).
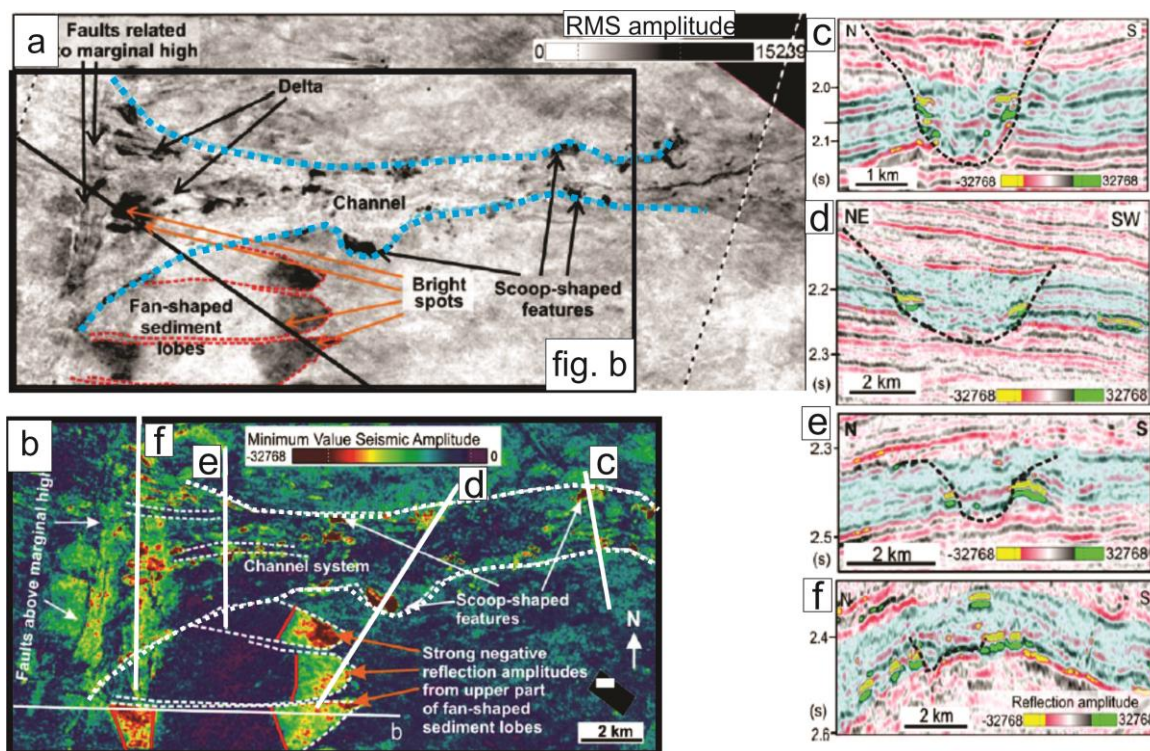

Figure 25 A) RMS map calculated for shaded zone (Plio-Pleistocene sedimentary succession of the SW Barents Sea), revealing different sedimentary environments. B) Minimum-value seismic amplitude attribute map with location indicated in a, showing minimum amplitude values for shaded zone. Strong negative amplitudes (red, yellow, green) indicate bright spots distribution. (C-F) Vertical seismic sections showing bright spots. Figure modified from (Karin Andreassen, et al., 2007).

In a fluvial-deltaic environment, channels are cut and filled with lithology which differs from one through which it is cut, giving rise to acoustic impedance contrast. Lateral changes in lithology give rise to differential compaction (Satinder Chopra & Kurt J. Marfurt, 2012). The channel levee system has a seismic appearance of high-amplitude, negative phase-reflection segments with a mounded outer shape. They

occur at the sides of a channel as a single reflection (Figure 25 C, D, E, F) or as several high amplitude reflections stacked upon each other (Karin Andreassen, et al., 2007; A. Gay, et al., 2005; Jair Weschenfelder, et al., 2010), where low amplitudes can be correlated with shales and/or mudstones, while high amplitudes indicate sands. The strong negative-phase seismic reflections might be associated with the channel levees and suggest that they are gas-bearing and, therefore, they consist most probably of sandy sediments (Karin Andreassen, et al., 2007). A well-marked, strong and continuous reflector of the overlying strata (Jair Weschenfelder, et al., 2010) truncates the upper reflectors of the seismic facies filling up these paleochannels. High RMS amplitudes (Figure 25 A), may indicate the presence of gas or may be caused by lithological contrasts. Minimum-value seismic amplitude attribute map (Figure 25 B) is generated to display strongest negative-amplitude values, or negative-amplitude bright spots, which indicate the gas presents in the fan-shaped sediment lobes, in continental slope channels and deltaic deposits, and in the sediments at the flanks of slide scars.

The study of channels is of great importance in hydrocarbon exploration since they can act as conduits for sediments transported to deep basins, act as repositories of coarse-grained sediment, and hence could represent promising hydrocarbon reservoirs. After Sites of preferential sand accumulation in channels can be listed as follows, after Pickering & Clark (1996, p. 217): (1) Channel bends; (2) Channel confluences; (3) Point-bars associated with high-sinuosity lateral accretion; (4) Channel benches and terraces; (5) Channel thalwegs; Frequent river course change due to regional tectonic activity results in frequent avulsion, whereas rapid subsidence rate and high quantity of sediment supply governs high proportion of fine deposits. Massive sands often form the basal units of channel sequences which grade upwards into a succession of horizontally laminated with fine sands and silts, overlain by wavy, lenticular bedded silts and interbedded muds (A. Gay, et al., 2005). Silts and sands, which compose the palaeochannel infills or sands, formed within fluvial deposits in channel belts, have high porosity. The palaeochannels may concentrate fluids migrating from the productive source rocks. Porous paleochannel deposits may act as effective longitudinal drains for the fluids to migrate (A. Gay, et al., 2005), or act as a

porous reservoirs where petroleum is found (Miall, 1992). As river meanders through the flatland, influencing the deposition of peat and associated sediments, coal could be deposited as peat along the channel in regions subjected to nonuniform sedimentation rates, which was controlled by interaction of migrating depositional environments and because peats bordering the river received nutrients and vegetation supply. The implication for petroleum exploration lies in the prediction that sand-rich, sinuous channels are important reservoir elements (Ian A. Kane, 2010). These depositional features are of particular interest offshore Angola, Brazil, Guinea, Gulf of Mexico and India. Gas in these features is interpreted to appear in high-porosity channel, levee and delta deposits (Karin Andreassen, et al., 2007), which may be easily identifies on seismic data due to appearance of strong negative-phase seismic reflections associated with gas presents.

Chapter 3 – Study area

3.1 Barents Sea

The study area is restricted to the Norwegian sector of the Barents Sea where it spans an area of about 600 by 350 km stretching from the northern coast of Norway to Svalbard (Figure 26). The SW Barents Sea is a part of the Arctic Ocean located north of Norway and north-west of Russia (Eva K. Halland, et al., 2013), in the junction of the North Atlantic and Arctic provinces (L. Gernigon, et al., 2013). It is bordered by the Norwegian Sea to the west, Novaya Zemlya in the east, Franz Josef Land and Svalbard to the north Figure 26). The bottom topography of Barents Sea is highly irregular and consists of complex structural features as numerous basins and highs (E. Henriksen, et al., 2011). It has largest continental shelf on the globe, covering area of 1.3 million km² and water depths averaging approximately 300 m (Doré, A.G., 1995). The Barents Sea is characterized by several shallow bank areas (100-200 m bsl) and deeper basins and troughs (200-500 m bsl) (Lilja R. Bjarnadóttira, et al., 2014), which characterize it as a shallow continental shelf with average water depth of about 400 m all over the Barents Sea (Smelror, et al., 2009). Barents Sea preserves a relatively complete succession of sedimentary strata ranging in age from Late Palaeozoic to Quaternary, locally exceeding 15 km in thickness (S. T. Gudlaugsson, et al., 1998).

The Barents Sea is the most productive of the Arctic seas. Marine source derived sediments (47%) exceed terrestrial sources, namely rivers, coastal erosion, and aeolian transport, where coastal erosion is probably the largest terrigenous sediment source (Agata Zaborskaa, et al., 2008). Sea-ice sediment entrainment, transport, and melting processes have an influence on the re-distribution of Arctic sediments, and up to 30% of modern sedimentation in the Barents Sea may be connected to sea-ice/sediment interactions (Agata Zaborskaa, et al., 2008).

Geophysical and geological investigations in the Barents Sea began during the 1970s, however, the exploration of the southern part started only in 1979, when the first licenses were awarded. Initial exploration was focused in and around the Hammerfest Basin (E. Henriksen, et al., 2011). The first gas discoveries were made in 1981, the Alke and Askeladd gas field (Doré, A.G., 1995).
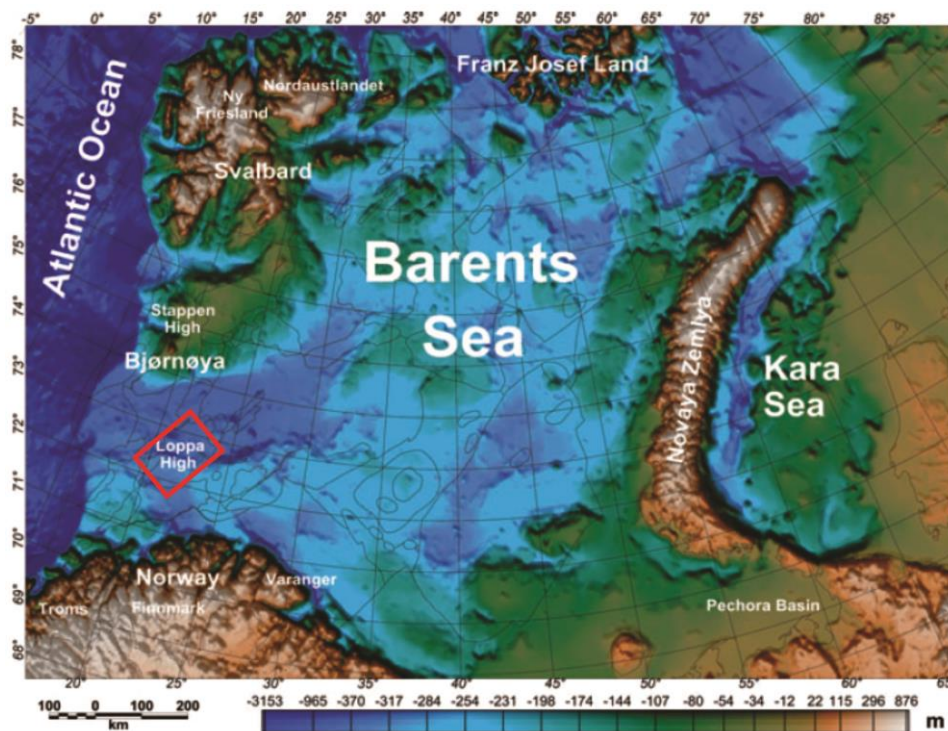
Figure 26 Map showing the location of the Barents Sea and adjacent areas. Approximate location of study area (LM09M01) is shown with red rectangle. Figure modified from (C. Barrereet al., 2011)

The Snøhvit field was discovered in 1984 and is the largest gas and oil discovery in the Norwegian Barents Sea up to date, which contains predominantly gas in reservoir rocks of Middle Jurassic age (Doré, A.G., 1995). In more recent years new discoveries have been found. In 2011 Skrugard field was discovered, following the year after by Havis discovery (Jørgensen, 2014). The level of exploration activity has increasing trend and has been maintained relatively high over past years (NPD, 2013). Various authorities place the currently discovered resources of the Norwegian Barents Sea in the region of 260–300 billion Sm3 (standard cubic meters) of gas. Norway's overall offshore area covers 2 040 000 square kilometers, about half of the area comprises sedimentary rocks which could contain petroleum (NPD, 2013). As many as seventy-three plays have been identified by the NPD on the Norwegian shelf, among them twenty-seven plays (ten confirmed) are identified in the Barents Sea (except for South-East Barents Sea).
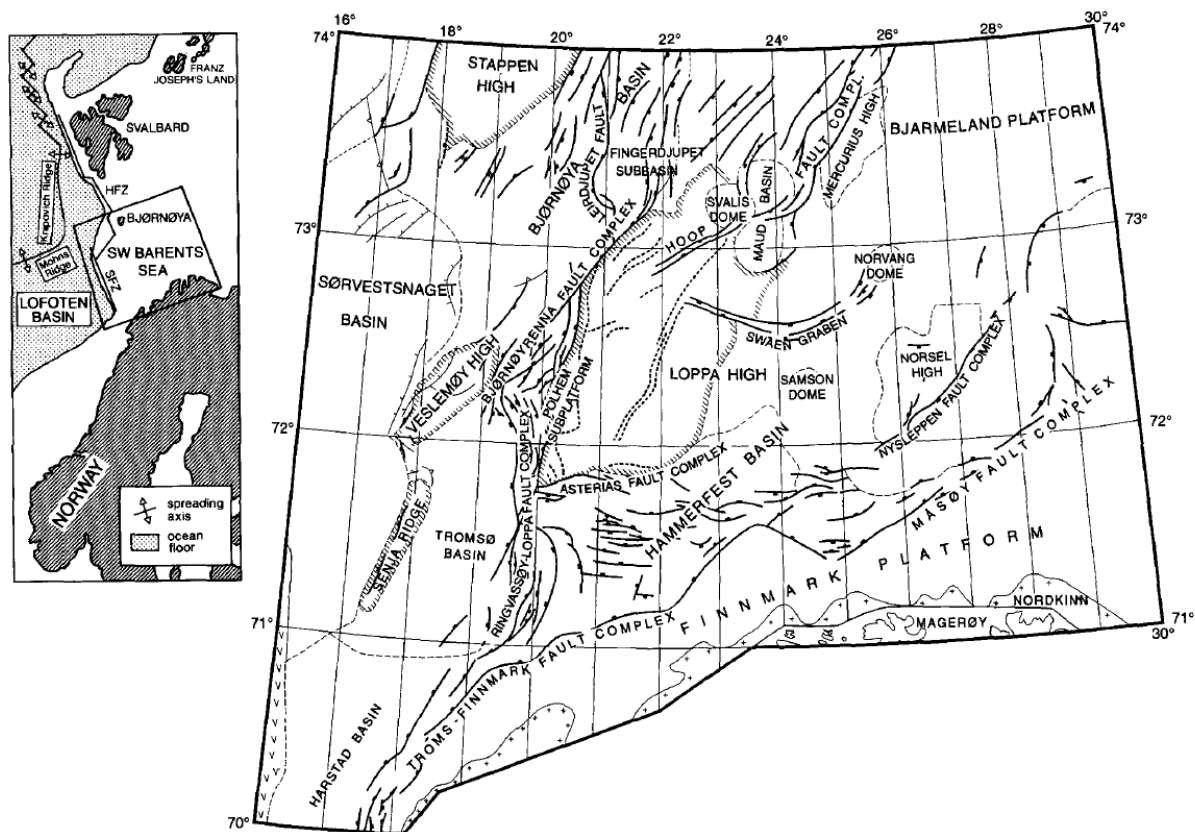
Figure 27 Main tectonic structures of the southwester Barents Sea. Figure from (Gabrielsen, R, et al., 1990).

Much larger fields are discovered in the Russian sector of the Barents Sea with the Stokmanovskaya, contains gas and condensate in a reservoir consisting of Middle-Upper Jurassic marine sandstones (Doré, A.G., 1995) and Ludlovskaya supergiant gas fields. Stokmanovskaya alone has gas reserves in the order of 2500 billion m³ (Doré, A.G., 1995). Today there are 53 active licenses, within 80 wildcats, which resulted in 35 discoveries (Eva K. Halland, et al., 2013). The western half of the Barents Sea is considered very challenging. It is characterized by few wells (80 boreholes over 160,000 km2, an area equivalent to the entire North Sea) and a variable quality of the seismic data, together with several highly tectonized basins and a complex uplift history (Carstens, 2011).

The Loppa High has a fair potential for oil and gas exploration, however there were uncertainties both about reservoir rocks and hydrocarbons migration back in the late 1980's. Estimates of recoverable hydrocarbons vary from negligible to 200×10^6 cu m oil equivalents (T. Sund, et al., 1986). However, in 2013 Lundin AS made a new oil and gas discovery in Late Permian carbonate rocks on the Loppa High, the Gohta discovery (Lundin, 2013).

The western part of the Barents Sea is a large Perm-Triassic platform, dominated by a system of NNW-SSE and N-S striking structural features (Gabrielsen Roy H, et al., 1997). It represents different structural style, affected by several episodes of crustal extension and rifting that cause severe thinning of the continental crust and graben-type basins (Smelror, M, et al., 2009). Eastern part of the Barents Sea will not further described since it is beyond study area of this study. There is a marked difference, both in time, trend and magnitude, between the tectonic and stratigraphic development in the western and eastern parts of the southern Barents Sea. This boundary is defined by the dominantly N-S to NNE-SSW trending Ringvassoy-Loppa and Bjornoyrenna Fault Complexes (Figure 27) (Eva K. Halland, et al., 2013). This master thesis therefore focuses on the western part of the Barents Sea, Loppa High (LM09M01) (Figure 26, Figure 27).

3.2 Tectonic evolution of the south-western Barents Sea.

The regional geology of the Barents Sea has been studied by several researches (Nøttvedt, A., et al., 1992; Gabrielsen Roy H, et al., 1997; Paul Reemst, et al., 1994; S. T. Gudlaugsson, et al., 1998). The tectonic and basement history, however, is still quite complex and therefor locally still debatable. The Caledonian Orogeny provided the fundamental structure framework for the southwestern Barents Sea. Today the Barents Sea can be divided into an Eastern and Western geological provinces. The present day geology of the Barents Sea area has been affected to a great extent by a complex combination of large-scale plate movements and varying climatic and depositional processes and, therefore, Barents Sea shelf can be divided into a series of basins and highs that were active at different stages during the geological history of the area (Nøttvedt, A., et al., 1992). The Western province experiences major post-Caledonian rifting phase, which eventually lead to continental break-up (Smelror, M, et al., 2009). Several periods of uplift and erosion have occurred in the south-western Barents Sea. The range between 500 and 3000m, increasing from west to east, is applicable for erosion estimation (Paul Reemst, et al., 1994). Since study area is located in the South-West Barents Sea, eastern province will not be considered in this study.
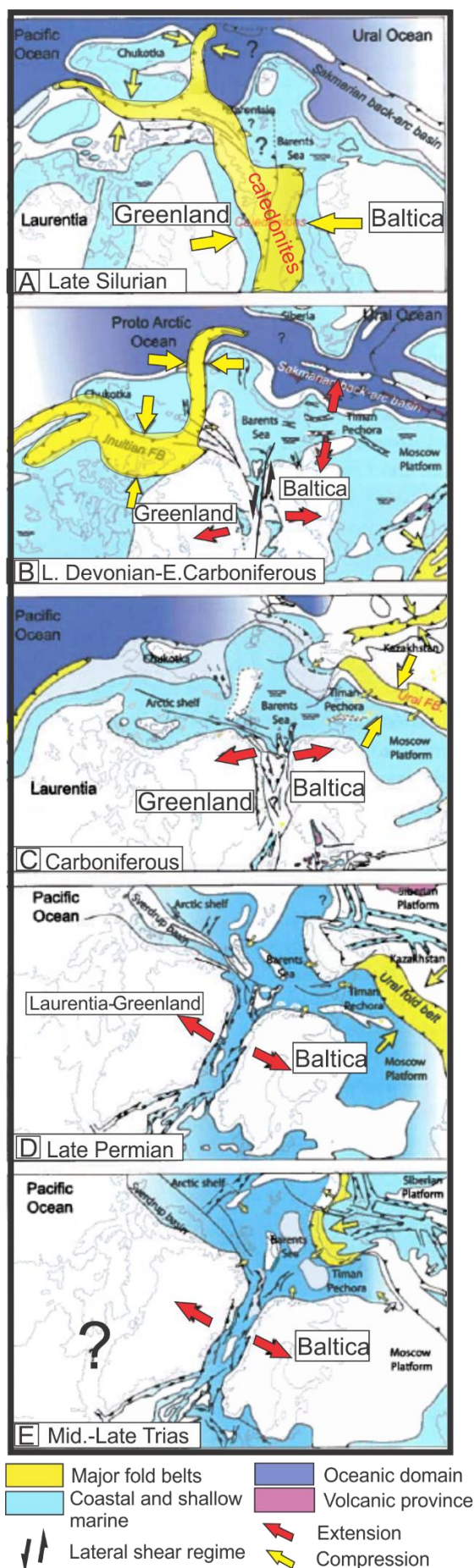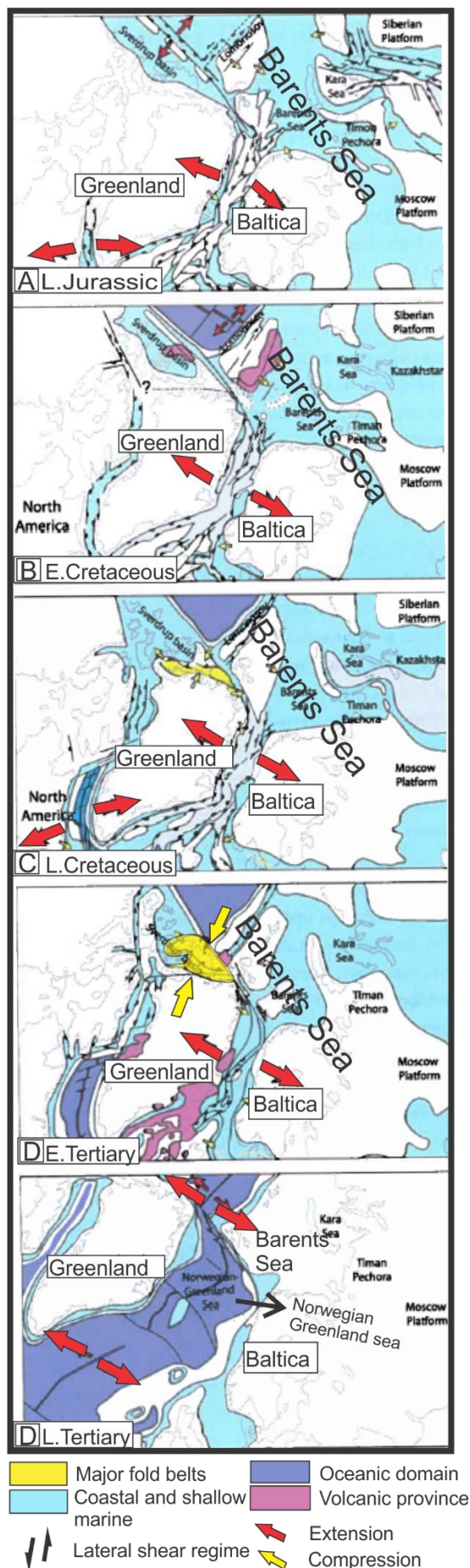
Paleozoic

The metamorphic basement of the Barents Sea developed during Caledonian orogeny, which occurred from Late Silurian to Earliest Devonian (Faleide, J. I., et al., 1984; Smelror, M, et al., 2009; S. T. Gudlaugsson, et al., 1998). Caledonian orogeny was a major continent–continent collision zone (Figure 28 A), which culminated approximately 400 Ma, resulted in consolidation of Laurentian and Baltic plates into Laurasian continent, tectonic thickening and closure of the Lapetus Ocean (Smelror, M, et al., 2009; David Macdonald, et al. , 2007; L. Gernigon, et al., 2013). This led to isostatic uplift and erosion, which removed 25–30 km of overburden matherials in the period 500–410 Ma, during the final stages of the Caledonian Orogeny (David Macdonald, et al. , 2007). The Caledonides in Scandinavia extended for nearly 2000 km from SW Norway to the far north, involving a large part of Sweden, and are now widely exposed in the country of Finnmark (L. Gernigon, et al., 2013). The depositional history of the western Barents Sea starts in Early Devonian (Lochkovian) which is directly overlaying crystalline basement (Gudlaugsson et al., 1998).

Figure 28 Main stages in the evolution of the western Barents Sea from Silurian to Triassic (A-E). Modified from (Smelror, M, et al., 2009).

Following the Calledonian orogeny, in the Lochkovian time, the area was dominated by breakdown of Caledonian orogeny, extension and was characterized by large scale erosion of hinterlands (Smelror, M, et al., 2009; L. Gernigon, et al., 2013). The western part of Loppa High aligns with a proposed Caledonian suture zone and following the collapse of the Caledonian orogeny acted as a transfer zone (S. A. Clark, et al., 2013), since considerable erosion of the hinterland and sediment deposition in foreland occurred (Smelror, M, et al., 2009). Post-Caledonian geological history of the western Barents Sea is dominated by Late Devonian-Carboniferous rift phase. In the Late Devonian (Figure 28 B) left-lateral shear regime with large-scale strike-slip movements (Faleide, J. I., et al 1984) formed nearly 300 km wide rift zone, extending at least 600 km in a north-easterly direction (Smelror, M, et al., 2009). Celedonian erosion continued, resulting in gradual flattening of Calledonial mountains (Smelror, M, et al, 2009). At the transition zone from Early to Middle Carboniferous the later lateral shear regime changed into a phase of extensional tectonics (Figure 28 C) (Faleide, J. I., et al., 1984). The Middle Carboniferous rifting ceased in Late Carboniferous, followed by regional subsidence and sediment accumulation in Tromsø, Bjørnøya, Nordkapp basins, which have been interpreted as rift basins formed at this time (S. T. Gudlaugsson, et al., 1998). At the onset of the Permian the transgression occurred, giving rise to an extensive marine shelf environment with temperate climate (Jørgensen, 2014).

Mesozoic

Triassic was tectonically quite period, with regional subsidence (Evy Glørstad-Clark, et al., 2010; Faleide, J. I., et al., 1984). Triassic rift and following mid-Triassic post-rift subsidence episodes (Figure 28 E) (Smelror, M, et al., 2009), contributed to Triassic regional subsidence in the western Barents Sea and amplifying the relief of the paleo Loppa High (Evy Glørstad-Clark, et al., 2010), which was uplifted and eroded in Early Triassic as a consequence of rifting to the west of the high (Smelror, M, et al., 2009). Calm regional extension, minor strike-slip movement and postrift thermal subsidence generally characterized Middle-Late Triassic times. At this time, a significant change in the paleogeography of the Barents Shelf area occurred due to uplift of northern, eastern and southern parts.

Figure 29 Main stages in the evolution of the western Barents Sea from Late Jurassic to Late Tertiary. Modified from (Smelror, M., et al., 2009).

This was followed by relative uplift in the east, shifting the area of maximum sediment accumulation westward. This event resulted in Carnian formation thickening (Smelror, M, et al., 2009). The tectonic activity during the Mesozoic can be divided into two main phases: the Mid-Kimmerian tectonic phase and the Late Kimmerian tectonic phase (Faleide, J. I., et al., 1984). The Mid-Kimmerian tectonic phase (Middle to Late Jurassic) is related to the rifting and opening of the central Atlantic Ocean. The second is the Late Kimmerian tectonic phase (Late Jurassic to Early Cretaceous), which is dominated by the development of large deep-seated normal faults along zones of weakness in the Caledonian basement, i.e. the Ringvassøy-Loppa Fault Complex. During this phase lateral variations in subsidence occurred in the south-western Barents Sea (Faleide, J. I., et al., 1984). At this point the main basins and highs were already developed, so the Late Kimmerian phase mainly leads to continuation in formation of structural elements, such as Ringvassøy-Loppa Fault Complex and Loppa High, internal changes in the sedimentary basins, such as horst-graben formation.

Figure 28 and Figure 29 show the change in tectonic settings before and after Late Jurassic.

Following Early Cretaceous uplift and associated regression continued (Figure 29 B) (Smelror, M, et al., 2009; Faleide, J. I., et al., 1984). Northern Barents Sea area during the Early Cretaceous was subsequently uplifted and large amounts of sediment were abraded from the uplifted continental areas in the Northeast into deeply subsiding basins in the west (L. Gernigon, et al., 2013). The Loppa High, being an island throughout the Cretaceous (S. A. Clark, et al., 2013), was inverted between the subsiding Bjørnøy and Hammerfest basins (Faleide, J. I., et al., 1984). The rate of subsidence at this stage was much faster to the west of the Ringvassøy-Loppa Fault Complex than on the east side. The main phase of subsidence took place in the end of Early Cretaceous when most of the Late Kimmerian fault movements had ceased (Faleide, J. I., et al., 1984). The Late Cretaceous rifting of Norway and Greenland continued well into the Palaeocene (Early Cenozoic) (Figure 29 C), but changed gradually into a strike-slip movement.

Cenozoic

Late Cretaceous to Paleocene period between Norway and Greenland was progressively taken up by strike-slip movements within De Geer Zone (Smelror, M, et al., 2009; L. Gernigon, et al., 2013) and deformation leading to the formation of pull-apart basins in the westernmost parts of the Barents Sea (Jan I. Faleide, et al., 1993). North Atlantic margin break-up and opening of Norwegian-Greenland Sea at around 55 Ma mark the Paleocene-Eocene transition (Smelror, M, et al., 2009). This time interval is also characterized by a major magmatic event, as witnessed by massive basaltic traps and the formation of volcanic rifted margins which have been identified from the Irish margin up to the Lofoten and NE Greenland shelves. Progressively developed shear-margin in Paleocene-Eocene time lead to break-up in Early Oligicene time and separation of the Barents Shelf and Greenland/North Antantic-Arctic marine connection in the Miocene (Smelror, M, et al., 2009). Separation of the Barents Sea Shelf and Greenland/North America has continued, leading to the opening of the Fram Strait and establishing a North Atlantic-Arctic marine connection in the Miocene (Faleide, J. I., et al., 1984).

Summary

The tectonic development of the Barents Shelf includes the Timanian and Caledonian orogenies, the Atlantic rifting in the west, basin opening in the North, and the subsequent break up and opening the Norwegian North Atlantic ocean along the western margin of the shelf (Smelror, M, et al., 2009). Basins and platforms were mainly established during processes of major collisions, followed by continental separation and opening of the northern North Atlantic along the western margin of the shelf (Smelror, M, et al., 2009). Triassic sedimentary succession, was deposited in relatively quiet and shallow epicontinental basin in the Norwegian part of the Barents Sea (Gabrielsen, et al., F, 1990; Evy Glørstad-Clark, et al., 2010). Late Jurassic to Early Cretaceous and Neogene uplifts and erosion has locally removed much of the upper part of the Triassic succession on the Loppa High.

3.3 Structural settings

Three geological provinces, separated by major fault zones, can be recognized within Barents Sea on basis of sedimentary fill, tectonic style and crustal structure: Cenozoic Basin of Lofoten, Cretaceous and Early Tertiary basins (Harstad, Tromsø, Bjørnøya and Sorvestsnaget), separated by intrabasinal highs (Senja Ridge, Veslemtiy High and Stappen High), and Mesozoic basins and highs (Finnmark Platform, Hammerfest Basin, Loppa High, Fingerdjupet Subbasin) (Faleide, J. I., et al., 1984). The Senja Fracture Zone and the Vestbakken Volcanic Province marks the western limit of the continental shelf and the transition to oceanic crust. In addition, the western Barents Sea holds several Jurassic-Cretaceous fault-zones that creates the boundaries of deep sedimentary basins: The Troms-Finnmark Fault Complex south of 71° N, the Ringvassøy-Loppa Fault Complex, Bjørnøyrenna Fault Complex and Leirdjupet Fault Complex (Figure 30) (Faleide, J. I., et al., 1984; Jan Inge Faleide, et al., 2008), where Ringvassøy-Loppa and Bjørnøyrenna Fault Complexes define the boundary between eastern and western parts of SW Barents Sea (Eva K. Halland, et al., 2013) and bound Loppa High to the west.

3.3.1 Loppa High

The dataset of this study has its eastern section of the western part of the Loppa High, which is named after an island and a district on Finnmark. The Loppa High, including the Polhem Subplatform is situated between 71°50'N, 20°E and 71°55'N, 22°40'E and 72°55'N, 24°10'E and 73°20'N, 23°E (Gabrielsen, R, et al., 1990), and also is one of the main structural and basement highs of the SWBS (Figure 26, Figure 27, Figure 30) (L. Gernigon, et al., 2013). The Loppa High is a marked (N-S) trending structural feature (Figure 30), dimond-shaped in outline (Gabrielsen, R, et al., 1990). It is a structurally complex basement high, which is surrounded by sedimentary basins, and a marked isolated structural high near the southwestern margin of the Norwegian Barents Sea (Jhosnella Sayago, et al., 2012).
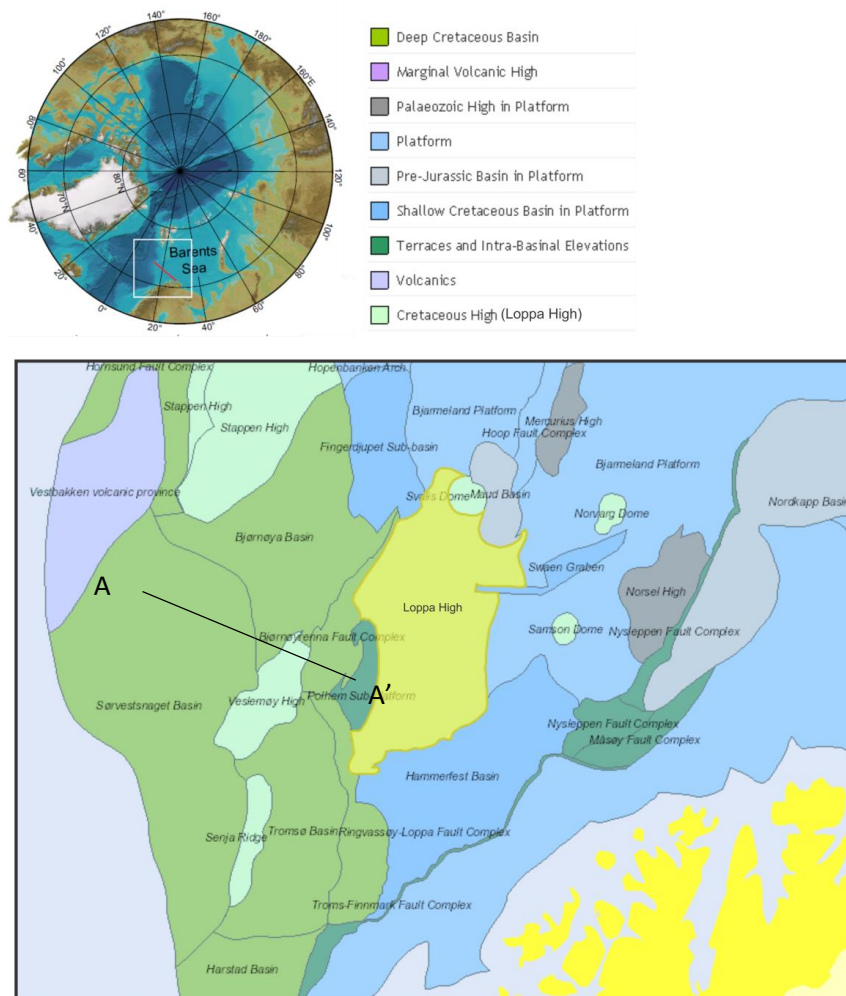

Figure 30 Transect of the geosection showing Structural elements of the western Barents Sea and regional profile AA' across the SW Barents Sea. Figure modified from (NPD, Factmaps, 2014).

Loppa High is separated from the Hammerfest Basin in the south by the E-W trending Asterias Fault Complex, from the Tromsø and Bjørnøya Basins to the west by the Ringvassoy-Loppa and Bjornoyrenna Fault Complexes and to the east, it grades into the Bjarmeland Platform (Eva K. Halland, et al., 2013).
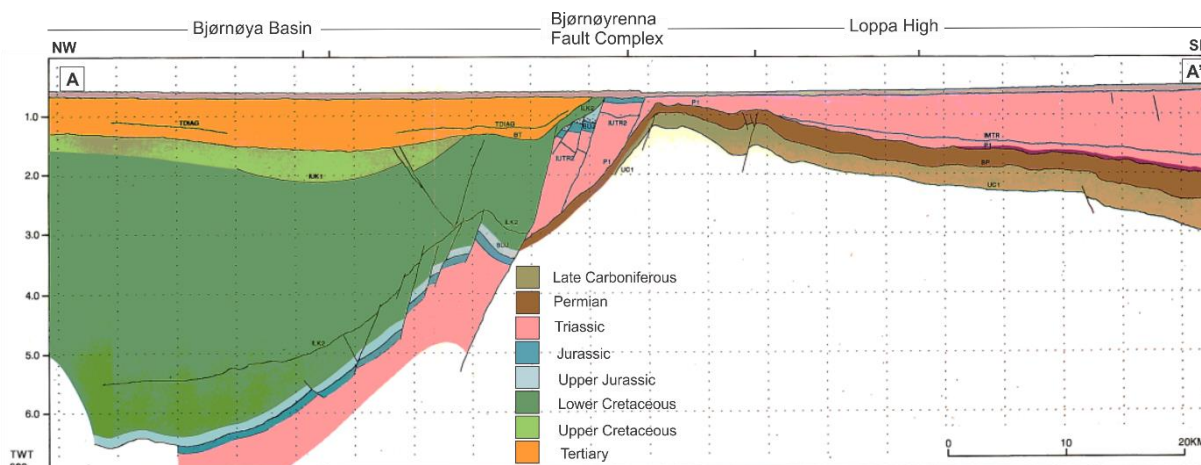

Figure 31 Schematic regional seismic cross- section from northwest to southeast of the Western Barents Sea, line AA' (see Figure for location). Triassic is shaded in pink. Modified from **(Gabrielsen, et al., F, 1990)**.

It incorporates the Polheim Platform (Gabrielsen, R, et al., 1990). The Svalis Dome, a major salt structure, marks the northeastern limit of the Loppa High (Gabrielsen, R, et al., 1990). The Loppa High has complex geological history with several phases of uplift/subsidence followed by tilting and erosion (Figure 32) (Eva K. Halland, et al., 2013; R. J. Wood, et al., 1989).

The Loppa High is a result of late Jurassic to early Cretaceous and Late Cretaceous-Tertiary tectonism (Gabrielsen, R, et al., 1990; E. Henriksen, et al., 2011). The schematic section AA' (Figure 31) and chronostratigraphic chart of the study area (Figure 32) indicates strong erosional truncation at several stratigraphic levels across Loppa High (R. J. Wood, et al., 1989; T. Sund, et al., 1986). Early Carboniferous terrigenous clastics were onlapped by Upper Carboniferous and Permian Carbonates, which were eroded during the Early Triassic (R. J. Wood, et al., 1989), as a result of rifting and uplift of Loppa High (Smelror, M., et al., 2009), and were onlapped by the Lower to Middle Triassic clastic sequences (Figure 32). Footwall uplift of the Loppa High during Late Jurassic to Early Cretaceous caused erosion of Jurassic sediments over the Loppa High (Figure 32 C) (R. J. Wood, et al., 1989). Loppa High became an island leading to erosion of exposed Jurassic and Triassic sediments.
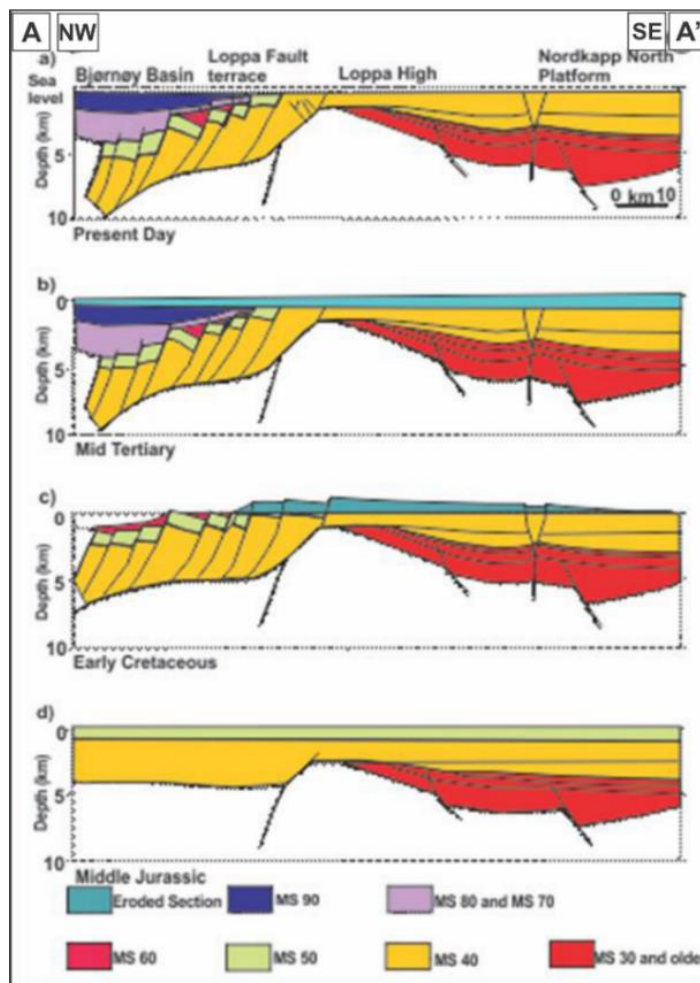
Figure 32 Schematic profiles showing geological evolution of Loppa High, line AA' (location Figure). Modified from (R. J. Wood, et al., 1989).

The high remained exposed until island gradually subsided and the crest was onlapped during the early Paleocene when high was fully submarine (Figure 32 B). Again, Loppa High was subjected to uplift and erosion, which formed an unconformity with low-angle tertiary and older sediments below Quaternary glacio-marine sediments (R. J. Wood, et al., 1989). This was the last stage of the formation of present day structure of Loppa High (Figure 32 A).

The high is defined by the subcrop of the Mid-Jurassic unconformity against Quaternary sequence (Gabrielsen, R, et al., 1990) and is of Early Cretaceous age. It is associated with positive gravity and magnetic anomalies caused by a relatively shallow metamorphic basement of Caledonian age underlying its western part (C. Barrere, et al., 2011; Gabrielsen, R, et al., 1990).
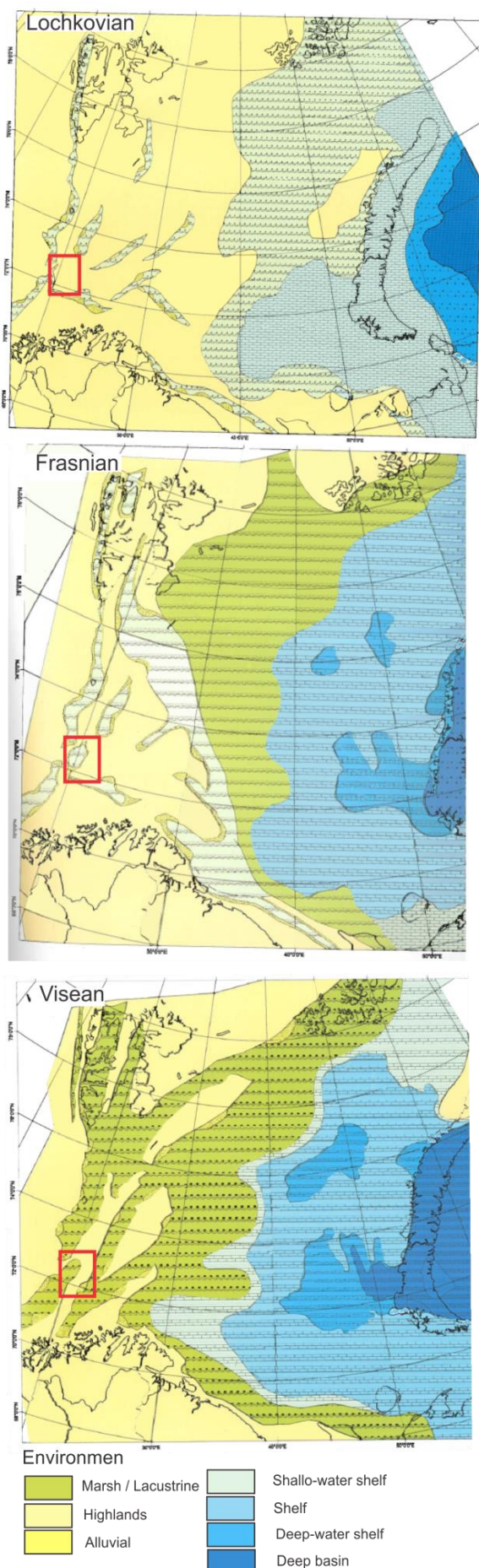
3.4 Lithostratigraphy and depositional environments

During Devonian land areas occupied almost the whole territory of South West Barents Sea in Lochkovoan-Frasnian, until depositional regime changed to dominated by fluvial plaints in Early Carboniferous (Visean). The general picture, with an emergent continental regime in the in the west BS, and broad marine carbonate platform in the east, is the dominant feature of Visean (Figure 33) (Early Carboniferous) (Smelror, M., et al., 2009). At the onset of the Moskovian (Late Carboniferous), the areas had expanded so that carbonate shelf condition subsequently reached western Barents shelf. Extensive shallow-marine carbonate shelves and deposition of warm-water carbonates took place in Asselian (Early Permian) (Smelror, M., et al., 2009). During periods with high sea-level changes, entire shelf areas were flooded and shallow-water platform carbonates, with up to 100 m thick algae build-ups developed on paleo-Loppa High and other structural highs, resulting in Polygonal Reef Pattern on Loppa High (Figure 33) (Smelror, M., et al., 2009).

Figure 33 Palaeogeographic reconstruction (Early Devon-Carboniferous). Red box indicates proximal location of paleo-Loppa high. Modified from (Smelror, M., et al., 2009).
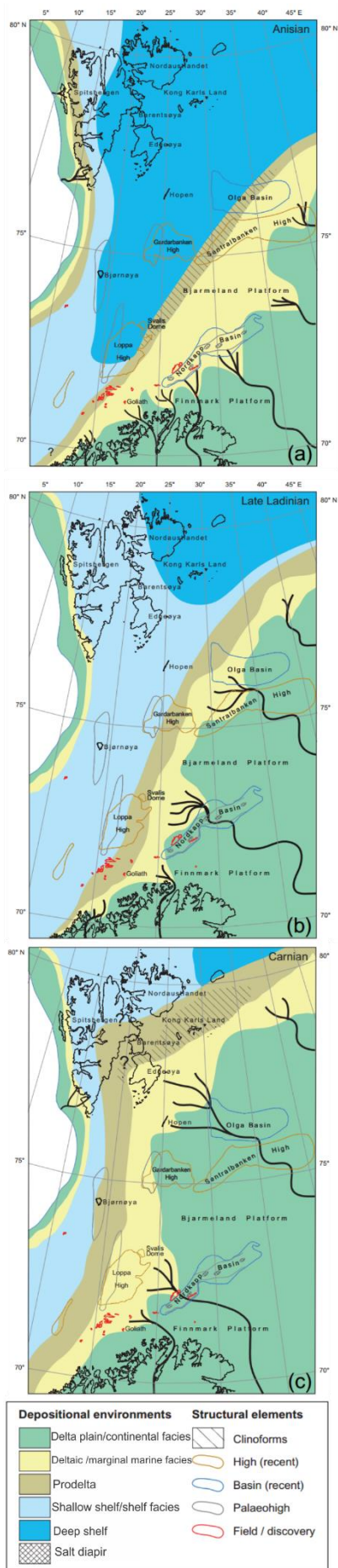
The late Carboniferous–late Permian megasequence is characterized by significant thickness variations in the south-west Loppa High, associated with local rift grabens. The basal surface reflects major rifting, defined as the initial rift phase at 320–300 Ma (S. A. Clark, et al., 2013). This rifting phase is also associated with the initiation of the western flank of the younger paleo- Loppa High (S. A. Clark, et al., 2013). The Carboniferous to Early Permian carbonate deposition regime changed to the siliclastic regime at the onset of Wordian (Middle Permian), which was the period of transgression and deep-marine depositional environments. In Wordian paleo-Loppa High is still a positive relief in the area with coastal and shallow water deposits while the area west of Loppa High consist of deeper shelf deposit (Smelror, M., et al., 2009).

In the Barents Sea area Triassic (Figure 34) was generally tectonically quite period, marked by regional subsidence (Smelror, M., et al., 2009; Evy Glørstad-Clark, et al., 2010; Fridtjof Riis, et al., 2008). General shallow shelf depositional environment filled with siliclastic sediments from the southeast, sourced by the Uralian orogeny, is characterized by a series of see transgression and regression. In the Early Triassic (Induan) to Middle Triassic marine conditions and clastic marine sediments existed in the western part of the Barents Sea (Faleide, J. I., et al., 1984). Paleo-Loppa High was uplifted and eroded due to rifting to the west of the Loppa High.

Figure 34 Palaeogeographic reconstructions (Early to late Triassic). Modified from (Evy Glørstad-Clark, et al., 2010) and (Fridtjof Riis, et al., 2008).
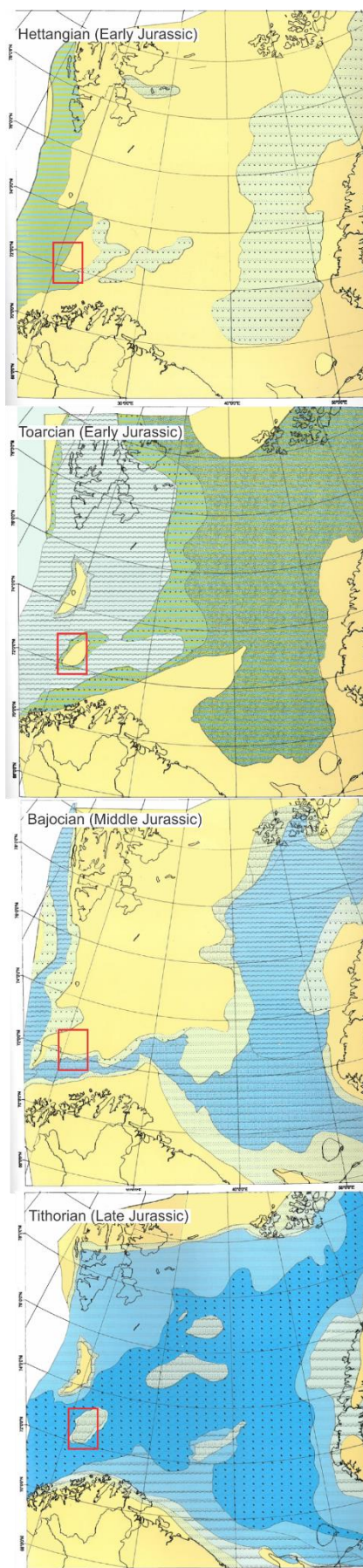
Uplift in the east, accompanied with subsidence within the South Barents Region Basin and extensive supply of sediments from developing Uralian orogen caused extensive north-westward progradation of siliclastic shelf deposits (Doré, A.G., 1995). Series of Early Induan shelf-margin progradations are observed on seismic section as a series of northwest prograding clinoforms (Smelror, M., et al., 2009). In general terms, clinoforms show the transition from shelf and offshore to deep marine basin in the distal part of prograding depositional system (Tore Grane Klausen, et al., 2015). Clinoforms have been used as a predictor for paleogeography and distribution of sandstones with reservoir potential in prograding delta system (Tore Grane Klausen, et al., 2015). A transition from marine settings of Middle Triassic (Anisian) (Figure 34 A) to a marginal marine settings of Late Triassic (Late Landian) (Figure 34 B) is marked by clinoform belt, which in this case represents the slope separating deep shelf area with deposition of organic-rich shales in the west from deltaic area in the east (Fridtjof Riis, et al., 2008). The Late Triassic (Carnian) (Figure 34 C) uplift and followed by overall regional regression in the eastern part led to extensive westward coastal progradation and the development of continental and coastal plain environments, with the Uralian highland in the east being an important sediment source (Figure 34) (Smelror, M., et al., 2009).

Figure 35 Palaeogeographic reconstructions Jurassic. Red box indicates proximate location of paleo-Loppa High. Modified from (Smelror, M., et al., 2009)

Figure 36 Palaeogeographic reconstructions (Cretaceous-Eocene). Red box indicates proximate location of Loppa High Modified from (Smelror, M., et al., 2009)
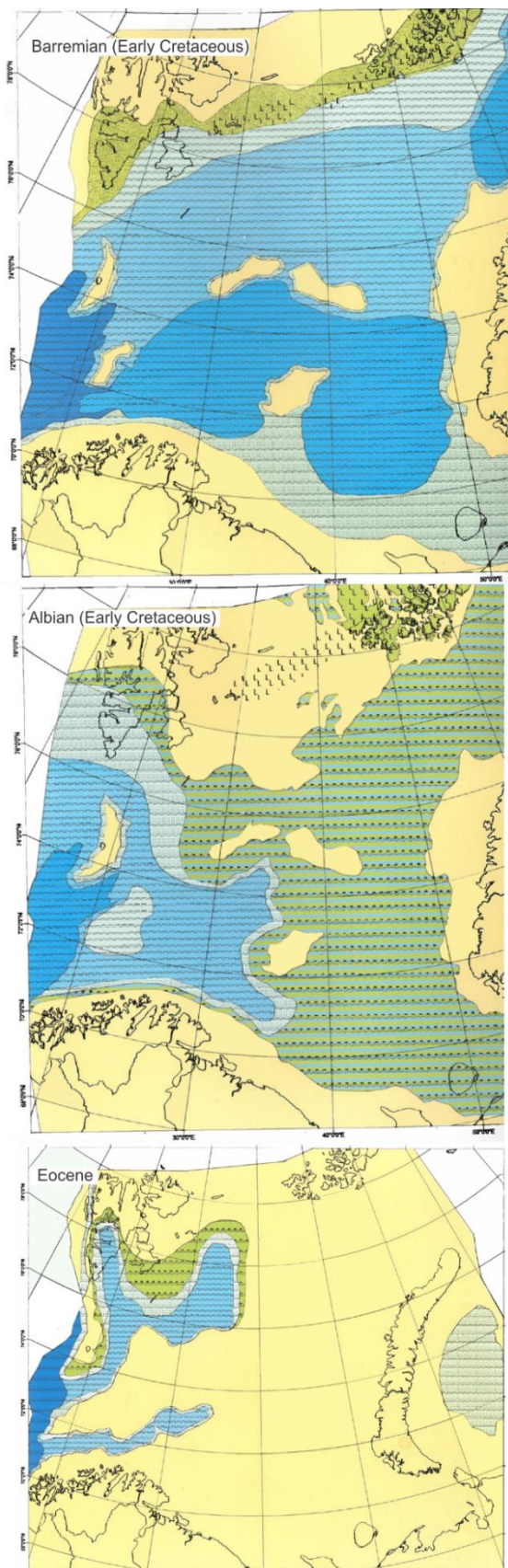
The generally shallowing depositional environment of the Triassic is illustrated from maps (Figure 34 A, B, C), reflecting the transition from Middle Triassic (Anisian) shallow shelf settings to a Late Triassic (Carnian) deltaic settings with fluvial sediments reaching all the way to Svalbard at the maximum regressive stage of this basin infillDuring the Late Triassic–Early Jurassic time (Figure 34, Figure 35), large areas were uplifted and eroded. Areas with shallow marine environment were restricted to the west, which were partially flooded (Smelror, M., et al., 2009). In Early Jurassic the Loppa High became submerged and as well as central part of the Barents Sea comprised wide continental lowlands. The climate changed from arid to humid leading to an increased run-off and transport of sediment. Toward Late Triassic – Middle Jurassic (Figure 35) sea level reached its maximum and shallow-shelf to deep-marine sedimentation prevailed over large area of the SW Barents Sea (Smelror, M., et al., 2009).

During most of the Cretaceous (Figure 36), the Loppa High was an island with deep canyons cutting into Triassic sequence. Increasing tectonic activity through the Late Jurassic in the western Barents Sea culminated in the Early Cretaceous (E. Henriksen, et al., 2011). Late Jurassic-Early Cretaceous rifting phase is associated with a focusing of subsidence west of Loppa High, in the deep Bjørnøya and Tromsø basins (S. A. Clark, et al., 2013). Early Cretaceous tectonic subsidence along the western margin resulted in deposition of extremely thick Cretaceous sandstones succession downflank of the Loppa High towards the Hammerfest basin (E. Henriksen, et al., 2011; Smelror, M., et al., 2009). A major marine transgression (Figure 36) developed a condensed marine succession during late Cretaceous, represented by the Kveite and Kviting Formations (Nøttvedt, A., et al., 1992).

The transition from Late Cretaceous to Early Paleocene in the Barents region is recognized as a significant hiatus in seismic data (Faleide, J. I., et al., 1984). Early Paleocene is characterized by massive transgression, which led to flooding of elevated areas such as the Loppa High and the Troms - Finnmark Platform. Eocene was dominated by subsidence succeeding the early rifting episode, and basins to the west of the Loppa High continued to subside and receive substantial amounts of sediments (S. A. Clark, et al., 2013). Neogene was characterized by uplift and erosion of the entire Barents platform, in conjunction with deposition of thick prograding sediment fans into the oceanic basins to the west and north, in response to northern hemisphere glaciations. The extensive uplift and erosion has been documented to estimate between 1000–1500 m in the Hammerfest Basin and Loppa High (S. A. Clark, et al., 2013). Limited distribution of Cenozoic strata is due to uplift and subsequent glacial erosion to the east, accompanied by contemporary subsidence along the western margin (E. Henriksen, et al., 2011), with erosion and re- deposition being particular intense during the Pleistocene glaciations (Doré, A.G., 1995). Cenozoic strata are absent (eroded away) below the base of the Quaternary in parts of the Loppa High (Smelror, M., et al., 2009). Glaciations, reaching the shelf edge in many episodes, have affected the south-western Barents Sea margin during the last 1.5 Ma (Jan Inge Faleide, et al., 1984; Karin Andreassen, et al., 2007). The eroding ice sheets have produced a massive prograding outer shelf sequence. The transition from erosion to

deposition is particularly well marked by the Upper Regional Unconformity (URU), which is a dominant feature of Barents Sea stratigraphy and is well-defined in most of the parts at the base of Quaternary (E. Henriksen, et al., 2011). This unconformity is due to recent Paleogene uplift and subsequent erosion, and it separates the preglacial Cenozoic from the overlaying glacigenic sediments (Chand, S., et al., 2008). The sequence of glacigenic sediments overly the URU with thickness ranging from 0 to 300 m (Tore O. Vorren, et al., 1991). An upper regional angular unconformity (URU) on the seismic record forms a strong, relatively even or smoothed reflector (Rafaelsen B., et al., 2002), which probably represents the erosional base for several continental shelf glaciations (Andreassen, K., et al., 2008).

3.4.1 Effect of the late Cenozoic uplift and erosion.

Since the opening of the Norwegian-Greenland Sea around 50 Ma ago, the Barents Sea has experienced different amounts of uplift and erosion that have important consequences on the reservoir quality, both positive and negative (Dore A. G. & Jensen L. N., 1996). The Cenozoic is characterized by large amount of uplift and erosion on the Barents shelf (Paul Reemst, et al., 1994), with the latest and most important uplift occurring during Pliocene-Pleistocene glacial period. Glaciation and subsequent erosion in the South West Barents Sea have a major impact on sedimentation and erosion over the entire area. Figure 37 A shows a preglacial topography of Early Tertiary phase, involving Plio-Pleistocene phase, which is characterized by glacial erosion on the whole shelf area with transport of erosional products to the present day margins (Figure 37 B), where transport path or ice-flow directions are shown in Figure 37 C by white arrows (Eiliv Larsen, et al., 2003). During Cenozoic most of the Barents Sea area was uplifted, however the uplift varied within southwestern Barents Sea, showing trends with the lowest values (<500m) in southwest, (500-1000m) on Loppa High, and increasing magnitude of uplift and erosion towards the north and northwest (>2000m) on the Stappen High (Eiliv Larsen, et al., 2003). It is important to discriminate between uplift and erosion. The erosion of sediments leads to isostatic adjustment followed by passive uplift, and in most cases erosion takes place whenever terrain is uplifted above sea level (Paul Reemst, et al., 1994).
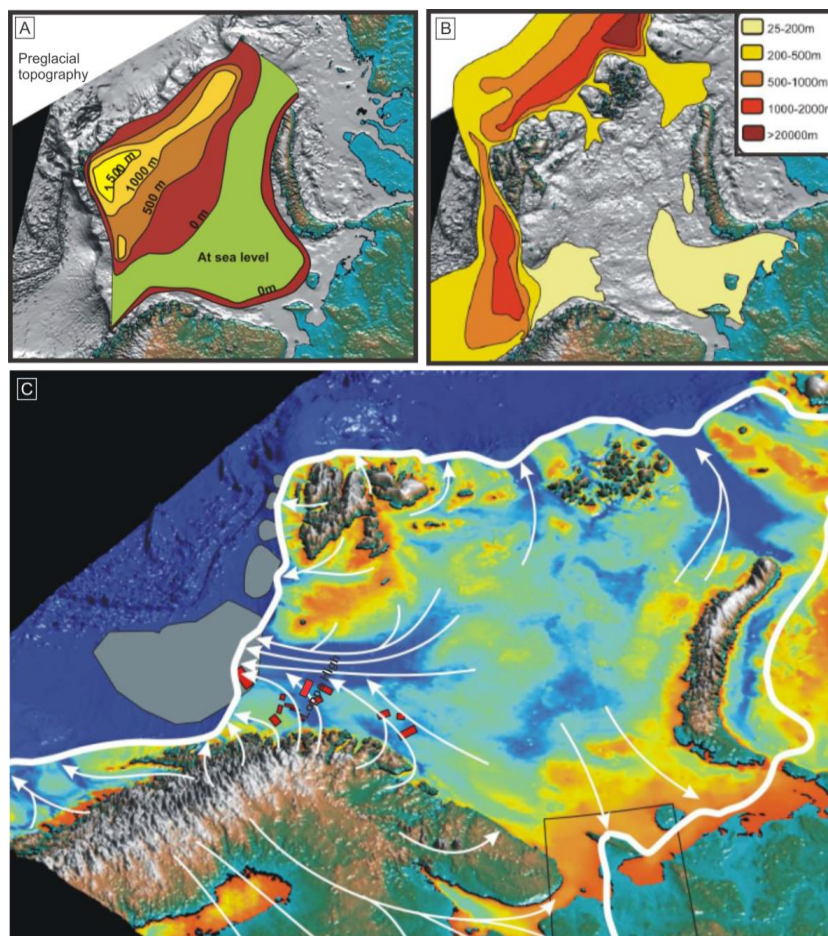
Figure 37 Effect of late Cenozoic upplift and erosion A) Reconstracted early Tertiary postrift topography of the Barents shelf. B) Present day thickness of Paleocene-Miocene sediments on the Barents shelf and margins. C) Ice extent (white lines) and large-scale ice-flow directions (arrows) during the Last Glacial Maximum. 3D seismic dataset in the southern Barents Sea (red boxes). Modified from (Eiliv Larsen, et al., 2003)

In the Barents Sea, 1000-3000 m of sedimentary overburden have been removed due to Cenozoic uplift and age of the this erosion has been subjected to considerable discussion (Eiliv Larsen, et al. 2003). It is considered an important factor, controlling the generation and migration of hydrocarbons. The uplift may have changed the structural attitude, which may have had an effect on preexisting hydrocarbon accumulation, fault reactivation and trap formation, since seal might fracture leading to spillage. The removal of sedimentary overburden is widely held responsible for reservoir properties, in particular structural and porosity change, gas expansion, and seal failure leading to leakage of hydrocarbons and causing the emptying of reservoirs or structures no being filled to spill responsible (Dore A. G. & Jensen L. N., 1996). However according to Dore A. G. (1996, p. 415), negative effects have been over-stressed and positive effect include mature source rocks at shallow

levels, liberation of natural gas from formation water, fracturing of tight reservoirs and remigration to shallower reservoirs.

3.5 Stratigraphy

The stratigraphy is based on reference well 7120/1-1 (Figure 46). The interpreted horizons are shown in Figure 53.

Basement

Available Information on nature of crystalline crust beneath Barents Sea sedimentary basins reveals evidence indicating that the basement underlying its western part was consolidated during the Caledonian orogeny (S. T. Gudlaugsson, et al., 1998). From many wells drilled, more than 50 wells have penetrated pre-Devonian rocks and in more than 30 of the wells basement rocks were cored. The thicknesses drilled have generally been in the order of a few meters. Five wells have drilled more than 100m of basement rock: 2/6-3 (142m), 16/1-4 (146m), 16/1-5 (195m), 35/3-2 (233m), 6306/10-1 (207m). The pre-Devonian rocks normally encountered include diverse rocks of low to high metamorphic grade, including metamorphosed igneous rocks such as granitic gneiss, and metasedimentary rocks such as mica schist, greenschist, quartzite and marble.

3.5.1   Paleozoic

Following the extensional collapse of Caledonian orogeny, Barents Sea acted as a transfer zone. During Late Paleozoic times most of the Barents Sea area was affected by crustal extension, and a 300 km wide rift zone, extending at least 600 km northeast, was established as a direct continuation of the northeast Atlantic rift between Greenland and Norway in the middle Carboniferous (S. T. Gudlaugsson, et al., 1998; Evy Glørstad-Clark, et al., 2010). Rifting resulted in in Late Paleozoic structures representing a fan-shaped array of NE-SW trend. Following deposition of continental clastics in rift basins, an extensive post-rift carbonate platform was established in the latest Carboniferous throughout Early Permian times with evaporite deposition in local basins (Faleide, J. I., et al., 1984).

3.5.1.1 Carboniferous

Gipsdalen gp

The group's sediments are found throughout the Norwegian Barents Sea, The Finnmark and Bjarmeland platforms and the Loppa High. Well 7121/1-1R has penetrated the thickest succession on the southern flank of the Loppa High, where the group is more than 1000 m thick (Factpages, 2015). Group's sediments are totally absent on the crest of the Loppa High. The group thickens towards the northwest of the Nordkapp Basin indicate thicknesses of several hundred meters. The group is composed of units generally showing shallowing upward trends continental red bed sandstones, siltstones and conglomerates dominate the basal part of the succession. These are overlain by mixed carbonates and siliciclastics (Factpages, 2015). Bedded limestones and dolomites with occasional small buildups dominate the upper part of the group, and minor evaporates on the platform areas.

3.5.1.2 Permian

Bjarmeland Group

The group is most thickly developed at the eastern flanks of the Loppa High and eastward across the Bjarmeland Platform, where it attains a maximum thickness of 488 m in well 7121/1-1 R at the eastern flank of the Loppa High (Factpages, 2015). It thins toward Bjarmeland Platform. The group onlaps palaeohighs and the margins of the depositional basin such as the eastern flank and crestal areas of the Loppa High and the southern parts of the Finnmark Platform (Factpages, 2015). White to light grey limestones containing a typical cool-water fauna dominate the group. Silty, dark grey to black limestones characterise the deeper-water succession. The group is also characterised by deposition of carbonates.

3.5.2 Mesozoic

3.5.2.1 Triassic

Triassic deposition was influenced by the erosion of Uralian Mountains, which acted as sediment source areas to the southeast (Evy Glørstad-Clark, et al., 2010). Thick and uniform Triassic siliciclastic deposit prograding predominantly towards the west and northwest, suggest an orogenic source (Smelror, M., et al., 2009). Northern Barents Sea demonstrates the development of prograding clinoforms from the east and southeast throughout the Triassic, controlled by sediment input from borderlands

and by sea-level changes (Fridtjof Riis, et al., 2008). In general, clinoforms show slope that separates deep shelf area with deposition of organic-rich shales in the west (Kobbe Formation) from the delta-front area in the east (Snadd Formation) (Fridtjof Riis, et al., 2008).
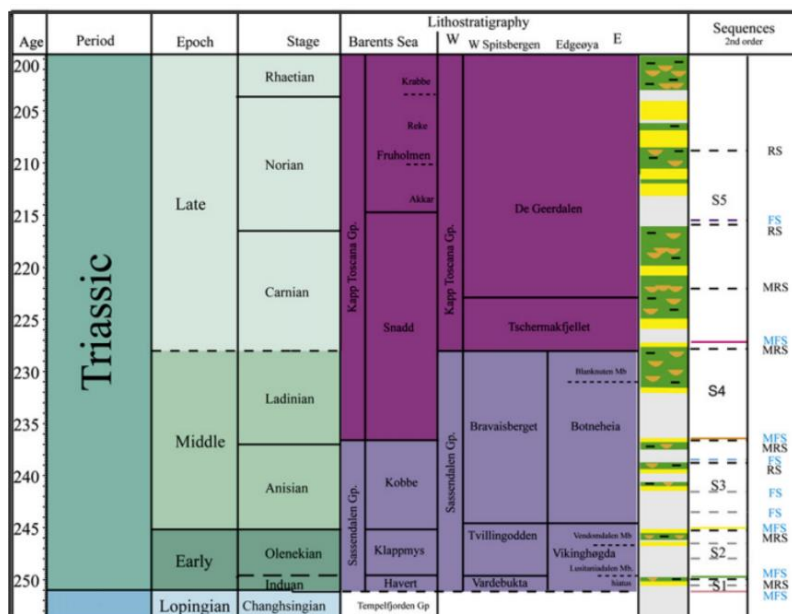

Figure 38 Schematic diagram of the Triassic lithostratigraphy in the western Barents Sea with the Triassic second-order sequences. Modified from (Evy Glørstad-Clark, et al., 2010)

Several studies have addressed the occurrence of well-defined clinoforms on seismic data referred to Lower-Middle Triassic in Barents Sea (Evy Glørstad-Clark, et al., 2010; Glørstad-Clark, E., et al., 2011). Based on these depositional features complete Triassic succession within Late Permian to Middle Jurassic megasequence was subdivided into sub-sequences (Figure 38, Figure 39), where bounding surfaces mark significant change in depositional conditions (Evy Glørstad-Clark, et al., 2010). The second-order Triassic surfaces were identified based on stratal termination, internal seismic character, reflection amplitude and continuity, geometry of seismic facies, sequence stratigraphic relationship of the Triassic deposits, where Snadd fm was effectively divided into lower (S4) and upper (S5) parts along a second order sequence boundary (Figure 39). Each sequence was analyzed in terms of time-thickness maps and paleogeographic interpretation. The present work is built on this observation.
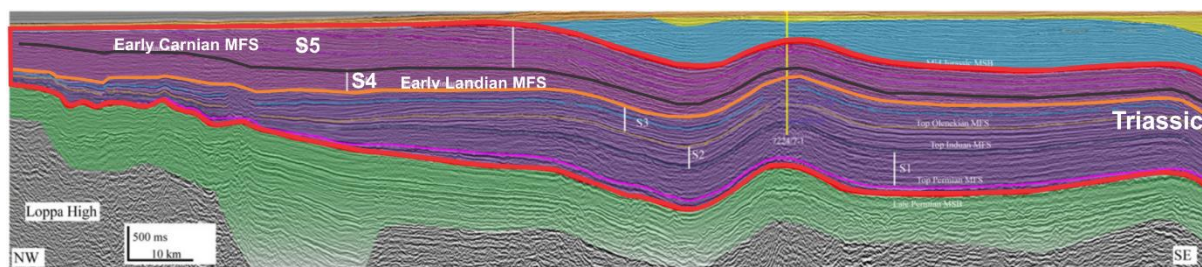
Figure 39. A northwest to southeast seismic line towards paleo-Loppa High showing the Triassic succession within one megasequence (outlined by red polygon), and displaying a general westward thinning of the Lower to Middle and thickening of the Upper Triassic sequences. Lower (S4) and upper (S5) parts of Snadd Fm, used in this study are identified as well as Early Carnian MSF (maximum flooding surface) and Early Landian MSF, indicating base S5 and base S4 respectively. Modified from (Evy Glørstad-Clark, et al., 2010).

Sassendalen Group

The Sassendalen Group comprises clastic sediments of Early and Middle Triassic age (Figure 40). Dominant lithologies are shales and siltstones with subordinate sandstones and minor amounts of carbonate rocks (Factpages, 2015). The group represents coastal, deltaic to shallow shelf deposits in western Spitsbergen. These coastal sediments grade eastwards and southwards into shelf mudstones. The upper part is very organic-rich. In the southwestern Barents Sea Shelf shallow to deep shelf sediments were deposited. The Sassendalen Group represents a series of stacked transgressive-regressive successions, each formation being initiated by a regionally significant transgression (MORK, 1999).

Havert Formation

The formation consists of medium to dark grey shales with minor inter-bedded pale grey siltstones and sandstones comprising two generally coarsening upwards sequences (Factpages, 2015). Thicknesses are moderate and show no marked trends. Palynomorphs suggest a Griesbachian to Dienerian age. The formation was deposited in marginal marine to open marine settings with coastal environments to the south and southeast (Factpages, 2015).

Klappmyss Formation

Medium to dark grey shales pass upwards into interbedded shales, siltstones and sandstones in the type well (Factpages, 2015). Marginal to open marine environments are indicated, with renewed northwards coastal progradation following the early Smithian transgression (Factpages, 2015).

Kobbe Formation

A basal 20 m thick shale unit passes up into interbedded shale, siltstone and carbonate cemented sandstone (Figure 40) (Factpages, 2015). The formation is defined by coarse proximal facies development, along the southern margin of the Hammerfest Basin and fines towards the basin axis. The formation thickens northwards from 140 m on the Troms - Finnmark Platform (Factpages, 2015). Thicknesses vary more from platform to basin than in the underlying units. An Anisian age is suggested, with a probable break in deposition in the early and/or late Anisian.

Snadd Formation

The Triassic sedimentary succession includes Snadd Formation, which was deposited in relatively quiet tectonically settings (Evy Glørstad-Clark, et al., 2010; Gabrielsen Roy H, et al., 1997; Jan I. Faleide, et al., 1993). The Snadd Formation overlies Kobbe Formation and is characterized by relatively thick and wide-spread sedimentary package of non-marine origin, which comprises river deposits. The base and top of Snadd Formation are both defined by regional marine flooding surfaces marked by thin anoxic mudstone above shallow-marine and non-marine deposits, which followed by terrigenous strata in the Snadd and the overlying Fruholmen Formations (Tore Grane Klausen, et al., 2015). The lower part of Snadd incorporates a Landian to Early Carnian interval (S4). The Ladinian sequence represents relatively distal marine environments, following a major transgressive trend and is dominated by marine shele and siltstones. The Landian succession is followed by an Early-Carnian interval. The Carnian is marked by extensive westward coastal progradation and the development of continental and coastal plain environments (Smelror, M., et al., 2009). Late Carnian to Norian constitute upper Snadd succession (S5).

The Landian to Norian Snadd fm in the Barents Sea comprises a thick, up to 1500 m siliciclastic interval dominated by fluvial deposits, with periods of flooding (A. Dalland, et al., 1988). Basal grey shales coarsen up into shales with interbeds of grey siltstones and sandstones. Limestones and calcareous interbeds are relatively common in the lower and middle parts of the unit, while thin coaly lenses are developed locally further up. Distinctive dusky red-brown shales occur near the top of the unit. The unit contrasts with under- and overlying sequences in terms of palaeogeographic controls

on sedimentation patterns, perhaps reflecting updoming of northern shelf margins. The Snadd fm is associated with large-scale channel sandstone bodies, of different size and extent. Late Jurassic to Early Cretaceous rifting, Late Cretaceous uplift and subsequent Neogene uplift and erosion has locally removed much of the upper part of the Snadd fm on the Loppa High (E. Henriksen, et al., 2011). Pleistocene glacial sediments cover the Mesozoic succession with a thick wedge of sediments along western margin (Faleide, J. I., et al., 1984).

Fruholmen Formation

Basal grey to dark grey shales pass gradually upwards into interbedded sandstones, shales and coals (Factpages, 2015). Sand dominates in the middle of the formation in several wells, while the upper part contains more shale. The base of the formation is early Norian. The top corresponds in general to the Triassic/ Jurassic transition.

3.5.3 Cenozoic

3.5.3.1 Paleogene

Sotbakken Group

The group shows thickness from approximately 300 m near the southern margins of the Hammerfest Basin, to approximately 1 km in the most sorthwestern wells in the basin (Factpages, 2015). It is dominated by claystones (Figure 40), with only minor siltstone, tuffaceous and carbonate horizons. Due to the fact that large areas of the Barents Shelf east of the Senja Ridge were uplifted and subjected to erosion, the upper part of the Sotbakken Group is not preserved in the eastern parts of Tromsøflaket. The lower parts are probably present throughout the Barents Shelf, but younger sequences are only preserved over the Ringvassøy - Loppa Fault Complex and in the Tromsø Basin (Factpages, 2015).

Torsk Formation

Light to medium grey or greenish-grey generally non-calcareous claystones with rare siltstone/limestone stringers dominate in the type well (Factpages, 2015).

3.5.3.2 Neogene

Nordland Group

Its upper boundary is the sea bed and sequences itself is mainly of glacial and post-glacial origin. Sand and clays grade into sandstones and claystones, the sand content increasing upwards (Factpages, 2015). Cobbles and boulders of quartzite, granite and different metamorphic rocks occur with clay in the upper parts of the group. The clay is grey to greyish greeen, soft to firm, blocky, non-calcareous, and in parts silty (Factpages, 2015). The base of the group coincides with the Oligocene unconformity (Figure 40).
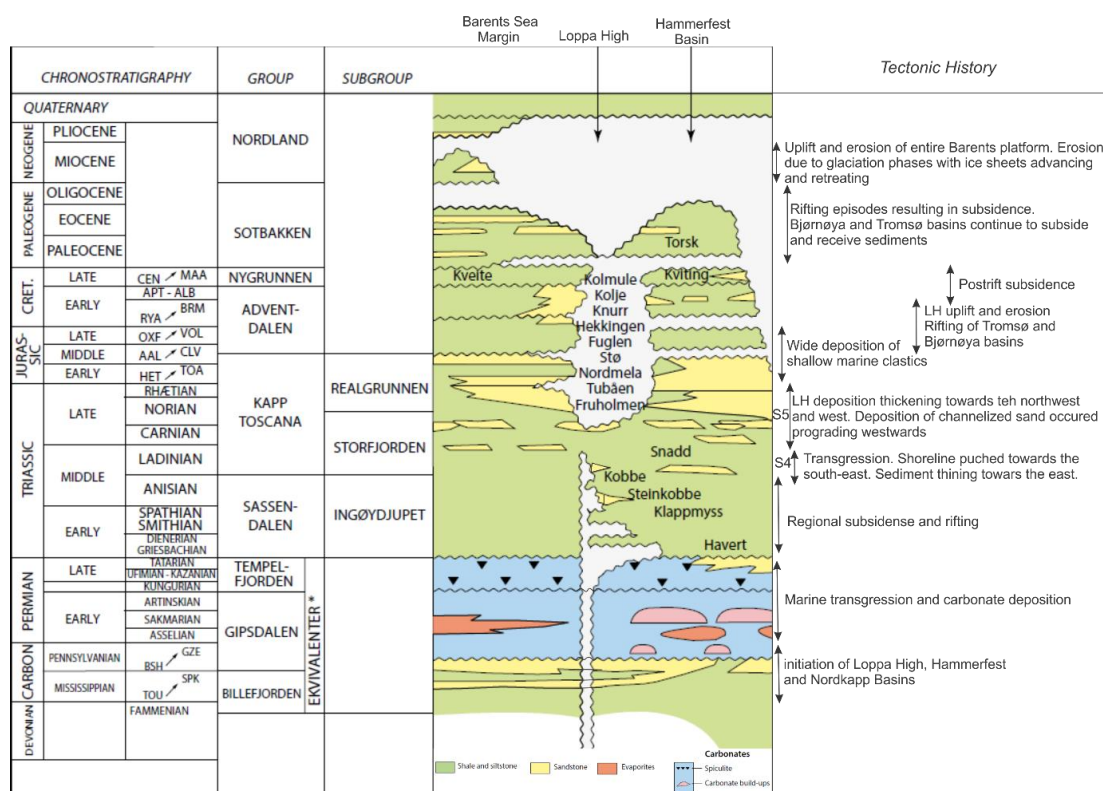
Figure 40 Chronostratigraphic chart of the study area with the Triassic S4 and S5 (Evy Glørstad-Clark, et al., 2010) second-order sequences. Modified from (E. Henriksen, et al., 2011).

Chapter 4 Data and Methods

4.1 Data

The dataset used for this work consisted of 3D processed seismic cube in SEG-Y format. The seismic dataset LN09M01 (Figure 41) from south-west of the Barents Sea acquired by Lundin. This seismic volume corresponds to an area of 298.94 km2.
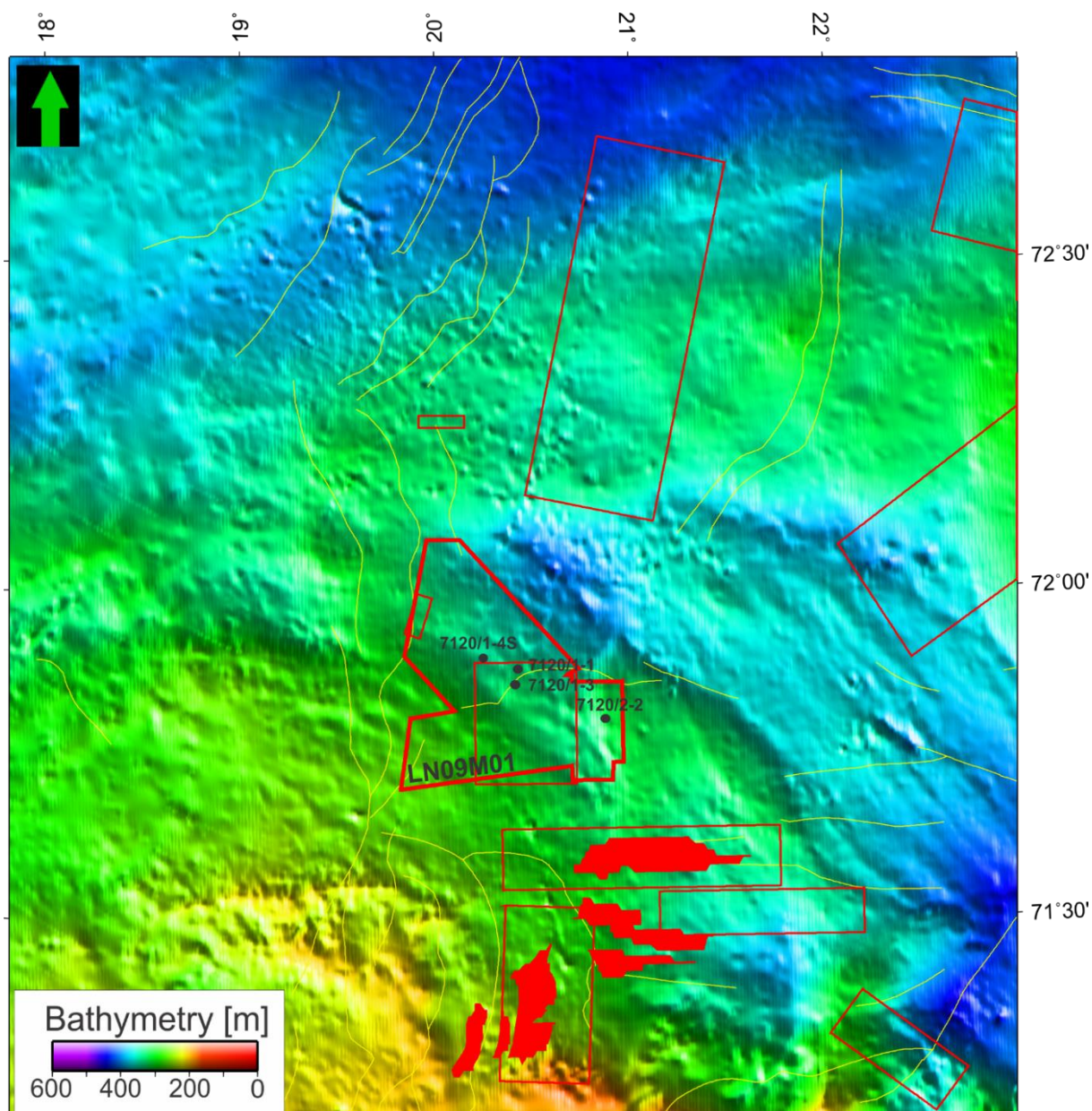

Figure 41 Overview map of the study area with geological structures and location of different datasets. 3D survey LN09M01 with location of wells in the area is highlighted by thick red polygon.

Dominant frequency of this dataset across the interval (from the seafloor to 1500 ms two-way-time (TWT)) (Figure 42). The data appears to be excellent in quality, shown by relatively high signal level and a broad frequency bandwidth between 5-70

HZ with flat top frequency distribution. Dominant frequency at the top of the flat top is at 34 Hz at -16 dB, in a travel time window of 0-1.5s (Figure 42).
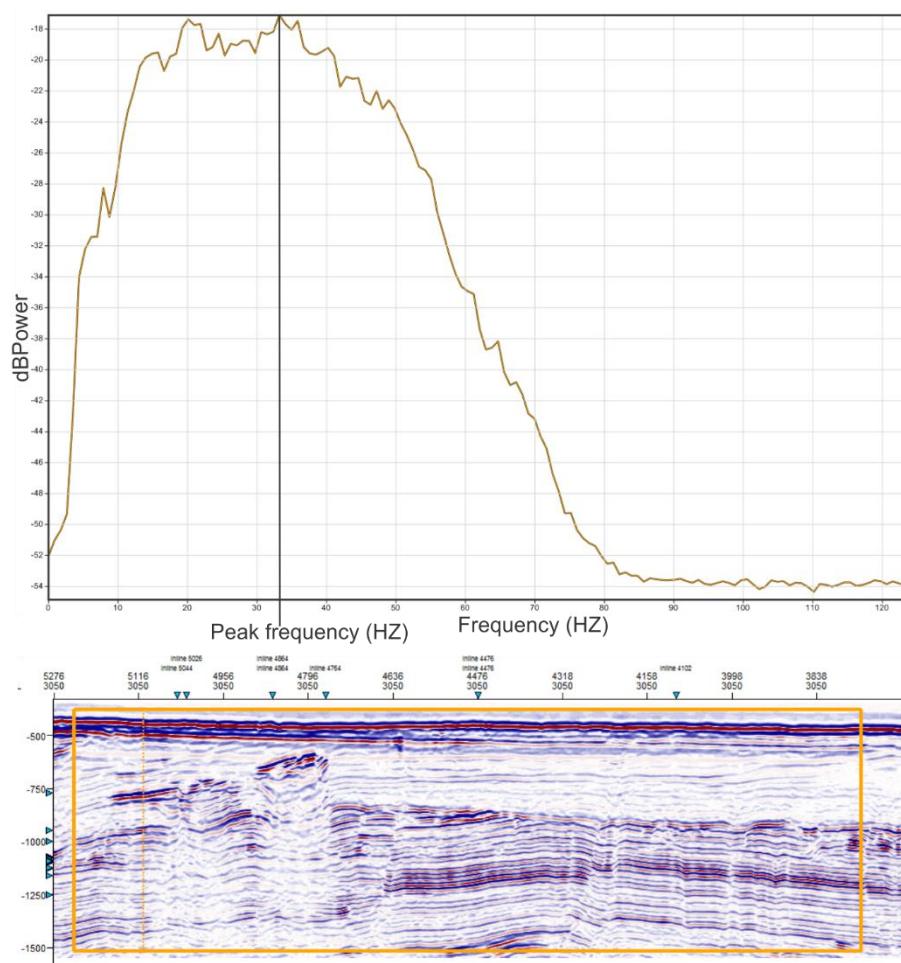

Figure 42 Spectral analyses from dataset LN0901 have flat top with dominant frequency of 34 Hz and a frequency spectrum of 15-40 Hz.

Various variance attributes were generated over the entire 3D seismic volume to define potential channel systems locations in the study area. Multi-attribute algorithm is an intensive process for the computer-processor and in order to reduce time consumption for computing various attributes and for easies manipulations of the data seismic cube was cropped to small volumes around areas of interest identified through several time-slices from the variance attribute volume. Cropping is an operation used reduce the cube volume in X, Y and/or Z domain and/or skip inlines and crosslines. The result is a smaller cropped volume that is faster and more suitable to work with, which greatly spares time of the testing. The process of realization must be carried out at the first place. Realization increases memory-loading speed and

converts original 32-bit 3D seismic cube into 16- or 8-bit format (Petrel, 2009), (Schlumberger, 2007). The delineated area has approximately 171.14 km2 and it was the base to apply various seismic attributes (Figure 44).
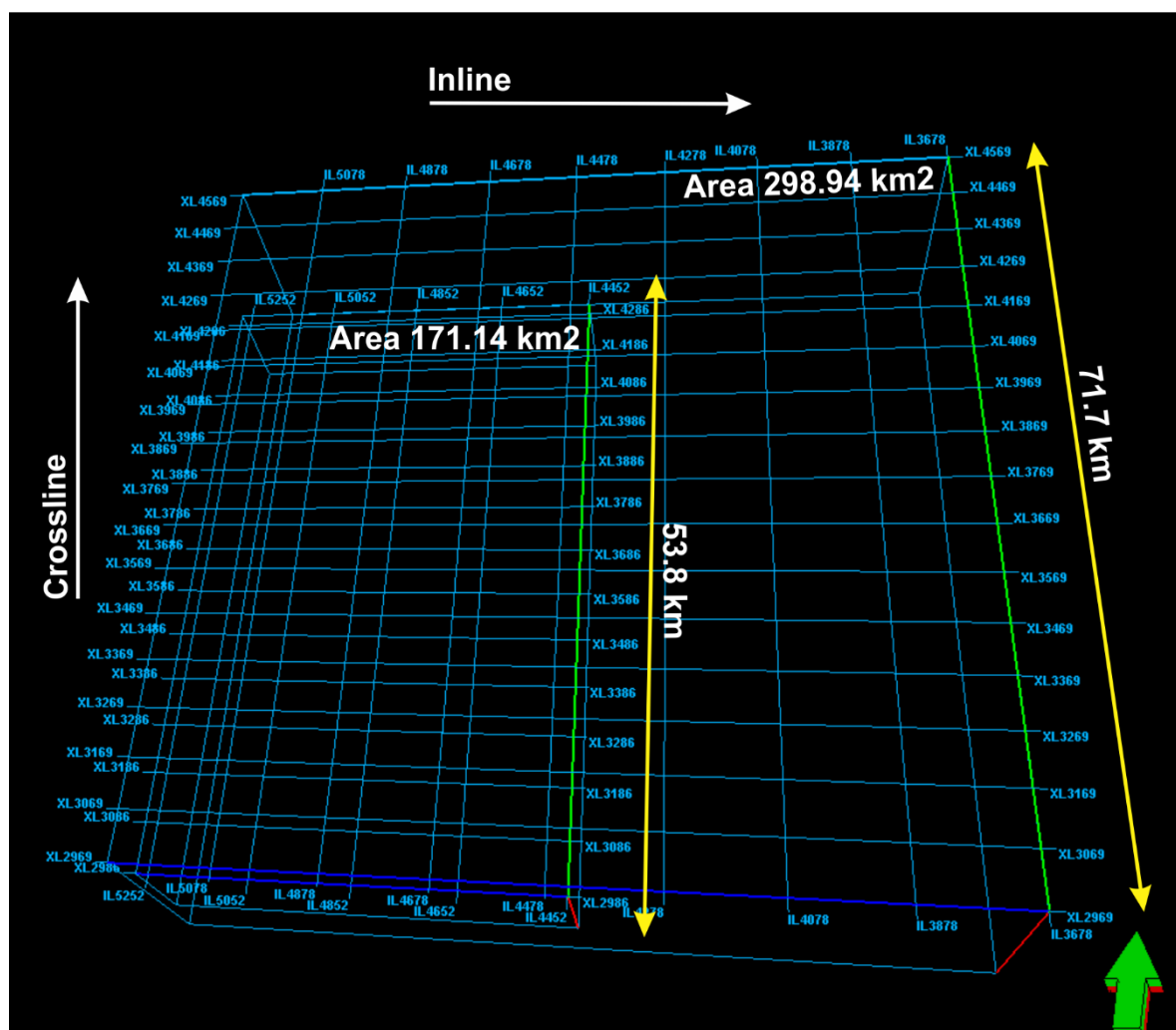

Figure 43 Grids of inlines/crosslines of the original and new cropped seismic cube used as a work base to compute seismic attributes.

The adopted methodology for this work was focused on improving definition, delineation and interpretation of stratigraphic targets of Triassic channels, the complexity of which in the region makes interpretation of original 3D seismic data challenging. The workflow was implemented and applied to improve imagining of channel features. It comprises data conditioning, attribute generation and advanced visualization methods as outlined in Figure 48.

4.2 Seismic resolution

Seismic data is an important tool when studying palaeo-environments and geomorphology (Rafaelsen, 2006). There are two aspects of seismic data resolution: vertical and horizontal, where both are depended on the frequency, velocity and wavelength of the signal. Resolution is the ability to distinguish between two individual reflectors (SHERIFF, 1997). The resolution depends on the seismic wavelength, which is determines by the formula wavelength=velocity/frequency ($\lambda = V/f$) (Andreassen, 2009). Seismic velocity increases with depth because of the processes of burification and compaction, and the frequency, on the hand, decreases with depth as seismic signals get more quickly attenuated (Brown, 1999). This results in poor resolution and increase in the wavelength with depth.

4.2.1 Vertical resolution

Vertical seismic resolution is a measure of thickness of a bed, so that reflections from top and base can be distinguished (SHERIFF, 1997). The vertical resolution is defined by the limit of separation, which is often given as ¼ of the wavelength, where wavelength is given by the equation $\lambda = v/f$. If the thickness of sedimentary package is thinner than $\lambda/4$, reflections begin to overlap and interfere (Andreassen, 2009). This is the closest separation of two wavelets in order to be distinguished.
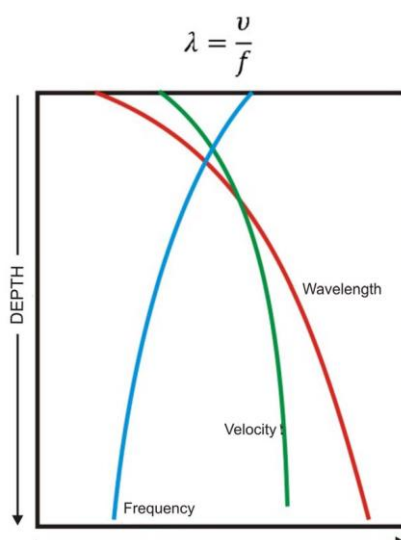

Figure 44 Relation and variation of frequency, velocity and wavelength with depth, and how they change. With increasing depth an increasing wavelength, increasing velocity and a decreased frequency can be observed. Figure modified from (Brown, 1999).

To improve vertical resolution, one has to shorten the wavelet shape, which requires higher frequencies or shorter wavelength. Relation and variation of frequency, velocity and wavelength are outline in Figure 44. The vertical resolution is calculated for the dataset with an average assumed velocity of 2200 m/s and a dominant frequency of 23 Hz:

$$\lambda = \frac{v}{f} = \frac{2400 \ m/s}{34 \ Hz}$$

$$\lambda \times \frac{1}{4} = \frac{1}{4} \times 70.5 \ m$$

Where λ is wavelenght (m), v is velocity in sediments (m/s), f is dominating frequency (Hz).

4.2.2 Horizontal resolution

As the wavefront affects considerable area of reflectors surface, the resulting reflection is produced from a circular zone, determined by the Fresnel zone (FZ) (Andreassen, 2009) (Figure 45). To distinguish lateral elements from each other on seismic data, the elements have to be greater than the FZ. Two elements falling within the radius of the FZ are so small that they cannot be seen on the seismic data. Migration is the principle technique used to improve the horizontal resolution. As the result of applying this technique FZ will be reduced to an ellipse perpendicular to the line using 2D migration, and a small circle for 3D migration (Figure 45).
The magnitude of the Fresnel zone can be approximated from the relationship:

$$rf = {v}/{2} \left({t}/{f}\right)^{1/2}$$

Where rf is radius of the Fresnel Zone, v is average velocity, t is two-way travel time in seconds, and f is dominant frequency in Hertz.

This equation shows that with increasing depth and velocities, and lower frequencies the resolution is getting poorer, while higher frequencies give better resolutions (Andreassen, 2009). Migration of the seismic data will further reduce the Fresnel Zone, to an ellipse perpendicular to the line for 2D migration and a small circle by 3D migration (Figure 45) (Rafaelsen, 2006).
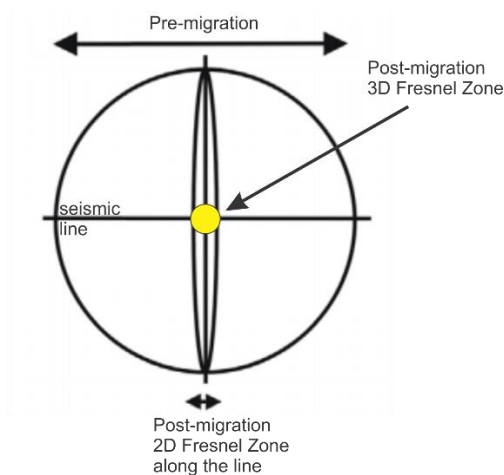
Figure 45 The focusing effect of migration in two and three dimensions. The Fresnel zone will be reduced to an ellipse perpendicular to the line for 2-D migration and to a small circle by 3-D migration. Modified from (Rafaelsen, 2006).

The vertical and horizontal resolution for 3D seismic data set in this study is listed in table. Peak frequency of 34 Hz has been applied for calculations. The calculation of dip is done at -1500 ms TWT, this will be used for horizontal resolution limit.

Table 2 Vertical resolution is calculated as wavelength=velocity/frequency, and that vertical resolution is λ/4. Peak frequency for a crop volume in 3D seismic data set is set to be 34 Hz. Horizontal resolution is calculated from Rf = (V/2) (t/f)1/2, where two-way-travel time for 2400 m/s is 1, 5s (well 7120/1-1).

Domiuat frequency (Hz)	Lithostratigraphy	Wavelength $X = V/f$	Vertical resolution	Horizontal resolution
34	Snadd Fm (2400m/s)	70.5 m	17.6 m	207.3 m

4.3 Well data

The lithostratigraphy within the seismic has been calibrated and determined from exploratory well data (7120/1-1). Well (7120/1-1) is located within the LN09M01 dataset (Figure 46). Well data from this well has therefore been used to correlate and interpret reflectors. The different formations penetrated by well (formation tops) gather from the well data are listed in Figure 46, and for this well can be identified with acceptable confidence to seismic correlation. The information of the different formations and their depositional environments stems from well information from NPD`s fact pages, along with the use of additional literature.

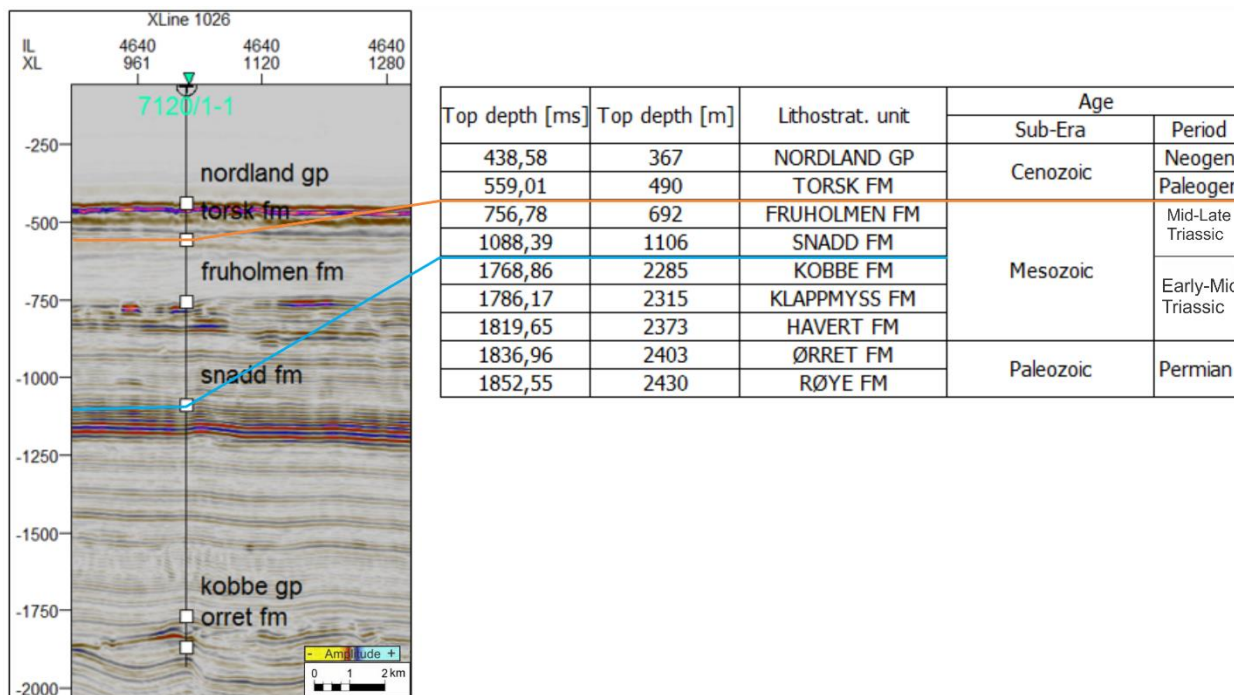| Top depth [ms]	Top depth [m]	Lithostrat. unit	Age	
			Sub-Era	Period
438,58	367	NORDLAND GP	Cenozoic	Neogen
559,01	490	TORSK FM		Paleogen
756,78	692	FRUHOLMEN FM	Mesozoic	Mid-Late Triassic
1088,39	1106	SNADD FM		
1768,86	2285	KOBBE FM		Early-Mid Triassic
1786,17	2315	KLAPPMYSS FM		
1819,65	2373	HAVERT FM		
1836,96	2403	ØRRET FM	Paleozoic	Permian
1852,55	2430	RØYE FM		

Figure 46 Formation tops within the survey LN09M01 of well 7120/1-1, and their ages (modified from NPD.no). The Snadd Formation ranges in two-way travel time between -1088 ms to -1768 ms with an average interval velocity of 2417m/s calculated from acoustic well log data.

4.4 Methods

In this master thesis three programs have been successfully used, Schlumberger Petrel 2014, Geoteric 2015 and CorelDraw X6. For interpretation of horizon and structural elements in the seismic volume, horizon interpretation, surface attribute and volume attributes Schlumberger Petrel 2014 along with Geoteric 2015 have been used. CorelDraw X6 was used for figures and editing purposes.

4.4.1 Petrel as geofluid interpretation tool

Schlumberger is the worldwide biggest company providing oilfield services on technology, information solution and integrated project management to consumers working worldwide in the oil and gas sector (slb.com). Petrel has been developed by Schlumberger in 1996, and since then many upgrades have been done from version to version in order to improve algorithms (Petrel, 2009). The data analysis was carried out at the University of Tromso. The Petrel software platform 2014 from Schlumberger was used as the interpretation and visualization tool. Petrel provides interpretation of horizons, structural elements and anomalies in the time-domain data on 3D seismic uses cross sections, 2D windows and 3D window with several different parameters

such as various seismic traces, attribute maps and seismic attribute analyses, volume cubes.

4.4.2 Geoteric

GeoTeric is a 3D interpretation software which directly translates geophysical data into geological information (GeoTeric, 2015). Geoteric has been used as interpreter guided approach for understanding and defining the 3D morphology of the geological elements imaged within the seismic data. GeoTeric is renowned as a market-leading innovator, establishing new standards for interpretation by bringing game changing Geological Expression workflows to the industry (GeoTeric, 2015).
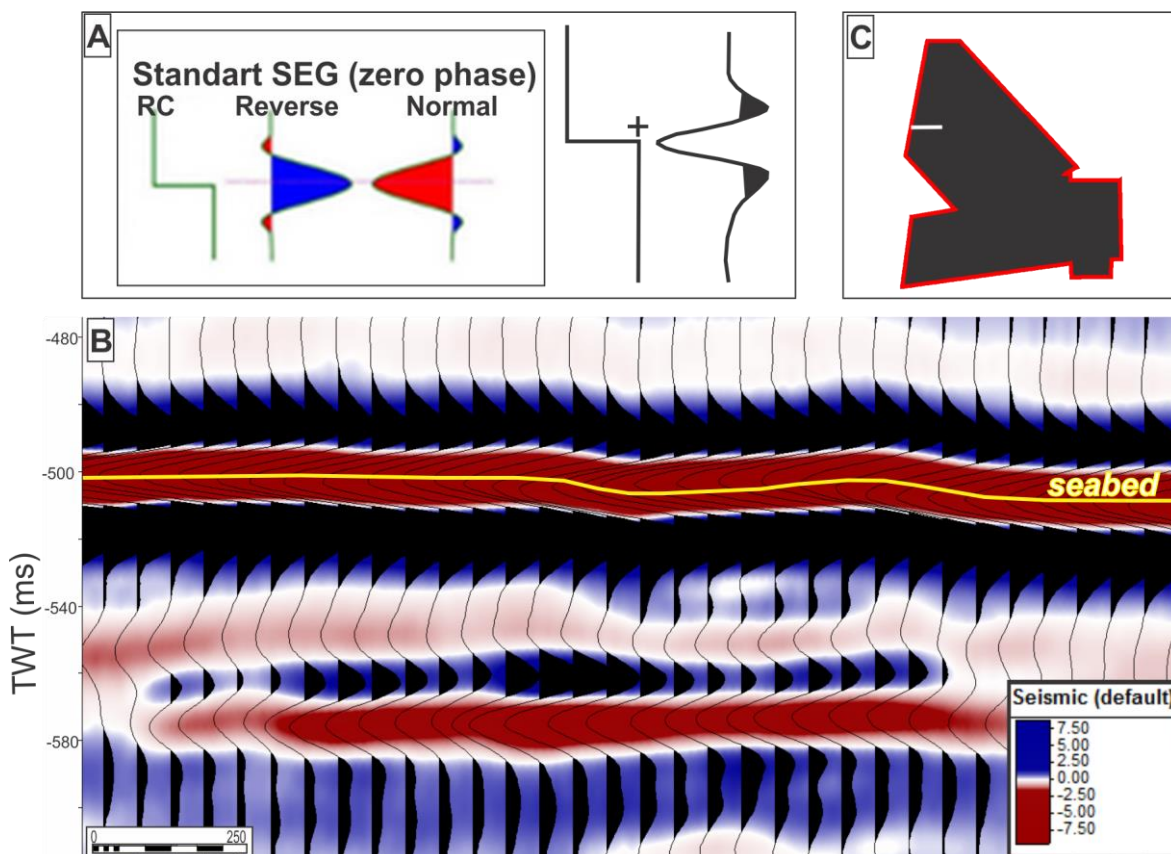

Figure 47 A) SEG standard polarity. For strong or positive reflection starts with a wave of minimum-phase (to the right) with negative trough. The seismic signal where trough is red, peak is blue and zero crossings (upper and lower) are white. Figure modified from (Sheriff, 2006) . B) Seismic cross-section of survey LM09M01, showing dataset being processed to zero-phase normal polarity signal. C) The white line indicates the position of the seismic cross-section in B.

4.4.3 Interpretation of 3D seismic data

Seismic interpretation involved a combination of basic methods in horizon interpretation: 1) Manual interpretation; 2) Guided autotracking; 3) Seeded 2D

autotracking; 4) Seeded 3D autotracking, as well as voxel-growing technique. For the purpose of this thesis the seeded 2D autotracking was appropriate and therefore mostly used. On which type of reflection the interpretation will be done is chosen manually; peak, trough, upper zero crossing or lower zero crossing (Figure 47). In this study the reflection, peak or trough, with the best continuity and the largest lateral extent was chosen for each of the horizons. To get a good interpretation it is recommended to start using restricted parameters, to interpret strong continuous reflections first. The seed confidence was therefore set to 80% to reduce the possibility of a misinterpretation. The interpretation was normally done for every 10th inline and cross line, depending on the continuity of the reflector. The seismic trace is visualized in Petrel as standart SEG zero-phase normal European polarity (SEG reverse) display for single pulse (Figure 47). The target channels were imaged using random seismic lines along, and perpendicular to, the channel axis (long profiles), together with a variety of attribute maps.

4.4.4. Workflow methodology

Advanced 3D seismic analysis methods was applied to Loppa High area. The methods applied were focused on improving definition, delineation and interpretation of stratigraphic targets of Triassic channels. The complexity of which in the region makes interpretation of original 3D seismic data challenging. The workflow was implemented and applied to improve imagining of these features. It comprises data conditioning, attribute generation and advanced visualization methods as described below and outlined in Figure 48. Geophysical data was performed using Geoteric software by applying four basic methods according to workflow schema: 1) Data Conditioning, 2) Stratigraphic Expression (High Definition Frequency Decomposition and multi-attribute colour blending), 3) Structural Expression (Multi-attribute Structural Expression), 4) Adaptive Interpretation (Geobody extraction).
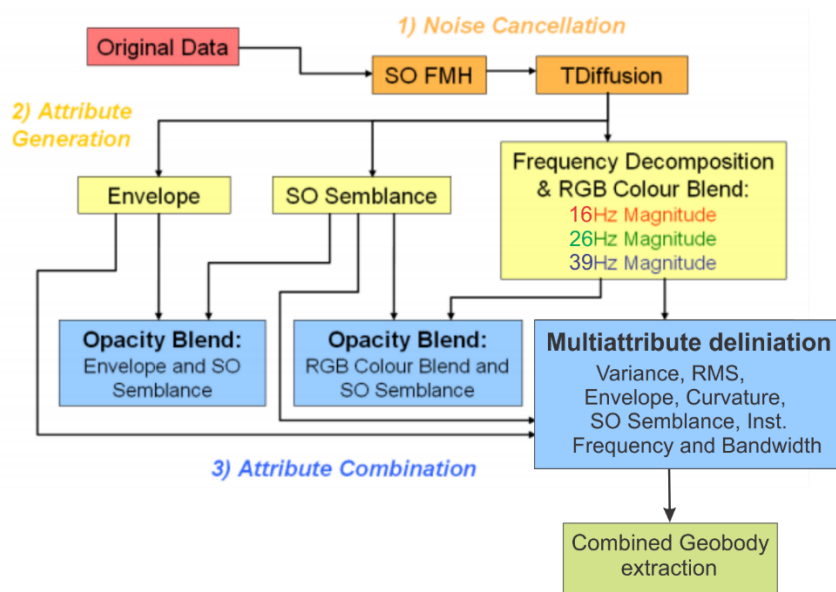
Figure 48 Workflow methodology applied in this work.

4.4.4.1 Data conditioning/Noise cancellation

Unwanted variations in data can arise from both acquisition and processing effects, and even though the seismic data is of good quality, the presence of noises is obvious by close inspection. The noise cancellation algorithms are designed to preserve all the useful for further interpretation information by aligning structurally oriented and adaptive-noise-cancellation filters with reflectors (McArdle Nickolas, et al., 2011). Noise reduction, or data conditioning, therefore becomes a very important step in the initial data processing (Alison T. Henning, et al., 2010).

My input data consists of a 3D post-stack seismic data volume from Barents Sea, which was acquired Lundin, focusing on channel systems. Channels are visible in the reflectivity data as high amplitude zones with continuous lower amplitude reflection events (Pavel Morozov, et al., 2013). By applying noise cancellation, I aimed to achieve a high level of continuity along the continuous reflectors, improve fault expression, and remove jitter effects and noise. Different filters have been used to attenuate noise, such as SO FMH (Structurally Orientated: Finite Median Hybrid), TDiffusion, and SO Noise Filter. Noise cancelled volumes, which are the products of single filter application on original data, have been carefully inspected and conclusion has been made, that it is imperative to run SO FMH filter to remove coherent noise before the TDiffusion filter to remove random noise.

It can be seen that in Figure 49 B below, noise that was present has been removed, reflectors are more continuous, while preserving signal and edges, faults are well seen and jitter effect has been attenuated. The difference volume using Voxel math process has been used to visualize and examine the noise removed from original data set (Figure 49 c). The improvement of noise cancelled data set, its degree of smoothing and distortion caused by application of noise cancellation filters can be judged by simply subtracting filtered image from the unfiltered one using Voxel math.

On the Figure 50 and Figure 49 the resolution of the final noise cancelled data set is tremendously improved as well as the lateral continuity. Jitter trending along most of the reflectors has been removed. On Figure 50 A, B original data versus noise cancelled data is hsown, where (A) Vertical seismic section after noise cancelling filters SO FMH and TDiffusion have been applied, (B) Vertical seismic section prior to noise cancelling.

4.4.4.2 Multiattribute analysis

Multiattribute approaches to seismic attribute analysis focus using number of individual attributes to create a clearer picture and complete description. All individual attributes were calculated on data conditioned 3D seismic volume. Attribute were chosen and tuned to enable the edges and internal architecture of the target stratigraphic features. The attribute 3D seismic volumes were sliced in depth and depth slices were examined. Numerous channels at different stratigraphic levels and typical elements of channel systems including levees, crevasse splays and ribbon-like channel belts. Seismic attributes that are most distinguished means and sensitive to mapping channel edges are curvature, frequency, variance and SO Semblance. Various other attributes were calculated, but are not displayed here. In general, they did not provide insight into the channel-levee systems. By the advancement to the seismic attributes, HD and Standard frequency decomposition has also been used to highlight the channels. Frequency or spectral decomposition and RGB blending have become powerful tool which aides in the imagining and mapping of geological both structural and stratigraphic changes in the geology that are represented by frequency variations along the reflected signal (Pavel Morozov, et al., 2013). Visualizing each frequency response independently reveals very limited amount of useful for interpretation

information, however when three frequency magnitude responses are combined using RGB (Red-Green-Blue) color bar, the interplay between different frequency responses becomes descriptive (Ingelise Schmidt, et al., 2013) and thus give a more detailed planview attribute image than conventional full-frequency amplitude extraction such as RMS amplitude (Tore Grane Klausen, et al., 2014).
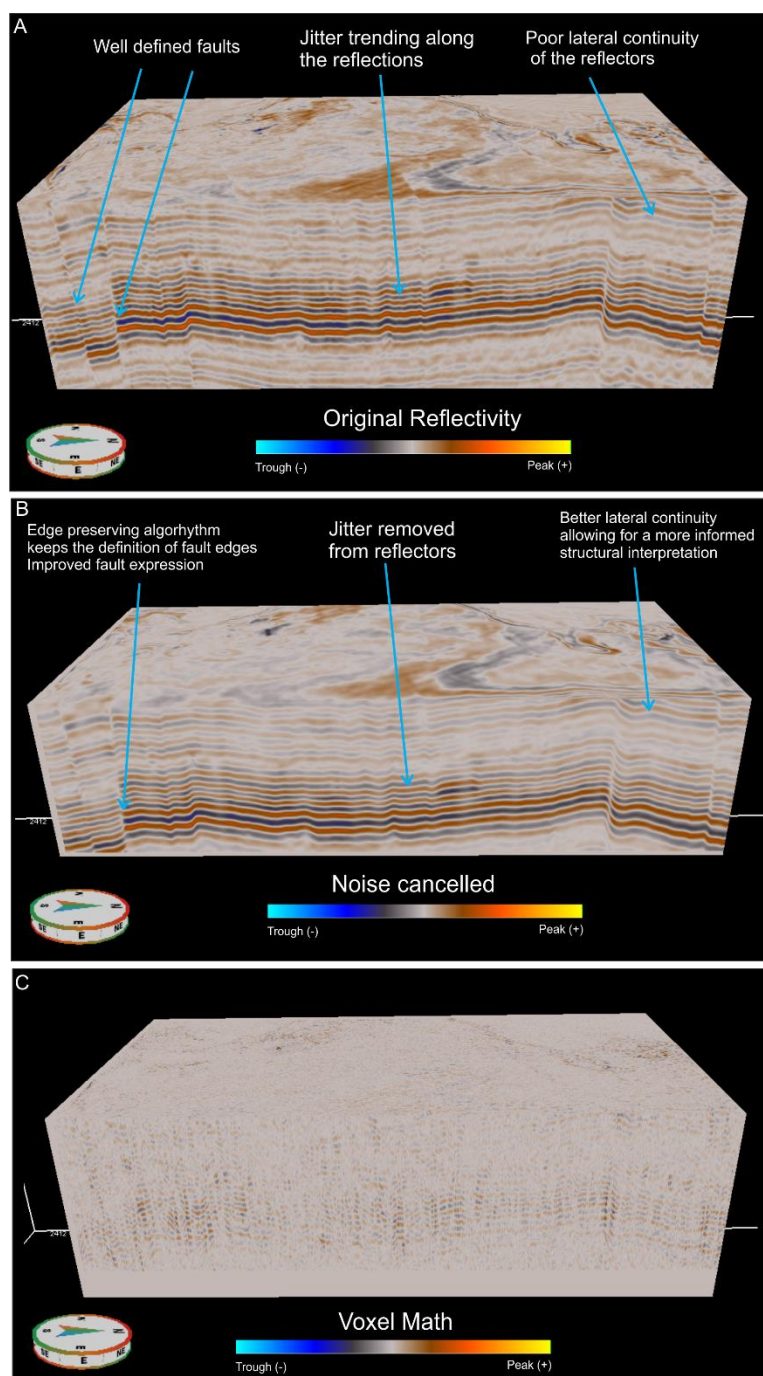

Figure 49 Result of noise cancellation of the seismic dataset. A) Seismic reflectivity data set prior to noise reduction, B) Data following application of SO FMH and TDiffusion filters, C) Result of subtracting the noise filtered data set from the original data set using VoxelMath. Inline 4740
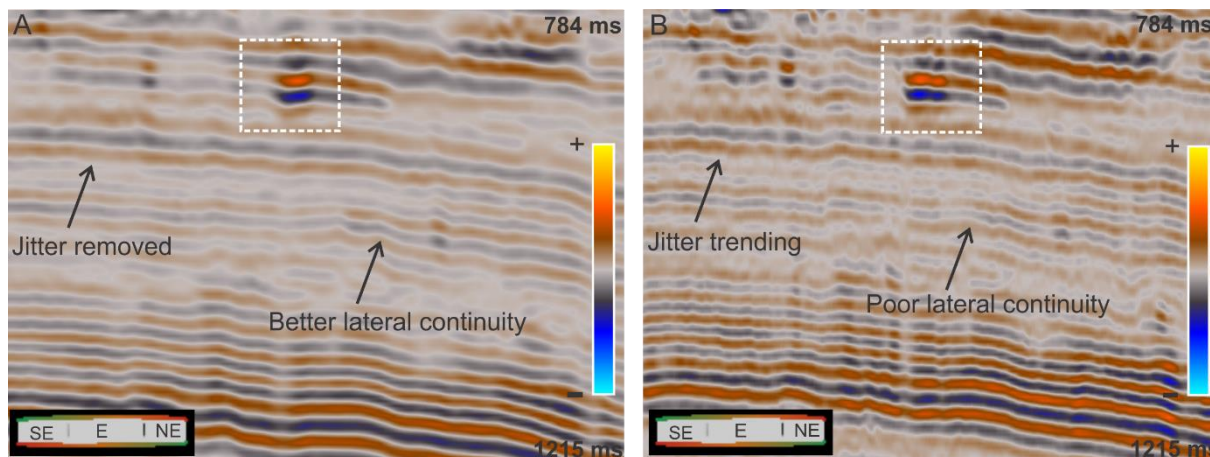
Figure 50 Original data versus noise cancelled data. A) Vertical seismic section after noise cancelling filters SO FMH and TDiffusion have been applied, B) Vertical seismic section prior to noise cancelling. The dotted rectangle highlights the interval of fluvial deposits. Inline 4764

4.4.4.2.1 Volume attributes

Variance

The variance attribute is an edge imaging and detection method, since it measures lateral changes in the seismic response caused by variation in structure and detecting lateral discontinuities in the change in acoustic impedance (dissimilarity of seismic data) (Pennington, 2002). Variance can be used in interpretation of faults and folds, depositional envornment and stratigraphy, such as channels and bedding characteristics (Chopra, 2006). Values of variance which are equal to 1 mean discontinuities within a continuous seismic even represented by zero values. When calculating variance, dip and azimuth values must be defined.

Envelope

Evelope or reflection strength attribute, is very well known seismic attribute. Envelope is defined as total absolute valueof the energy signature of the entire trace and represent mainly acoustic impedance contrast and hence reflectivity (D.Subrahmanyam, 2008). Changes in the amplitude strength in may reflect changes in lithology and pore fluid content (Chopra, 2006). High envelope values appear due to major lithological changes and sedimentary sequences boundaries, whereas gradual lateral changes of envelope are correlated with lateral lithology variations. Lithologic changes are enhanced by envelope attribute.

RMS

RMS or "Root mean Square" amplitude is a measure of reflectivity. RMS amplitude maps may be useful as indicators for porous lithologies, fluid accumulation areas and geological features due to amplitude response, and is an important attribute for characterizing different sedimentary environments (Petrel, 2009).

Curvature

Curvature is one of the discontinuity attributes and is a measurement of bending (dip) or how deformed a seismic reflections is at particular point (Chopra, 2006), (Lucia Torrado, et al., 2014). Features that have undergo differential compaction rate can also be revealed by curvature attribute.

SO Semblance

As a part of structural attribute analysis, a structurally oriented SO Semblance edge attribute was generated in Geoteric and was mainly chosen to highlight channels edges.

4.4.4.2.2 Surface attributes

In this work, an interpretation of the upper and lower channel boundaries of the target channel systems was attempted using manual interpretation of closely spaced inlines/crosslines. Using 3D noise cancelled seismic cube was the best approach to create reliable surface. Attribute maps, or surface attributes, were extracted from interpreted surfaces. RMS, Envelope and Gradient Magnitude attributes were extracted using different search window above or below boundary of interpreted surface. The surface attribute extract values was used in this master thesis allow to better present the seismic interpretation of features. Extract values are favorable to extract the input seismic value relative to a single horizon (Schlumberger, 2007). An interpretation of the surface of the target channel system was done by manual interpretation of closely spaced set of inlines/crosslines.

4.4.4.2.3 Frequency decomposition and RGB blending

Frequency or spectral decomposition has become powerful tool which aides in the imagining and mapping of geological both structural and stratigraphic changes in

the geology that are represented by frequency variations along the reflected signal (Pavel Morozov, et al., 2013). Visualizing each frequency response independently reveals very limited amount of useful for interpretation information, however when three frequency magnitude responses are combined using RGB (Red-Green-Blue) color bar, the interplay between different frequency responses becomes descriptive (Ingelise Schmidt, et al., 2013). The amplitude response at different frequencies tunes in to specific bed thickness, which helps highlight faulted areas, interpret discontinuities and delineate channels with more confidence (Lucia Torrado, et al., 2014) (Chopra, 2006). Changes in thickness, lithological and fluid variations causing acoustic impedance variations is one of the main cause of frequency variations in seismic data (McArdle, 2013).
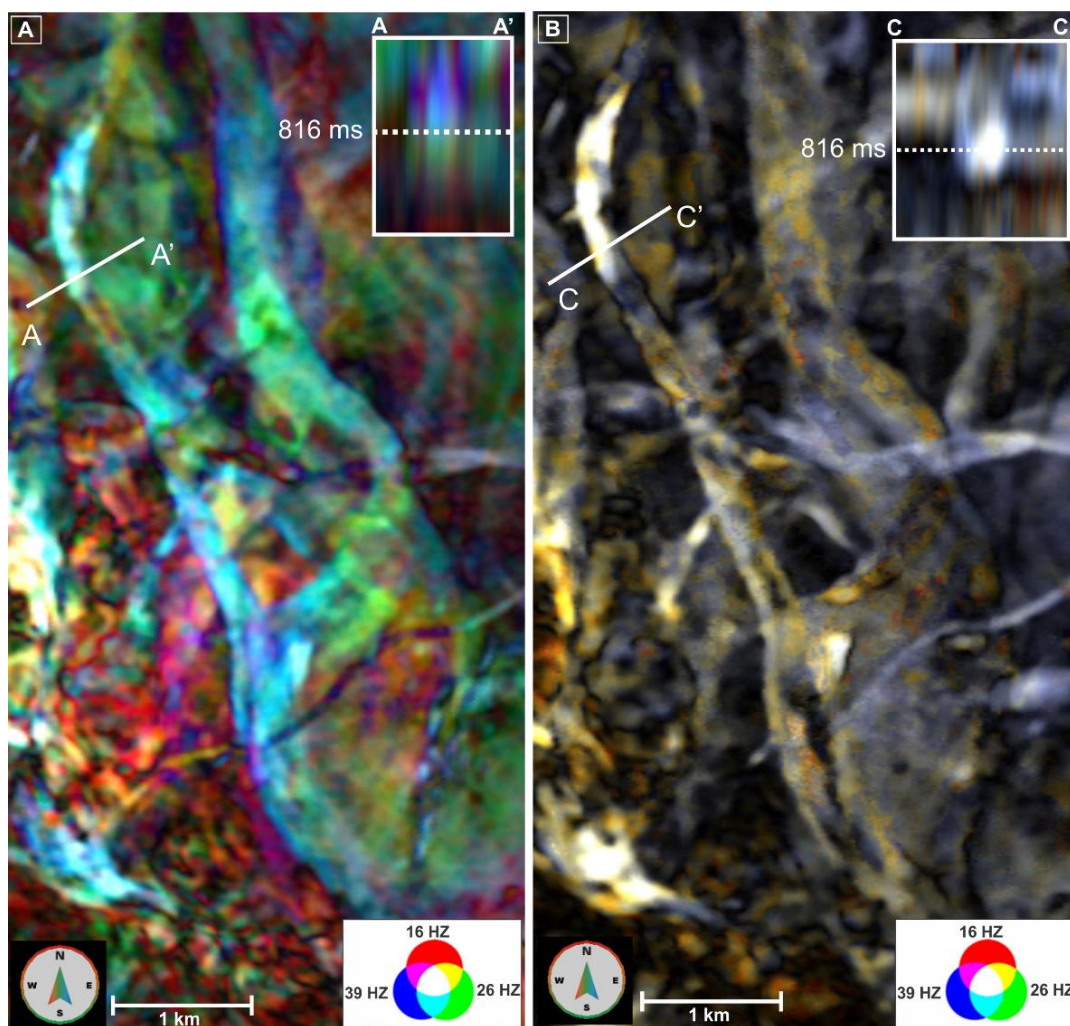

Figure 51 Comparison of Standard (A) and HD (B) RGB blends composed of frequency decomposition showing channel system imaged 816 ms below seabed. A) Standard frequency decomposition better identifies the elements of the flow. B) High Definition Frequency Decomposition is less precise in detail laterally, but gives a clearer deep understanding of the position of the sedimentation components.

Low frequencies are assigned to as red, mid - green, high frequencies – blue, and blended to look at the interplay between different frequency information. As a result of superposition, it becomes possible to identify portions of the wave field with a predominance of individual frequencies in the RGB color space. Methods for combining multiattribute information can include the use of visual (color and opacity blending) techniques, which are well established in seismic attribute analysis (McArdle Nickolas, et al., 2011). In fact, the white or grey colors indicate a strong response (high frequencies) from all three frequencies involved in summation (Pavel Morozov, et al., 2013), which may be exhibited by thinly laminated shale (Tayyab Muhammad Naseer, et al., 2014). Black, on the contrary, indicates the low response from all three frequencies (Pavel Morozov, et al., 2013; Ben Kilhams, et al., 2011), and is indicative of more massive bedding geometries, such as sand-prone lithologies (Tayyab Muhammad Naseer, et al., 2014). Standard decomposition (Figure 51) "highlights" core of the system of sedimentation in the lower frequencies (reds). With increasing distance from the center of the sedimentation system, however, the sediment thickness is reduced and the color sum manifests itself in the form of bright white, as the amplitude of the signal increases at all frequencies. Frequency Decomposition methods available in GeoTeric can be divided into two categories: Standard frequency decomposition (constant bandwidth and constant Q) and HDFD technique. Both RGB blends reveal more detail about the channels extent and morphology when compared with single attribute data (envelope). The comparison of Standart and HDFD frequency decomposition applied to noise cancelled data set is shown in vertical cross-sections of RGB color sums (Figure 51), obtained by standard methods (A) and high-resolution spectral decomposition (B). If comparing the sections of AA 'and CC' lines, it's possible to evaluate the vertical resolution of the two decomposition techniques. Here HDFD decomposition has the certain advantage, as it gives clearer picture of the object lateral intervals. As the result, it's possible to get a clear understanding of the deposits thickness and their spatial localization. Both methods can successfully identify channel geometry. Figure 51 also show an example where the application of spectral decomposition on 3D seismic data helped map geometry of sinuous channel system.

4.4.4.2.4 Opacity Blending

Methods for combining multiattribute information can include the use of visual (color and opacity blending) techniques, which are well established in seismic attribute analysis (McArdle Nickolas, et al., 2011). Opacity blending is a visualization technique in which multiple attribute or colour blend volumes can be combined and viewed simultaneously (McArdle N.J., et al., 2010). In fact, the technique showed the best practice and effectiveness in visualization of channel systems when SO Semblance edge attribute is blended with Envelope and frequency decomposition HD RGB blend to allow simultaneous view. (Figure 52). It is very noticeable how opacity blend successfully highlights channels edges and internal morphology, and greater level of information can obtained from this volume.
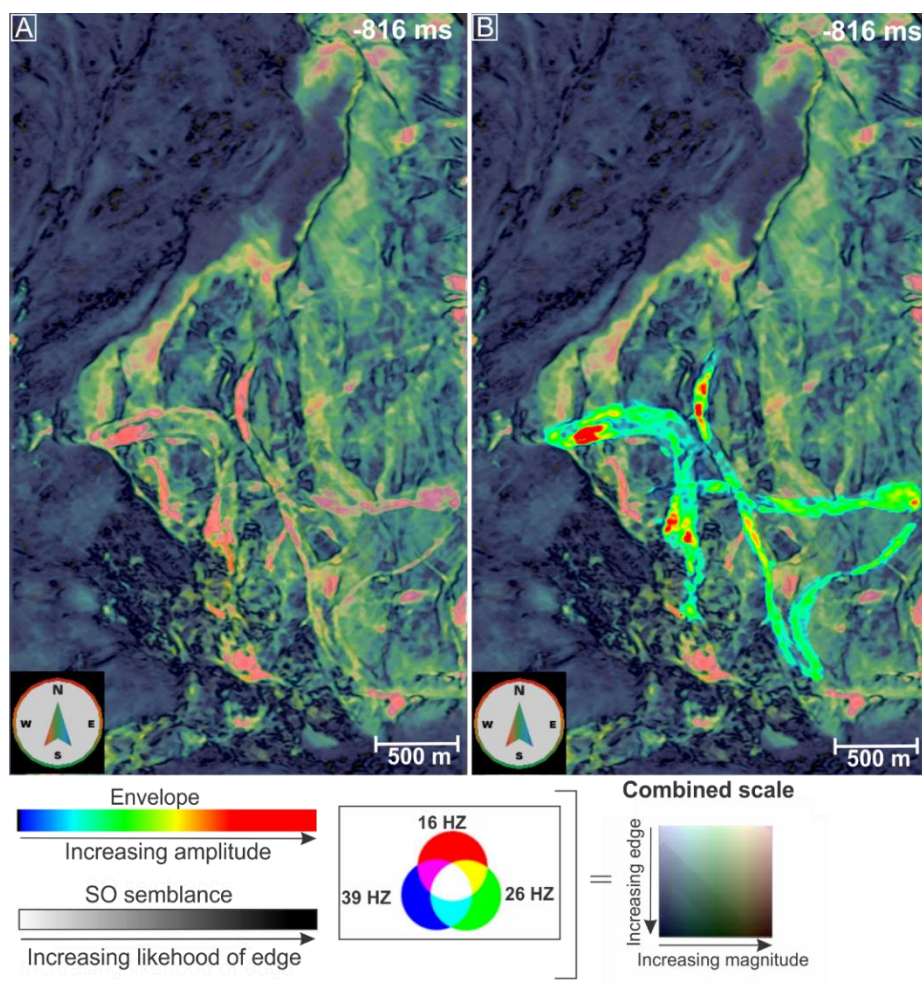

Figure 52 A) RGB, SO Semblance and Envelop opacity blend resolves greater level of extent and infill of the channel features of interest. Combined scale is the result of blending of Envelop, SO Semblance and RGB attributes, used further in this study. B) Envelope "cookie cut" dropped on RGB, SO Semblance and Envelop opacity blend. "Cookie cut" into geobody used as mask, populated with Envelope values.

4.4.4.2.5 Geobody Extraction

Geobody extraction is very useful utility in Geoteric that allows visial extraction of the features of interest. First, 3D geobodies delineation was performed using Body Labelling applied to single Envelope volume. The output of this technique is a volume in which all connected voxels having values within the given threshold range are assigned a label (Jonathan Henderson, et al., 2008), with high envelope values included as geobodies and low values ignored. Eventhough, segmentation of channel systems was done independently, it is evident that neighboring bodies can merge together and smaller bodies occur that are not of geological significance. Another method of Geobody extraction is by tracking the contours of overtime stream wanders through the whole volume independently, and combining extracted geobodies sets into single volume. To focus on data within particular geobogy (channel of interest), geobogy was first converted into a geobody volume, and then information within geobogy volume was extracted from (repopulated with) Envelope attribute data volume (Envelope "cookie cut") to help define the variations in lithology within the geobody. Figure 52 B shows Envelope Cookie Cut into 816 ms geobogy dropped RGB, SO Semblance and Envelop opacity blend.

Chapter 5 Results

5.1 Seismic stratigraphy

Several fluvial depositional elements have been traced out within the study area Snadd Formation interval and interpreted as Triassic in age. Stratigraphic intervals were defined by using exploratory well data (7120/1-1), which is located within the LN09M01 dataset, and correlated by tracing the corresponding seismic reflectors of sequence stratigraphic significance. Complete Triassic succession within Late Permian to Middle Jurassic megasequence was subdivided into sub-sequences (Figure 39), where bounding surfaces mark significant change in depositional conditions (Evy Glørstad-Clark, et al., 2010). For the purpose of this study, Triassic was further subdivided into Lower Snadd (S4) and Upper Snadd (S5) sub-sequences, and each sub-sequence was analyzed in terms of time-thickness maps and paleogeographic interpretation. The present work is built on this observation.

Landinian-early Carnian Lower Snadd (S4) sequence is bounded at the top and base by strong amplitude surfaces with significant extent (Evy Glørstad-Clark, et al., 2010). This sequence represent definable easterly thinning and development of local depocenters to the west. The base of upper part of Snadd Fm (S5), deposited from late Carnian to Norian, is marked by major transition from marine (S4) to non-marine (S5) deposits. Upper Triassic (S5) sequence is bounded at its top and bottom by strong, continuous seismic amplitude surfaces, well developed over the study area (Figure 39 B). Fluvial depositional environments within Snadd formation range conformably from offshore through shelf in S4 and shallow marine to deltaic in S5, where MFS marks the period of marine inflow or the transition from S4 to S5, indicating unconformable overlay and change in facies association of offshore marine deposits by shallow- (S4) and non-marine (S5) (Figure 53).

The horizons interpreted in this study correspond to Top and Bottom S5 (Figure 53). Based on (Evy Glørstad-Clark, et al., 2010), the major marine flooding surface (MFS) separating the lower (S4) and upper (S5) Snadd Formation has been assigned to as intra-Carnian in age.
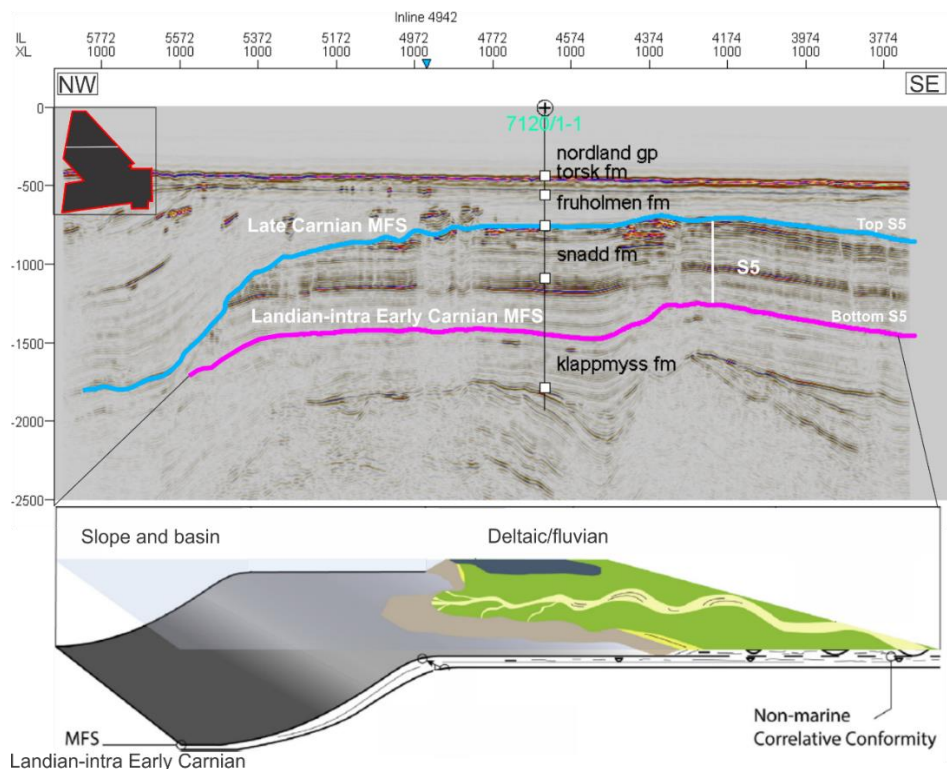
Figure 53 A west to east seismic line through LN09M01 survey, with interpreted upper Snadd (S5) sequence and Landian-intra Carnian MFS. Schematic overview of depositional environments in parts of Snadd Formation is shown in the sketch below. The white line on the inset picture in the left upper corner indicates the location of the seismic line. Modified from (Evy Glørstad-Clark, et al., 2010), (Tore Grane Klausen, et al., 2015).

Landian-intra Carnian MFS (Figure 54 B, bottom of S5) has been interpreted and used in this study to divide the Snadd formation into S4 and S5 stratigraphic sequences (Evy Glørstad-Clark, et al., 2010; Tore Grane Klausen, et al., 2015). Figure 53 summarizes the depositional environments in part of Snadd Formation and where they are located relative to 3D seismic data.

The time-thickness map calculated between Top and Bottom of upper Snadd Formation (S5) (Figure 54 C) represents that the area was progressively filled with sediments from the east and southeast over Triassic times, where Uralian orogeny was still active and sediments were spreaded toward the northwest and into the Barents Sea. This observation agrees with the one made by (Tore Grane Klausen, et al., 2014), where interpretation of Snadd Formation being comprised by westward-thickening package of siliciclastic sediments was stated.
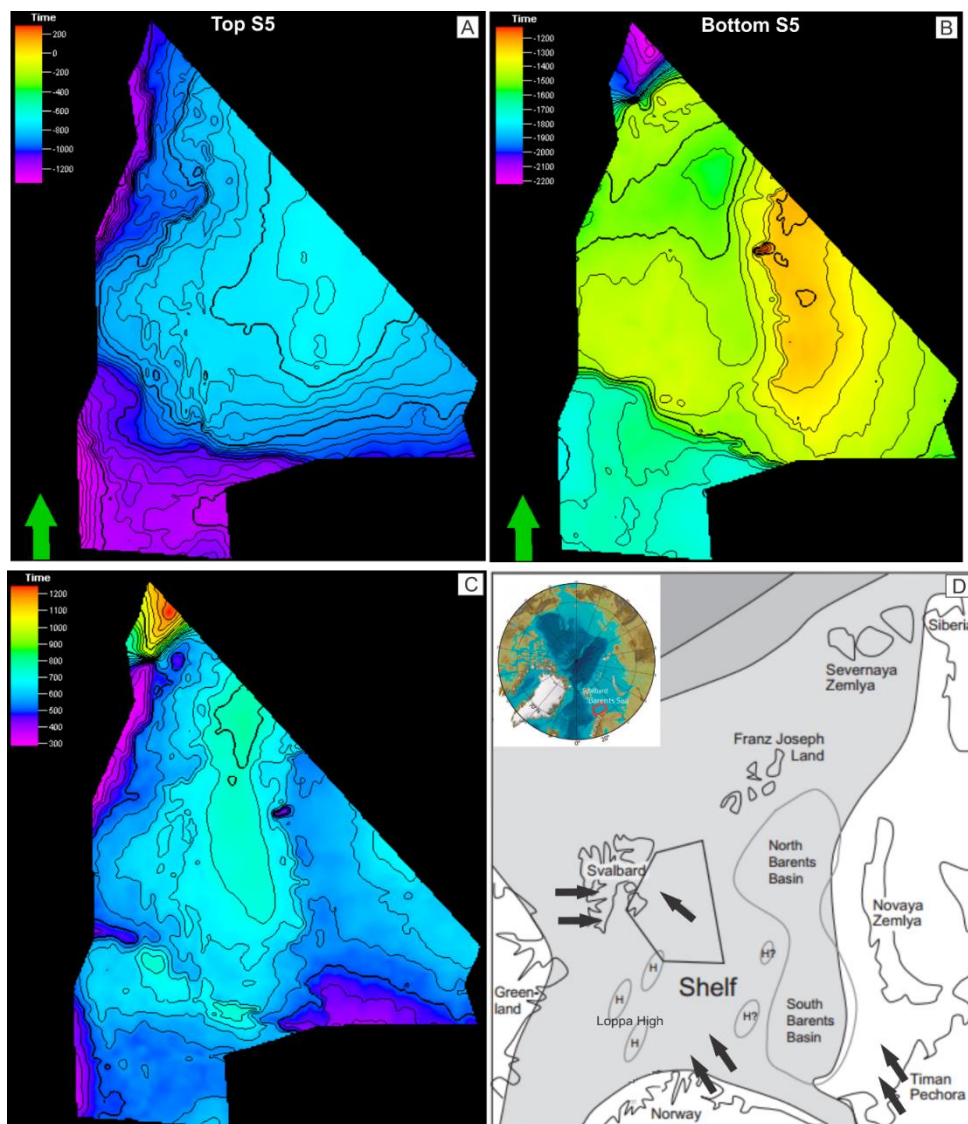
Figure 54 A) Top S5 isochron surface map contoured in TWT. B) Bottom S5 isochron surface map contoured in TWT. C) Thickness map for S5 generated between S5 bottom and top surfaces. D) Reconstruction of the regional setting of the Barents Sea in early Triassic times, showing the continents and the area of Triassic deposition. Major Triassic topographical highs (H) are also identified. Arrows show the directions of the main sediment transport. Modified from (Fridtjof Riis, et al., 2008).

Since Barents Sea was undergoing relatively quiet tectonic regime while siliciclastic Triassic succession was being deposited, the Loppa High area thus became a sedimentary basin. The observed trend of westward and northwestward thickening of the Late Triassic sequence (Figure 54 C) marks a major location of depocenter in the study area. Main focus of deposition occurred toward west and northwest in the study area with depocenter located in the central part. Here sedimentary succession thickens, signifying a relative increase in accommodation rate. On Figure 54 D the reconstruction of the regional setting of the Barents Sea in late Triassic times shows

the directions of the main sediment transport. Paleo-Loppa High developed from a barrier to sediment propagation from the south and southeast in Early to Middle Triassic, to become the main depocenter from Early Late Triassic (Evy Glørstad-Clark, et al., 2010), that fact significantly affected sediment dispersal patterns.

5.2 Interpretation of channel systems

Fluvial depositional environments were defined on the basis of planform seismic attribute ribbon-like geometries and distinctive cross-sectional seismic facies. Seismic interpretation was carried out using Schlumberger's Petrel 2014 for standart attribute analysis and Geoteric 2015 for spectral decomposition and RGB blending. A total of nine channels were analyzed within the Snadd formation of the study area, and the result presented in this work is the description of three of these channels in detail to show range of channel dimension parameters, channel deposits, seismic geomorphological and architectural patterns, channel migration pattern and meander bends development. Planform and cross-sectional geometries were measured from three channels and compared on the basis of their sinuosity, lengths and migration mode. Figure 69 shows representation of the parametrs that were measured and presented in Table 3. Channel sinuosity index was calculated for initial sinuosity (measured at the earliest stages of channels evolution) and for the secondary sinuosity (at the latest stages of channels evolution) on the basis of bend thalweg length-to-bend wave axis length ratio.

Particularly these three channels were picked for further analysis because they are continuous, extensive and are best to identify. The three target channels represent the focus of this study are numbered in stratigraphic order: channel Grid 1, channel Grid 2 and channel Grid 3. Channels have been identified by distinctive seismic signature, V- or U-shaped geometry, level of incision, and different morphological elements associated with channel valley.

Figure 55 A shows interpreted seismic section through the 3D seismic dataset, illustrating formations and the bounding surfaces within Triassic sequence. Schematic diagram on Figure 55 B summarizes the distribution of different fluvial channels with different geometries, relative to time lines based on mapping of Top and Base of upper (S5) Snadd Formation and marine flooding surface (Intra Carnian MFS).
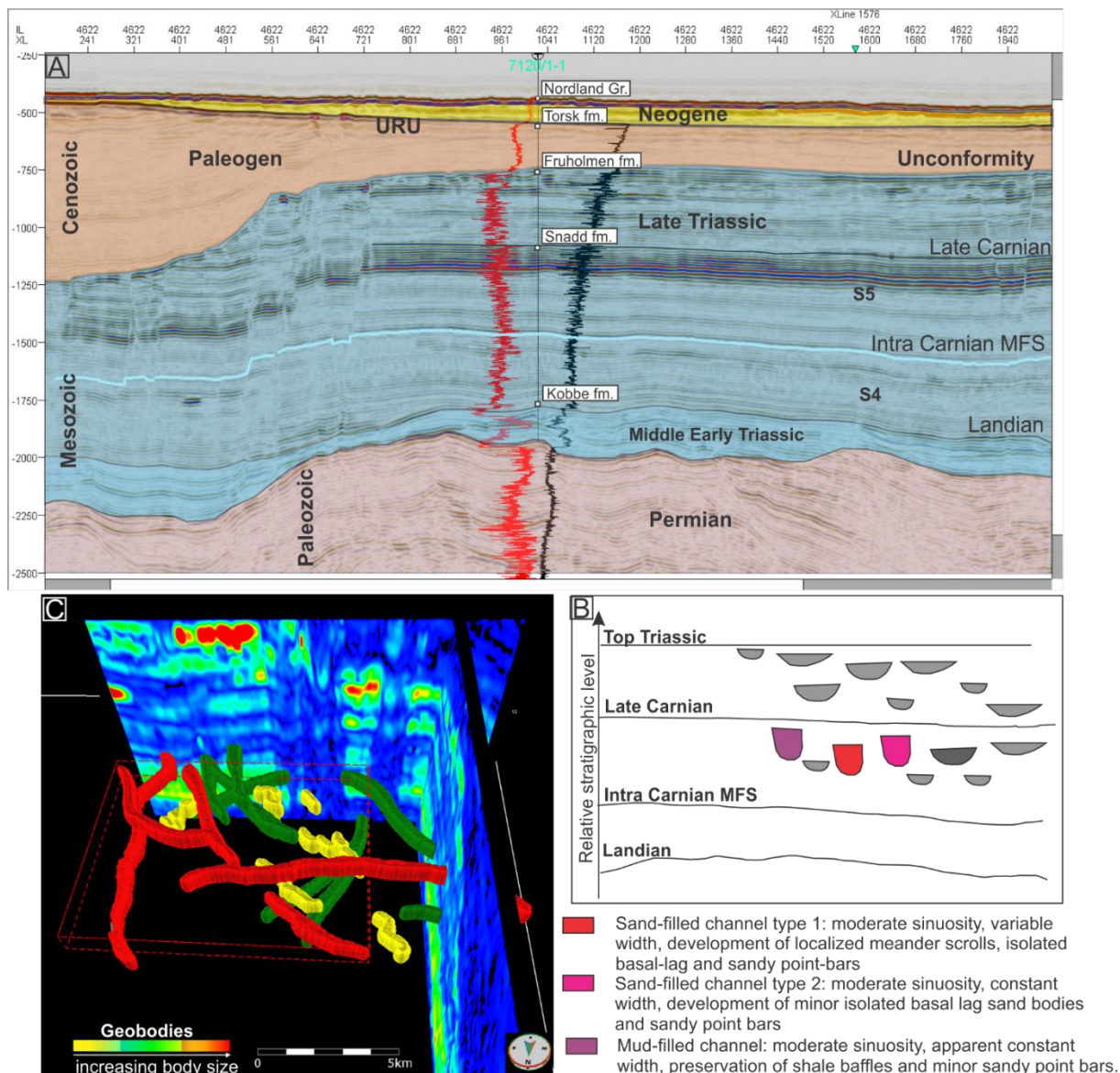
Figure 55. A) Interpreted seismic section, illustrating formations and the bounding surfaces within Triassic formation. Triassic formation is shaded in blue. The intra-Carnian MFS (bright blue line) divides the formation into lower (S4) and upper (S5) units, terminology after (Evy Glørstad-Clark, et al., 2010). B) Schematic diagram illustrating formations and the bounding surfaces and summarizing the distribution of different fluvial channel types with different geometries, relative to time lines based on mapping of Top and Base S5 and marine flooding surface. Channels identified by colors were analyzed in this work. C) Channel system geobodies generated through tresholding of the single Envelope attribute within -1088 ms to -1152 ms interval corresponding to Snadd Formation. Geobodies are ranked by body size: large geobodies are red and small are yellow.

Channel, which are further described in this work, are highlighted by colors, indicating classification into three different types: sand-filled of type 1 and 2, mud-filled channels. Figure 55 C shows geobodies of all observed channel system within -1088 ms to -1152 ms interval of the Snadd Formation, generated through tresholding of the single Envelope attribute, where geobodies are ranked by body size (large geobodies are red and small are yellow).

5.2.1 Channel 1

Grid 1. - is elongated NNE-SSW. It was initially defined on the basis of its sinuosity on the Variance attribute time slice (Figure 56 A), the interpretation of which allowed the definition of an area with relatively clear boundaries, emphasizing well-defined, sinuous channel complex elongated NNE-SSW. Moderate channel sinuosity (1.200), after (Rosgen, 2007), linked to channel low gradient of ≤ 0.02 degrees, are consistent with a type C rivers, which are classified in (Rosgen, 2007) as meandering. The channel is best resolved for the interval from -1128 ms to -1116 ms (Snadd formation, Triassic) and located between two major tectonic faults, trending from North to South, which bound downlifted area, where main paleochannels of this study area have been found.

For further analysis of the channel Grid 1, seismic attributes, which are most distinguished means and sensitive to mapping channel, were calculated (Instantaneous frequency, Spectral decomposition RGB-Envelope-SO Semblance opacity blend). A horizon-based approach did not provide any useful information. The interpretation was carried out on attribute time slices. The interpretation of both instantaneous frequency and RGB-Envelope-SO Semblance opacity blend allow definition of channel morphology to a certain degree. Channel is clearly distinguished by constant values of instantaneous frequency, contrasting to the abrupt lithological variations outside the channel boarders (Figure 56 B) (Leonardo Azevedo, et al., 2009). Since the channel belt itself tends to be mostly constant in values, there are no major lithological variations inside the channel belt as interpreted from Instantaneous frequency attribute, however, zones of sediment accumulation cause slight drop-off of high frequencies indicating major sediment accumulation (Figure 56 B).

The continuity of a particular dark color shade on the RGB-Envelope-SO Semblance opacity blend time slice (Figure 56 C) indicates continuous homogenous body. Dark color shade, which is characteristic of channel belt and meander bends (even darker), indicate the low response from all three frequencies involved in spectral decomposition sum (Red-Gren-Blue) (Pavel Morozov, et al., 2011), and is indicative of massive bedding geometries, such as sand-prone lithologies (Tayyab Muhammad Naseer, et al., 2014).
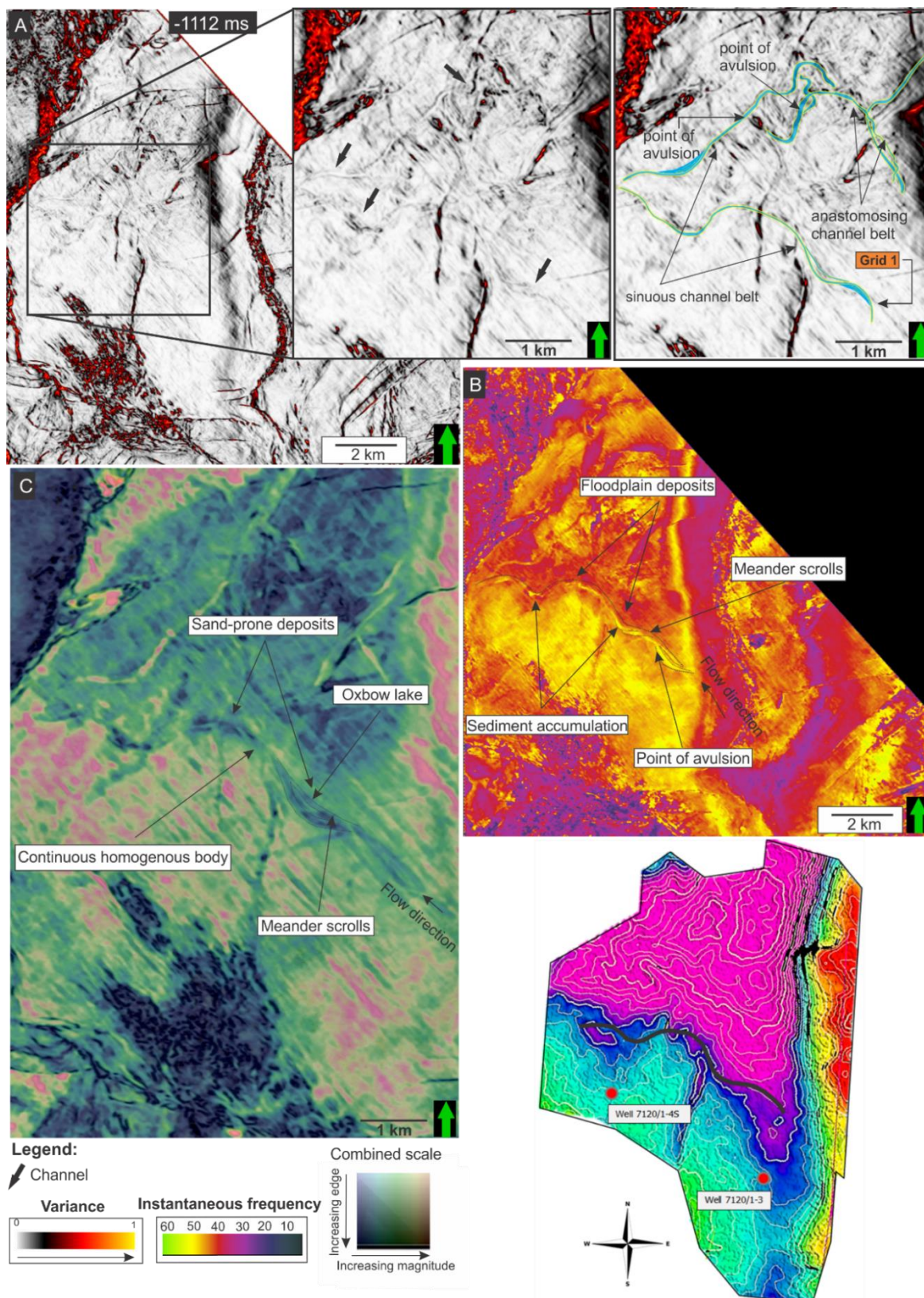
Figure 56. Channel Grid 1. A) Variance time slice at -1112 ms, showing close up to the target channel Grid 1, where several sinuous channel belts can be identified. B) Time slice of an instantaneous frequency cube. In the central part, a channel extends to the left part of the figure and is clearly distinguished, by constant values of instantaneous frequency. C) RGB-Envelope-SO Semblance opacity blend resolves greater level of extent and infill of the channel Grid 1. The location of the channel is shown on the surface map by solid line.

With increasing distance from the channel belt axis, sediment thickness is reduced and the color sum manifests itself in the form of red and green (Figure 56 C), as the frequency increases, which may be exhibited by thinly laminated shale (Tayyab Muhammad Naseer, et al., 2014). Therefore, the channel belt deposits are interpreted be to mainly represented by homogeneous, well-sorted, fine- to medium-grained sandstones, and the deposits of flood-plain zones are represented by alternating layers of clay and fine silt. In fact, the technique of RGB-Envelope-SO Semblance blend showed the best practice and effectiveness in visualization of channel systems. In the case of Grid 1 channel system delineated previously by single Variance attribute (Figure 56 A), it is likely now that it exhibits migration pattern and hence is laterally instable and dimensional. It is also noticeable from Figure 56 how RGB-Envelope-SO Semblance blend in this particular case successfully highlights channels edges, meander scrolls and internal morphology, and greater level of information can obtained from this volume.

For this study, a Curvature most positive and Curvature most negative attribute cube was generated for 3D seismic volume and stratal slices were extracted and examined to study internal lithology. In Figure 57 the most positive curvature attribute highlights flanks (potential levee deposits) with red, whereas the channel axis fill is highlighted by most negative curvature attribute with blue (6.6 Criteria for distinguishing between mud- and sand-filled channels). Based on observation of stratal slice through curvature cube, the definition of internal architecture for Grid 1 as of sand-filled channel constrained by mud-rich levee deposits, and showing migration patterns (meander scrolls) and hence being laterally instable is defined. Levee deposits are the largest and most extensive mud-prone architectural element of channel belt Grid 1. The interpretation of internal lithology of Grid 1 channel belt as being sand-filled and indicating successive migration patterns of relatively long-lived meander river channels is revealed by RGB-Envelope-SO Semblance blend, and is supported by closer examination of combined Curvature attribute.
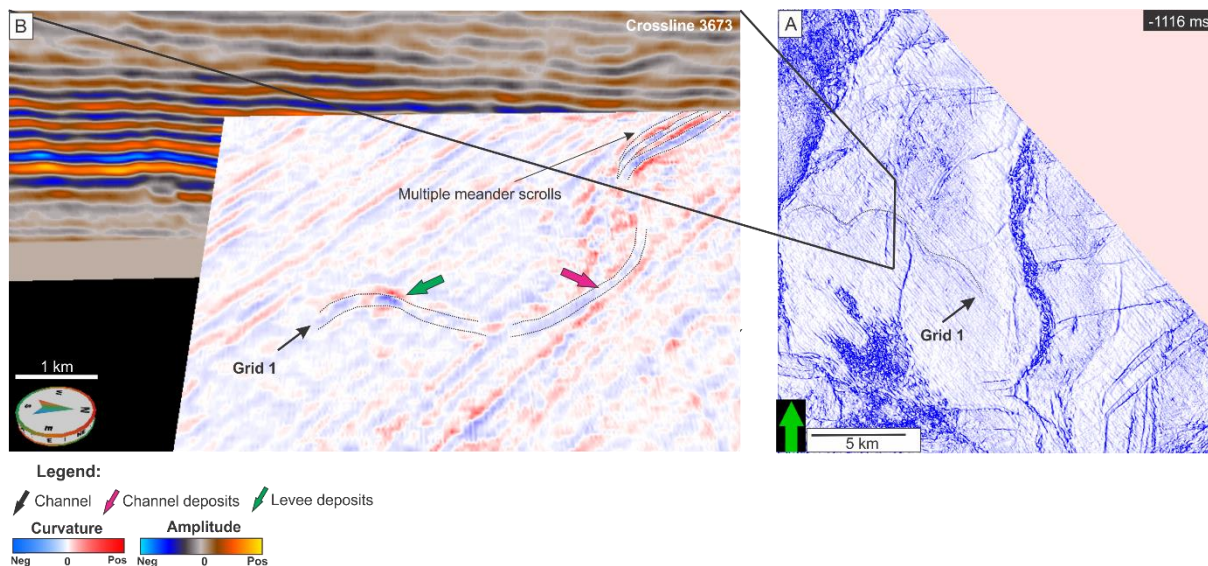
Figure 57 Channel Grid 1. A) Stratal slice at -1116 ms through most negative curvature attribute (black arrow show location of Grid. B) Zoomed-in chair display showing crossline and stratal slice through combined most negative and most positive curvature attribute. Pink and green arrows show channel fill and channel edges (flanks) of Grid 1 respectively.

High accurate 3D model of the Grid 1 channel was created in Geoteric and combined with Envolope attribute (Figure 58) in order to calculate the channel parameters/metrics (Table 3) and analyze channel morphology. The Envelop attribute shows a limited, localized area with high values, having typical meandering distribution, were therefore interpreted as sandy deposits of channel point-bar and concave-bank (Figure 58 B), deposited in stable homogenous depositional environment. Meander-loop has been interpreted as migrating by both lateral extension and downstream translation (6.4.1 Channel 1), leading to preservation of accreted channel deposits, which maintain their irregular elongated patterns and amount of connectivity (closely connected) with each migration step. The accretion trend is an important component of paleo-flow record. The lateral accretion deposits translate downstream relative to the initial mapped bend apex and indicate a paleo-flow direction to the west and north-west, which is consistent with general propagation of the sediment dispersal system (5.1 Seismic stratigraphy).

Quantitative Geomophology of channel valley

Grid 1. - meandering channel of moderate sinuosity (≤1.200), up to 200 m wide and approximately 19 km long, which appears at the lowest stratigraphic level (Table 3). It varies relatively from being low sinuous at its initial stage of channel

evolution (at 1132 ms, sinuosity 1.08) to moderate sinuous (at 1112 ms, sinuosity 1.2), according to Rosgen (2007, p. 10) stream classification. It has been interpreted as well-defined meander channel belt elongated NNW-SSE, with levees, meander scrolls patterns, point bar and concave-bank deposits, and chute channel within a channel belt. Channel-levee system is characterized by distinct, sub-parallel to chaotic reflectors of low to moderate amplitude, which appear as vertical U-shaped packages with smoothed to sharp lateral edges incised into the sediment beneath (Figure 59). It is flanked by topographic highs of the well-developed proximal levees, which are positive relieve features flanking the channels (Satinder Chopra K. J., 2012) and mainly consist of moderate amplitude, continuous, wing-shaped sub-parallel reflections, which slope down toward the distal levees, downlaping into strong acoustic base reflector (Figure 59).
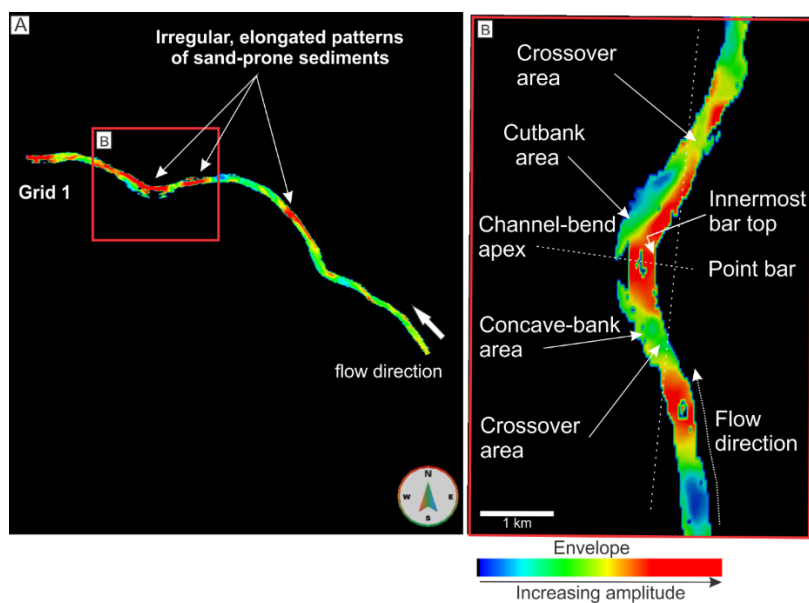

Figure 58. Channel grid 1. A) Channel Grid 1 3D Geobody with extracted Envelop attribute values. B) Zoomed in plan view of channel bend showing areas of sediment preservation along channel bend.

Internal principal architecture of the channel-levee system is defined by different type of facies found in between flanking levees and on proximal levees (6.3 Seismic facies). The interpretation of channel Grid 1 as being avulsive has been built on the observation that channel is not entirely well laterally constrained by levees. The channel flow has been interpreted as continuous, since channel fill grade laterally into finer, thinner levee deposits on inner meander bend side, whereas the contact between channel fill deposits and outer-bend levees is mostly erosive.
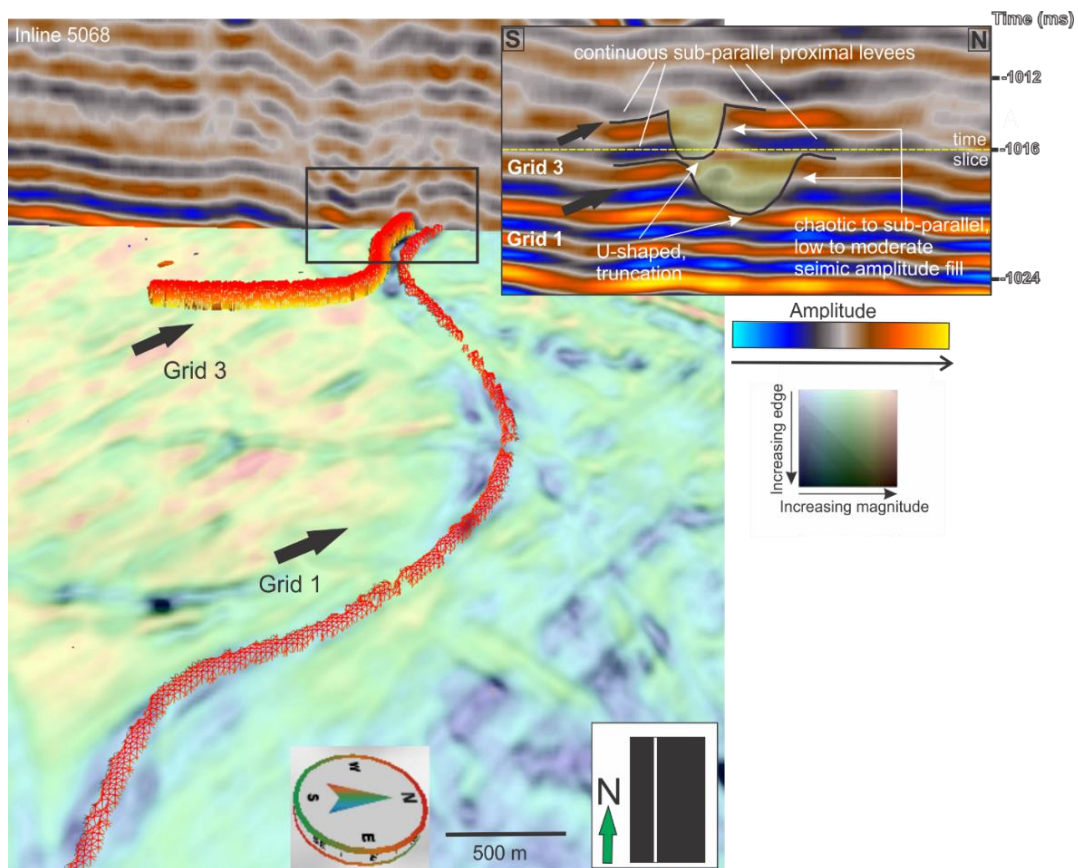
Figure 59. Chair display showing incised channels Grid 1 and Grid 3 on Evelope-SO Semblance blend stratal slice (1116 ms, Inline 5068). Vertical seismic section reveals the seismic amplitude signature for Grid 1 and Grid 3 (Inline 5068).
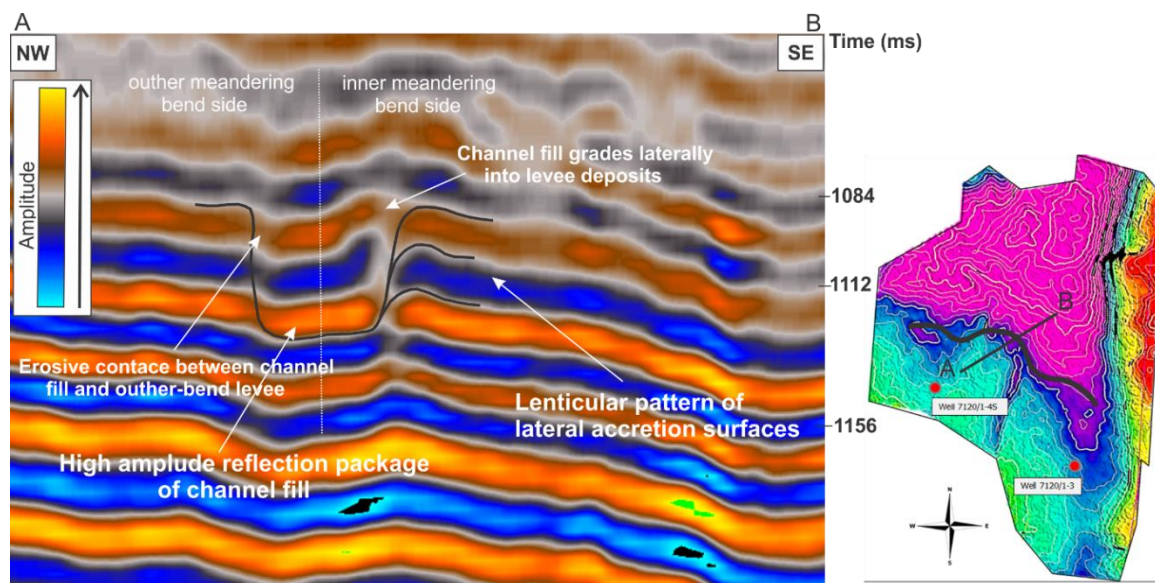

Figure 60 Interpretation of vertical seismic section of Grid 1 target channel (inline 5073). Location of seismic AB is shown on the inset map.

Successive migration and deposition patterns of relatively long-lived meander river channel and associated point bar deposits has been identified by weaker reflections dipping toward the channel center (Figure 60). They occur at an angle to the channel centerline orientation, are interpreted as lateral-accretion packages, and represent lateral accretion surfaces of meander scrolls, previously identified by Curvature attribute and RGB-Envelope-SO Semblance blend.

The channel Grid 1 interpreted as being incised into previous deposits due to the presents of reflection truncation at the channel base (Paivi Heinio & Richard J. Davies, 2009) and hence being formed by erosional processes. Incisions are mappable stratal surfaces and record the existence and migration of depositional environments on continental margins (Sylvia Nordfjord, et al., 2005). Channel Grid 1 is mildly incised (≈ 3 ms ≈ 4.5 m) into underlying sediments in its distal (western) reach, but the amount of incision fluctuates along the length of channel, with obvious decrease in its proximal (eastern) reach. The maximum incision (4 ms ≈ 5 m) has been calculated on outer meander bends, where due to continues erosion of the outer bank, flow scours deeper along the outside of the mender bend apex (6.2 Fluid flow controls on sediment sorting within meander bend). The base Grid 1 surface is generally slightly dipping to the south and channel has low (≤ 0.02 degrees) average gradient, which slightly increases toward the distal end (westward), thus showing positive correlation with channel sinuosity. For longer reaches 15 km in length, sinuosity and gradient increase.

5.2.2 Channel 2

Grid 2. - is elongated SSE-NNW and is running from SSE to NNW. It was initially defined on the basis of its sinuosity on the Variance attribute time slice (Figure 61). The interpretation of which allowed the definition of an area with relatively clear boundaries, emphasizing well-defined, sinuous channel complex, elongated SSE-NNW. Moderate channel sinuosity (1.260), after (Rosgen, 2007), linked to channel low gradient of ≤ 0.02 degrees, are consistent with a type C rivers, which are classified in (Rosgen, 2007) as meandering. The channel is best resolved for the interval from -1116 ms to -1100 ms (Snadd formation, Triassic) and located between two major tectonic faults, trending from North to South, which bound downlifted area, where main paleochannels of this study have been found. Several following surface attributes,

with different parameters were extracted from the interpreted surface of the Grid 2 channel system: RMS amplitude, Envelope and Gradient Magnitude, were the most helpful attributes to detect potential porous lithologies and trace out the lateral extent (Figure 62). The interpretation of RMS, Envelope and Gradient magnitude attribute revealed channel belt, marked by strong ribbon–like amplitude anomaly with sinuous bends, running from SSE to NNW. The generated RMS attribute map show well defined area of high RMS amplitude values inside the Grid 1 channel system (Figure 62, inside the white circles). The area is interpreted to correspond to high porosity sand lithologies. Generated Envelope attribute map is equivalent to RMS attribute map, where porous lithologies appear as high attribute values. However, Envelop attribute map better resolves low amplitude values corresponding to low porosity levee deposits (Figure 62, inside the white circles) and allows better spatial delineation of the interpreted earlier high porosity areas. The interpretation of surface attribute Gradient Magnitude was complimented with the information given by both RMS and Envelope attribute maps, already discussed above. On Gradient Magnitude attribute map, the channel is shown with constant magnitude value along the channel belt, and high values corresponding to meander bends. The interpretation of the attribute map shown on Figure 62, allows better delineation of the channel belt. Examining single Envelope and/or RMS attribute maps, prediction of the planform geometry at a point of confluence (junction) or bifurcation (split) of two channels is not possible to resolve. It is clear that channel bifurcation and confluence are processes not applicable in this case as might have been concluded from examination of single Envelop and RMS attribute maps. Here, the best practice is using Gradient Magnitude attribute map, allowing better delineation of the channel system, and revealing the presence of two channels having a confluence point. The interpretation of Curvature most positive and Curvature most negative attribute time slice along 3D combined seismic volume (Figure 61 B), reveals the positive potential levee deposits (highlighted by most positive Curvature attribute with red), and channel fill (highlighted by most negative Curvature attribute with blue). In this case, channel Grid 2, as well as channel Grid 1 was defined as sand-filled channels mainly represented by homogeneous well- sorted, fine- to medium-grained sandstones.
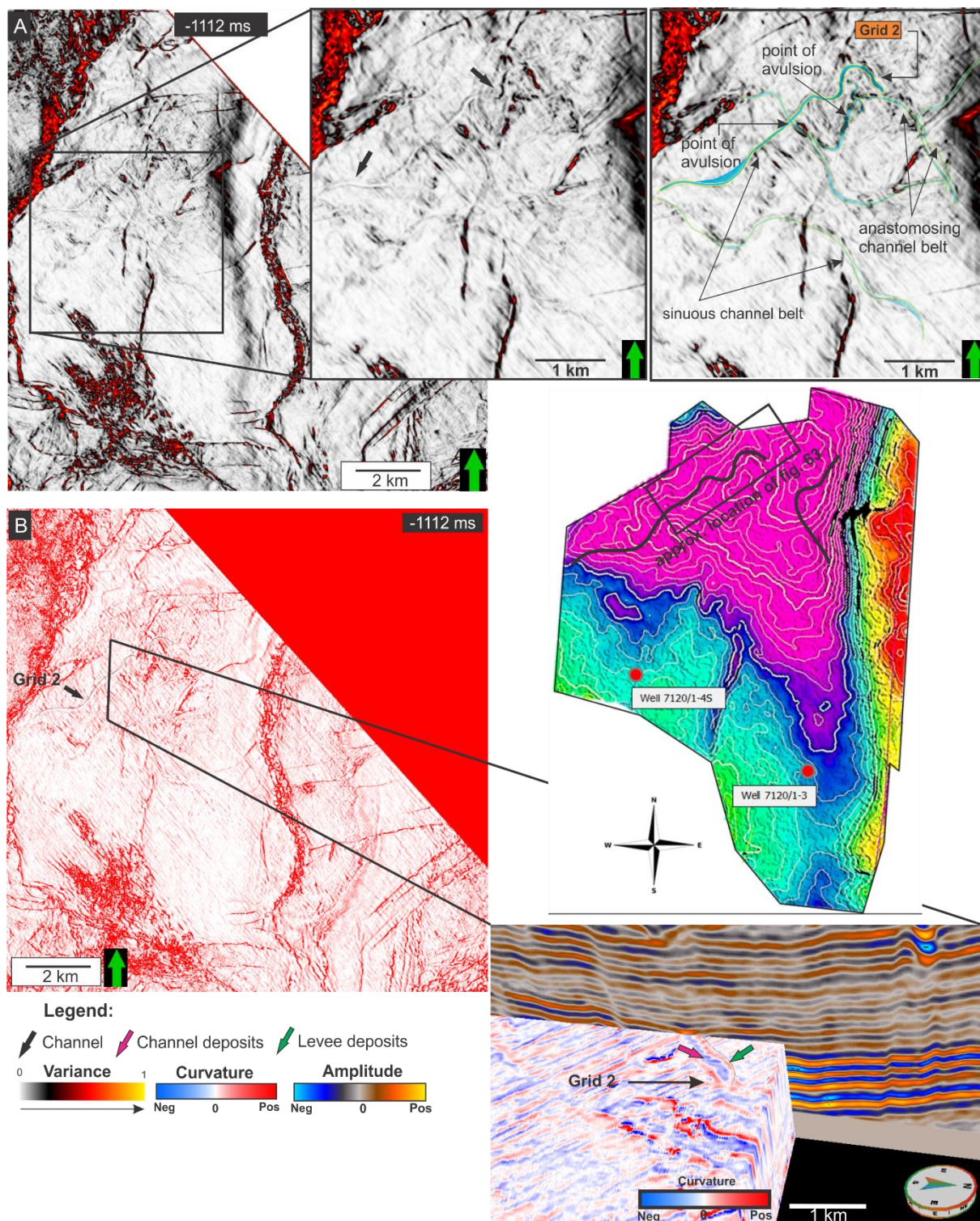
Figure 61 Channel Grid 2. A) Variance time slice at -1112 ms, showing close up to the target channel Grid 2, where several sinuous channel belts can be identified. B) Stratal slice at -1112 ms through most positive curvature attribute (black arrow show location of Grid 2) and zoomed-in chair display showing crossline and stratal slice through combined most negative and most positive curvature attributes. Pink and green arrows show channel fill and channel edges (flanks) of Grid 2 respectively. The location of the channel is shown on the surface map by solid line.

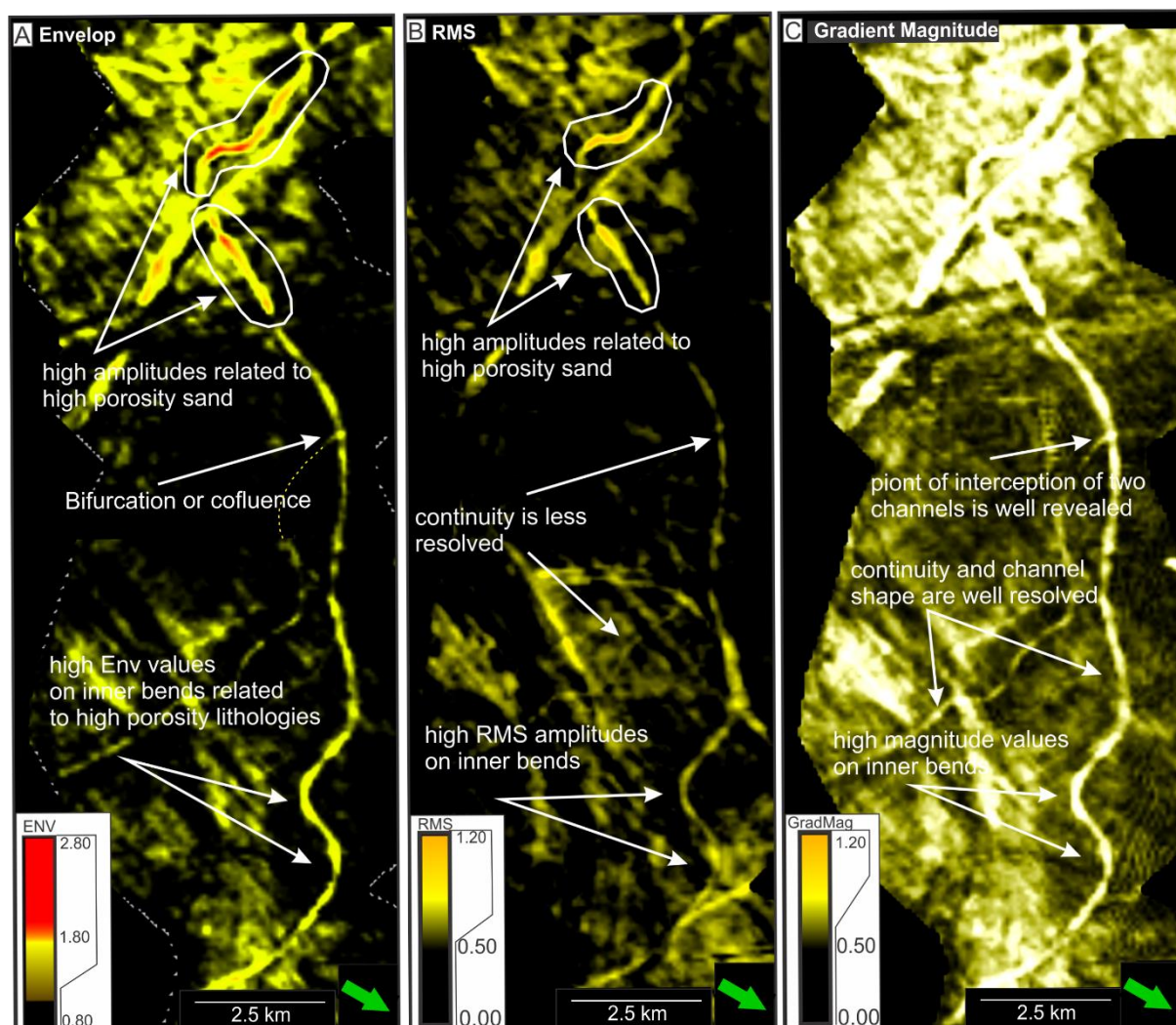Figure 62. Channel Grid 2. A) Envelope amplitude computed to a surface with 50 ms search window. Channel features are followed with greater continuity, than on RSM, however it is difficult to distinguish between neighboring and overlapping channels. B) High RMS amplitudes extracted from RMS 3D seismic cube and computed to a surface with 50 ms search window. Ribbon-like high amplitudes define channel body. C) Gradient magnitude attribute extracted from 3D seismic cube and computed to a surface with 50 ms search window. Two channel bodies with common confluence/interception point are resolved.

Whereas, channel-levee deposits are defined as the largest and most extensive mud-prone architectural element represented by alternating layers of clay and fine silt.

High accurate 3D model of the Grid 2 channel was created in Geoteric and combined with Envolope attribute (Figure 63) in order to calculate the channel parameters (Table 3) and analyze channel morphology. The Envelop attribute shows a limited area with localized high values of Envelope attribute, having a typical meandering distribution, were therefore interpreted as high porosity, sand-prone deposits of channel point-bar and concave-bank (Figure 63), accumulated in stable homogenous depositional environment. Where sand-prone thick deposits formed on

the inside of meander bends and shaped by lateral accretion, resulting from meander bend lateral expansion and downstream translation migration modes (6.4.2 Channel 2). With each migration step, accreted point bar and concave-bank deposits maintain their irregular elongated shape and amount of connectivity (closely connected) (Figure 63 C). The accretion trend of the channel belt deposits helps to identify paleo-flow direction. The lateral accretion deposits translate downstream relative to the initial mapped bend apex and indicate a paleo-flow direction to the west and south-west, which is consistent with general propagation of the sediment dispersal system (5.1 Seismic stratigraphy).
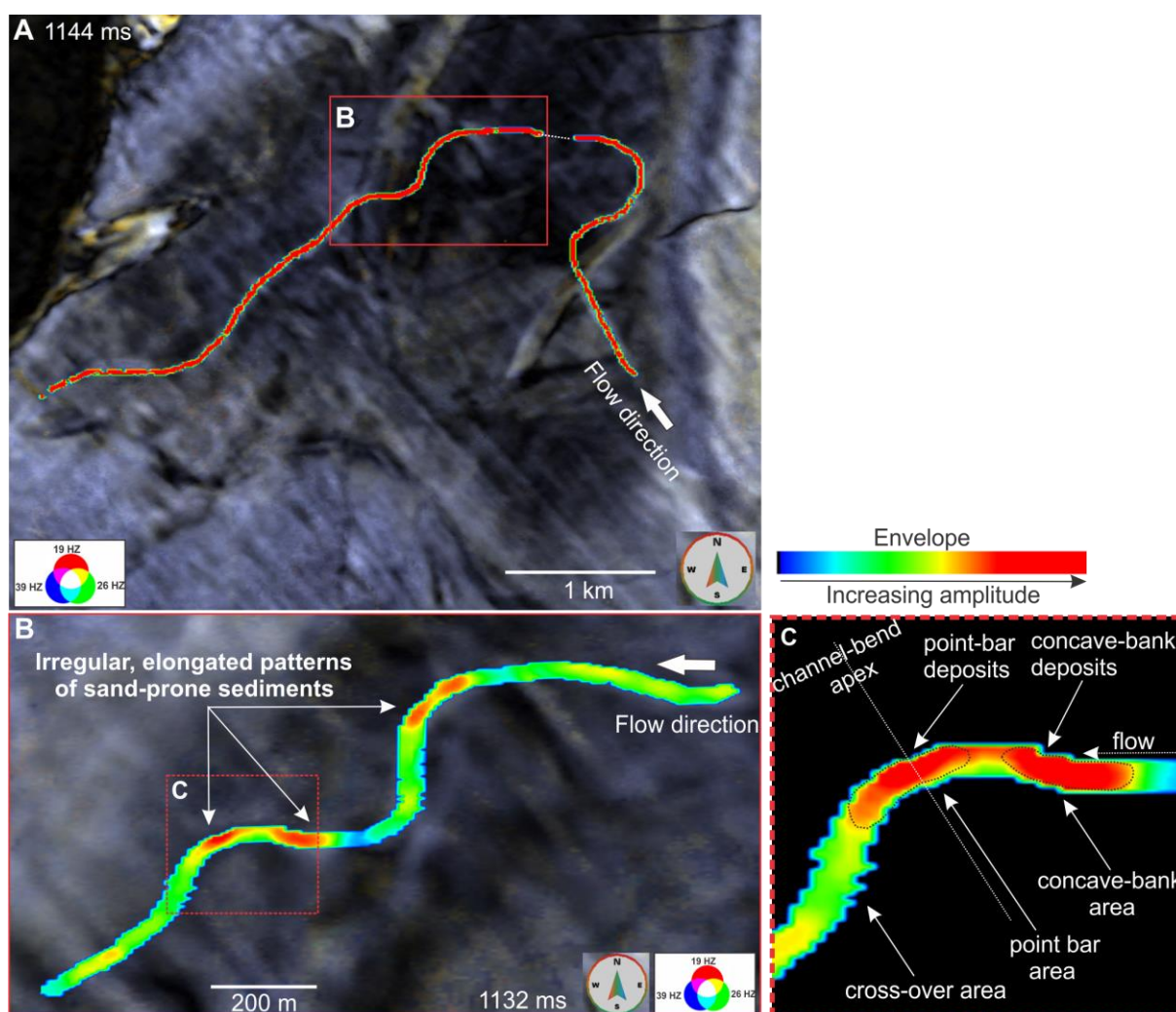

Figure 63 Channel grid 2. A) Plan View of spectral decomposition cube at a frequency subband of 19-26-39 HZ at -1144 ms, showing Grid 2 channel system. B) Channel Grid 2 3D Geobody "cookie cut" with extracted Envelop attribute values. B) Plan View of channel bend showing areas of sediment preservation along channel bend.

Quantitative Geomophology of channel valley

Channel Grid 2. – meandering channel has moderately (but highest of three studied channels) sinuous channel axis (≤1.260). It varies relatively from being low sinuous at the initial stage of channel evolution (1.13) to moderate sinuous (1.26) (Table 3), according to Rosgen's stream classification. The channel width decreases markedly down-system, from approximately 118 m to less than 100 m in width. The overall morphology of the channel valley of channel Grid 2 is similar to channel Grid 1, but is it reveals most distinctive and clearly visible patterns of channel fill (Figure 64), which is mainly characterized by high amplitude V-shaped reflectors packages, flanked by downlaping, continuous, wing-shaped moderate amplitude reflections of internal levees. Channel is therefore well-confined by levees.
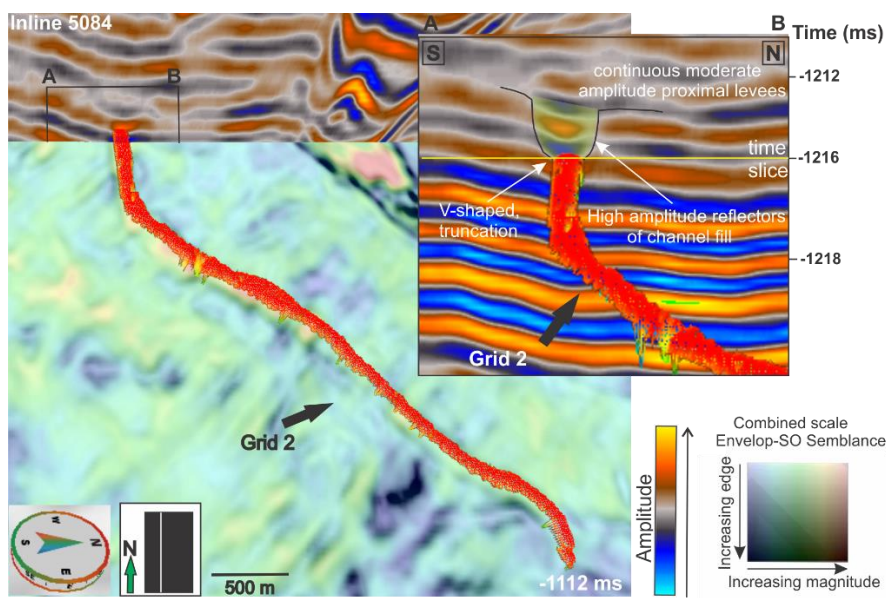
Figure 64 Chair display showing an incised channel Grid 2 on Envelope-SO Semblance blend slice (-1112 ms) and its seismic amplitude signature (Inline 5084).

The high-amplitude packages of channel fill deposits is associated with erosional and mounded channel base architecture. Channel Grid 2 incises into underlying sediments (≈ 7 ms ≈ 8.5 m), and therefore is interpreted as being formed by erosional processes, but its amount of incision fluctuates along the entire length, being slightly more significant at the distal reach (westward). In few areas, the initial erosion is deep enough so that high-amplitude seismic reflections, inferred to be the seismic expression of sandstone-prone channel fill, do not have a visible contact with proximal levee walls. Sand-prone channel fill is then fully confined within mounded incised part,

interpreted as isolated basal-lag sand bodies. In other areas (Figure 64), sand bodies are well confined by levees. On inner bend side, channel fill grade laterally into finer, thinner levee deposits, which in fact suggests flow continuity. The internal channel's geometry is characterized by very distinctive high seismic amplitude within upstream and central reach, which decrease toward the downstream reach. Downstream, channel Grid 2 is more lens-shaped, broader system with thicker levees in cross-section. Channel has overall low (≤ 0.02 degree) average gradient, which slightly increases toward southeast.

5.2.3. Channel 3

Grid 3.- Interpretation of planform Variance attribute map on time slice (Figure 65 A), combined with the original seismic data, allowed definition of area with relatively clear boundaries emphasizing well-defined, sinuous, elongated NN-SSW and running from north to SSW channel complex, defined at stratigraphic interval from -1108 ms to – 1080 ms (Snadd Formation, Triassic) on the basis of its sinuosity. Moderate channel sinuosity (1.203), after (Rosgen, 2007), linked to channel low gradient of ≤ 0.02 degrees, are consistent with a type C rivers, which are classified in (Rosgen, 2007) as meandering. Plan view of the initial Grid 3 channel varies relatively from being low sinuous at intial stage of channel evolution (at -1108 ms, sinuosity 1.04) to moderate sinuous (at -1080 ms, sinuosity 1.202), according to Rosgen's stream classification. The channel thalweg lenght is approximately 4.5 km, and its width varies from 100 m to 110 m. Channel Grid 3 is identified on the instantaneous frequency time slices (Figure 65 B) by constant values of instantaneous frequency, contrasting with surrounding environment of alternating frequencies. There are no zones of sediment accumulation which cause slight drop-off of high frequencies along the channel belt, and since the channel tends to be constant in values, there are no major lithological variations inside the channel belt.

The following morphological features have been identified within channel valley: channel belt, crevasse-splays and overbank deposits (Figure 65.). The response from Grid 3 show a continuity of a particular white or grey color shade on the Standart spectral decomposition RGB attribute time slice, which indicates continuous homogenous body.
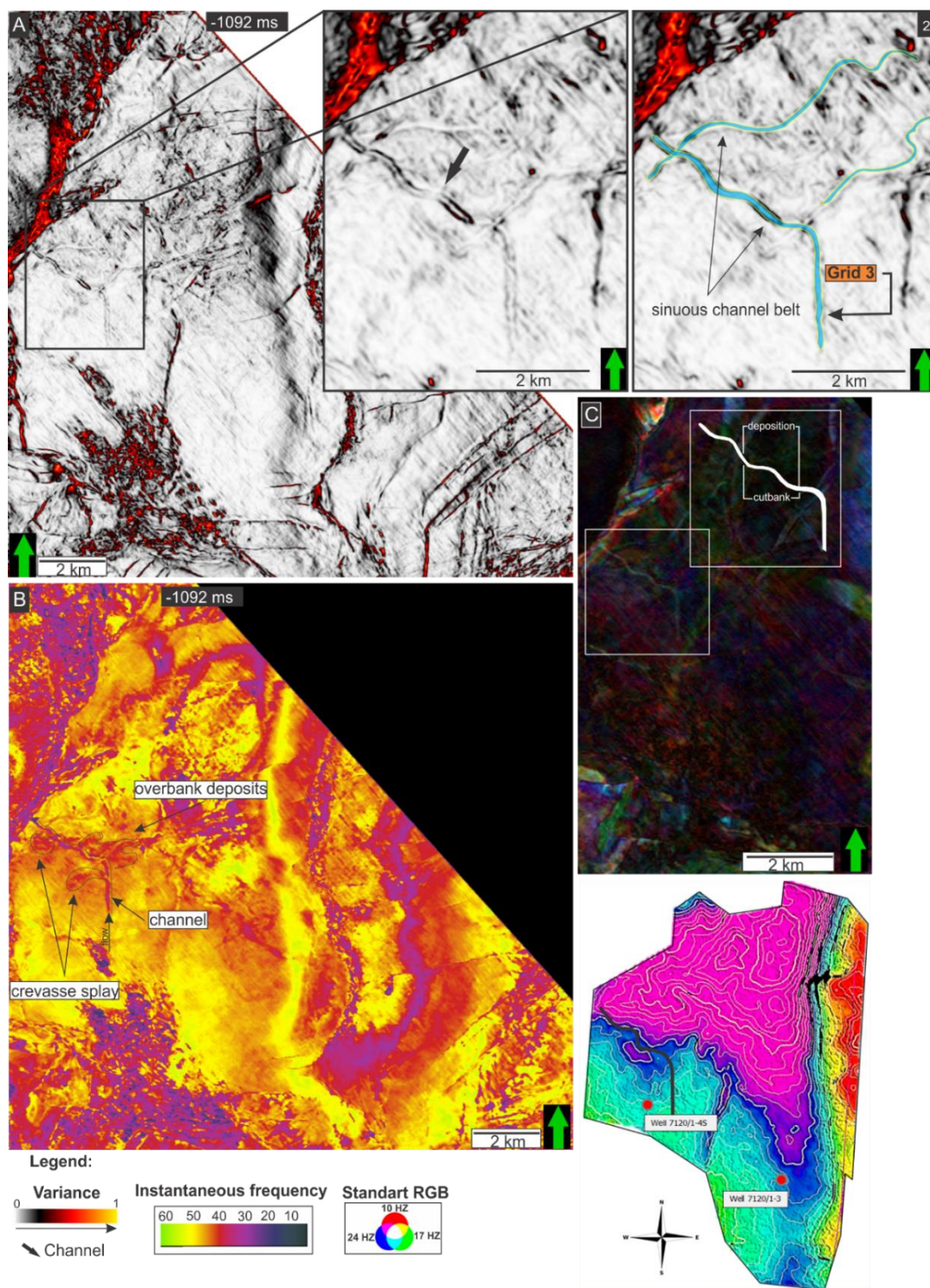
Figure 65 Channel Grid 3. A) Variance time slice at -1092 ms, showing close up to the target channel Grid 3, where several sinuous channel belts can be identified. B) Time slice of an instantaneous frequency cube. NN-SSW channel which extends to the left part of the figure is clearly distinguished, by constant values of instantaneous frequency. C) Standart frequency decomposition RGB resolves white continuous color shade, where the schematic channel model indicates areas of erosion and deposition along channel belt. The location of the channel is shown on the surface map by solid line.

White or grey color of channel belt indicate a strong response (high frequencies) from all three frequencies involved in RGB (Red-Green-Blue) summation (Pavel Morozov, et al., 2013), which may be exhibited by thinly laminated shale (Tayyab Muhammad Naseer, et al., 2014).

Figure 66 Channel Grid 3. A) Stratal slice at -1104 ms through most positive and most negative curvature attributes (black arrow shows location of Gri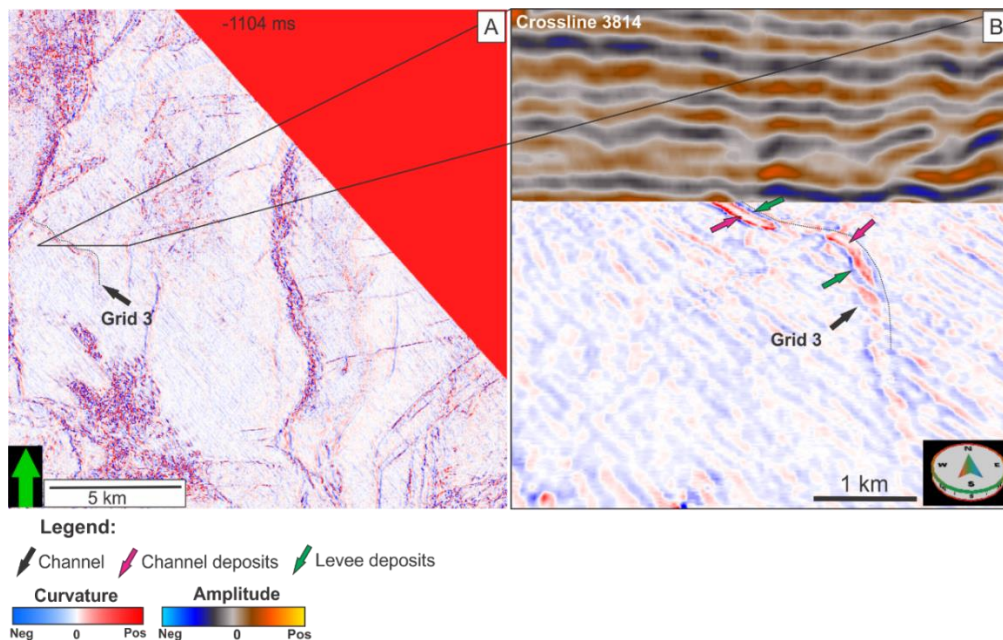d 3. B) Zoomed-in chair display showing crossline and stratal slice through combined most negative and most positive curvature attribute. Pink and green arrows show channel fill and channel edges (flanks) respectively.

By combining most positive and most negative curvature attributes for Grid 3 (Figure 66), the definition of internal morphology as that of low-energy, mud-filled channel is revealed by Curvature attribute. The most positive curvature attribute highlights channel fill by most positive curvature attribute with red. Differential compaction accounts for aspect of channel fill being substantially more compactable and therefore more mud-rich than the adjacent levee deposits (Posamentier, 2003). Potential levee deposits highlighted by most negative curvature attribute with blue and are defined as sand rich. Levee deposits are thus the largest and most extensive sand-prone architectural element of channel belt.

High accurate 3D model of the Grid 3 channel was created in Geoteric and combined with Envolope attribute (Figure 67) in order to calculate the channel parameters (Table 3) and analyze channel morphology. The Envelop attribute shows a limited area with almost circular localized values of high envelope attribute,

associated with point-bar and concave-bank areas and having typical meandering distribution, were interpreted as sandy deposits of channel point-bar and concave-bank areas, accumulated in stable homogenous depositional environment. Where sand-prone point bars preserved on the inside of meander bends and concave-bank deposits preserved in concave-bank areas (Figure 67 B). Channel Grid 3 migrated by lateral expansion and therefore maintained distinctive, completely separated, circular bodies of accreted point bars and concave-bank deposits defined in plan view (Figure 67 B). The sediment accretion patterns are important to characterize paleo-flow direction. The accretion deposits show very weak sign of downstream translation relative to the initial mapped bend apex and indicate a paleo-flow direction to the west and north-west, which is consistent with general propagation of the sediment dispersal system (5.1 Seismic stratigraphy).
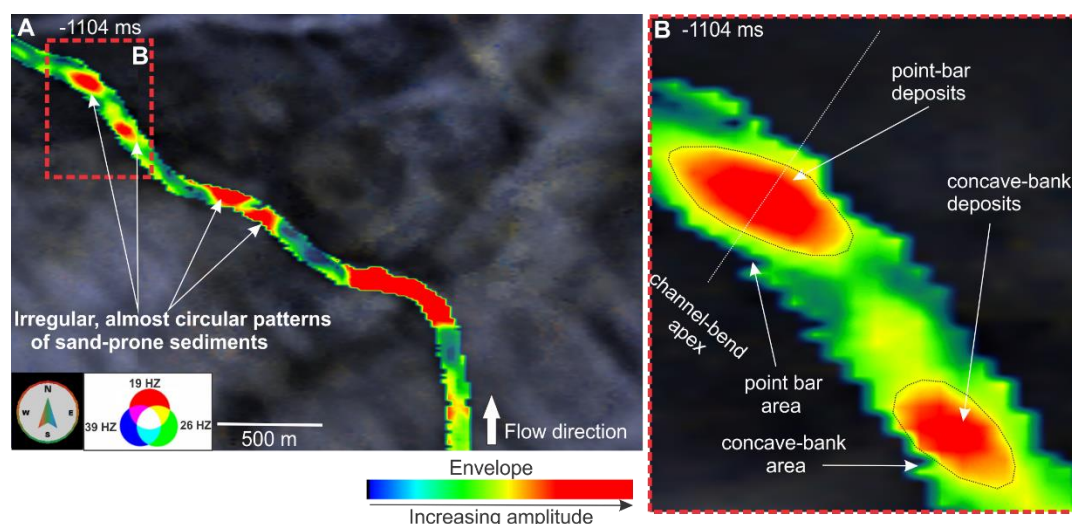
Figure 67 A) Channel Grid 3 3D Geobody with extracted Envelop attribute values. B) Plan View of channel bend showing areas of sediment preservation along channel bend.

Quantitative Geomophology of channel valley

Channel 3. – The overall morphology of the channel valley of meandering channel Grid 3 is similar to channel Grid 1 and Grid 2. It has moderate average sinuosity (≤1.202), but is characterized by low sinuosity (≤ 1.000) up-system and moderate to high sinuosity (≥1.400) down-system. Furthermore, the channel width decreases markedly down-system, from approximately 110 m km to less than 100 km in width. It reveals distinctive and clearly visible patterns of channel fill, flanked by downlaping continuous wing-shaped moderate amplitude reflections of internal levees (Figure 68).

Its amount of incision fluctuates along the entire length. The amount of incision varies along the channel, having its maximum value at the distal reach (westward) (≈ 4 ms ≈ 4.5 m), thus showing positive correlation with channel sinuosity, and interpreted as being formed by erosional processes.
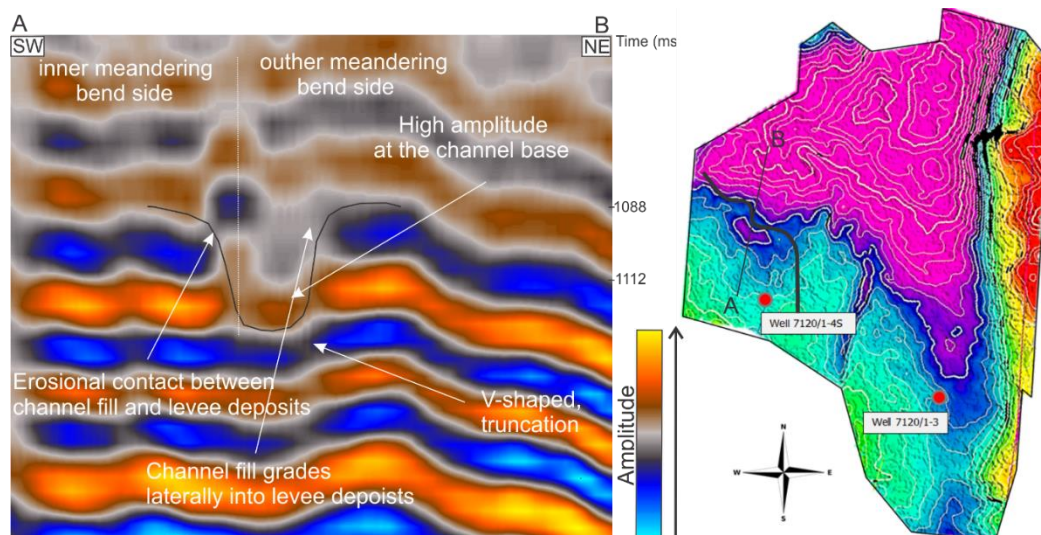
Figure 68 Interpretation of vertical seismic section of Grid 3 target channel (Inline 5048). Location of the seismic line AB is shown on inset map.

Mud-filled channel is associated with lower energy system. Narrow, aggradational channel fill deposits shows no distinctive signs of meander-loop downstream translation are therefore preserved as narrow ribbon along the channel belt. Low to moderate amplitude reflections of channel belt fill, are characterized by some localized high amplitudes at the bottom, interpreted to indicate basal-lag sand bodies. They have strong non-uniformity and uncertainty in its spatial distribution, since they are un-equal distributed along the channel belt, making it hard to refer is to specific location trend. Considering the presence of the basal-lag sand bodies, deposition of fluvial facies with lithology referring to interbed siltstone and mudstone-bearing fine sandstone with unequal thickness is proposed.

6.1 Channel dimensions

In order to quantify and describe the fluvial geometries interpreted from the 3D seismic data, the centerline of each channel body was mapped independently as a polygon and measurements were taken (Table 3). It displays the range in hydraulic parameters calculated for the channels analyzed in this study. On Figure 69, the

example of a planform of Grid 1 meandering stream showing definitions of: valley axis, channel-thalweg length Lt, bend apex, bend width, local centerline radius of curvature Rc, bend-thalweg length Lc, bend-wave length Lb and the results of sinuosity measurements, depth and width of the channel bodies and channel complex thickness.

Table 3 Channels dimentions

	Grid 1	Grid 2	Grid 3
Channel-thalweg lenght, Lt (m)	18847.126	7504.139	4453.089
Channel valley axis, Lv (m)	8027.062	2512.040	1013.017
Bend thalweg lenght, Lc (m)	7744.596	1689.632	924.556
Bend wave axis lenght, Lb (m)	5020.000	1348.905	850.006
Initial sinuosity (Lc/Lb)	1.080	1.130	1.040
Rosgen's sinuosity classification	Moderate	Moderate	Moderate
Secondary sinuosity (Lc/Lb)	1.200	1.260	1.202
Local centreline radius of bend curvature, Rc (m)	2100.00	602.00	221.151
Channel body width (m)	180-200	100-118	100-110
Thickness (ms) Geoteric	43.66	39.40	20.35
Thickness (m) Geoteric (100ms=122m)	53.26	48.068	24.80
Total surface area (km^2)	4.180	3.270	0.860
Migration mode	Expansion/translation	Expansion/translation	Expansion
Channel gradient (degrees)	≤ 0.02	≤ 0.02	≤ 0.02

Planform geometries were measured from three individual channel bodies (Grid 1, Grid 2and Grid 3) and compared on the basis of their extend, width, sinuosity and thickness. The sinuosity is the result of changes in channel course (J. D. Clark & K. T. Pickering, 1996). This measurement indicates the degree of meandering and channel migration within a valley that the channel exhibits (Rosgen, 2007). The initial sinuosity (Figure 69 B) was measured at the earliest stages of channels evolution and the secondary sinuosity (Figure 69 A) at the latest as the ratio between bend thalweg length (Lc) and bend wave axis length (Lb). Noteworthy features of Figure 69 is the increasing sinuosity with increasing channel migration through time of channel evolution and hence increasing of bend-thalweg length. Varying through evolution time local centerline radius of curvature Rc is also a product of increasing bend-thalweg length and hence channel migration. Increasing Rc by one-half from its initial value produces more sinuous channel planform and apparently expands meander bend loop (Figure 69). Channel-belt width and channel sinuosity for each of three channels vary

along the length of the channel belt. Within all three channels described in this study, the increase of lateral continuity or extend (channel-thalweg length, Lt) during channel evolution goes along with increase in bend-thalweg lenght and local centreline radius of bend curvature. None of the streams have bends with similar shapes. Variations of parameters other than bend-thalweg length (Lc), meander bend wave axis length (Lb), as well as channel-thalweg lengths (Lt) and channel valley axis length (Lv) cannot affect sinuosity. The largest variation of initial channel sinuosity and secondary sinuosity of developed channel was calculated for Grid 3. Thickness was measured in millisecond as two-way travel time (TWT) from seismic data and converted to depth using a velocity-depth relationship 100ms = 122m, based on seismic interval velocities of 2417m/s.
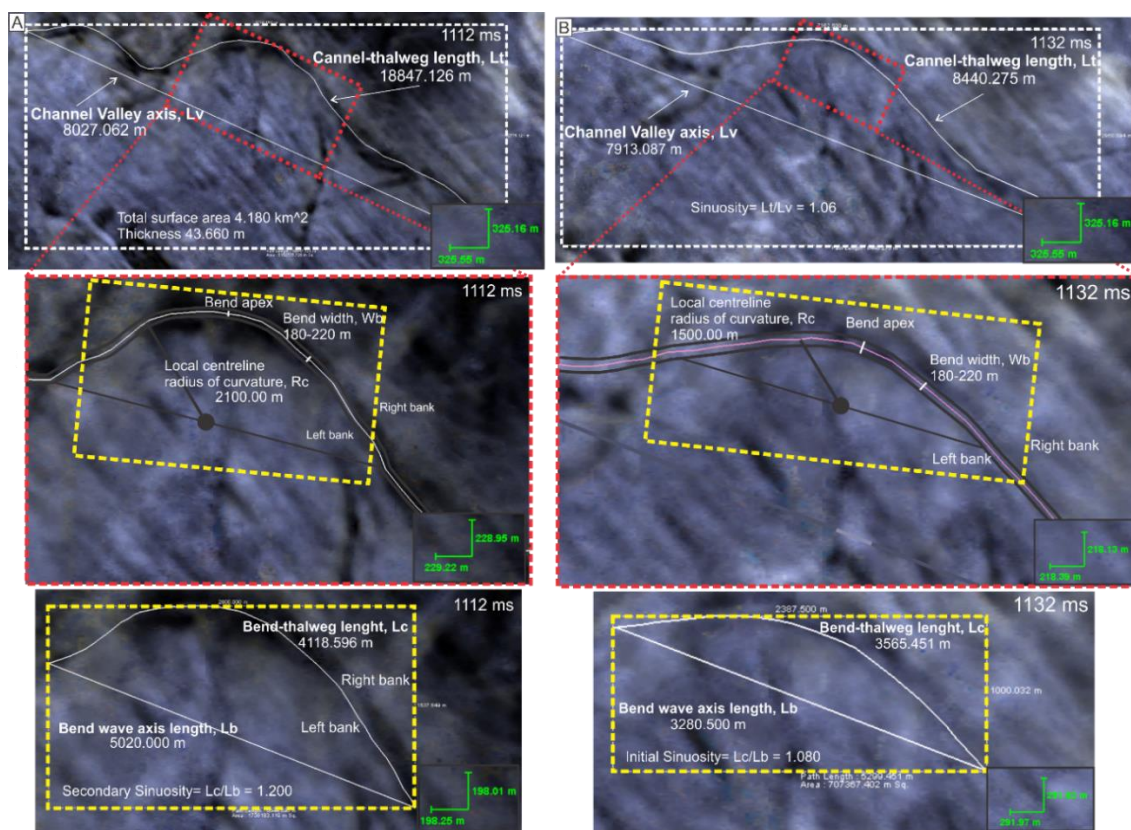
Figure 69 Channel Grid 1. Planform geometries of a meandering stream showing definitions: Valley axis, channel-thalweg length Lt, Bend apex, Bend width, Local centerline radius of curvature Rc, Bend-thalweg length Lc, bend-wave length Lb and measurements of channel sinuosity using Lb and Lc. A) Channel Grid 1 planform geometries are measured at the latest stage of channel evolution (1112 ms). B) Channel Grid 1 planform geometries are measured at the earliest stage of channel evolution (1132 ms).

Chapter 6 Discussion

In the following discussion, channel migration patterns have been identified for channels Grid 1, Grid 2 and Grid 3. It has also been discussed how channel migration patterns lead to preservation of point bar and concave-bank deposits and predict their geometry, shape and grain-size distribution along the curved bend segments of fluvial channels. The understanding of the control over direction of accretion of channel deposits is important to indicate paleo-flow direction. The data generated for this study allows analyzing seismic facies associated with fluvial paleo-channels, its architecture and planform geometries.

6.3 Seismic facies

Channel bodies of different sizes and shapes are found in non-marine part of upper part of the Snadd Formation. A series of facies have been identified from integrated seismic data analysis. Four seismic facies were used to identify the channel systems on the basis of reflection amplitude, architecture, geometry and lateral continuity. Four of mentioned seismic facies represent three specific depositional environments: 1) overbank deposits and levees, 2) internal channel fill deposits, and 3) accreted surfaces of point bar and concave-bank deposits. The study of the internal geometry of Grid 1, Grid 2 and Grid 3 channels reveals them to have a range of following seismic facies.

Seismic facies 1

Seismic facies 1 appear as low to moderate, continuous reflections dipping towards the last-stage channel thalweg and confined within channel in vertical seismic sections and interpreted to as lateral-accretion packages (LAPs) (M. Janocko & W. Nemec, 2012) (Figure 70, seismic section CD). LAPs are commonly related to longitudinal moderate to high amplitude patches in the meander bend apex zones in attribute maps for sinuous channels. Lateral accretion packages similar to those in Figure 70 (seismic section CD) can be found for Grid 1 and Grid 2 channel systems and are interpreted to be meander-scroll patterns, represented by accreting channel belt deposits of point bars and concave-bank, where meander scrolls reflect deposition of relatively long-lived meandering rivers (Tore Grane Klausen, et al., 2014).

Concave bank deposits

Concave-bank deposits accumulate in concave-bank area (Figure 74 A, B), which extends from a channel-bend crossover into the area where thalweg deepens along the outer bank (Brian J. Willis & Hong T., 2010). The downstream translation through crossover area necessitates sediment used by accumulations, which caused by erosion at the head of the upstream point bar (Woodyer, K.D, 1975; Brian J. Willis & Hong T., 2010). Accretion of concave bar deposits produce fining up succession of muddy, or at least more heterolithic than adjacent point bar deposits (Brian J. Willis & Hong T., 2010).

Point bar deposits

Point bar deposits are formed in the initial meander bends (Figure 74 A, B). During individual flow events bank erosion on the outer side of the channel bend provided sediments to form a point bar on the inner side downstream. Development of the initial point bar triggered the formation of the downstream point bar, which in its turn triggers the formation of the third bar (Wietse I. van de Lageweg, 2012).

Seismic facies 2

Seismic signature of seismic facies 2 is characterized by wing-shaped, continuous, dipping away from the channel axis, low to moderate amplitude reflectors, downlapping onto strong acoustic base reflector and immediately adjacent to channels (Figure 70, seismic sections AB, CD and EF) (Schwenk, T. & M. Breitzke, 2005). Seismic facies 2 are highly variable in their thickness and internal architecture along the data set. They are typically two or more reflection thick in vertical cross sections for Grid 1, Grid 2, and Grid 3. Seismic facies 2 is interpreted as overbank deposits that form gull-wing proximal levees (M.J.R. Gee & R.L. Gawthorpe, 2006). Proximal levees along the outer bend side show initial thickening and then thinning trend toward distal levees. This principal structure is identified in the levees of all channel-levee systems in the study area. However, thickness-to-width ratio of these units is obviously different and varies from system to system. The seismic architecture of positive relieve levees depends on the distance away from the channel and on the side of the channel it belongs to (Conveners Mike Mayall & Ian Kane, 2011). The contact between channel fill deposits and outer-bend levee is mostly erosive. On inner bend side, on the other

hand, channel fill onlap levee deposits or grade laterally into finer, thinner levee deposits, which in fact suggests flow continuity.

Levee deposits

These deposits have been interpreted as fining upward deposition of fine-grained sediments, which have been deposited as the current travelling through the channel over spilled and built up levees on the sides of the channel. In this study channel-levee deposits are divided by into two "end-member" facies: sand rich, with and mud rich and are the largest and most extensive architectural element of channel belts. In seismic attribute maps, the levees appear as areas of low amplitude reflections contouring high continuous refection amplitude of single channels. Levee deposits might not be clearly distinguished along the entire channel-levee system, meaning that the channel belt is not entirely well laterally constrained by levees, indicating avulsive character of the channel segment. The contact between channel fill deposits and outer-bend levees is mostly erosive. On inner meander bend sides, channel fill grade laterally into finer levee deposits, which in fact suggests flow continuity, and is characterized by weaker reflections dipping toward the channel center (LAPs).

Seismic facies 3

Seismic facies 3 is widespread mostly parallel high-amplitude continuous reflectors (Figure 70, seismic section AB), which are adjacent to channel-levee systems and extend away from channel axis. Many seismic facies 3 can be traced over longer distances than the others cannot, and some are disrupted and discontinuous. Seismic facies 3 may also consist of high-amplitude, discontinuous reflections at the base of channel valleys. Seismic facies 3 is interpreted as High amplitude reflections (HARs). Interpretation based on the internal architecture in seismic data reveals the packages of high amplitude parallel reflectors. Continuous, high amplitude packages, which correspond to thick beds of fine to medium grained massive to graded sand, were identified on Amazon River (Schwenk, T. & M. Breitzke, 2005). Accordingly, these reflectors have been interpreted as splays or overbank deposits, representing thick package of fine to medium grained massive sand, which can be identified for Grid 1, marking the channel-bend axes, since over-spilled deposits occur outer bends (Henry W. Posamentier & Roger G. Walker, 2006). On Amazon River, these packages are

interpreted to be deposited as the result of levee avulsions and represent sandy lobes (Schwenk, T. & M. Breitzke, 2005). If high amplitude reflectors packages are building dipping blocks, they might be deposited by simultaneous lateral migration of the channel axes (Schwenk, T. & M. Breitzke, 2005).
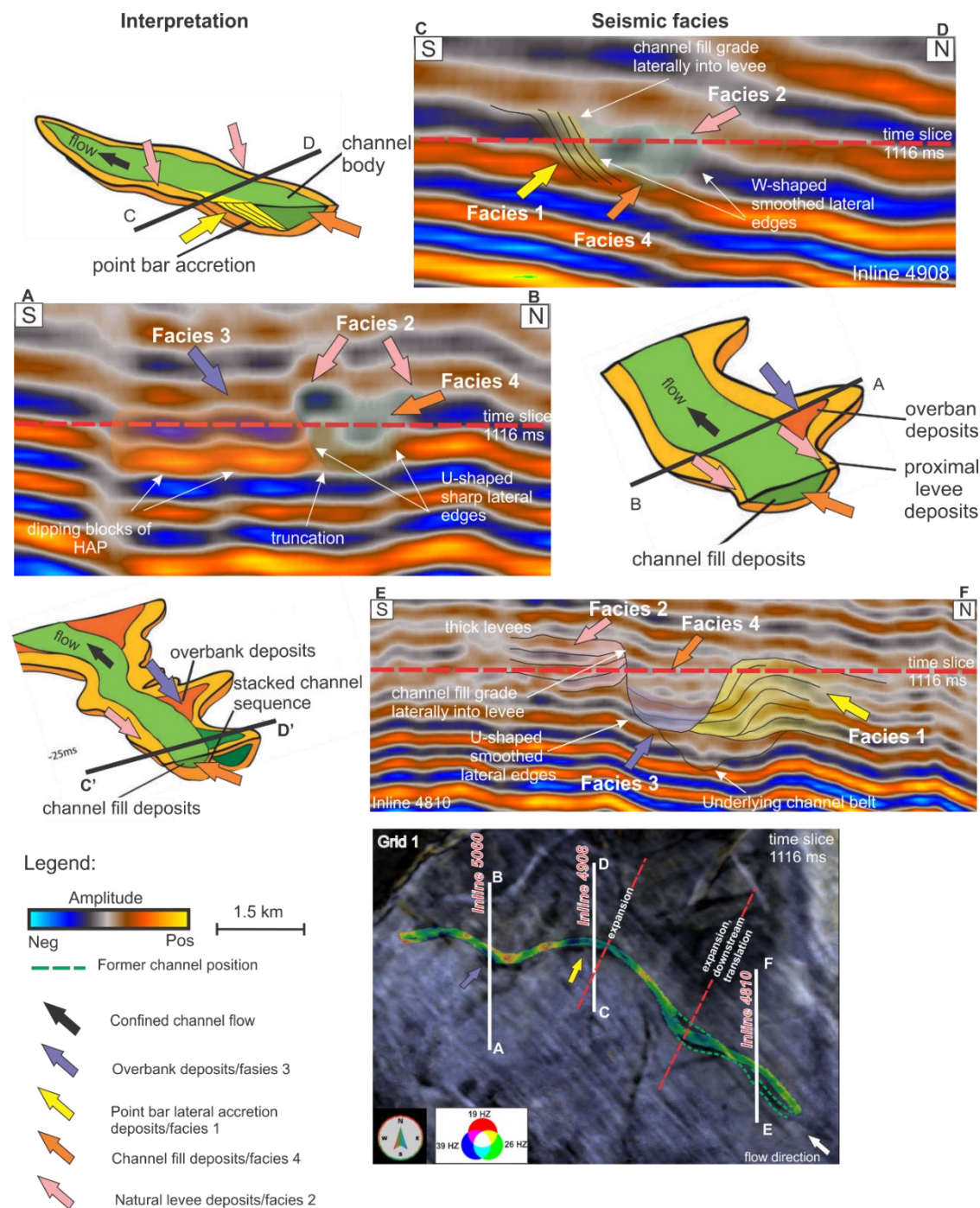

Figure 70 Vertical seismic sections AB, CD and EF showing different architectural elements. Examples are taken from Grid 1 channel-levee system. For detailed description and discussion, see txt. Plan view of Grid 1 channel plotted against spectral decomposition slice, showing the location of AB, CD and EF seismic lines.

Lateral migration distances generally do not exceed lateral extent of these overflow deposits, they can ensure the lateral connectivity between the single channels or can also connect main channel conduits laterally. The lack of the recognizable localized overbank deposits have been reported from few meandering channels. However there's no doubt that the channelized flows were spilling out and spreading sediments in overbank areas, which means that flow was sufficiently confined by channels, and spill outs were moderate or they dissipated within a relatively short distance from the channel, resulting in levee build-up (M. Janocko & W. Nemec, 2012). Discontinuous high amplitude packages, which occur at the base of the channels analyzed in this study, are interpreted as coarse-grained lithologies deposited in the channel axis (Figure 70, seismic section AB) (M.J.R. Gee & R.L. Gawthorpe, 2006).

Seismic facies 4

Seismic facies 4 is characterized by most distinct discontinuous to chaotic and discordant, or parallel reflectors of low to high amplitude, which appear as vertical W- or V-shaped packages with sharp or smoothed lateral edges (Figure 70, seismic sections AB, CD and EF). This seismic signature is found within dipping, low to moderate amplitude reflectors of seismic facies 2, previously interpreted as levee deposits. The vertical high amplitude packages of channel fill deposits are often associated with erosional and mounded channel body architecture incised into the sediment beneath. Seismic facies 4 shares its internal architecture with a vast majority of the channels fills observed in the study area. Higher reflection amplitudes compared to the levees indicate that channel fill deposits are comprised of coarser grained sediments (Schwenk, T. & M. Breitzke, 2005).

Channel fill deposits

The channel fill deposits are interpreted as being formed by scour and fill processes within a channel and represent ribbon-shaped bodies of sandstone- and mudstone-filled channels with or without associated lateral migration packages (LAPs). Due to its interpreted sandstone fill of Grid 1 and Grid 2 channels, these channel fill bodies are considered as being more affected by accretion, rather than mud-prone Grid 3 channel. The extent of lateral accretion vary considerably within the channel valley, resulting in a broad spectrum of channel shapes and lateral instability. The

seismic character of the channel infill pattern varies in cross section along the channel belt and suggests changes in flow conditions throughout the channel system evolution (Paivi Heinio & Richard J. Davies, 2009).

6.2 Fluid flow controls on sediment sorting within meander bend

Sinuous channels become more asymmetric because of the downstream translation and lateral expansion migration through time of channel evolution, which leads to successive preservation of point bar and concave-bank deposits. The fluvial channel migration pattern discussed here also predicts grain-size distribution (sediment sorting) along the curved segments of fluvial channels.

Thickness maps were generated for three channels Grid 1, Grid 2 and Grid 3 to analyze time-thickness variations in milliseconds between Top and Base generated surfaces. An expected thickness profile of a channelized body, where thickness decreases away from the channel axis toward the channel edges was aquired. Thickness map (Figure 71 C) shows the time-thickness variations in milliseconds between Top and Base surfaces generated for channel Grid 1. The thickness for Grid 1 channel ranges from around 38 to 40 ms (approximatelly 49 m, 100ms = 122m where average interval velocity of 2417m/s from well log data) along the channel axsis to around 32-36 ms (approximatelly 39 m) at the channel edges. However, the maximum thickness of 40-42 ms (TWT) is clearly corresponds to the location of meander bends (Figure 71 C, D).

Due to continued erosion of the outer bank and deposition of bedload on the inner bank, channel bend migrates by increasing in sinuosity and flow scours deeper along the outside of the bend apex (closest bank to thalweg). Scour near the apex of mender bend can be twice as deep as channel depth (Brian J. Willis & Hong T., 2010). The maximum thickness sections found corresponding to meander bends location, have been interpreted to indicate the location of the closest bank to the thalweg, which experienced relatively fast flowing water against it. These changes in topography within a channel belt have an impact on the grain size distribution (sorting), since coarser grain sediments have a tendency to move toward and accumulate in outside deeper part of the channels bend.
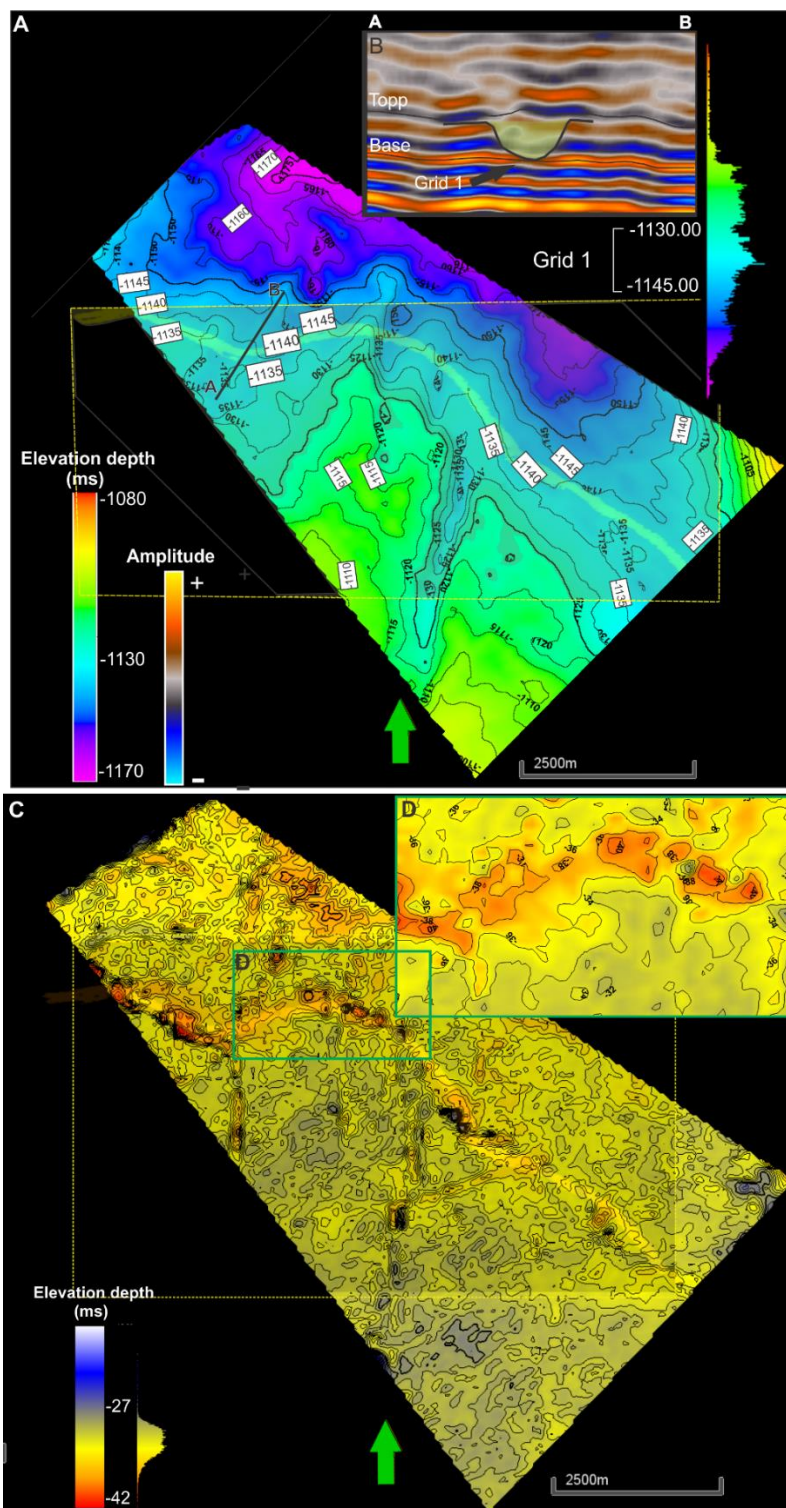
Figure 71 A) Grid 1 geobody plotted against Grid 1 Bottom Surface Isochron map contoured in TWT (ms). B) Vertical seismic section showing the Top Grid and Bottom Grid 1 surfaces used to calculate thickness map, C) Grid 1 thicknes map contoured in TWT (ms) and generated between Top and Base Grid 1 surfaces. Thicker deposits are shown in red colors. D) Zoomed in section of the maximum thickness interval, showing topography variations within the meander bend, where outer bank experiences fast flowing water against it, which results in meander bend being scoured deeper along the outer bend of the meander.

Figure 72 A) Time-map showing location of AA' seismic line traced along Grid 1 channel. B) AA' seismic line. Yellow boxes indicate location of meander bend apexes, which correspond to variations in internal seismic amplitude 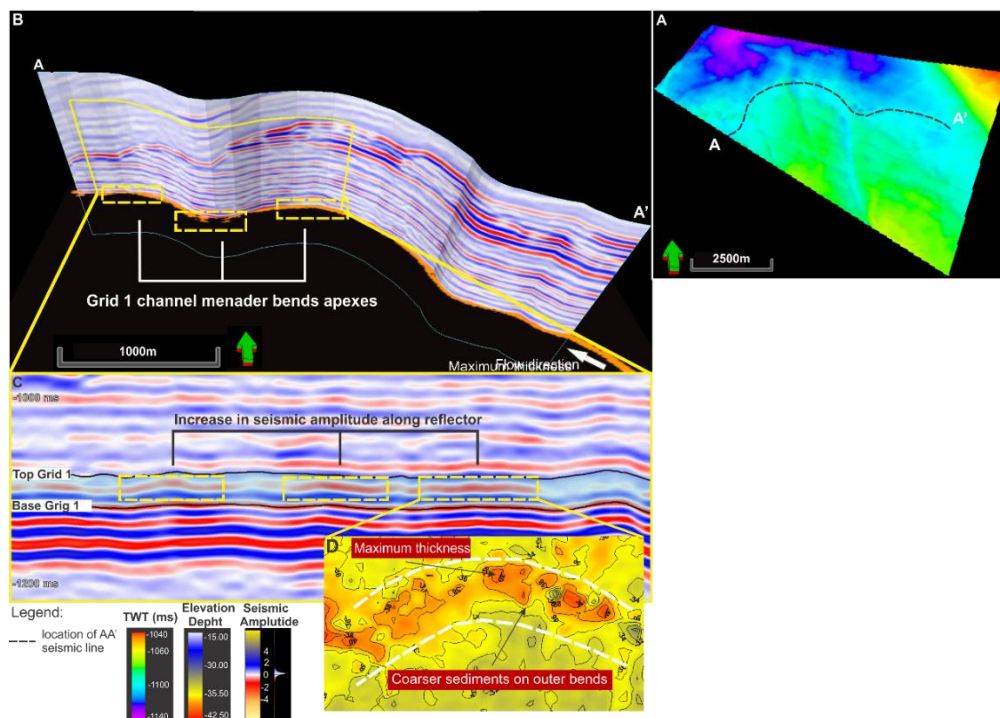along seismic reflectors (C). C) Long profile seismic section down the main axis of channel Grid 1, showing increased amplitude packages. D) Thickness map generated between Top and Base Grid 1 depth surfaces (see location in figure 71), indicating coarser sediment accumulation on outer parts of the meander apex.

Figure 72 C shows longitudinal profile of channel Grid 1 and variation in internal seismic amplitude along seismic reflector. Where increased amplitude packages (inside yellow boxes) correspond to the location of meander bend apex, indicating coarser sediment accumulation in the outside deeper part of the channel bends.

6.4 Channels migration patterns

The migration of channel segment in position over time has always been the subject of the research, because of its importance for a channel-belt deposit growth (Brian J. Willis & Hong T., 2010). River meandering is a complicated process, involving the interaction of the flow through channel bends, as well as bank erosion and sediment transport (Stephen T. Lancaster & Rafael L. Bras, 2001). During individual flood events, erosion along the outside of the channel bend caused cutbank retreat, and deposition occurred along the inside of the bend, resulting in the successive lateral migration of river channel and associated point bars and resulting in channel following the sinuous path (Brian J. Willis & Hong T., 2010; Randle, 2006). Based on this theory, several meander migrations models are recognized: lateral expansion (increase in

meander bend sinuosity and amplitude), downstream translation (movement of meander loop downstream) and rotation (asymmetry development of meander bend) (Nils Janbu, et al., 2007). Meander loop migration is common attribute of the developing channel, with both meander swing and sweep patterns (Henry W. Posamentier & Roger G. Walker, 2006), whereas swing in common for expansion model and sweep for translation.

Meander river channels were identified on the basis of their moderate sinuosity, ribbon-like continuous reflections and low gradient. Expansive and downstream translating meandering channel segments leading to accretion and therefore preservation of channel belt deposits formed in bar and concave-bank areas, resulting in their enlargement with each migration step. The important implication of studying sediment accretion patterns is the identification of paleo-flow direction, since lateral accretion deposits translate downstream relative to the initial mapped bend apex and indicate a paleo-flow direction, which is genarally consistent with wets-northwest general propagation of the sediment dispersal system (5.1 Seismic stratigraphy).

6.4.1 Channel 1

In plan view, channel Grid 1 has a moderate sinuous channel axis for all 18.8 km length (Table 3), with some morphological features identified within a channel belt: point bars, meander scrolls and chute channel (Figure 73 A). In this example, the seismic expression of meander channel Grid 1 can be interpreted as regions dominated by fill of underlying channel segments highlighted by yellow and associated with meander scrolls patterns and region dominated by inner levees and floodplain deposits highlighted by green. Successive migration of the river channel, resulting in channel widening the formation of the meander scrolls. In Figure 73 D, E the stacking of meander-bends against and upon each other implies a meander-bend evolution by lateral expansion combined with a less pronounced downstream translation, where it shows a series of channel alignments over the period from -1132 ms to -1112 ms. Lateral expansion mode is associated with meander loop swinging and cause its widening. Whereas downstream translation, associated with sweep patterns, formed as thalweg is exercising maximum erosive force on the outer bend, forcing river to migrate across the river valley.
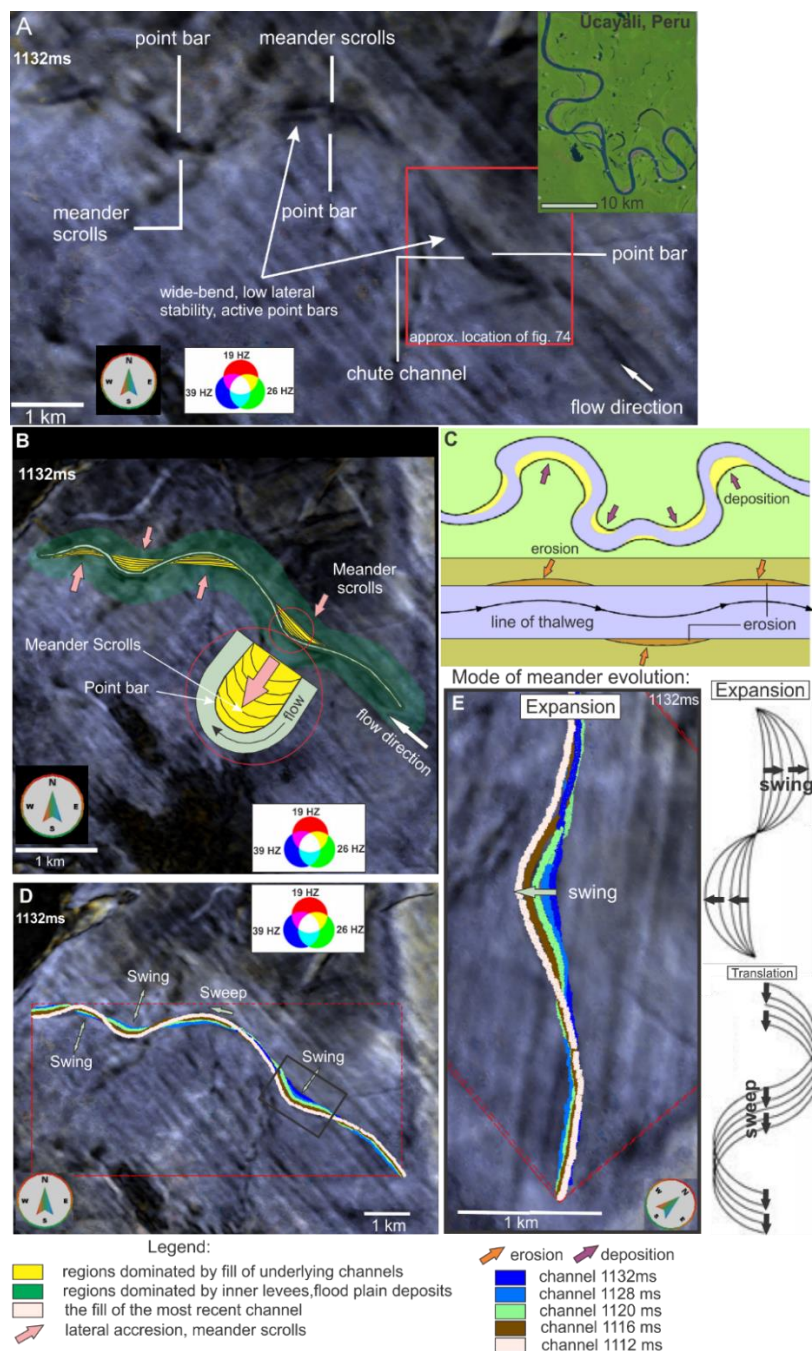
Figure 73 Meander-loop development for Grid 1 channel. A) Uninterpreted spectral decomposition cube at a frequency subband of 19-26-39 HZ at -1132 ms, showing single meandering channel Grid 1 and revealing morphology of the channel belt. The inset picture in the upper right corner shows a clear analogy of Grid 1 channel with wide-bend, active point bars, low lateral stability Ucayall River channel in Peru. B) Interpreted spectral decomposition cube at -1132 ms, showing regions dominated by fill of underlying channels highlighted by yellow and region dominated by inner levees and floodplain deposits highlighted by green, and the fill of most recent channel by highlighted by white. Pink arrow point at successive migration of the river channel, resulting in the formation of the meander scrolls. C) Schematic meandering river channel, with purple arrows indicating lateral accretion direction, and meander scrolls location. Flow in the channel follows sinuous thalweg resulting in erosion (orange arrows indicating erosion sites) of the bank in place. D) Spectral decomposition slice shows a series of channel alignments over the period from -1132 ms to -1112 ms, illustrating meander-loop swing and sweep features within the channel. Cannel color threads indicate order of formation. (E) Meander-bend evolution by lateral expansion, after (Nils Janbu, et al., 2007). Diagrams show Expansion and Translation meander modes, associated with Grid 1 fluid flow.

Maximum rate of bank erosion is located along the outer bend. Concave-bank area (Figure 74 B) is located at some phase lag distance upstream of the meander bend apex (Figure 74 C). Since channel experienced downstream translation, the greater the planform phase-lag was, the more channel bend migrated across valley axis (Randle, 2006). Figure 74 A, B shows channel's Grid 1 geobogy populated with Envelope attribute values, showing areas of sediment preservation along channel bend. Limited localized areas with high Envelope values are indicative of porous lithologies (Leonardo Azeved, et al., 2009) and therefore were interpreted as sandy deposits of channel point-bar and concave-bank areas. It can be seen, that the channel sandbodies have a typical meandering distribution (Pu Renhai, et al., 2009), with sand-prone thick point bars formed on the inside of meander bends and concave-bank deposits accumulated in concave-bank areas. Patterns of meander bend migration by translation and expansion lead to preservation of deposits formed in point bar and concave-bank areas and show successive accretion of concave-bank and point bar deposits, leading to an increase in deposits length and width and amount of connectivity with each migration step (Figure 74 D) (Wietse I. van de Lageweg, 2012). Significance of the accretion rate for sediments differs from step to step. In this example, accretion is compared on the basis of channel Grid 1 evolution through time, where more significant point bar and concave-bank sediments accretion is identified on the latest stages of channel evolution (Figure 74 D).

Initially channel Grid 1 of low sinuosity (1.080) with narrow point bars and concave-bank deposits developed through lateral expansion and downstream translation into meandering river channel with 5 meander bends of moderate sinuosity of 1.200 (Table 3). Bend expansion continued over the 300 m, bend translation over 100 m. The amount of connectivity of point bar and concave-bank deposits is increasing with each migration step, as sediments get more accreted. Meander bend migration patterns provide interpretation of Grid 1 channel as being developed by significant bend extension and less significant downstream translation of sand-bed meandering fluvial channel. The bar and bend stretched out to a length longer than initial, resulted in formation and growth of bends and increased sinuosity until the firs upstream bend was cut off to for chute channel.
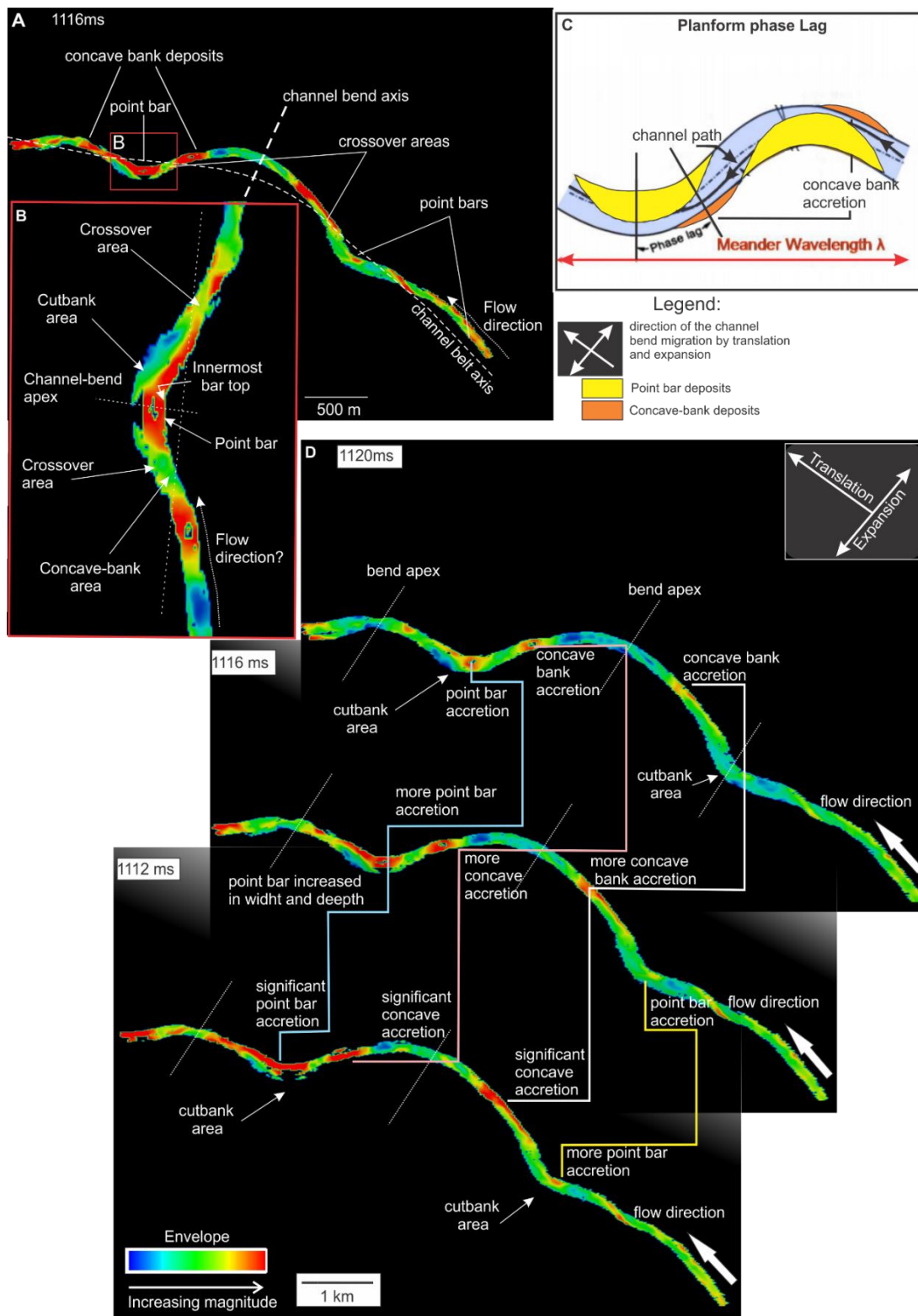
Figure 74 Envelope Cookie Cut into Grid 1 geobogy A) Plan View of channel bend showing areas of high Envelope values at -1116 ms. B) Zoomed in plan view of channel bend showing areas of sediment preservation along channel bend. C) Planform Phase lag. The greater the planfrom phase lag, the greater downstream migration of the meander bend along valley axis (Randle, 2006). D) Patterns of meander bend migration by translation and expansion leading to preservation of deposits formed in point bar and concave-bank areas and showing successive accretion of concave-bank and point bar deposits leading to an increase in deposits length and width with each migration step. In addition, identifying paleo-flow direction.

6.4.1.1 Chute channel

Initially low sinuosity sand-filled Grid 1 meandering channel developed by both lateral expansion and downstream migration, where outer bend erosion was balanced by formation of scroll-bars. Significant bend displacement/bend growth for upstream meander bend between channel's color threads (Figure 75 A, B) indicates significant area of bend expansion, increase in curvature and sharper bends. Since rapidly extending bends of sand-filled meandering rivers are vulnerable to dissection by chute channels (Grenfell, 2012), meander bend growth was alternated by chute cutoff formation, when critical bend amplitude was reached (W. M. van Dijk et al., 2012), and flow advances onto and over the point bar (Figure 75 C). The probability of chute cut-off increases as sinuosity increases (Bridge & Demicco, 2008). It has been suggested, that the formation of chute cutoff would be favored at bends with particular characteristics, such as high meander bend sinuosity, lower values of curvature and bend geometry (Grenfell, 2012). Single bend cutoffs occur as the meander bend growth proceeds due to downstream migration, lateral expansion and bank erosion produces a higher amplitude bend (Figure 19 A) (W. M. van Dijk, et al., 2012). Termination of bend growth and main channel flow pathway shifting were coupled to the occurrence of chute cutoff, which prevented the development of high sinuosity meander (W. M. van Dijk et al., 2012)

Chute channel is located close to the inner-bend apex of Grid 1 upstream meander bend and is connected to inner bend at the bifurcation point (Figure 75 D). Single bend cutoff occurred as bend significantly migrated both laterally and downstream. And chute cutoff development was most likely the result of overbank flow, which occurred when upstream meander bend became sharper as meander segment sinuosity increased. Figure 75 (inset picture in upper right corner) shows a clear analogy of Grid 1 channel with wide-bend, active point bars with stable chute channel of Strickland River in Papua New Guinea, where bend is also subjected to rapid extension.

6.4.2 Channel 2

In plan view, channel Grid 2 has a moderate sinuous channel axis for all 7.5 km length (Table 3, Figure 76 A). For channel Grid 2 migration patterns are quite similar to these previously identified for Grid 1.
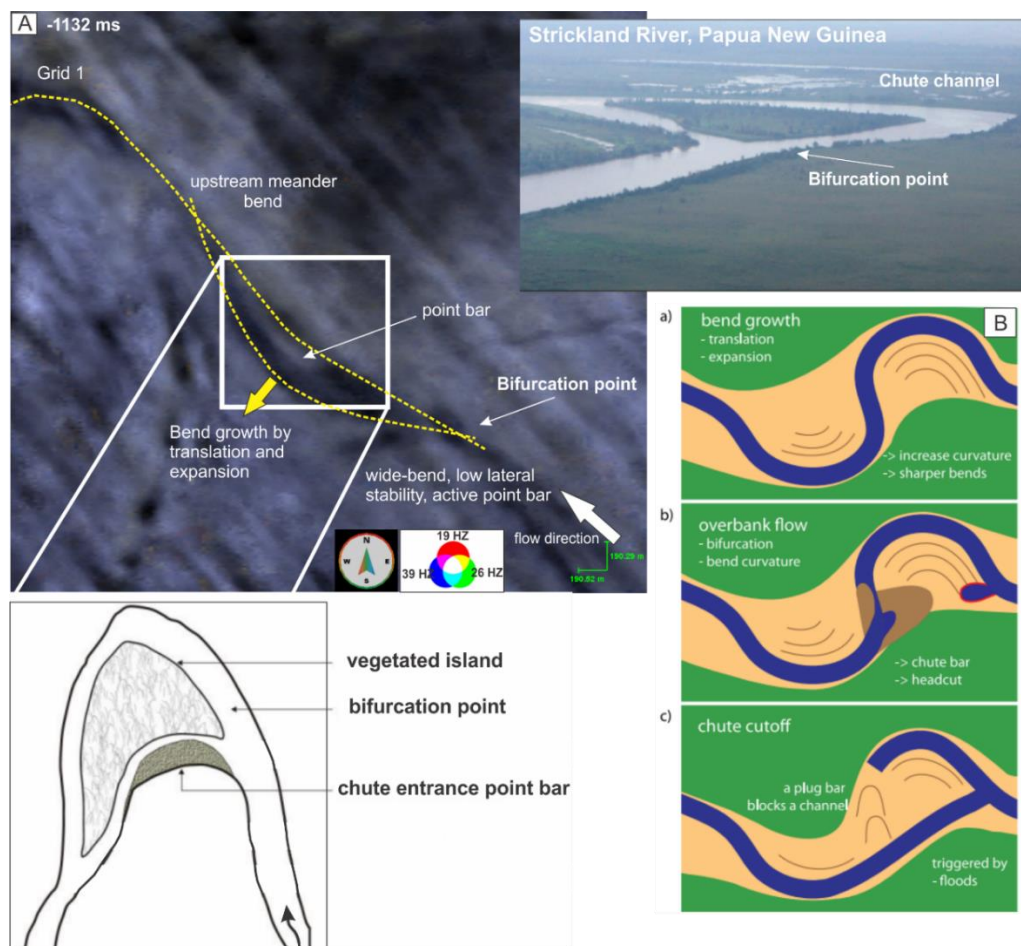

Figure 75 A) Spectral decomposition cube at a frequency subband of 19-26-39 HZ at -1132 ms showing single meandering channel bend of Grid 1 undergoing significant lateral extension and morphology of a bifurcate meander bend. The dotted yellow lines indicate first and last order of bend formation. The inset picture in the upper right corner shows a clear analogy of Grid 1 channel with wide-bend, active point bars with stable chute channel Strickland River in Papua New Guinea (Grenfell, 2012). B) The development pathway, illustrating the formation of stable chute channel: a) A conceptual model for chute cutoff development in meandering river with bend expansion and translation, b) Flow goes over the point bar, causing further development of chute through the chute bar, c) Once the chute channel established, the old meander bend has an unfavorable entrance curvature and is eventually disconnected from the channel. Modified from (W. M. van Dijk, et al., 2012).

In Figure 76 B the stacking of series of channel alignments over the period from -1144 ms to -1120 ms against and upon each other implies a meander-bend evolution by lateral expansion combined with a less pronounced downstream translation, where it shows both swing and sweep features. Meander bend stretched out to a length longer than initial, resulted in meander loop growth and increase in channel sinuosity.
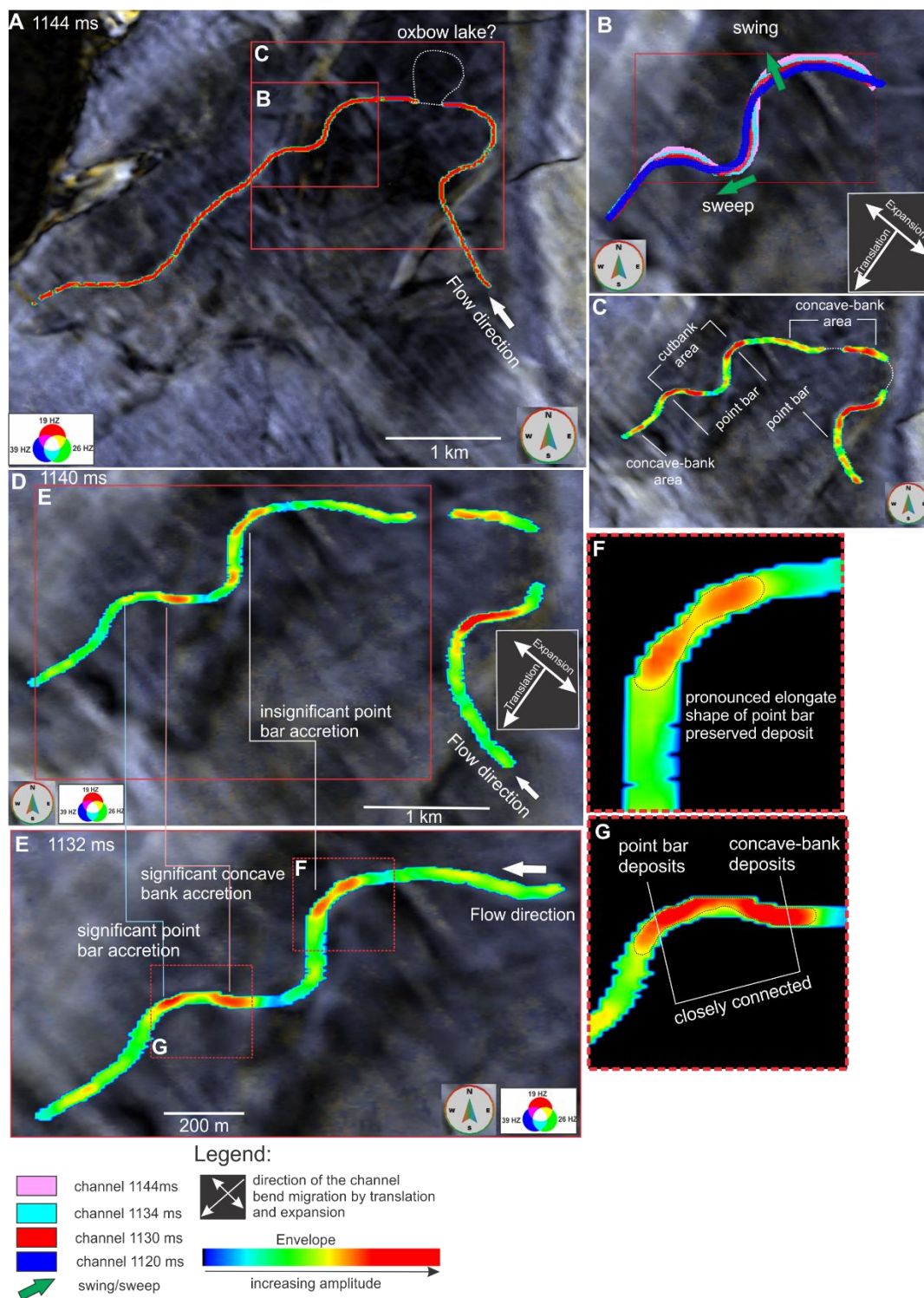
Figure 76 Plan View of Grid 2 channel belt. A) Spectral decomposition cube at a frequency subband of 19-26-39 HZ at -1144 ms showing the meandering Grid 2 single channel. B) Series of channel alignments over the period from -1144 ms to -1120 ms, illustrating meander-loop swing and sweep features. Channel color threads indicate order of formation. C) Plan View of channel bend showing areas of sediment preservation along channel belt. (D-E) Patterns of meander bend migration by translation and expansion leading to preservation of deposits formed in bar and concave-bank areas and showing successive accretion of concave-bank and bar deposits leading to an increase in deposits length and width with each migration step. (F-G) Zoomed-in section of meander bend showing shape and connectivity between single point bar and concave-bank deposits with each migration step of sediments preserved along channel bend.

Figure 76 C shows channel's Grid 2 geobogy populated with Envelope attribute values, showing areas of sediment preservation along channel bend: point bar and concave-bank areas, where limited, localized areas of irregular elongated high Envelope values are indicative of porous lithologies (Leonardo Azevedo, et al., 2009) and therefore were interpreted as sandy deposits of channel point-bar and concave-bank areas. Point bar and concave-bank deposits also have a typical meandering distribution (Pu Renhai, et al., 2009), with sand-prone thick deposits formed on the inside of meander bends and concave-bank areas (Figure 76 C). Earlier discussed patterns of meander bend migration by translation and expansion lead to preservation of these deposits and successive lateral accretion, leading to an increase in deposits length and width and the amount of connectivity between single point bar and concave-bank deposits with each migration step (Figure 76 D, E) (Wietse I. van de Lageweg, 2012). In this example, accretion is compared on the basis of channel Grid 2 evolution through time, where more significant point bar and concave-bank sediments accretion is identified on the latest stages of channel evolution (Figure 76 D). Initially low sinuosity (1.130) channel Grid 2 with narrow point bars and concave-bank deposits developed through lateral expansion and downstream translation into meandering channel of moderate sinuosity (1.260) (Table 3).

6.4.3 Channel 3

In plan view, channel Grid 3 has a moderate sinuous channel axis for all 4.4 km length (Figure 77 A, Table 3). Figure 77 B shows the stacking of channel alignments over the period from -1112 ms to -1096 ms against and upon each other and implies a meander-bend evolution by lateral expansion, where it shows swing features associated with channel bend lateral migration. Lateral expansion mode of channel migration, associated with meander loop swinging, cause channel widening. There is no phase lag, as meander bend evolution doesn't show any signs of downstream translation.   Figure 77 C, D shows channel's Grid 3 geobogy populated with Envelope attribute values, showing areas of sediment preservation along channel belt. Limited localized almost circular areas with high Envelope values are indicative of porous lithologies (Leonardo Azevedo, et al., 2009) interpreted as sandy deposits of channel point-bar and concave-bank areas.
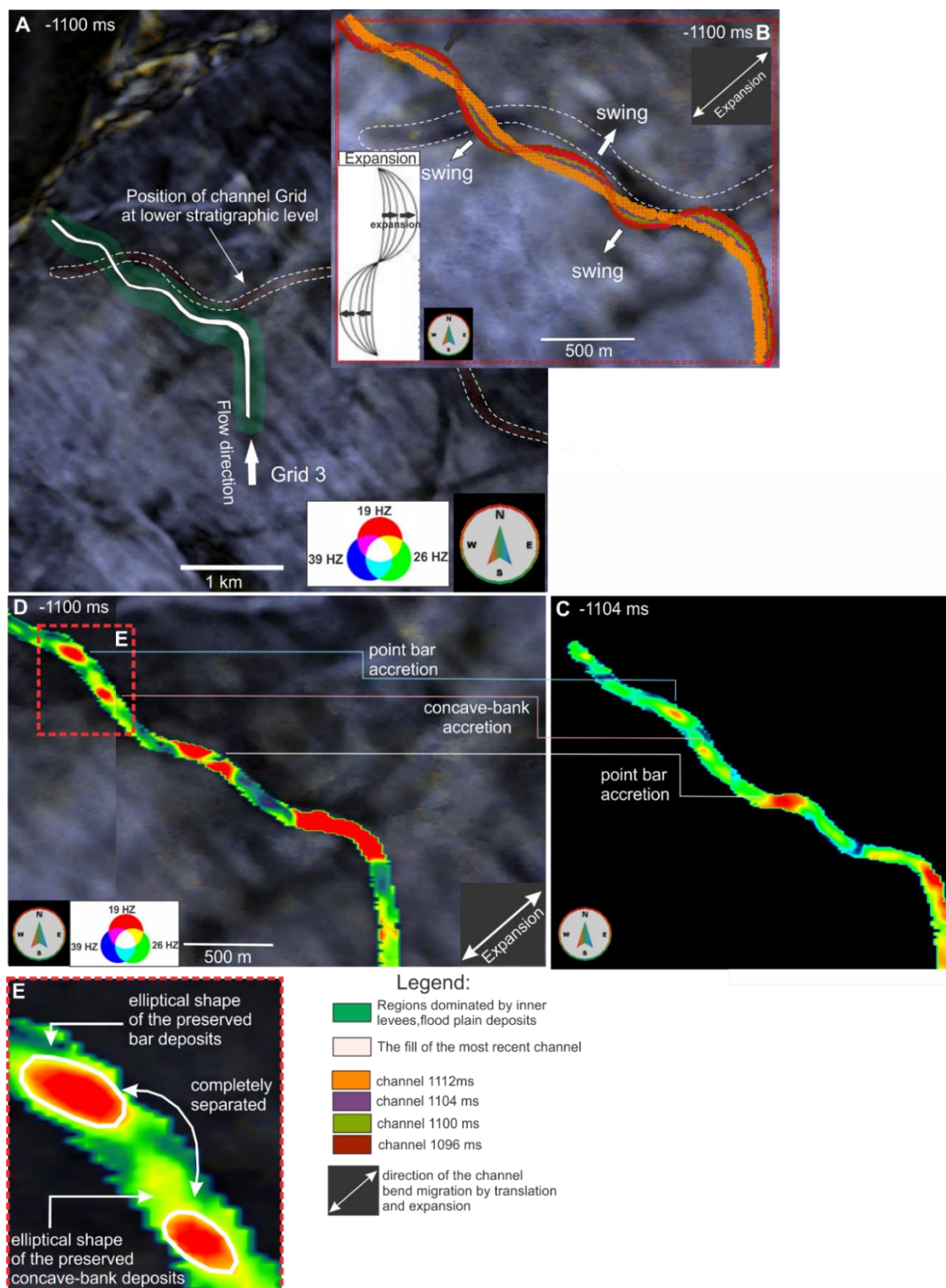
Figure 77 Meander-loop evolution for Grid 3 channel. A) Interpreted spectral decomposition cube at a frequency subband of 19-26-39 HZ at -1100 ms, showing meandering single channel Grid 3 and position of channel Grid 1 at lower stratigraphic level. B) B) Series of channel alignments over the period from -1112 ms to -1096 ms, illustrating meander-loop swing features. Channel color threads indicate order of formation. C) Plan View of channel bend showing patterns of meander bend migration by expansion leading to preservation of deposits formed in bar and concave-bank areas and showing successive accretion of concave-bank and bar deposits leading to an increase in deposits length and width with each migration step. E) Zoomed-in section of meander bend showing shape and complete separation of sediments preserved along channel bend.

Patterns of meander bend migration by expansion lead to preservation of these deposits formed in point bar and concave-bank areas and show successive accretion of concave-bank and point bar deposits leading to an increase in deposits length and width with each migration step (Figure 77 D) (Wietse I. van de Lageweg, 2012). In this example, accretion is compared on the basis of channel Grid 3 evolution through time, developed from being low sinuous (1.040) with narrow point bars and concave-bank deposits to moderate sinuous (1.202), where sediment accretion led to more massive sediment geometries (Figure 77 D).

6.4.4 Summary

In this work the migration modes of three studied channels have been described and discussed. Since channel Grid 1 and Grid 2 have been developed by both lateral expansion and downstream translation and channel Grid 3 only shows expansion bend migration mode, it's possible to compare the effect of bend migration on accretion and hence preservation of deposits.

Grid 1 and Grid 2 channels migrated by lateral expansion and downstream translation and maintained to develop pronounced, elongated shape and closely connectivity of single point bar and concave-bank sandbodies with each migration step (Figure 76 F, G). Figures suggest that preserved point bar and concave-bank deposits are not compleately separated sediment bodies with some link of attachment and the volume of sediment preserved as a concave bank deposits is nearly the same as that preserved as a point bar deposits (Brian J. Willis & Hong T., 2010). According to Brian J. Willis & Hong (2010, p. 440), more point bar and concave-band deposits are preserved when meander bend grows/migrate by both extension and translation (channels Grid 1 and Grid 2) with each migration step. Point bar and concave bank deposits of channel Grid 3 has more elliptical or even circular shapes of point bar and concave-bank deposits (Figure 77 E), which appear to be completely separated from each other (point bar deposits from adjacent concave-bank deposits (Figure 77 E).

6.5 Fluvial Channels

Channel bodies of different extend and shapes are the most identifiable depositional elements within Snadd Formation (Tore Grane Klausen, et al., 2014). They

have been found and categorized as fluvial meander channel belts. All the seismic attribute map images of fluvial channels presented in this study show ribbon-like high-to moderate-amplitude continuous reflections of well-developed, sinuous, evolving meander bends with high-magnitude facies within them, suggestive of a sand prone fill of point bars and concave-bank deposits (Posamentier, 2003). Point bars in some of the examples also exhibit meander scrolls, which appear as closely spaced multiple channel threads. They are interpreted to indicate continuous channels migration pattern, typical of fluvial channels (V. Kolla & H.W. Posamentier, 2007). Channel belt migration patterns are characterized by downstream translation (sweep) and lateral expansion (swing) of meander bends during their growth, typical of fluvial systems (V. Kolla, et al., 2007). These dominantly laterally migrating channels do not exhibit significant component of vertical aggradation seen on vertical seismic cross-sections.

The channel deposits in the Snadd Formation are interpreted as the products of fluvial depositional systems, which were observed to have westward dispersion of channel orientations. The relatively consistent thickness of the channels observed on the long profiles for all three channels (Figure 78), where the acoustic properties of the channel deposits formation determine the possibility of its delineation in the wave field. Such consistent values of thickness suggest stable homogeneous depositional environment (Tore Grane Klausen, et al., 2014), where discharge in the rivers did not change much from upstream toward downstream parts of the channels (M.J.R. Gee & R.L. Gawthorpe, 2006). A long profile sections AA', BB' and CC' do not show any significant variations in internal seismic amplitude, gradient and channel consistent thickness, with the exception of downstream channel thickness gradual decrease toward the farthest end (Figure 78). A long profile section AA' of channel axis Grid 1 shows that upper channel surface is defined by weak but continuous reflections which marks a change to layered, laterally continuous reflections. Low to variable amplitude, highly discontinuous, chaotic reflections associated with channel bend axis, indicating erosion (M.J.R. Gee & R.L. Gawthorpe, 2006). Chaotic pattern make it difficult to track target reflections. Continuous high seismic amplitude reflections are associated with channel bend axis (Figure 78 A, red box corresponds to meander bend location on surface 1) and indicate erosion. The top of channel in long profile section BB' of

channel axis Grid 2 is characterized by low amplitude generally chaotic seismic character, indicating possible fining upward channel fill (Figure 78 B) (M.J.R. Gee & R.L. Gawthorpe, 2006). In both profiles well traced both positive and negative reflections formed near the bottom, thus showing higher amplitude for the target interval. Chaotic seismic character is associated with channel bend axis (Figure 78 B, red box corresponds to meander bend location on surface 1). A long profile CC' of a channel axis Grid 3 is characterised by relatively laterally continous reflecton at the bottom and weak, discontinuous reflection of upper channel surface, indicating finning upward succession (Figure 78 C).
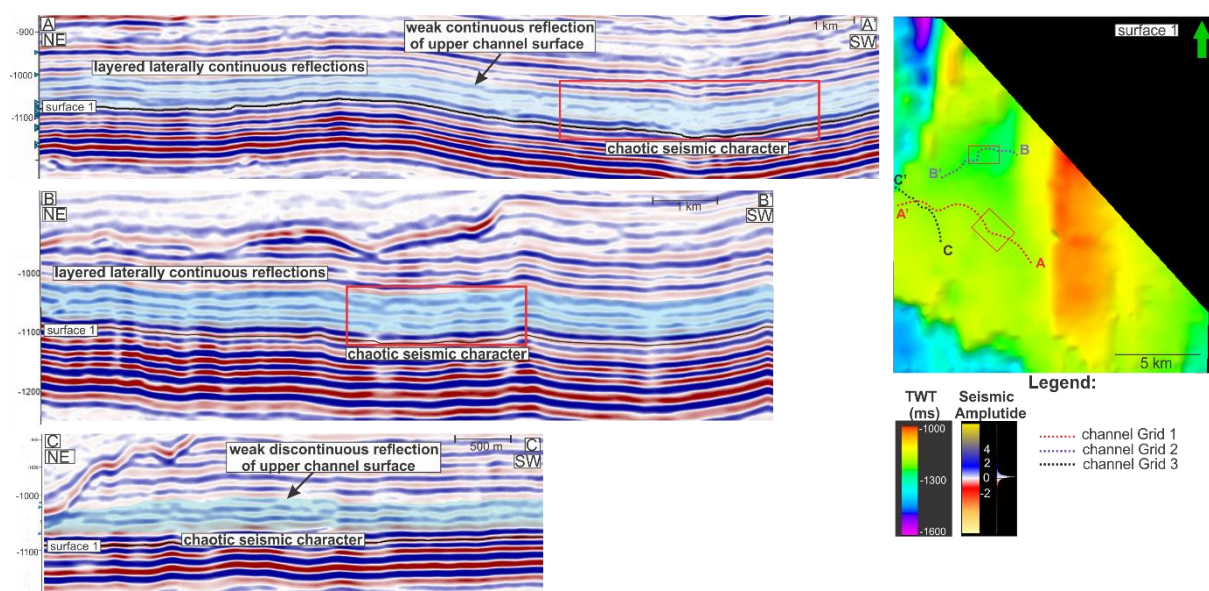
Figure 78 Long profiles of channel systems illustrating A) Internal seismic facies and thickness variation along the Grid 1 channel axis, B) along Grid 2 channel axis and C) along Grid 3 channel axis. See inset picture on the ight of Surface 1 time-maps showing location of AA', BB' and CC' seismic lines for Grid 1, Grid 2 and Grid 3 respectively.

6.6 Criteria for distinguishing between mud- and sand-filled channels

To carry out the following analysis of distinguishing between mud- and sand filled channels, the definition of internal lithology of studied channels has been identified by combining most positive and most negative curvature attributes. Features that have undergo differential compaction rate can be revealed by curvature attribute. Since shales may have enormous porosity up to ~ 80%, they compact easier than finer sediments as the overburden pressure increases and hence appear as a 'structural' heights on most positive curvature attribute (Lucia Torrado, et al., 2014), whereas less

compactable and therefore more sand-prone lithology highlighted by most negative curvature attribute.

For channel Grid 1 and channel Grid 2 the most positive curvature attribute highlights flanks (potential levee deposits) with red and channel axis fill by most negative curvature attribute with blue (Figure 57, Figure 61 B). In this case, channels are defined as sand-filled. Series of closely spaced multiple sinuous threads, which resemble meander scrolls form typical ridge and swale topography (Lageweg, 2012) for channel Grid 1 (Figure 57). They appear as structural heights (highlighted by the most positive curvature attribute) and are interpreted to indicate channel migration patterns. Channel Grid 3, on the other hand, has been interpreted by combining most positive and most negative curvature attribute, as mud-filled channel, since the most positive curvature attribute highlights channel axis fill with red (Figure 66). Channel Grid 3 is therefore defined as relatively low energy, mud-rich channel with siltstone channel lithology, which contrasts with higher-energy setting of Grid 1 and Grid 2 sand-filled channels. Very cohesive mud may be laid down on the channel Grid 3 bottom and on point bar and concave-bank deposits upper surfaces. But since point bar and concave-bank deposits are distinguished by their high Envelope values, these mud layer was eroded away due to strongest current flow at the top of the point bars and around meander bend apex.

Based on information provided by examination of Curvature, Variance and Spectral decomposition attributes coupled with observation of geomorphology and internal seismic architectures for Grid 1, Grid 2 and Grid 3 channels, allowed channel classification as that of sand-filled channels of two types (type 1 and type 2) and mud-filled channels.

6.6.1 Type 1 sand-filled channel

Type 1 sand-filled channels are characteristics of Grid 1 channel. Type 1 sand-filled channel appear as wide, poor laterally confined, avulsive, single channels with variable width and moderate sinuosity. Vertical seismic section shows that channels are expressed with low to moderate amplitudes, moderate reflectivity, weakly-laterally confined reflections (Figure 79 A, red rectangle), flat or locally wavy base reflection over the most of channel belts lenght. In the case of Grid 1, type 1 channel exhibit

moderate sinuosity, significant lateral point bar and concave-bank accretion, with formation of pronounced and elongated sand-bodies (Figure 74 D), resulting in development of isolated meander scrolls (seen as sinuous threads on attribute maps), and as lateral accretion surfaces (on vertical seismic cross-sections).
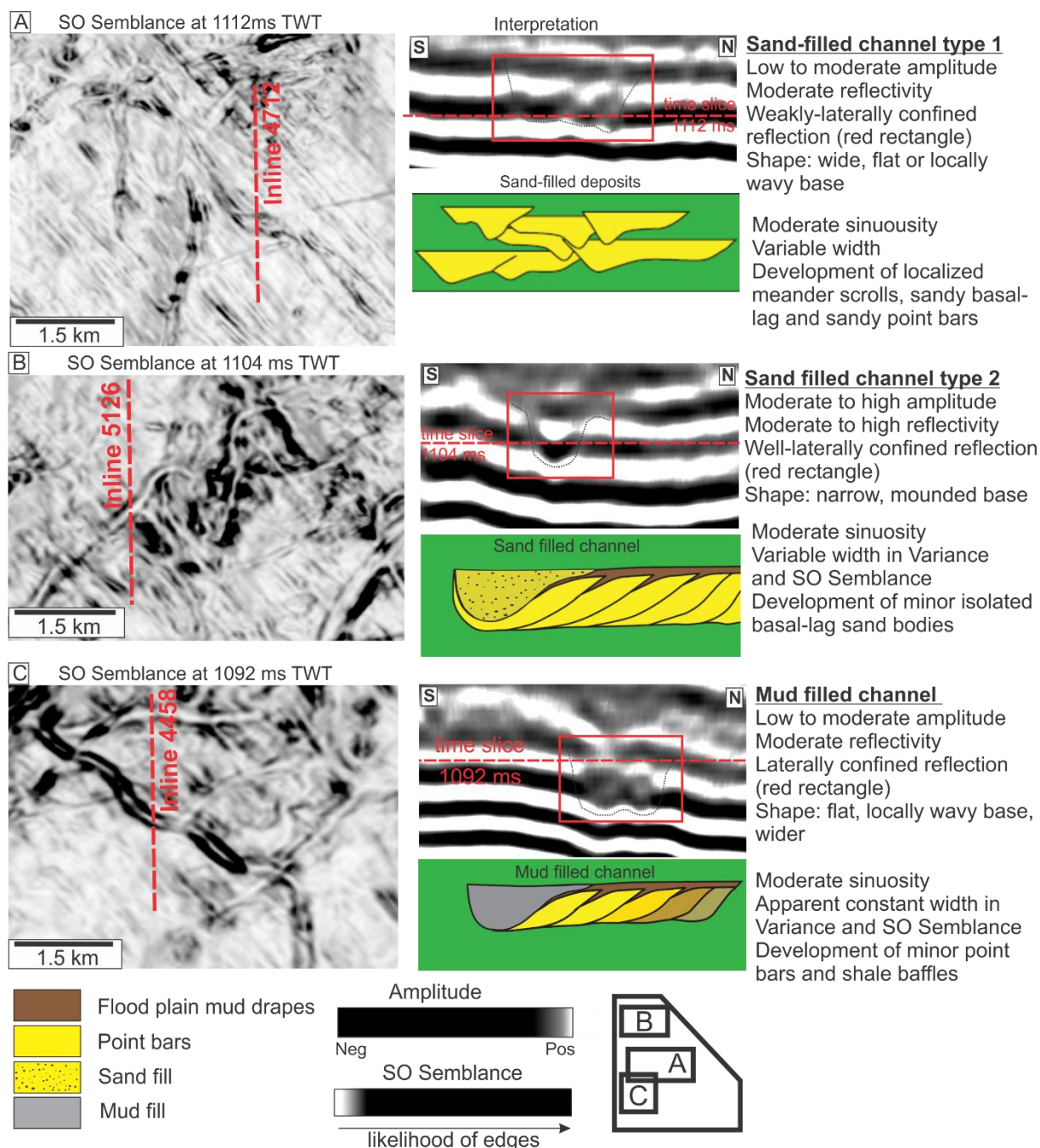

Figure 79 Characteristics of mud- and sand-fill channel belts of Grid 1, Grid 2 and Grid 3 in SO Semblance 3D seismic cube and vertical seismic display. A) Example of a sand-filled channel type 1 Grid 1. B) Example of a sand-filled channel type 2 Grid 2. C) Example of a mud-filled channel Grid 3.

6.6.2 Type 2 sand-filled channel

Type 2 sand-filled channels are characteristics of Grid 2 channel. Highly confined sand-filled channels appear as mostly narrow, single channels with variable width and moderate sinuosity. In a vertical seismic section, channels are expressed with moderate to high amplitudes, moderate to high reflectivity, well-laterally confined reflection (Figure 79 B, red rectangle), and locally mounded channel basal seismic reflections, interpreted as isolated, basal-lag sand bodies. In the case of Grid 2, sand-filled channel of type 2 exhibit moderate sinuosity and less significant lateral point bar and concave-bank accretion (if comparing to sand-filled channel type 1) with formation of pronounced and elongated sand-bodies (Figure 76 F, G), resulting in development of lateral accretion surfaces in vertical seismic cross-sections.

6.6.3 Mud-filled channel

Mud-filled channels are characteristics of Grid 3 channel. Low-energy system mud-filled channels appear as narrow ribbon-like, single, entrenched channels with variable width and moderate sinuosity. In a vertical seismic section, channels are expressed with low to moderate amplitudes, moderate reflectivity, laterally confined reflection (Figure 79 C, red rectangle), and isolated, flat, locally wavy base reflection. In the case of Grid 3, mud-filled channel exhibit moderate sinuosity, insignificant lateral point bar and concave-bank accretion (Figure 77 D, C) with formation of elliptical or even circular shapes of point bar deposits, showing no signs of meander-loop downstream translation and lateral accretion surfaces in vertical seismic cross-sections. Locally mounded channel basal higher seismic reflections are un-equally distributed along the channel belt bottom and have non-uniformity and uncertainty in its spatial distribution, are interpreted as the basal-lag sand *bodies*, the presence of which refferes to interbed siltstone and mudstone-bearing fine sandstone with unequal thickness lithology.

6.7 Stacking architecture

Connectivity of channel belt depend on the lateral and vertical stacking (aggradation) of point bar and concave-bank deposits (Brian J. Willis & Hong T., 2010; J. D. Clark & K. T. Pickering, 1996). The stacking architecture of channel bodies

demonstrates channel growth patterns originally forming from the interaction between lateral and vertical amalgamation processes (Figure 80 A) (J. D. Clark & K. T. Pickering, 1996). Differences in the stacking architecture of Grid 1, Grid 2 and Grid 3 channel systems is interpreted to be related to differences in channel sinuosity and nature of channel migration patterns. Three patterns of channel migration (expansion, translation, both expansion and translation) were identified and discussed earlier as related to channel development. Poorly confined Grid 1 channel is interpreted to be wide, not well laterally constrained by levees, moderate sinuosity system, developed by both expansion and downslope translation. Highly-confined channels (Grid 2 and Grid 3) are related to comparatively narrow flow in moderate sinuous channels, whereas Grid 2 has developed by both expansion and translation and Grid 3 by lateral expansion only. These differences in flow behavior have its impact on the aggradation patterns (Brian J. Willis & Hong T., 2010) and the stacking architecture of channel bodies described bellow.

Lateral stacking

If meander bend migrates by downstream translation and expansion (Grid 1 and Grid 2), which is typical for more continuous flow through channel belt (Brian J. Willis & Hong T., 2010), preserved point bar and concave bank deposits mandates similar volumes and similar elongate shape (Figure 74, Figure 76 F-G). The stacking architecture in this case will alternate along the channel belt edges from concave-bank to point bar preserved porous sand deposits and will be associated with predominantly lateral organized stacking. In the case, when meander bend migrates by expansion only (Grid 3), coarser grained deposits of point bars increase in volume due to point bar accretion and tend to be isolated on the alternate sides of the channel belt (Figure 77 E) (Brian J. Willis & Hong T., 2010). Laterally stacking architecture is less pronounced since point bar deposits are restricted by channel belt deposits, since no or little downdip accretion is associated with elliptical shaped point bar deposits (Figure 77 D).

Vertical stacking

Despite some point bar and concave-bank deposits lateral migration through both expansion and translation, the channel vertical stacking pattern features were not

identified (no vertical aggradation, no rise of the channel margin over previous migration step) (Brian J. Willis & Hong T., 2010). The lack of vertical aggradation pattern suggests that there were no signs of thalweg vertical migration. The lack of vertical thalweg migration in its turn indicates that the system was dominated by equilibrium flows with rate of lateral deposition balanced by the rate of lateral erosion (M. Janocko & W. Nemec, 2012).
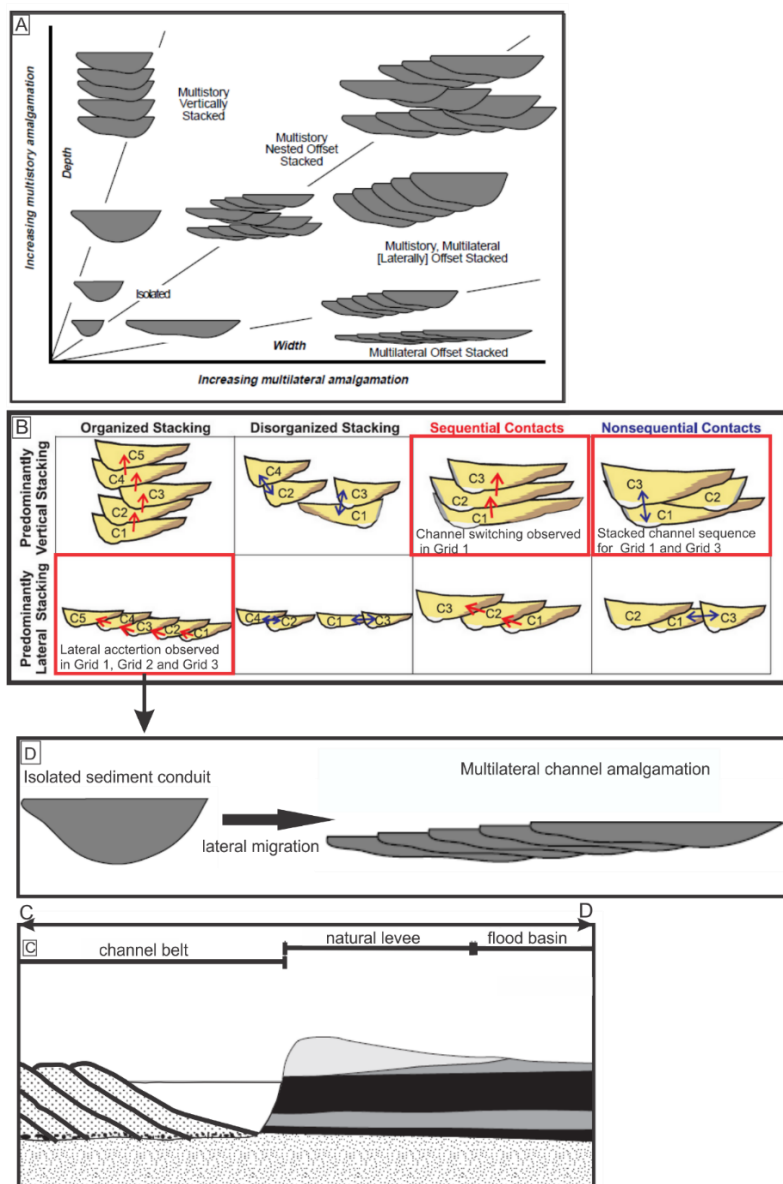
Figure 80 A) Schematic graph showing how the width and depth of stacked channel complexes result from the interplay between lateral and vertical amalgamation of channels bodies (J. D. Clark & K. T. Pickering, 1996). B) Figure shows four categories of static connectivity. Stacking patterns common for Grids is predominantly lateral stacking sequential contacts (STRATA, 2015). C) Schematic diagram showing architecture elements of the channel, as well as lateral amalgamation process of channel causing accretion of bar deposits D) Schematic diagram to show how the process of lateral amalgamation transform isolated sediment conduit into multilateral channel amalgamation.

Vertical aggradation patterns have only been observed on the vertical seismic section for Grid 1 and Grid 3 (Figure 81, seismic section AB), where, channel Grid 3 aggrades on top of channel Grid 1, resulting in predominantly vertical stacking with nonsequential contact. In this case channels Grid 1 and Grid 3 are characterized by two distictintive channel fill deposits (sand- and mud-filled respectively), deposited on top of each other, but lacking joined incising base.

Verticaly stacked channel sequence has been observed on vertical seismic cross-section (Figure 81, seismic section EF) of NE tip for Grid 1, and has been associated with sequential contact of predominantly vertical stacking architecture pattern. Stacked channel sequence has been interpreted as being related to an offset of flow pathways along the channel belt. Flow through channel must have had experienced channel switching, which might indicate progressive lateral shifting in channel axis due to either channel migration or avulsion, and which has produced distinctive pattern of lateral aggradation and vertical aggradation (however it doesn't aggrade to significant heights). Here, the secondary channel (upper stratigraphic level, Figure 81) is observed to incise slightly deeper into sediments below, however is in general weakly incised. It has well-defined channel axis. Initial channel (lower stratigraphic level, Figure 81) is even more weakly incised, almost lacks incised notch, indicating less basal erosion (M.J.R. Gee & R.L. Gawthorpe, 2006). Channel at lower stratigraphic level has been interpreted as an older abandoned channel. Channel-belt stacking architecture is the result of channel lateral switching, occurred where the channel become plugged with sediment to a point when it couldn't contain the flows any longer and avulsion occurred (M. Janocko & W. Nemec, 2012).
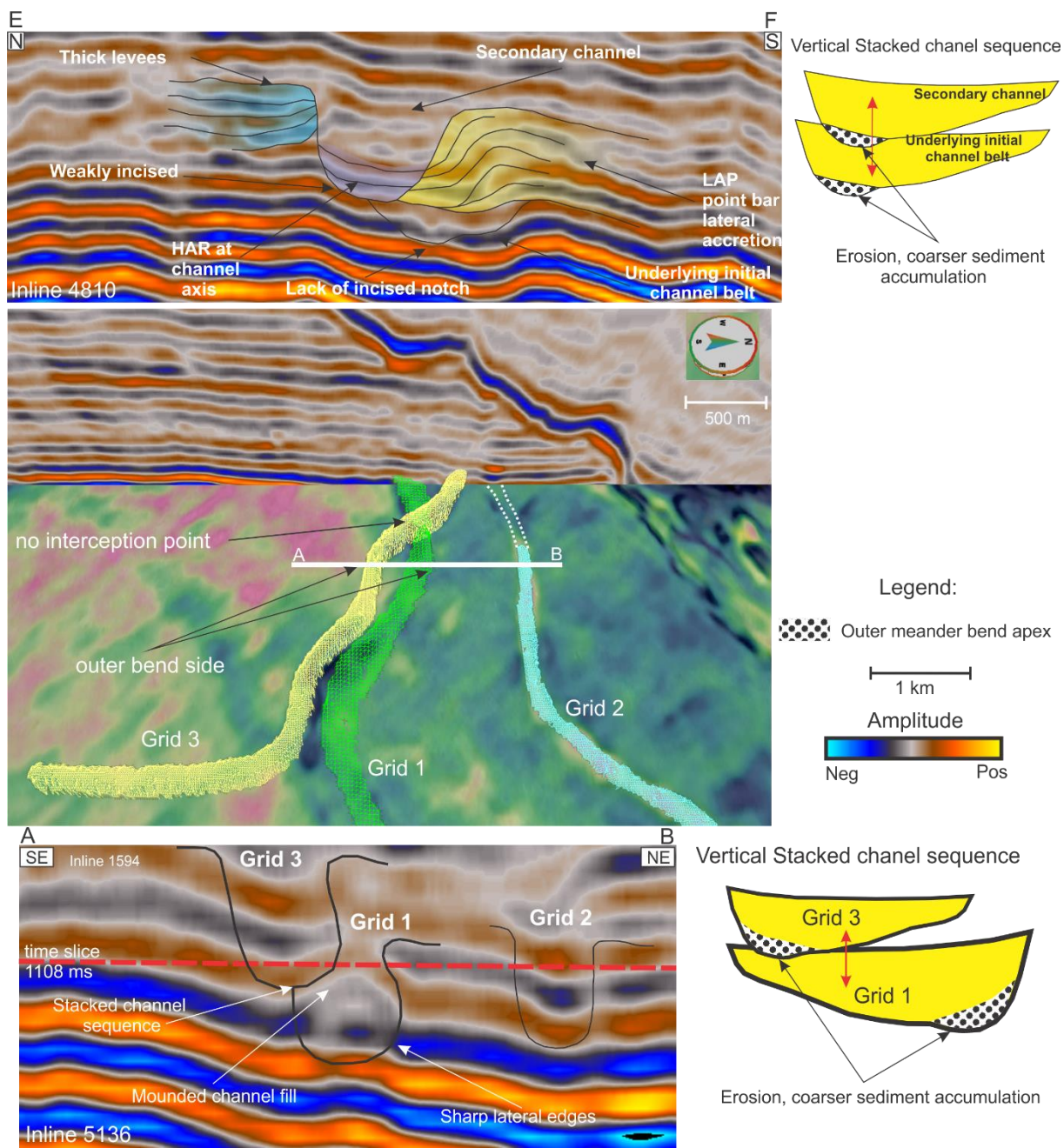
Figure 81 A) Vertical seismic section EF, showing different architectural elements and sequential contact of vertical stacking architecture, where intial channel experienced channel switching. Location of the seismic line EF see in Figure 70 (Inline 4810). B) Plan view of Grid 1, Grid 2 and Grid 3 channels plotted against spectral decomposition-SO Semblance opacity blend slice (at -1108 ms), showing the location of AB seismic line. C) Vertical seismic cross section AB along Grid 1, Grid 2 and Grid 3 channels, showing reflection geometry and stacked channel sequence interpreted as nonsequential contact vertical stacking architecture of Grid 1 (lower stratigraphic level) and Grid 3 (upper stratigraphic level) (Inline 5136).

Conclusions

In the SW Barents Sea the Middle to Late Triassic Snadd Formation accumulated as north-west prograding low-gradient sequence of siliciclastic sediments, sourced from still active Caledonian orogeny in the east-southeast. An interval of fluvial channel bodies is defined within upper (S5) part of the Snadd formation, above major intra-Carnian marine flooding surface. The general westward paleo-flow direction of fluvial channel bodies in the Snadd formation is consistent with general propagation of the sediment dispersal system during Triassic.

The fluvial depositional systems of Snadd Formation are analyzed from 3D seismic data (LN09M01) located in the southwest Barents Sea, southwestern flank of the Loppa High, where they are traced over kilometers. Sinuous channels become more asymmetric because of the downstream translation and lateral expansion migration through time of channel evolution. The fluvial channel sand-bodies show range of geomorphic features including point bar, concave-bank and channel-levee deposits. The fluvial channel migration leads to accretion and preservation of point bar and concave-bank deposits within fluvial channel belts and affects their geometry and shape. The coarse-grain deposits in fluvial channel belts are defined as elongated-, elliptical to circular- bodies of accreted point bars and concave-bank deposits, where the shape and amount of their connectivity depend on relative significance of channel-bend migration through time. This in turn affects lateral connectivity of the accreted deposits. More point bar and concave-band deposits are preserved when meander bend grows/migrate by both extension and translation. The maximum thickness of coarse-grained deposits found on the closest bank to the thalweg, corresponding to the location of meander bends.

Channels have been classified into three types based on their geomorphology and internal seismic architectures into three types: type 1 sand-filled channel, type 2 sand-filled channel and type 3 mud-filled channel. The quantitative analysis of meander patterns demonstrates the relation between channel-thalweg length, bend-thalweg lenght and local centreline radius of bend curvature, thus showing positive correlation with channel sinuosity.

7. References

A. Dalland, D. Worsley, & k. Ofstad. (1988). A Lithostratigraphic Scheme for the Mesozoic and Cenozoic Succession Offshore Mid- and Northern Norway. Norwegian Petroleum Directorate Bulletin v. 4, p. 42-65.

A. Gay, M. Lopez, H. Ondreas, J.-L. Charlou, G. Sermondadaz, & P. Cochonat. (2004). Seafloor facies related to upward methane flux within a Giant Pockmark of the Lower Congo Basin. Marine Geology 226 (2006) 81– 95.

A. Gay, M. Lopez, P. Cochonat, M. Seranne, D. Levache, & G. Sermondadaz. (2005). Isolated seafloor pockmarks linked to BSRs, fluid chimneys,polygonal faults and stacked Oligocene–Miocene turbiditic palaeochannels in the Lower Congo Basin. Marine Geology, 25-40.

Agata Zaborskaa, Jolynn Carroll, Carlo Papucci, Leonardo Torricellic, Michael L. Carroll, & Jolanta Walkusz-Miotka. (2008). Recent sediment accumulation rates for the Western margin of the Barents Sea. Deep Sea Research Part II: Topical Studies in Oceanography.

Alison T. Henning, Ryan Martin, & Gaynor Paton. (2010). Data conditioning and seismic attribute analysis in the Eagle Ford Shale Play: Examples from Sinor Ranch, Live Oak County, Texas. SEG Denver 2010 Annual Meeting. Foster Findlay Associates Limited (ffA).

Andreassen, K. (2009). Lecture Notes for Geo-3123. In K. Andreassen, MARINE GEOPHYSICS. Tromsø.

Andreassen, K., Laberg, J.S., & Vorren, T.O. (2008). Seafloor geomorphology of the SW Barents Sea and its glaci-dynamic implications. Geomorphology, v. 97, p. 157-177.

Andrew J. Cavanagh, R. Di Primio, M. Scheck-Wenderot, & B. Horsfield. (2006). Severity and timing of Cenozoic exhumation in the southwestern Barents Sea. Journal of the Geological Society, v. 163, p. 761-774.

Arvid Nøttvedt, E. P. (2008). The Mesozoic of Western Scandinavia and East Greenland. Episodes, Vol. 31, No. 1.

Ben Kilhams, Stuart Godfrey, & Adrian Hartley. (2011). An integrated 3D seismic, petrophysical and analogue core study of the Mid-Eocene Grid channel complex in the greater Nelson Field area, UK Central North Sea. Petroleum Geoscience, Vol. 17, pp. 127–142.

Best, J. L. (1987). FLOW DYNAMICS AT RIVER CHANNEL CONFLUENCES: IMPLICATIONS FOR SEDIMENT TRANSPORT AND BED MORPHOLOGY. The Society of Economic Paleontologists and Mineralogists (SEPM).

Bevis, K. A. (2013). The Geology of Sedimentary Rocks. In the Playground of Giants.

Bjorlykke, K. (2010). Petroleum Geoscience: from sedimentary environments to rock physics. Springer.

Brian J. Willis, & Hong T. (2010). Three-dimensional connectivity of point-bar deposits. Journal of Sedimentary Research, v. 80, 440–454.

BRICE, J. C. (1974). Evolution of Meander Loops. Geological Society of America Bulletin v. 85, p. 581-586.

Bridge, J. S. (1999). Alluvial architecture of the Mississippi valley: predictions using a 3D simulation model. Geological Society of London.

Bridge, J., & Demicco, R. (2008). Earth Surface Processes, Landforms and Sediment Deposits.

Brown, A. (1999). Interpretation of three-dimensional seismic data. 5th edition. AAPG Memoir 42, pp. 514. .

C. Barrere, J. Ebbing, & L. Gernigon. (2011). 3-D density and magnetic crustal characterization of the southwestern Barents Shelf: implications for the offshore prolongation of the Norwegian Caledonides. Geophysical Journal International.

Carstens, H. (2011). Unlocking the Secrets of the Barents Sea. GeoExPro Vol. 8, No. 4 .

Castro, J. (2003). Geomorphologic Impacts of Culvert Replacement and Removal: Avoiding Channel Incision . USFWS .

Chand, S., Mienert, J., Andreassen, K., Knies, J., Plassen, L., & Fotland, B. (2008). Gas hydrate stability zone modelling in areas of salt tectonics and pockmarks of the Barents Sea suggests an active hydrocarbon venting system. Marine and Petroleum Geology, v. 25, p. 625-636.

Chopra, S. M. (2006). Seismic Attributes – a promising aid for geologic prediction. Seismic attributes.

Chris Perry, & Kevin Taylor. (2007). Environmental sedimentology:introduction. In K. T. Chris Perry, Environmental Sedimentology (pp. 1-32). BLACKWELL PUBLISHING.

Collinson, J. (1996). Alluvial sediments. In H. Reading, Sedimentary Environments:Processes, Facies and Stratigraphy. Wiley-Blackwell.

Conveners Mike Mayall, & Ian Kane. (2011). Internal architecture, bedforms and geometry of turbidite channels. Geological Society.

D. Bowman, T. Svoray, S. Devora, I. Shapira, & J.B. Laronne. (2009). Extreme rates of channel incision and shape evolution in response to a continuous,rapid base-level fall, the Dead Sea, Israel. Geomorphology.

D.Subrahmanyam. (2008). Seismic Attributes- A Review. 7th international Conference and Exposition on Petroleum Geophysics.

D.V. Ramana, S. D. (2006). Seismic Expressions of Submarine Channel - Levee Systems and Their Architectural Elements. 6th International Conference & Exposition on Petroleum Geophysics "Kolkata 2006".

D.V. Ramana, Santanu De, & Kalyanbrata Datt. (2006). 6th International Conference & Exposition on Petroleum Geophysics "Kolkata 2006". Seismic Expressions of Submarine Channel - Levee Systems and Their Architectural Elements, (pp. 678-682).

Dalla Valle, G., & Gamberi, F. (2011). Slope channel formation, evolution and backfilling in a wide shelf, passive continental margin (Northeastern Sardinia slope, Central Tyrrhenian Sea). Marine Geology.

DAVID MACDONALD, B. A. (2007). Modelling and comparing the Caledonian and Permo-Triassic erosion surfaces with present-day topography across Highland Scotland: implications for landscape inheritance. Sedimentary Processes, Environments and Basins: A Tribute to Peter Friend.

David Macdonald, Barry Archer, Selma Murray, & Kieren Smith . (2007). Modelling and comparing the Caledonian and Permo-Triassic erosion surfaces with present-day topography across Highland Scotland: implications for landscape inheritance. Sedimentary Processes, Environments and Basins: A Tribute to Peter Friend.

Dore A. G., & Jensen L. N. (1996). The impact of late Cenozoic uplift and erosion on hydrocarbon exploration: offshore Norway and some other uplifted basins. Global and Planetary Change, Volume 12, Issue 1, p. 415-436.

Doré, A.G. (1995). Barents Sea Geology, Petroleum Resources and Commercial Potential. Arctic VOL. 48, NO. 3 P. 207–221.

Dru Germanoski, & S. A. Schumm. (1993). Changes in Braided River Morphology Resulting from Aggradation and Degradation1. The Journal of Geology v. 101.

E. Henriksen, A.E. Ryseth, G.B. Larssen, T. Heide, K. Rønning, & K. Sollid. (2011). In T. o. systems, Tectonic and stratigraphic evolution.

Edie, R. W. (2005). Meander Belt Entrapment of Hydrocarbons, Campbell-Namao Field, Alberta. Search and Discovery .

Eiliv Larsen, Karin Andreassen, Lena Charlotte Nilssen, & Ståle Raunholm. (2003). The prospectivity of the Barents Sea:Ice ages, erosion and tilting of traps. Geological Survey of Norway, N-7491.

Einsele, G. (1992). Sedimentary Basins. Evolution, facies and Sediment Budget.

Eva K. Halland, Andreas Bjørnestad, Ine Tørneng Gjeldvik, Maren Bjørheim, Christian Magnus, & Ida Margrete Meling. (2013). CO2 storage atlas Barents Sea. NPD, Chapter 4 Geological description of the Barents Sea.

Evy Glørstad-Clark, Jan Inge Faleide, Bjørn Anders Lundschien, & Johan Petter Nystuen. (2010). Triassic seismic sequence stratigraphy and paleogeography of the western Barents Sea area. Marine Geology.

Factpages. (2015, 12 21). Retrieved from NPD: http://factpages.npd.no/factpages/?culture=en&nav1=wellbore&nav2=Statistics%7cEntryYear

Faleide, J. I., Gudlaugsson, S. T., & Jacquart, G. (1984). Evolution of the western Barents Sea. Marine and Petroleum Geology, 123-150.

Faruk O. Alpak, Mark D. Barton, & Stephen J. Naruk. (2013). The impact of fine-scale turbidite channel architecture on deep-water reservoir performance. AAPG Bulletin v. 97 no. 2.

Fridtjof Riis, Bjørn A. Lundschien, Tore Høy, & Atle Mørk. (2008). Evolution of the Triassic shelf in the northern Barents Sea region. Polar Research.

Gabrielsen Roy H, Grunnaleite Ivar, & Eigil Rasmussen. (1997). Cretaceous and tertiary inversion in the Bjørnøyrenna Fault Complex, south-western Barents Sea. Marine and Petroleum Geology Volume 14, Issue 2, Pages 165–178.

Gabrielsen, R, Færseth, R, Jensen, L, Kalheim, J, & Riis, F. (1990). Structural elements of the Norwegian continental shelf, Part 1: The Barents Sea Region. NPD bulletin, v. 6, p. 1-33.

Galloway, H. (1996). Alluvial fans. In Terrigenous Clastic Depositional Systems.

GeoTeric. (2015). Geoteric Software. Retrieved from GeoTeric: www.geoteric.com

Gloppen, & Stell. (1980). Late Caledonian (Devonian) basin formation, western Norway signs of strike-slip tectonics infilling. Spec. Publ. int. Ass. Sediment, 79-103.

Glørstad-Clark, E., Birkeland, E.P., Nystuen, J.P., Faleide, J.I., & Midtkandal, I. (2011). Triassic platform-margin deltas in the western Barents Sea. Marine Geology v. 28, 1294-1314.

Gonzalo D. Veiga, Luis A. Spalletti, & Stephen S. Flint. (2007). Anatomy of a fluvial lowstand wedge: the Avilé Member of the Agrio Formation (Hauterivian) in central Neuquén Basin (northwest Neuquén Province), Argentina. Sedimentary Processes, Environments and Basins: A Tribute to Peter Friend.

Grenfell, M. C. (2012). Dynamics and Morphodynamic Implications of Chute Channels in Large, Sand-Bed Meandering Rivers.

Grenfell, M. C. (2012). Dynamics and Morphodynamic Implications of Chute Channels in Large, Sand-Bed Meandering Rivers.

Harrelson. (1994). Stream channel reference sites: an illustrated guide to field technique.

Henry W. Posamentier, & Roger G. Walker. (2006). facies Models Revisited.

Henry W. Posamentier, & Roger G. Walker. (2006). FACIES MODELS REVISITED.

HENRY W. POSAMENTIER, V. K. (2003). SEISMIC GEOMORPHOLOGY AND STRATIGRAPHY OF DEPOSITIONAL ELEMENTS IN DEEP-WATER SETTINGS. JOURNAL OF SEDIMENTARY RESEARCH, VOL. 73, NO. 3, P. 367–388.

Hongtao Zhu, Xianghua Yang, Xinhuai Zhou, & Keyu Liu. (2014). Three-dimensional facies architecture analysis using sequence stratigraphy and seismic sedimentology: Example from the Paleogene Dongying Formation in the BZ3-1 block of the Bozhong Sag, Bohai Bay Basin, China. Marine and Petroleum Geology.

Hudson-Edwards, K. (2006). Fluvial environments. In K. T. Chris Pery, Environmental Sedimentology. Wiley-Blackwell.

Ian A. Kane, V. C. (2010). Submarine channel response to intrabasinal tectonics:The influence of lateral tilt. The American Association of Petroleum Geologists.

Ian A. Kanea, Mason Dykstrac, Ahmed Kassemd, William D. McCaffrey, & Benjamin C. Knellerb. (2007). Anatomy of a submarine channel–levee: An example from

Upper Cretaceous slope sediments, Rosario Formation, Baja California, Mexico. Marine and Petroleum Geology 24 (2007) 540–563.

Ingelise Schmidt, Sebastien Lacaze, & Gaynor Paton. (2013). Spectral Decomposition combined with geo-model interpretation: Creating new workflows by integrating advanced technologies for seismic imaging and interpretation. 75th EAGE Conference & Exhibition incorporating SPE EUROPEC. London.

J. D. Clark, & K. T. Pickering. (1996). Architectural Elements and Growth Patterns of Submarine Channels: Application to Hydrocarbon Exploration1. The American Association of Petroleum Geologists.

J. Dufek, & G. W. Bergantz. (2007). Suspended load and bed-load transport of particle-laden gravity currents: the role of particle–bed interaction. ORIGINAL ARTICLE.

Jair Weschenfelder, Iran Carlos Stalliviere Corrêa, & Salvador Aliotta. (2010). PALEOCHANNELS RELATED TO LATE QUATERNARY SEA-LEVEL CHANGES IN SOUTHERN BRAZIL. BRAZILIAN JOURNAL OF OCEANOGRAPHY.

Jan I. Faleide, Erling Vågnes, & Steinar T. Gudlaugsson. (1993). Late Mesozoic-Cenozoic evolution of the south-western Barents Sea in a regional rift-shear tectonic setting.

Jan Inge Faleide, Filippos Tsikalas, Asbjørn Johan Breivik, Rolf Mjelde, Oliver Ritzmann, Øyvind Engen, & Jonas Wilson. (2008). Structure and evolution of the continental margin off Norway and the Barents Sea. Episodes, Vol.31 No.1.

Jhosnella Sayago, Matteo Di Lucia, Maria Mutti, Axum Cotti, Andrea Sitta, & Kjetil Broberg. (2012). Characterization of a deeply buried paleokarst terrain in the Loppa High using coredata and multi attribute seismic facies classification. AAPG Bulletin, v. 96, no. 10.

Jobe, Z. (2013). Lateral accretion in submarine canyons, offshore Equatorial Guinea. Virtual Seismic Atlas.

John S. Bridge, & Ian A. Lunt. (2005). Depositional models of braided rivers. DEPOSITIONAL MODELS OF BRAIDED RIVERS, pp. 11-51.

Jonathan Henderson, Stephen J. Purves, Gaynor Fisher, & Chris Leppard. (2008). Delineation of geological elements from RGB color blending of seismic attribute volumes. THE LEADING EDGE.

Jonathan M. Nelson, Paul J. Kinzel, & Mung Dinh Thanh. (2011). MECHANICS OF FLOW AND SEDIMENT TRANSPORT IN DELTA DISTRIBUTARY CHANNELS. Geomorphology and Sediment Transport Laboratory, U.S. Geological Survey.

Jørgensen, K. (2014). Development of fault complexes in time and space at Loppa High – SW Barents Sea. Tromsø: UIT.

K. El Kheiashy, J. M. (2010). Three dimensional hydrodynamic modeling over bed forms in open channels. International Journal of Sediment Research 25.

Karin Andreassen, Espen Glad Nilssen, & Christian M.Ødegaard. (2007). Analysis of shallow gas and fluid migration within the Plio-Pleistocene sedimentary succession of the SW Barents Sea continental margin using 3D seismic data.

Keylock, C. (2004). Reviewing the Hjulstrom curve. GeographyReview.

L. Gernigon, M. Brönner, D. Roberts, O. Olesen, A. Nasuti, & T. Yamasaki. (2013). Crustal and basin evolution of the southwestern Barents Sea: From Caledonian orogeny to continental breakup.

Labourdette, R. (2007). Integrated three-dimentional modeling approach of stacked turbidite channels. AAPG v. 91, 1603-1618.

Langbein, W. B., & Leopold, L. B. (1968). River Channel Bars and Dunes-Theorv of Kinematic Waves. PHYSIOGRAPHIC AND HYDRAULIC STUDIES OF RIVERS.

Lawrence M. Gochioco, J. I. (1990). HIGH-RESOLUTION SEISMIC SURVEY TO MAP PALEOCHANNELS IN AN UNDERGROUND COAL MINE. CANAD,ANJO"RNN.OF EXPLORATION GEOPHISICS.

Leeder, M. (2011). Alluvial fans and fan deltas. In M. Leeder, Sedimentology and sedimentary basins (pp. 330-337).

Leeder, M. R. (2011). River and Fan Deltas. In Sedimentology and sedimentary basins:From Turbulence to Tectonics, 2nd Edition. Wiley-Blackwell.

Leeder, M. R., & Mack, G. H. (2007). Basin-fill incision, Rio Grande and Gulf of Corinth rifts: convergent response to climatic and tectonic drivers. In G. Nichols, E. Williams, & C. Paola, Sedimentary Processes, Environments and Basins: A Tribute to Peter Friend.

Leonardo Azevedo, & Guerra Raposo Pereira. (2009). Seismic Attributes in Hydrocarbon Reservoirs Characterization. Universidade de Aveiro, Departamento de Geociências.

LeRoy, N., Bain, M., & David Allan, J. (1997). A paradigm for river conservation and restoration. The Natural Flow Regime.

Lilja R. Bjarnadóttira, Monica C.M. Winsborrow, & Karin Andreassen. (2014). Deglaciation of the central Barents Sea. Quaternary Science Reviews.

Lucia Torrado, Paul Mann, & Janok Bhattacharya. (2014). Application of seismic attributes and spectral decomposition for reservoir characterization of a complex fluvial system: Case study of the Carbonera Formation, Llanos foreland basin, Colombia. GEOPHYSICS, VOL. 79, NO. 5.

Lundin. (2013). Gohta: Et nytt oljefunn i Barentshavet. Retrieved 09.11.2015, from http://www.lundin-norway.no/2013/10/16/gohta-et-nytt-oljefunn-ibarentshavet/.

M. E. Oskin, D. W. Burbank, F. M. Phillips, S. M. Marrero, B. Bookhagen, & J. A. Selander. (2014). Relationship of channel steepness to channel incision rate from a tilted and progressively exposed unconformity surface. Journal of Geophysical Research: Earth Surface.

M. Janocko, & W. Nemec. (2012). The diversity of deep-water sinuous channel belts and slope valley-fill complexes. Marine and Petroleum Geology.

M. Janocko, & W. Nemec. (2012). The diversity of deep-water sinuous channel belts and slope valley-fill complexes. Marine and Petroleum Geology.

M.J.R. Gee, & R.L. Gawthorpe. (2006). Submarine channels controlled by salt tectonics: Examples from 3D seismic data offshore Angola. Marine and Petroleum Geology 23 (2006) 443–458.

Major, J. J. (1996). Depositional Processes in Large-Scale Debris-Flow Experiments. U.S. Geological Survey.

Makaske, B. (2000). Anastomosing rivers: a review of their classification, origin and sedimentary products. Earth-Science Reviews, 149–196.

Matsuda, I. (2004). RIVER MORPHOLOGY AND CHANNEL PROCESSES . Encyclopedia of Life Support Systems (EOLSS) .

McArdle N.J., Kristensen T., & Lowell J. (2010). Spits, channels and beaches: advanced imaging and delineation of Jurassic and Triassic stratigraphic targets. PETEX 2010 Technical Conference. London.

McArdle Nickolas, Purves Steve, & Lowell James. (2011). Advanced Multiattribute imaging and Geology Deliniation of jurassic and Triassic Startigraphic Targets.

McArdle, D. N. (2013). Frequency Decomposition and colour blending of seismic data - More than an image. Petroleum Exploration Society of Great Britain. London.

McDonough, J. M. (2007). COMPUTATIONAL FLUID DYNAMICS OF INCOMPRESSIBLE FLOW. University of Kentucky.

Miall, A. D. (1992). Alluvial Deposits. In N. J. Roger Walker, Facies Models Response to Sea level change.

MORK, E. (1999). Lithological description of subcropping Lower and Middle Triassic rocks from the Svalis Dome, Barents Sea. Polar Research 18(1).

Nichols, G. (2007). Fluvial systems in desiccating endorheic basins. In G. Nichols, E. Williams, & C. Paola, Sedimentary Processes, Environments and Basins: A Tribute to Peter Friend.

Nils Janbu, Wojciek Nemec, & Ediz Kirman. (2007). Facies anatomy of a sand rich channelized turbiditic system: the Eocene Kusuri Fm in the Sinop Basin, Turkey. In E. W. Gary Nickols, Sedimentary processes, Environments and Basins.

Npd. (2012). Delineation of the 7220/8-1("Skrugard") gas/oil discovery - 7220/5-1. Retrieved 18.11.2015. Retrieved from http://www.npd.no/en/news/Exploration-drillingresults/.

NPD. (2013). Petroleum resources on the Norwegian continental shelf.

NPD. (2014). Factmaps. Retrieved 18.11.2015. Retrieved from http://gis.npd.no/factmaps/html_20/.

Nøttvedt, A., Cecchi, M., Gjelberg, J., Kristensen, S.E., Lønøy, A., Rasmussen, A., . . . Veen, V., P.M. (1992). Svalbard - Barents sea correlation, a short review. Arctic geology and petroleum potential, Elsevier, p. 363-375.

P. Huggenberger, & C. Regli. (2009). A sedimentological model to characterize braided river deposits for hydrogeological applications. In Gregory H. Sambrook Smith, James L. Best, Charlie S. Bristow, & Geoff E. Petts, Braided Rivers: Process, Deposits, Ecology and Management. International Association of Sedimentologists.

P. Morozov, H. Y. (2015). Geological Model of Channel Deposits Based on. EAGE.

Paivi Heinio, & Richard J. Davies. (2009). Trail of depressions and sediment waves along submarine channels on the continental margin of Espirito Santo Basin, Brazil.

Paul Reemst, Sierd Cloetingh, & Stein Fanavoll. (1994). Tectonostratigraphic modelling of Cenozoic uplift and erosion in the south-western Barents Sea. Marine and Petroleum Geology.

Pavel Morozov, Gaynor Paton, A. M. Milyushkin, & V. V. Kiselev. (2013). Application of High Definition Frequency Decomposition techniques on Western Siberia reservoirs. GEOTERIC ffA.

Pennington, W. D. (2002). Calibration of Seismic Attributes for Reservoir Characterization.

Petrel. (2009). Seismic interpretation and visualization. Schlumberger.

Phillip A. Labrecque, Stephen M. Hubbard, Jerry L. Jensen, & Haley Nielsen. (2011). Sedimentology and stratigraphic architecture of a point bar deposit, Lower Cretaceous McMurray Formation, Alberta, Canada. BULLETIN OF CANADIAN PETROLEUM GEOLOGY VOL. 59, NO. 2, 147–171.

Pickering, J., & Clark , K. (1996). Architectural Elements and Growth Patterns of Submarine Channels: Application to Hydrocarbon Exploration. The American Association of Petroleum Geologists, 194-221.

Posamentier, H. W. (2003). Depositional elements associated with a basin floor channel-levee system: case study from the Gulf of Mexico. Marine and Petroleum Geology, 677–690.

Posamentier, H. W. (n.d.). Depositional elements associated with basin floor channel-levee system: Case study from the Gulf of Mexico.

Pu Renhai, Zhu Li, & Zhong Hongli. (2009). 3-D Seismic Identification and Characterization of Ancient Channel Morphology. Journal of Earth Science, Vol. 20, No. 5, p. 858–867.

R. J. Wood, S. P. Edrich, & I. Hutchison. (1989). Influence of North Atlantic Tectonics on the Large-Scale Uplift of the Stappen High and Loppa High, Western Barents Shelf: Chapter 36: North Sea and Barents Shelf. AAPG, 559-566.

Rafaelsen B., Andreassen K., & Kuilman L.W. (2002). Geomorphology of buried glacigenic horizons in the Barents Sea from three-dimentional seismic data. The geological society of London.

Rafaelsen, B. (2006). Seismic resolution (and frequency filtering. Tromsø: University of Tromsø.

Randle, T. J. (2006). CHANNEL MIGRATION MODEL FOR MEANDERING RIVERS. PROCEEDINGS of the Eighth Federal Interagency Sedimentation Conference , (pp. 241-248).

Robert W. Dalrymple. (2010). Introduaction to siliclastic facies models. In Noel P. James, & Robert W. Dalrymple, Facies Models 4.

Rosgen, D. (2007). Rosgen Stream Classification . Technique—Supplemental Materials. In T. S. 3E, National Engineering Handbook.

S. A. Clark, E. Glorstad-Clark, J. I. Faleide, D. Schmid, & E. H. Hartz. (2013). Southwest Barents Sea rift basin evolution:comparing results from backstripping and time forward modelling. Basin Research (2013) 25, 1–17.

S. T. Gudlaugsson, J. I. Faleide, S. E. Johansen, & A. J. Breivik. (1998). Late Palaeozoic structural development of the South-Western Barents Sea. 174.

Satinder Chopra, & Kurt J. Marfurt. (2012). SEG Las Vegas 2012 Annual Meeting. Seismic attribute expression of differential compaction. SPE.

Satinder Chopra, K. J. (2012). Seismic attribute expression of differential compaction. SEG Las Vegas 2012 Annual Meeting.

Schlumberger. (2007). Interpreter's Guide to Seismic Attributes. Schlumberger.

Schwenk, T., & M. Breitzke. (2005). The architecture and evolution of the Middle Bengal Fan in vicinity of the active channel–levee system imaged by high-resolution seismic data. marine and petroleum geology.

SHERIFF, R. E. (1997). Seismic Resolution a Key Element. Geophysical Corner Geophysical Corner.

Sheriff, R. E. (2006). Encyclopedic Dictionary of Applied Geophysics. Tulsa, Oklahoma, U.S.A.

Smelror, M, Petrov O.V., Larssen, B.B, & Werner S. (2009). Atlas Geological History ofthe Barents Sea. Geological Survey of Norway, Trondheim.

Stephen M. Hubbard, Derald G. Smith, & Haley Nielsen. (2011). Seismic geomorphology and sedimentology of a tidally influenced river deposit, Lower Cretaceous Athabasca oil sands, Alberta, Canada. AAPG Bulletin, v. 95, no. 7.

Stephen T. Lancaster, & Rafael L. Bras. (2001). A simple model of river meandering and its comparison to natural channels. HYDROLOGICAL PROCESSES, 1-26.

STRATA, S. (2015). Channel stacking. Retrieved from STRATA Terminology: http://www.sepmstrata.org/Terminology.aspx?id=channel%20stacking#

Sunil Vadakkepuliyambattaa, S. B. (2013). Distribution of subsurface fluid-flow systems in the SW Barents Sea.

Sylvia Nordfjord, John A. Goff, & James A. Austin Jr. (2005). Seismic geomorphology of buried channel systems on the New Jersey outer shelf: assessing past environmental conditions. Marine Geology 214, 339 – 364.

T. Euzen, E. A. (2007). Reservoir architecture of a turbidite channel complex in the Pab Formation, Pakistan. AAPG.

T. Schwenka, V. Spiessa, M. Breitzkea, & C. Hubscherb. (2005). The architecture and evolution of the Middle Bengal Fan in vicinity of the active channel–levee system imaged by high-resolution seismic data. Marine and Petroleum Geology 22 (2005) 637–656.

T. Sund, O. Skarpnes, L. Norgard Jensen, & R. M. Larsen. (1986). Tectonic Development and Hydrocarbon Potential Offshore Troms, Northern Norway. AAPG, 615-627.

Tayyab Muhammad Naseer, Shazia Asim, & Mirza Naseer Ahmad. (2014). Application of Seismic Attributes for Delineation of Channel Geometries and Analysis of Various Aspects in Terms of Lithological and Structural Perspectives of Lower Goru Formation, Pakistan. International Journal of Geosciences.

Tore Grane Klausen, Alf Eivind Ryseth, & William Helland-Hansen. (2014). SPATIAL AND TEMPORAL CHANGES IN GEOMETRIES OF FLUVIAL CHANNEL BODIES FROM THE TRIASSIC SNADD FORMATION OF OFFSHORE NORWAY. Journal of Sedimentary Research, 2014, v. 84, 567–585.

Tore Grane Klausen, Alf Eivind Ryseth, & William Helland-Hansen. (2015). Regional development and sequence stratigraphy of the Middle to Late Triassic Snadd Formation, Norwegian Barents Sea. Marine and Petroleum Geology, 102-122.

Tore O. Vorren, Geir Richardsen, & Stig-Morten Knutsen. (1991). Cenozoic erosion and sedimentation in the western Barents Sea. Marine and Petroleum Geology, v. 8, p. 317-340.

University of Cambridge. (2008). Devensian (Weichselian) Late-glacial - Holocene (Flandrian) fluvial sequence as an analogue. Retrieved from http://www.qpg.geog.cam.ac.uk/.

V. Kolla, & H.W. Posamentier. (2007). Deep-water and fluvial sinuous channels—Characteristics, similarities and dissimilarities, and modes of formation. Marine and Petroleum Geology 24 (2007) 388–405.

Veiga-Pires, C., Moura, D., & Bruno, R. (2007). Provenance of Quaternary sands in the Algarve (Portugal) revealed by U–Pb ages of detrital zircon. In E. W. Gary Nichols, Sedimentary Processes, Environments and Basins: A Tribute to Peter Friend. International Association of Sedimentologists.

W. M. van Dijk, & W. I. van de Lageweg. (2012). Experimental meandering river with chute cutoffs. JOURNAL OF GEOPHYSICAL RESEARCH, VOL. 117.

W. M. van Dijk, & W. I. van de Lageweg. (2012). Experimental meandering river with chute cutoffs. JOURNAL OF GEOPHYSICAL RESEARCH, VOL. 117.

Wietse I. van de Lageweg. (2012). Sedimentology.

Wikipedia. (2015).

Wilcock, P. (2001). Relations between streamflow, sediment transport, and aquatic habit in regulated rivers. Water science and application, v.4, 185-198.

Woodyer, K.D. (1975). Concave-bank benches on Barwon River. Australian Geography, v. 13, p. 36–40.

Wooster, J. (2002). A Braided River System in a Glacial Environment, the Copper River, Alaska.

Zoltán Sylvester, Carlos Pirmez, & Alessandro Cantelli. (2010). A model of submarine channel-levee evolution based on channel trajectories:Implications for stratigraphic architecture. Marine and Petroleum Geology.

А.А., П. (2007). Изучение неоднородности пласта по геофизическим данным. Вестник недропользователя Ханты-Мансийского автономного округа .

GeoTeric Software

www.GeoTeric.com

Channel stacking. sepmstrata org. (2013).
http://www.sepmstrata.org/Terminology.aspx?id=channel%20stacking

Lundin. (2013). *Gohta: Et nytt oljefunn i Barentshavet.* Retrieved 09.11.2015, from
http://www.lundin-norway.no/2013/10/16/gohta-et-nytt-oljefunn-ibarentshavet/.

NPD. (2014). *Factmaps. Retrieved 18.11.2015*. Retrieved from http://gis.npd.no/factmaps/html_20/

Wikipedia. (2015).